University of Pécs
Faculty of Sciences
Doctoral School of Earth Sciences

Geomorphometric application of quasi-global DEMs for semi-automated geomorphological mapping

PhD Dissertation

Author:
Edina JÓZSA

Supervisor:
Dr. Szabolcs Ákos FÁBIÁN
associate professor

Pécs, 2019

Contents

List of Figures

List of Tables

List of Abbreviations

ACE/ACE2:	Altimeter Corrected Elevations
ALOS:	Advanced Land Observing Satellite
AOI:	Area of Interest
ASI:	Agenzia Spaziale Italiana (Italian Space Agency)
ASTER:	Advanced Spaceborne Thermal Emission and Reflection Radiometer
AW3D30:	ALOS World 3D 1" model
CGIAR:	Consultative Group for International Agricultural Research
CLC2006:	Corine Land Cover 2006
CSI:	Consortium for Spatial Information
DCW:	Digital Chart of the World
DEM:	Digital Elevation Model
DLR:	Deutsches Zentrum für Luft- und Raumfahrt (German Aerospace Center)
DLSM:	Digital Land Surface Model
DMA:	Defense Mapping Agency
DoD:	DEM of Differences
DSM:	Digital Surface Model
DTED:	Digital Terrain Elevation Data standard
DTM:	Digital Terrain Model
EEA:	European Environment Agency
EGG08:	European Gravimetric Geoid model 2008
EGM96/EGM2008:	Earth Gravitational Model 1996 and 2008
EM:	Eastern Mecsek 3rd level study area
EOTR:	Egységes Országos Térképrendszer (Hungarian Unified National Map System)
EOV:	Egységes Országos Vetület (Hungarian Unified National Projection System)
EROS:	Earth Resources Observation and Science Center
ERS-1, ERS-2:	European Remote-sensing Satellite
ESD:	Error Standard Deviation
ETC/ULS:	European Topic Centre on Urban, Land and Soil systems
ETRS89-LAEA:	European Terrestrial Reference System 1989-Lambert Azimuthal Equal Area projection
FOSS:	Free and Open Source Software
GCP:	Ground Control Point
GDEM:	Global Digital Elevation Model
GEOBIA:	Geographic Object-Based Image Analysis
GeoPAT:	Geospatial Pattern Analysis Toolbox
GEOSS:	Global Earth Observation System of Systems
GHP:	Great Hungarian Plain

GIS:	Geographic Information Science / Geographic Information System
GLAS:	Geoscience Laser Altimeter System
GLOBE:	Global Land One-km Base Elevation Project
GMES RDA:	Global Monitoring for Environment and Security Reference Data Access project
GmIS:	Geomorphological Information System
GRASS GIS:	Geographic Resources Analysis Support System
GTOPO30:	Global 30 Arc-Second Elevation
GUI:	Graphical User Interface
HRTI:	High Resolution Terrain Information standard
ICESat:	Ice, Cloud, and land Elevation Satellite
IDW:	Inverse Distance Weighting
InSAR/IfSAR:	Interferometric Synthetic Aperture Radar
ITP:	Integrated TanDEM-X Processor
JAXA:	Japan Aerospace Exploration Agency
JPL:	Jet Propulsion Laboratory
LE90:	Linear Error at 90% confidence level
LHP:	Little Hungarian Plain
LiDAR:	Light Detection and Ranging
LP DAAC:	Land Process Distributed Active Archive Center
MADOP:	Magyarország Digitális Ortofotó Programja (Hungarian Digital Orthophoto Program)
MCP:	Mosaicking and Calibration Processor
ME:	Mean Error
MEaSUREs:	Making Earth System Data Records for Use in Research Environments
MERIT:	Multi-Error-Removed Improved-Terrain
METI:	Ministry of Economy, Trade and Industry of Japan
NASA:	United States National Aeronautics and Space Administration
NGA:	National Geospatial-Intelligence Agency
NGDC:	National Geophysical Data Center
NHR:	North Hungarian Range
NIMA:	National Imagery and Mapping Agency
NOAA:	National Oceanic and Atmosphere Administration
NSIDC:	National Snow & Ice Data Center
PRISM:	Panchromatic Remote-sensing Instrument for Stereo Mapping
QGIS:	Quantum GIS
RMSE:	Root Mean Square Error
SAGA GIS:	System for Automated Geoscientific Analyses
SRTM:	Shuttle Radar Topography Mission
SRTM1:	SRTM model with 1” horizontal resolution
SRTM3:	SRTM model with 3” horizontal resolution
SWBD:	SRTM Water Body Data
TanDEM-X, TDX:	TerraSAR-X add-on for Digital Elevation Measurements
TDH:	Transdanubian Hills
TDR:	Transdanubian Range

TDX12:	TanDEM-X 12 m model
TG:	Topographic Grain
TIN:	Triangulated Irregular Network
TPI:	Topographic Position Index
TS:	Tolnai-Sárköz 3rd level study area
TSX:	TerraSAR-X satellite
TWI:	Topographic Wetness Index
USGS:	United States Geological Survey
VNIR:	Visible and Near-Infrared
WAM:	Water Indication Mask
WGS84:	World Geodetic System 1984
WHB:	West Hungarian Borderland

'A földfelszín egész valóságának, térben és időben tapasztalt realitásának felderítése a geomorfológia súlyos feladata. Súlyos pedig különösen azért, mert segédtudományaitól kell olyan, mégpedig rengeteg adatmennyiséget átvennie, melyeket maga nem tud, sőt nem is tudhat begyűjteni.'
(Prinz, 1950, p. 153)

1. Introduction

1.1. Research context and significance

Nearly two decades have passed since the *Shuttle Radar Topography Mission* and ten years since the handbook *'Geomorphometry: Concepts, Software, Applications'* was published. Following these scientific milestones, the quantitative transition of geomorphological research accelerated, GIS-software has provided a series of novel possibilities for (semi)-automated landform analysis (Farr et al., 2007; Pike, Evans, & Hengl, 2009). Geomorphometry is an active field, dominated by the development of automated landform delineation and classification methods, all of which intend to overcome the influence of expert subjectivity and to extract information from DEMs in a robust and repeatable fashion (Drăguţ, Eisank, & Strasser, 2011; Minár, Krcho, & Evans, 2016; Pike et al., 2009). The improving quality and spatial coverage of digital elevation models coupled with the technological innovations have led to the spread of GIS-based geomorphological mapping, while the classical techniques are being gradually replaced (Demek, Kirchner, Mackovčin, & Slavík, 2012; Griffiths, Smith, & Paron, 2011; Gustavsson, Kolstrup, & Seijmonsbergen, 2006; Seijmonsbergen, Hengl, & Anders, 2011; Verstappen, 2011). Over the years various specialised software packages have been developed (e.g. LandSerf, MicroDEM, ILWIS, TauDEM, Whitebox Geospatial Analysis Tools, etc.), and as geomorphometry became a central part of Earth Sciences the general-purpose GIS software (ArcGIS, GRASS GIS, SAGA GIS, QuantumGIS) integrated the digital terrain analysing tools as well (Bishop, James, Shroder, & Walsh, 2012; Lindsay, 2016; Wilson, 2018; J. D. Wood, 2009b).

To date the development of digital terrain analysis and GIS-aided geomorphological mapping is driven by the new sources of digital elevation data, exploration of uncertainty in output products, conceptualisation and standardisation of workflows, efforts towards exactness of derived land-surface parameters and development of new tools to facilitate DEM-based mapping (Hebeler & Purves, 2009; Minár, Minár Jr, & Evans, 2015; Reuter,

2018; M. J. Smith & Clark, 2005; Wilson, 2018). Recent studies demonstrated that GIS-aided surface analysis is more cost- and time-effective, transparent, reproducible, objective and systematic than conventional field-based and visual interpretation methods (De Reu et al., 2013; Dekavalla & Argialas, 2017; Drăguţ & Blaschke, 2006; Evans, 2012; Florinsky, 2017; Jasiewicz & Stepinski, 2013; Minár & Evans, 2008; Pike et al., 2009; Seijmonsbergen et al., 2011).

The variety of quasi-global DEM products (*GMTED2010, MERIT DEM, SRTM, ASTER GDEM, AW3D30, TanDEM-X*) at the disposal of the scientific community is rapidly increasing, and all of these models exhibit potentials and limitations with regard to coverage, temporal and horizontal resolution and accuracy. Readily available DEMs with improving resolution mean that most researchers no longer perform the data acquisition or interpolate their own models, instead plausibility analyses need to be conducted to ensure the fitness-of-use for a particular application (Carabajal & Harding, 2006; Purinton & Bookhagen, 2017; Reuter, Hengl, Gessler, & Soille, 2009; Wessel et al., 2018). Besides the free of charge availability for scientific purposes, amongst the advantages of these GDEMs should be mentioned the unified data structure, the lack of time-consuming data acquisition, avoidance of interpolation related DEM errors, and compared to topographic maps the actuality of the data (Király, 2005; G. Szabó, Mecser, & Karika, 2013). GDEMs have already been successfully applied in numerous regional and global geomorphological studies (e.g. Bubenzer & Bolten, 2008; Bugnicourt et al., 2018; Csillik & Drăguţ, 2018; Dekavalla & Argialas, 2017; Demoulin, 2011; Drăguţ & Eisank, 2012; Grohmann, 2018; Iwahashi, Kamiya, Matsuoka, & Yamazaki, 2018; Iwahashi & Pike, 2007; Seres & Dobos, 2010), however, a common conclusion regarding these models is that despite their general plausibility in digital terrain analysis, quality assessment and pre-processing steps are strongly advised to avoid misleading interpretations (Guth, 2010; Hengl & Reuter, 2011; Hirt, 2018; Mukherjee et al., 2013; Rodríguez, Morris, & Belz, 2006; Tachikawa et al., 2011). GDEM users are often unaware of the effects of error propagation to the derivatives and validation techniques are not applied systematically, which is compromising the reliability of the scientific output (Minár et al., 2016; Reuter et al., 2009; G. Szabó, 2007). The application of GDEMs has not yet been widely adopted in Hungary (Józsa, Fábián, & Kovács, 2014; Józsa & Kalmár, 2014; G. Szabó, Mecser, & Karika, 2015; G. Szabó & Szabó, 2010; Ungvári, 2015b); thus, further validation and exploration of geomorphological applicability is required to provide an overview for researchers planning to use these datasets within the Carpathian Basin.

Despite the medium resolution and the outlined drawbacks, the quasi-global DEMs provide uniformity of quality and coverage, which enables the synthesis and comparison of mapping projects across broad spatial extents and encourages international research cooperation. Sophisticated (semi)-automated mapping techniques expand the horizons of GIS-aided geomorphology: the reliability of the algorithms is increasing with the advance of explicit semantic models, 'black-box' procedures are constantly replaced by open source tools and standardisation of the derived landform maps is also in progress (Bishop et al., 2012; Evans, 2012; Gustavsson et al., 2006; Minár & Evans, 2008; Minár et al., 2015; Verstappen, 2011). While fieldwork will always be an integral part of geomorphology, surveys can greatly benefit from using the more objective geomorphometric mapping in identifying areas of interest (Walsh, Butler, & Malanson, 1998; Wieczorek & Migoń, 2014).

The recent work is focusing on the general and specific geomorphometric applications of GDEMs, shedding light on the regional error characteristics and uncertainties in the derived land-surface parameters and objects. The author's scientific interest towards GDEMs eventually originated from the need of input data to tackle geomorphological questions. The duality of the research is inevitable because the geomorphological investigation of the complex terrain in Hungary requires the thorough review of the available DEM products, and conducting the analysis successfully is only possible by correct application of the terrain analysing tools. Therefore, a significant portion of the presented work is dedicated to DEM-based terrain analysis, the optimisation of the selected methods and the presentation of self-developed tools to handle the operational scale problem of geomorphometry, the delineation of landforms and geomorphological landscapes and the approach to analyse terrace remnants in the Danube Valley.

1.2. Aims and Objectives

In one sentence, the aim of this study is to perform robust and reproducible GIS-based geomorphological mapping in Hungary, applying only public elevation datasets and open source software. Considering the potentials and limitations of digital terrain analysis on GDEMs, this ambitious goal has to be rephrased as a contribution to the specific geomorphometric analysis of landform elements, geomorphologic landscapes and terrace remnants at a variety of spatial extents. In order to ensure that this research benefits the geoscientific user community, the presented work is primarily conducted using free statistical (*R*) and GIS software (*GRASS GIS*), and the source code of the developed tools is shared on *GitHub* (Józsa, 2017a, 2017b).

Geomorphometric analysis is commonly implemented in the following steps: (1) acquiring or generating a digital land surface model that matches the research objectives, (2) performing quality assessment of the DEM, (3) correcting errors and removing artefacts to the best possible extent, (4) deriving land-surface parameters and objects, (5) conducting application specific analysis and synthesising geomorphologically relevant information (Bishop et al., 2012; Pike et al., 2009; Wilson, 2012). The objectives of this study are formulated according to this workflow.

1. Public domain quasi-global digital elevation models date back to the mid-1990s and ever since an increasing number of products has been released for scientific or commercial purposes. Finding the DEM that is fitting the objectives of the task at hand is a crucial step in designing the research framework. While users tend to choose models with smaller cell sizes, coarse resolution datasets are still essential to certain global or continental applications (Lisenby & Fryirs, 2017). Therefore, the present work is dedicating a longer section to the detailed description of free-of-charge DEMs available for Hungary.
2. Quality assessment is intended to determine the common error statistics (e.g. ME, RMSE, LE90) and more importantly to reveal the spatial arrangement of the different error components. This step is performed on a reduced selection of DEMs (*TanDEM-X 0.4", SRTM v3.0, AW3D30 v2.1, MERIT DEM*) and contour-based DTMs as reference datasets.
    a. Systematic analysis of DEM errors is necessary in advance of application to set the expectations straight and avoid misinterpretation of the outputs (Grohmann, 2018). The key steps of this analysis are the visual interpretation of models (shaded relief map, exaggerated 2.5D display, difference surface), calculation of absolute and relative error statistics (vertical and horizontal accuracy), inspection of the spatial arrangement of errors and regression analysis based on auxiliary datasets to explore the underlying causes of elevation bias.
    b. Land-surface parameters generated from the models and the reference datasets are used to evaluate the reliability of DEM derivatives and the effect of error propagation in the frame of general geomorphometry (Reuter et al., 2009).
3. Since the appearance of quasi-global DEMs, the user community expressed keen interest in reducing the uncertainties associated with data voids, vegetation offset and noise on the models (Robinson, Regetz, & Guralnick, 2014; Su & Guo, 2014; Walker, Kellndorfer, & Pierce, 2007; Yamazaki et al., 2017). For geomorphological analysis, it

is important that the relative representation of the topography is as reliable and accurate as possible (Reuter et al., 2009; Wecklich, Gonzalez, & Bräutigam, 2015). For this reason, a pre-processing algorithm is compiled to enhance the quality of the selected *SRTM1* model.

4. Even though the number of available algorithms to derive land-surface parameters and objects is constantly increasing, one important objective of geomorphometry is to find a minimal set of tools, which are universal, flexible and easily feasible, while also being capable to reveal the maximum geomorphological information content from DEMs (J. D. Wood, 1996). In order of complexity, this study is focusing on semi-automated GIS approaches for the identification and extraction of landform elements, geomorphological regions and terrace-top surfaces, tackling the problem of objective and adaptive parametrisation.

   a. For the delineation of landform elements, the novel *geomorphons* approach (Jasiewicz & Stepinski, 2013) is used, however, in order to fully exploit the efficiency of this tool the parameters require optimisation. Similarly to other digital terrain analysis methods, the weakness of the algorithm is the search parameter, which limits the scale of the analysis (Drăguţ et al., 2011; J. D. Wood, 1996). No readily available tool was found to tackle the scale problem; thus, revisiting the *topographic grain principle* (Pike, Acevedo, & Card, 1989) and developing an *extension* (r.tg.geom) to improve the geomorphometric output map is necessary.

   b. The simple landform elements, such as ridges, footslopes or pits, that are delineated from the DEMs with the geomorphometric tools, are suitable to characterise the terrain on the available operational scale. On the other hand, they are unable to describe the complexity of actual landforms or show the relationships of morphometric features and geomorphologic processes (Evans, 2012; Minár & Evans, 2008; J. D. Wood, 1996). To retrieve the underlying geomorphological information the landform elements are classified into physiographic units by pattern-based landscape analysis implemented in the *GeoPAT* toolbox (Jasiewicz, Netzel, & Stepinski, 2014, 2015).

   c. Significant watercourses in the hilly and mountainous regions of the Pannonian Basin are often accompanied by terrace remnants. As a result of the socio-economic role of these surfaces and their importance in paleo-environmental reconstructions, terrace research along the Danube has established

itself as a major topic of Hungarian traditional geomorphology (Bugya, 2008; Pécsi, 1959). For the automatic delineation of these discrete landforms conceptual issues need to be addressed first. The terrace extraction is based on the method of Demoulin et al. (2007). To fill in the gap between the semantics and technical domain a *synthetic DEM* is created to test and improve the methodology. The algorithm to extract terrace remnant candidates from DEMs is worth-wile to be implemented as a user-friendly *'push-the-button' tool* (r.terrace.geom).

5. In this research geomorphometry serves a dual purpose: it is a tool for the quality assessment of the GDEMs, but more importantly the GIS-based, semi-automated geomorphological mapping is also the final aim of the present dissertation. The DEM quality influences the accuracy of the digital terrain analysis, however, the derived maps and statistics are still valuable outputs. To validate the results of the *geomorphometric mapping* process it is necessary to create reference datasets based on the available literature and expert-based geomorphological maps. Transforming traditional maps into GIS layers can be a challenging task and requires reinterpretation of the delineated landforms (Gustavsson et al., 2006; Wieczorek & Migoń, 2014). From a technical point of view, the results are reflecting on the GDEMs plausibility in geomorphometry and the applicability of the selected and self-developed landform mapping algorithms. From the geomorphological aspect the resulting maps reveal further details about the spatial arrangement of landforms, terrace-remnants and geomorphic regions in Hungary.

Geomorphometry is truly an amalgam of geomorphology and GIS, and in case of such interdisciplinary research it is difficult to present the results in a way pleasing both involved disciplines. The structure of the research is following the outlined framework of geomorphometric analysis from the acquisition and quality assessment of the GDEM data, through the application of readily available or self-developed terrain-analysing tools, to the validation and interpretation of the output maps. The current research has a stronger connection to the field of GIS, and so, the presented results might appear incomplete from a geomorphological point of view.

2. Theoretical background and literature review

2.1. Digital land surface representations

The digital representation of Earth's topography is a mathematical model where elevation value (*Z*) is assigned to a large number of known points on the horizontal plane (*X, Y coordinates*). The digital model is providing a continuous surface, where only one elevation data is stored for one spatial location (discontinuities or overhangs cannot be handled in this sense). The digital land surface models should, therefore, be interpreted as 2.5D models instead of true 3D representations (Li, Zhu, & Gold, 2005c; Maune, Heidemann, Kopp, & Crawford, 2007; Telbisz, Székely, & Timár, 2013).

Based on the height that the Z-value represents, one could distinguish between the types of digital land surface models (DLSM) as detailed below. On the other hand, over time and in different countries alternative terms came into use, which leaves room for confusions and misinterpretations (Li, Zhu, & Gold, 2005b; Pike et al., 2009). Nevertheless, the terminology is not consistent between the top Google search results[1] either, which further confirms the need to clarify on a per study basis.

The most common terms in practice are DEM (Digital Elevation Model), DTM (Digital Terrain Model) and DSM (Digital Surface Model), which are often assumed to be synonymous or used as complete opposites (in)between studies. According to 'The DEM Users Manual' (Maune, Heidemann, et al., 2007) the term DEM implies to elevations of the terrain (meaning the bare earth), on the contrary, data providers and the user community have favoured DEM to be used as an umbrella term for digital land surface models irrespective of the Z-value the dataset captures (Guth, 2018; Hengl & Evans, 2009). The latter meaning is a better fit for the interpretation of quasi-global digital land surface models as well, considering the generally coarse horizontal resolution and different correction attempts commonly applied on GDEMs (e.g. smoothing, partial removal of vegetation offset) (Gallant & Read, 2016; Yamazaki et al., 2017). As the cell size covers a larger portion of the Earth's surface, the spatial variations caused by the natural and built features are averaged, so it is advised not to interpret the GDEMs strictly as DTMs or DSMs either

[1] Top search results for the term digital elevation model: "DEM, DSM & DTM Differences – A Look at Elevation Models in GIS" 2018 and "Digital elevation model – Wikipedia article" 2018

(Tachikawa et al., 2011). *Table 1* summarizes the meaning of the terms both in English and in Hungarian[2], while *Figure 1* provides a visual overview of the different models used in this study.

Table 1. Types of digital land surface models according to the represented surface (Based on Telbisz et al., 2013)

Represented surface	***Bare earth without surface objects***	***Terrain with natural and built features***
Term in English	*DTM* = Digital Terrain Model	*DSM* = Digital Surface Model
Term in Hungarian	*DTM* = Digitális Terepmodell *DDM* = Digitális Domborzatmodell	*DFM* = Digitális Felszínmodell
Generic term in English	*DEM* = Digital Elevation Model *GDEM** = Quasi-Global Digital Elevation Model	
Generic term in Hungarian	*DMM* = Digitális Magasságmodell	
Common source of data	topographic maps	remote sensing

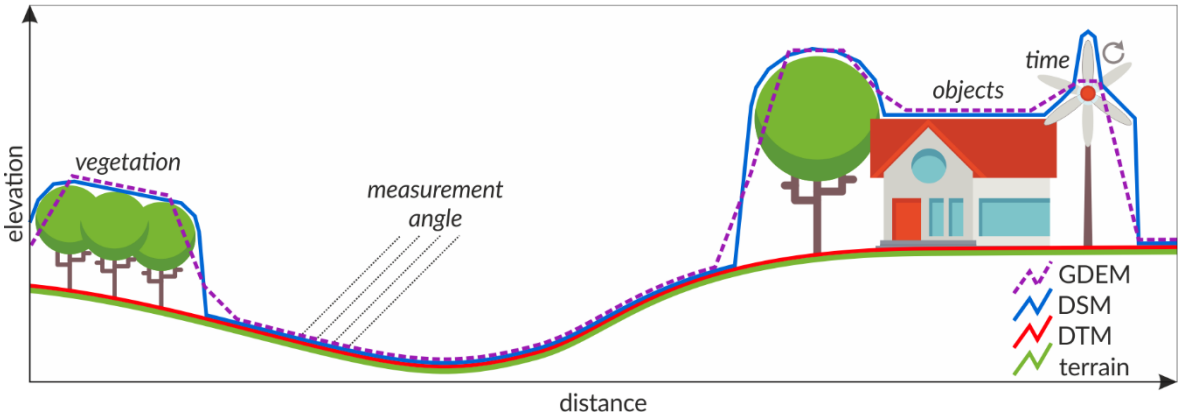

Figure 1. Differences in the land surface represented by DTM, DSM and GDEM.[3]

From a technical aspect, the digital elevation data is organised into a data structure, which is related to the type of the data model. The two commonly used data model types are rasters (grid format) and vectors (triangulated irregular networks, digital contours, point clouds) depending on the data source, further analysis purposes and preferred methods (Li et al., 2005b; Telbisz, Székely, et al., 2013; Wilson & Gallant, 2000a).

Grid meshes cover the surface by squares (optionally rectangles or hexagons) organised to rows and columns, the elevation is referring to the centre or the node of the grid cells. This data structure is favoured because of the simplicity of data storage (same as digital

[2] Hungarian terms are listed for the help of the reader considering the main audience of the dissertation.
[3] Basic design of the figure is from Freepik repository.

images) and ease of computer handling (from visualisation to calculation of derivatives). The disadvantage of the model is that the cell size is limiting the representation of complex topography, while redundant data is stored over smooth surfaces. Recording the elevation data in whole meters such as in GDEMs aggravates this issue. On the other hand, smaller horizontal resolution affects the storage requirements and computational efficiency. The precision of hydrological modelling is also impacted by the different distances of cardinal and diagonal directions, and zigzag course of derived flow paths (Hengl & Evans, 2009; Telbisz, Székely, et al., 2013; Wilson & Gallant, 2000a).

TINs are modelling the surface with triangular elements (facets), which are constructed by Delaunay triangulation. Advantages of TINs are the more accurate handling of abrupt changes in the topography and matching a wide variety of terrain roughness with different density of the triangles (Telbisz, Székely, et al., 2013; Wilson & Gallant, 2000a). Terrain analysis is, nevertheless, more difficult because the common algorithms are based on the raster design, and thus geomorphometric analysis often requires the TIN data to be rasterized (Hengl & Evans, 2009).

Further advancement is the concept of hybrid models, where the surface specific points, ridge- and streamlines could be incorporated in the model by breaking the regular grid into triangles and inserting local TINs to the grid mesh (Li et al., 2005b). Square-grid models can also be improved so that the model respects the surface drainage better, for example by using the ANUDEM (*Topo to Raster* tool in ArcGIS) interpolation method (Hutchinson, 1989; Hutchinson, Xu, & Stein, 2011). The technical implementation of storing raster datasets (e.g. DEMs) with different resolutions in the same file was also presented recently (Bugya & Halmai, 2013).

During the past 20–30 years DEM data acquisition techniques evolved rapidly and the previously common ground surveying and secondary data collection from topographic maps were gradually replaced by passive and more recently active remote sensing methods (Wilson, 2012). Conducting field surveys with theodolites and total stations are labour intensive and costly, however, provide high accuracy measurements. GPS/differential GPS measurements can be carried out quickly and with good precision, therefore, serving as a reasonable alternative data source (Li, Zhu, & Gold, 2005d). The conversion of topographic maps to digital contour lines is considered as a worst-case scenario and nowadays it is rarely the main source of elevation data. Even though the recorded elevations represent the bare Earth, the precision is highly dependent on the reliability of the base map, the quality of the scanned hard-copy and the skills of the human operator (Nelson, Reuter, & Gessler, 2009).

On the contrary, remote sensing techniques are able to cover large areas with significantly lower costs, thus it is no surprise that ever-growing attention is devoted to the airborne and spaceborne sources of elevation data. According to an estimation provided by Li et al. (2005d) 85% of topographic maps have been produced or updated by stereo-photogrammetric techniques around the world. As aerial images capture the land surface with the natural and built features, the resulting model is a DSM. Camera distortions, misregistration of stereopairs, cloud cover and terrain characteristics can impair the accuracy of the elevation data. Among the GDEMs, ASTER GDEM (Urai, Tachikawa, & Fujisada, 2012) and AW3D (Takaku, Tadono, & Tsutsui, 2014) were created by the stereo-photogrammetric processing of extensive spaceborne imagery repositories. In the framework of the MADOP project, launched in 2003, orthophotos and stereophotogrammetric DSMs are prepared for Hungary in 3 to 4-year periods (Winkler, 2003).

Laser ranging surveys (LiDAR) are using active sensors, which are able to operate under less-than-ideal weather conditions as well, providing a high density of sampled elevations with high vertical accuracy and allowing the derivation of different surface models by classifying the returned signals. The number of regional and national LiDAR projects is growing, in 2018 the mapping agencies of Norway, the Netherlands, Belgium, Denmark, the United Kingdom, Slovenia, Finland, the United States and Spain had already conducted surveys (Guth, 2018). Another notable elevation data source is the globally distributed, but not seamless coverage, ICESat/GLAS high accuracy, spaceborne laser altimetry measurements provided by NSIDC. The main objective of this mission was monitoring the polar regions, so accordingly the data tracks are separated by a maximum of 80 km around the Equator (Abshire et al., 2005; Schutz, Zwally, Shuman, Hancock, & DiMarzio, 2005). The GLA14 Land Elevation Product has been used as ground control points during the TanDEM-X creation (Rizzoli et al., 2017) and in several GDEM quality assessment projects (Carabajal & Harding, 2006; Satgé et al., 2016; Tachikawa et al., 2011). NASA also planned to conduct the LiDAR Surface Topography (LIST) mission in the near future to gather accurate measurements of the land surface globally ("Lidar Surface Topography (LIST)" 2007).

In the last decades, satellite-based radar systems are particularly important in the creation of global DEMs, as InSAR/IfSAR techniques are capable of mapping large areas rapidly, and with longer radar wavelengths the operation is almost independent of weather conditions. The elevation data is based on the phase difference between two radar images covering the same location from different angles. In the case of repeat-pass interferometry

the accuracy is limited due to temporal decorrelation and atmospheric disturbances. A single-pass operation was used for the creation of the SRTM DEM, where an additional, passive antenna was deployed to acquire the second image (Massonnet & Elachi, 2006; Nelson et al., 2009). During the TanDEM-X mission, the radar satellites were flying in a close helix formation to perform quasi-simultaneous data takes in order to achieve a high accuracy of the images (Krieger et al., 2007).

Digital elevation models are offering diverse possibilities to scientific and commercial activities, and thus it is practically impossible to provide an exhaustive list regarding DEM usage. A course of books attempts to familiarise the reader with user applications (Hengl & Reuter, 2009; Li, Zhu, & Gold, 2005a; Maune, 2007; Wilson & Gallant, 2000b). DEM data is essential for the orthorectification of satellite imagery. Geomorphology, hydrology, pedology, ecology and meteorology are considered amongst the traditional scientific fields using DEMs for mapping and modelling processes. On the other hand, early on civilian and military engineering were the main facilitators of DEM developments. Studies from humanitarian or economic perspectives are using DEMs for management purposes, such as flood risk modelling, city planning, precision farming and forestry, natural resource management and transportation planning. Digital elevation data has potentials in archaeology as well, like the detection of ancient settlement sites. With the rapid development of 3D visualisations, the digital representations of the surface gained importance in the field of cartography as base maps, even more with the advance of online maps such as OpenStreetMap and Google Maps.

For decades now, DEMs form the backbone of quantitative terrain analysis (e.g. Csillik & Drăguţ, 2018; Franklin, 1987; Iwahashi & Pike, 2007; Seijmonsbergen, Hengl, & Anders, 2011; J. D. Wood, 1996) and have major role in terrain visualisation (Mitasova, Harmon, Weaver, Lyons, & Overton, 2012), digital geomorphological mapping (Bishop et al., 2012; Gustavsson et al., 2006; Verstappen, 2011), as well as in exploring and modelling landscape evolution (Demoulin et al., 2007; Geach et al., 2014; Troiani & Della Seta, 2011).

2.2. Digital geomorphological mapping vs. Geomorphometry

Modern geomorphology is utilising a combination of GIS tools for geomorphic analysis and the knowledge of geomorphological experts, eventually forming a new subsystem referred to as geomorphological GIS or Geomorphological Information System (GmIS) (Mentlík, Jedlička, Minár, & Barka, 2006; Minár, Mentlík, Jedli, & Barka, 2005; Wu, Wang, Han, Ren, & Chen, 1993). GmIS includes the geodatabase structure to manage relevant

geomorphological layers (DEMs and its derivatives, hydrological and geological data, topographic and thematic maps, field and remote sensing data, etc.), and the special terrain analysis toolset to create new geomorphological information with statistical and cartographic outputs (Minár et al., 2005). The discipline still focuses on exploring the spatial arrangement and formation of landforms, while taking advantage of the vital numerical inputs and analytical options that can be handled via GIS (Evans, Hengl, & Gorsevski, 2009).

Geomorphological mapping is the link between theoretical geomorphology and its applications from civilian engineering to operative decision support (Ádám & Pécsi, 1985; Demek, Embleton, Gellert, & Verstappen, 1972; Evans, 2012; Griffiths et al., 2011; Gustavsson et al., 2006). Traditional geomorphological maps were produced by meticulous ground mapping of landforms, surface materials and the incorporation of already available maps. In order to depict the shape, age, origin and forming processes of the different landforms the maps have a complex colour scheme and several different symbols (Demek et al., 1972; Gustavsson et al., 2006; Verstappen, 2011). The information content of the maps can be organised into layers during digitisation with a graphics editing software, but such a vector or raster file cannot be directly imported to GmIS. The geomorphological database can include point, line, polygon vectors and raster data as well, but the spatial relationships and attributes of the mapped phenomena have to be maintained for the sake of GIS operations (e.g. buffering, overlaying, etc.) (Bédard, 2005). In addition, the elementary forms layer in GmIS is not supposed to contain overlaps or gaps (Mentlík et al., 2006). The heavy use of symbols (gully, cliff, etc.) and the ambiguously drawn boundaries of geomorphic units make reinterpretation of the traditional maps unavoidable. The forms need to be crisply delineated and the symbols eliminated, so that the map only depicts information that could also be retrieved from DEMs and the above-mentioned auxiliary layers (Gustavsson et al., 2006; Verstappen, 2011; Wieczorek & Migoń, 2014). With the advent of GIS-aided geomorphological mapping, attempts were made to standardise and simplify legends, and also to facilitate scale flexibility of combination legends (Gustavsson & Kolstrup, 2009; Gustavsson et al., 2006; Verstappen, 2011).

Besides the digitisation and revision of traditional maps, (semi-)automatic mapping of landform elements has significantly increased over the last decade (e.g. Cunha, Magalhães, Domingos, Abreu, & Withing, 2018; Demek, Kirchner, Mackovčin, & Slavík, 2012; Frankl, Lenaerts, Radusinović, Spalevic, & Nyssen, 2016; Jasiewicz & Stepinski, 2013). Compared to the expert-drawn maps, these completely GIS-based geomorphological maps show two major differences. The latter approach is a classification of the input maps into common

landform elements, landforms and landscape types without providing further information on the age, genetics or current processes over the represented area (Bishop et al., 2012; Bugya, 2008; Demek et al., 2012; Wieczorek & Migoń, 2014). GIS-based delineation of the units is limited by the cell-based design of the tools – these mapping strategies are mostly considering the cells independently from each other, thus adjacent cells might be assigned to different categories resulting in the so-called 'salt-and-pepper' effect (Drăguţ & Eisank, 2011). The automatic classification is much faster and the output is easily reproducible based on clearly defined rules, however, there are ambiguous situations, where the expert-knowledge is required to avoid misinterpretation (e.g. eroded fluvial terraces and pediment surfaces). A geomorphologist is able to interpret the visual interrelations in DEMs along with auxiliary data to delineate and classify coherent regions of the terrain on multiple scales simultaneously (Stepinski, Jasiewicz, Netzel, & Niesterowicz, 2015). On the other hand, subjectivity cannot be eliminated from the manual mapping process, as a priori experience and domain knowledge of practitioners vary (Ardelean, Drăguţ, Urdea, & Török-Oance, 2013; Bishop et al., 2012; Hegedűs, 2012).

GIS-based geomorphological mapping from DEMs rather belongs to the discipline of geomorphometry. Geomorphometry is the quantitative study of topography, being an amalgam of Earth sciences, mathematics, engineering and computer science. The operational focus of geomorphometry is the extraction of land-surface parameters and objects typically from DEMs, resulting in so called geomorphometric maps (Pike, 2000; Pike et al., 2009). *General geomorphometry* applies to the analysis of the continuous surface by the means of land-surface parameters, while *specific geomorphometry* aims at analysing geometric and topological characteristics of landforms and landform elements (Evans, 1972, 2012). In order to conceptualise the transition of the continuous terrain into objects of geomorphic meaning Drăguţ & Eisank (2011) proposed *discrete geomorphometry* as the local description of land-surface divisions defined by the homogeneity of given input parameters.

General geomorphometry describes the characteristics of the topography by land-surface parameters, also referred to as geomorphometric variables. The fundamental parameters include local and regional as well as gravity field-specific and field-invariant variables (Evans, 1972; Evans & Minár, 2011; Florinsky, 2017; Olaya, 2009). Starting from a DEM, altitude is a zero order, field-specific, scale-free and local primary variable; derivatives are based on arbitrary regular areas (squares or circles) around each elevation point (Minár et al., 2016; Wilson & Gallant, 2000a). First order (e.g. slope, aspect), second order (different types of curvature) and third order (change of curvatures) local variables are

commonly used to describe surface characteristics and to identify possible boundaries of landforms at abrupt changes (Evans, 2012; Evans & Minár, 2011; Florinsky, 2017). Regional morphometric variables are based on the topological relations of cells, determined mainly by the hydrological properties of the terrain (e.g. catchment area, flow-path length, proximity to local streams and ridges) (Olaya, 2009). Field-invariant variables are the descriptive statistics of any land-surface parameters (Evans & Minár, 2011; Florinsky, 2017).

Specific geomorphometry is operating on the level of geomorphological units, however, these are organised into a nested hierarchy (Bishop et al., 2012; Drăguţ & Eisank, 2011; Minár & Evans, 2008). Landforms are morphologically meaningful, discrete features of the Earth's surface with recognisable shapes formed by natural and/or anthropogenic processes. The landforms are composed of landform elements that are bounded by topographic discontinuities of the so-called form-defining land-surface parameters. On the other end of the scale repeating landforms, patterns of the terrain are organized into geomorphological landscapes or physiographic units (MacMillan & Shary, 2009; Pike et al., 2009). Due to technical limitations, specific geomorphometry is treating these geomorphometric units as discrete forms, but this is only a necessary idealisation. In reality, sudden changes in the form-defining parameters are rare, considering fuzzy memberships of the boundaries is advisable (Evans, 2012; Minár & Evans, 2008; Pike et al., 2009).

From implementation point of view the procedures of automated landform extraction and classification can be grouped into those that attempt to retrieve repeating types of landforms (e.g. plateaus, hills) or delineate landform elements along a toposequence from divide to channel (e.g. ridge, footslope) (Evans, 2012; MacMillan & Shary, 2009; Minár et al., 2016). Multivariate classification techniques are commonly based on land-surface parameters such as elevation, slope and curvature, and the landforms are distinguished by arbitrary thresholds (e.g. Csillik & Drăguţ, 2018; Dikau, Brabb, & Mark, 1991; Hammond, 1964; Speight, 1990; Weiss, 2001; J. D. Wood, 1996). While other studies conducted unsupervised cluster analysis for a rather data-driven approach of partitioning the topography (e.g. Burrough, van Gaans, & MacMillan, 2000; Iwahashi, Kamiya, Matsuoka, & Yamazaki, 2018; Iwahashi & Pike, 2007; MacMillan, Pettapiece, Nolan, & Goddard, 2000). Promising techniques imported from outside of geographic disciplines are the segmentation of landform elements using object-based image analysis (Drăguţ & Blaschke, 2006; Drăguţ & Eisank, 2012) or pattern analysis (Jasiewicz & Stepinski, 2013). An exhaustive list of landform segmentation and classification methods is presented by Iwahashi & Pike (2007) and Cunha et al. (2018).

2.3. The scale problem

Geomorphological landscapes are made up of the pattern of landforms with varying sizes, which are commonly categorised as microforms (1–100 m), mesoforms (100–10 000 m), macroforms (10–1000 km) and megaforms (>1000 km) in the literature (Horváth, 1991). As the landscape is potentially carrying the signatures of multi-scale geomorphological processes, geomorphometry aims to extract descriptive land-surface parameters and objects on several characteristic scales and synthesise the information into a more realistic representation of the complex terrain (De Reu et al., 2013; Gorini & Mota, 2011; Schmidt & Andrew, 2005). However, geomorphometry is restricted by the cell size of the DEM intended to represent the real topography and the 'window of perception' applied in digital terrain analysis. A number of studies confirmed this dual scale dependency of DEM-based land-surface parameters and objects (Demeter, Szabó, Szalai, & Püspöki, 2007; Deng, Wilson, & Bauer, 2007; Drăguţ, Eisank, Strasser, & Blaschke, 2009; Fisher, Wood, & Cheng, 2004; Grohmann, 2015; Kienzle, 2004; Schmidt & Andrew, 2005; J. D. Wood, 1996).

In case of the digital land surface models the scale implies the level of spatial detail; the cell size gives the shortest distance over which change is recorded, the variation within the cell is lost (Goodchild, 2001). The Nyquist-Shannon sampling theorem dictates that the smallest unambiguously represented surface element is twice the grid resolution (Elek, 2004a, 2004b; Hengl, 2006; Pike, 1988; Shannon, 1949). There is no universally 'right' cell size, yet it is possible to find a 'good enough' surface representation for the targeted application. The recommended grid resolution is a compromise between the coarsest legible cell size – which is still capable to provide valid information regarding the analysed phenomena; and the finest legible grid resolution – which represents 95% of the spatial variability (Hengl, 2006). The working scale has to be accounted for in order to avoid misleading conclusions by omitting the influence of smaller or larger scale features and processes (Goodchild, 2011; Hengl & Evans, 2009). In practice the scale of the analysis is also limited by the costs of the input data, therefore the accessibility of GDEMs with improving resolution is an important step towards feasible multi-scale analysis (Drăguţ & Eisank, 2011; Goodchild, 2011).

The traditional *cartographic scale* – the ratio of the map distance to the corresponding distance on Earth's surface – has a less explicit meaning in digital terrain modelling. Firstly, the contour lines digitised from a topographic map to interpolate a DEM impose an effective

limit on the represented surface variability and the positional accuracy. A generally accepted accuracy of paper maps is 0.5 mm, which is in practice related to the printing technology as narrower features are hard to distinguish (Goodchild, 2001; Hengl, 2006). From another aspect, the set of contour lines or a LiDAR point cloud is also defining the support size, the area over which the sampled heights are representative of the surface. One should strive to select a cell size that complies with the *support size* of the sampling; unreasonably fine resolution could lead to local artefacts and higher computational requirements (Arundel, Li, & Zhou, 2018; Hengl & Evans, 2009). From another perspective, DEMs are widely used as a base layer of topographic or thematic maps, and the range of scales over which the model is sufficiently representing the terrain variability needs to be determined (Ungvári, 2015a). The level of detail possibly retrieved from the surface model is the *effective spatial resolution*, which is not necessarily the same as the *horizontal spacing*. Typically, some kind of smoothing is applied to the DEMs – especially to the GDEMs – to reduce the effect of noise at the cost of losing short-range variability (Hengl & Reuter, 2011; Józsa, 2015a; B. Smith & Sandwell, 2003; Tachikawa et al., 2011).

In order to capture the nested hierarchy of the terrain, geomorphometry needs to shift from the fixed-scale approaches to advanced multi-scale techniques. *Figure 2* illustrates three principally different, but commonly used methods to analyse the land-surface parameters and objects on multiple scales. Regardless of the applied method, it is still typical to determine the suitable search distances by following a trial-and-error method and visually reviewing the topography and the surface derivatives (Frankl et al., 2016; Kramm et al., 2017; Zwoliński & Stefańska, 2015). This confirms that the establishment of the optimal search parameter remains a key challenge in geomorphometry.

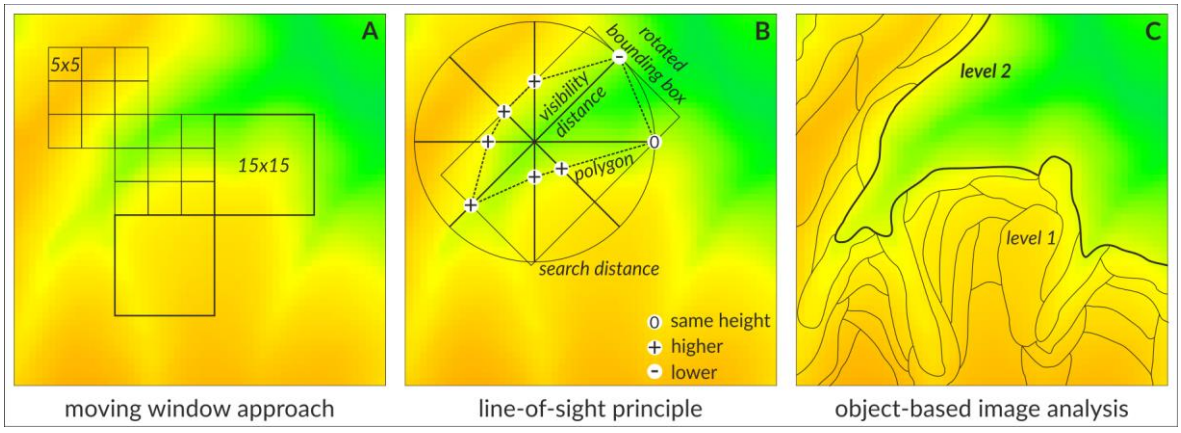

Figure 2. Common multi-scale approaches in landform mapping. (A – moving window operations, B – openness-based techniques, C –multi-level, multi-resolution segmentations)
(Figure 2B is based on the r.geomorphon GRASS GIS manual (Jasiewicz & Stepinski, 2016))

Incorporating multiple scales through growing neighbourhood sizes is a straightforward and widely used approach in digital terrain analysis (*Figure 2A*). Measuring land-surface parameters over a range of spatial scales is essential to the design of the Topographic Position Index (Jenness, 2006; Weiss, 2001) and the r.param.scale GRASS GIS tool or the related LandSerf software package (J. D. Wood, 1996, 2009a). Combining the output maps derived at characteristic scales yields a more realistic representation of the landscape (F. E. Gruber, Baruck, & Geitner, 2017; Weiss, 2001; J. D. Wood, 1996). The application of varying size moving windows to retrieve the scale signatures has appeared early in geomorphometry (Pike et al., 1989; W. F. Wood & Snell, 1960). These data-driven methods propose the characteristic scale based on the reduction of recorded relief energy (a difference between the maximum and minimum elevation) over a series of growing search windows. This concept is in line with Tobler's First Law of Geography and spatial autocorrelation (MacMillan & Shary, 2009). However, neighbourhood operations are computationally intensive and over a certain range the analysis becomes unfeasible (Grohmann & Riccomini, 2009). To overcome the limitations of neighbourhood operations, techniques could be taken over from the field of computer vision and graphics. Integral image analysis has been efficiently applied as an alternative to detect scale signatures over broad ranges (Lindsay, Cockburn, & Russell, 2015; Newman, Lindsay, & Cockburn, 2018).

Local ternary patterns technique – another reinterpreted image analysis concept – has proven to be useful for describing the texture of the land surface and delineating landform elements (Liao, 2010; Stepinski & Jasiewicz, 2011). Furthermore, the geomorphon tool is also achieving scale flexibility and orientation independency by introducing the line-of-sight principle (*Figure 2B*). The technique is based on the positive (zenith angle) and negative (nadir angle) topographic openness, which relates the surface relief and the horizontal distance along the eight principal directions (Yokoyama, Shirasawa, & Pike, 2002). According to the authors, the absolute scale independency could be theoretically reached by selecting an infinitely large search parameter to identify landform elements irrespective of their size (Jasiewicz & Stepinski, 2013; Stepinski & Jasiewicz, 2011).

Geographic object-based image analysis (GEOBIA) is a data-driven approach to decompose the terrain into elements of maximum internal homogeneity and external heterogeneity (*Figure 2C*). The approach has gained visibility in digital terrain analysis over the last years as an effective tool for multi-scale hierarchic landform delineation (Anders, Seijmonsbergen, & Bouten, 2011; Drăguţ & Blaschke, 2006; Drăguţ & Eisank, 2012; van Asselen & Seijmonsbergen, 2006). A key factor of the segmentation process is the 'scale

parameter', which can be objectively determined by the ESP2 tool (Drăguţ, Csillik, Eisank, & Tiede, 2014). In a bottom-up approach the tool is executing an iterative segmentation of the input maps until the recorded local variance in the segmented objects is increasing, then based on the rate of change between the iterations it suggests characteristic spatial scales for mapping at the different hierarchy levels (Drăguţ et al., 2014, 2011, 2009).

MacMillan and Shary (2009) and Li (2008) provide an overview of less well-known approaches to tackle the scale problem. These algorithms are usually either not readily available in the terrain analysis GIS packages or the attainable results are not worth the complicated execution. Among the possibilities are, for example, variogram calculations, derivation of hydrological spatial entities, fractal analysis or Fourier and wavelet transformations. As such methods are not applied in the present study, their detailed description is beyond the scope of this chapter.

3. Description of the study area

3.1. Different AOIs for different objectives

Considering the above-mentioned research interests, it is necessary to perform the validation of GDEMs and the landform mapping over different areas. By reviewing the physical and human geography of the selected study sites one can better design the framework of the specific geomorphometric applications and get a preliminary picture of the local factors influencing the quality of quasi-global DEMs.

During the delimitation of the AOIs the geographic characteristics of the Pannonian Basin and the general orographic features of Europe were taken into consideration. Based on the absolute altitudes and relative elevation differences, Hungary can be divided into three height levels, or so-called relief steps: lowlands, hills and low mountains (Bulla, 1962). Approximately 20–20% of the country is characterised by mountainous and hilly environments, and accordingly, its major area belongs to plains (Pécsi, 1984). On the other hand, Schweitzer (2009) claims that 73% of Hungary should be considered as plains, 20% belongs to hills and pediment surfaces and only 7% can be categorised as mountainous. This division is also reflected in the typical landscape classifications (Dövényi, 2010; Mészáros & Schweitzer, 2002). Another notable aspect in selecting the study sites was the prior knowledge and field experiences of the author. The detailed quality assessment of GDEMs is performed on designated areas over Southern Transdanubia in line with previously executed analyses (Józsa, 2014, 2015a; Józsa, Fábián, & Kovács, 2014). However, considering the topographic characteristics of Hungary, these AOIs are appropriate in spatial extent and representative from a geographical point of view. As per the presented objectives the necessary study areas are organised into four hierarchy levels (*Figure 3*).

- *1st level*: The main geomorphological landscapes were examined over the total area of Hungary. As a prerequisite of this step the SRTM1 model was improved over the whole country as well.
- *2nd level*: A 20 500 km^2 region, mainly in Southern Transdanubia, was selected to test the geomorphons tool and the topographic grain approach over heterogenous terrain. The study area is covering 36 microregions of the Transdanubian Hills, Great Hungarian

Plain and West Hungarian Borderland macroregions. The section along the Drava and southernmost course of the Danube has been excluded as the vegetation offset has an irreducible effect on the terrain roughness and the delineated landform elements. The selected microregions are listed in *Appendix 1*.

- *3rd level*:
  - In order to analyse the terrace levels of the Danube, a 320 km^2 region was designated between Almásfüzitő and Esztergom (*Appendix 7*). The area includes the microregions of the Győr-Tata Terrace Region, the Almás-Tát Danube Valley and the Gerecse Mountains, but the borders were drawn according to the available expert-based geomorphological map (*Appendix 9*).
  - For the quality assessment of the GDEMs two additional territories were selected. The models were compared over a 960 km^2 region covering the southern section of the Tolnai-Sárköz microregion (580 km^2) and the accompanying hills (380 km^2) and another 350 km^2 area including the Eastern Mecsek Mountains and its southern pediment surface. These regions were delimited along the kilometre network of the 1:10 000 scale EOV map sheets instead of natural boundaries.

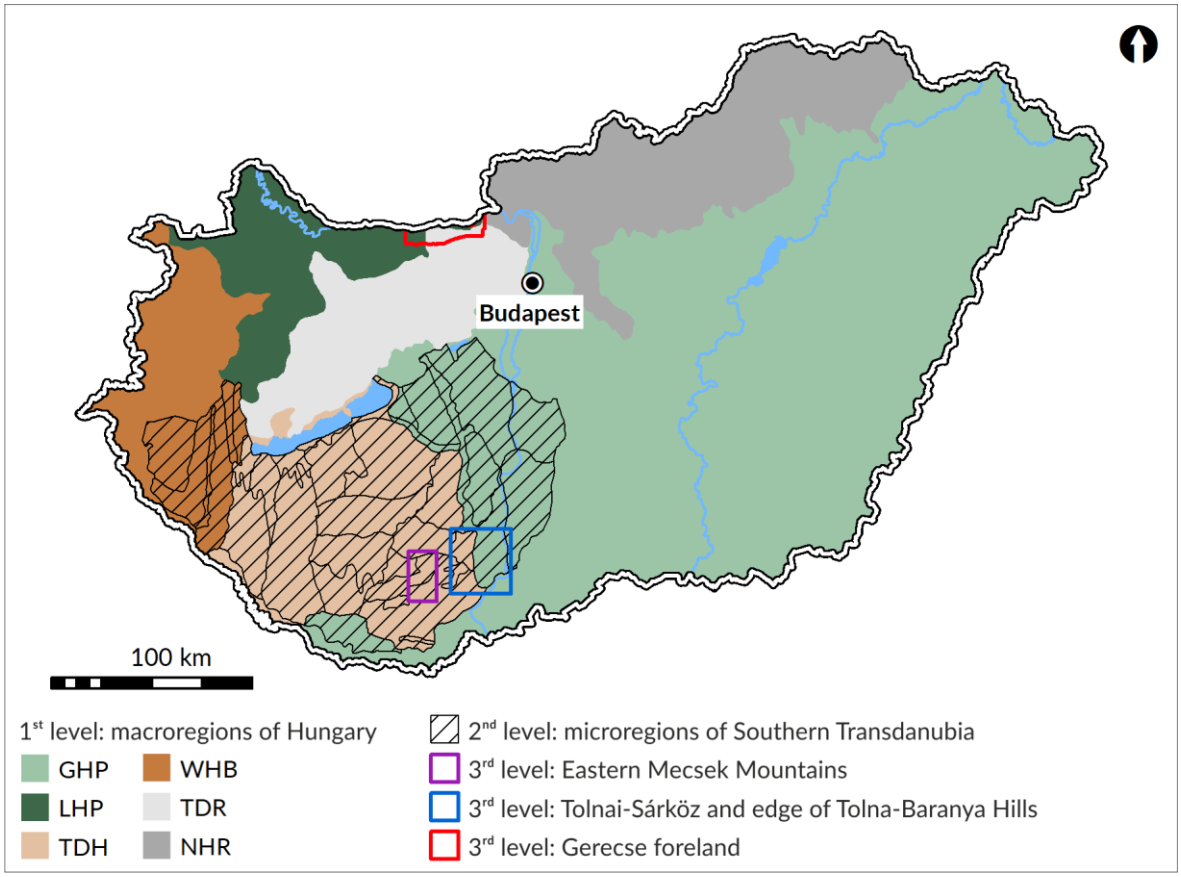

Figure 3. Location of the 1st, 2nd and 3rd level study areas.

- *4th level*: The contour-based reference DTMs used for the GDEMs' validation are subsets of the above-mentioned floodplain, hilly and low mountainous regions. The sites were selected to represent clear relief types (e.g. plain, upper section of a small catchment) and heterogenous surfaces as well. The multiple reference areas allow for the comparison of local characteristics and regional bias. Considering the labour intensity of digitisation these models cover only local landscapes that are representative of the topography (*Table 2*). The DTMs are named after the nearest settlement or stream for identification purposes in the following sections of the dissertation.

  - *Decs DTM*: Partially covers the area of Decs village and the Holocene terrace island in the Tolnai-Sárköz (Leél-Őssy, 1953; Pécsi, 1959). Besides the built-in areas it represents the extensive bare surfaces of agricultural fields.
  - *Bátaszék DTM*: Located at the adjoining section of the three hilly regions (Szekszárd Hills, Geresd Hills and South-Baranya Hills) the area is dominated by the NW–SE valley of the Lajvér Stream. The landcover is heterogenous, forest patches, shrubs, vineyards and agricultural fields are all represented.
  - *Báta DTM*: Covering the area of Báta village at the steep edge of the South-Baranya Hills towards the floodplain of the Tolnai-Sárköz. The major features of the landcover are the extensive agricultural fields, parts of the Gemenc Forest and the Danube itself.
  - *Váralja DTM*: The upstream section of a small catchment in the central unit of the Eastern Mecsek Mountains, dominantly covered by oak-hornbeam forests.
  - *Vasas-Belvárd DTM*: The upper section of the Vasas-Belvárd Stream's catchment area, also covering the highest parts of the Mecsek around Zengő. The landcover is diverse, representing forested, built-in and agricultural areas as well.

Table 2. Basic characteristics of the reference DTMs with 30 m resolution.

Name	**Extent (km^2)**	**Elevation**		
		min (m)	**max (m)**	**absolute local relief (m)**
Decs DTM	20	85.79	92	*6.21*
Bátaszék DTM	15	96	236.90	*140.90*
Báta DTM	54	84.15	174.63	*90.48*
Váralja DTM	6.14	289.44	592.67	*303.24*
Vasas-Belvárd DTM	125.62	138.27	680.44	*542.17*

3.2. Physical geography of the study sites

The following sections provide a brief description about the geography of the 3rd level AOIs (*Figure 4*). These areas are of key importance by the GDEMs' quality assessment and the complex specific geomorphometric analyses.

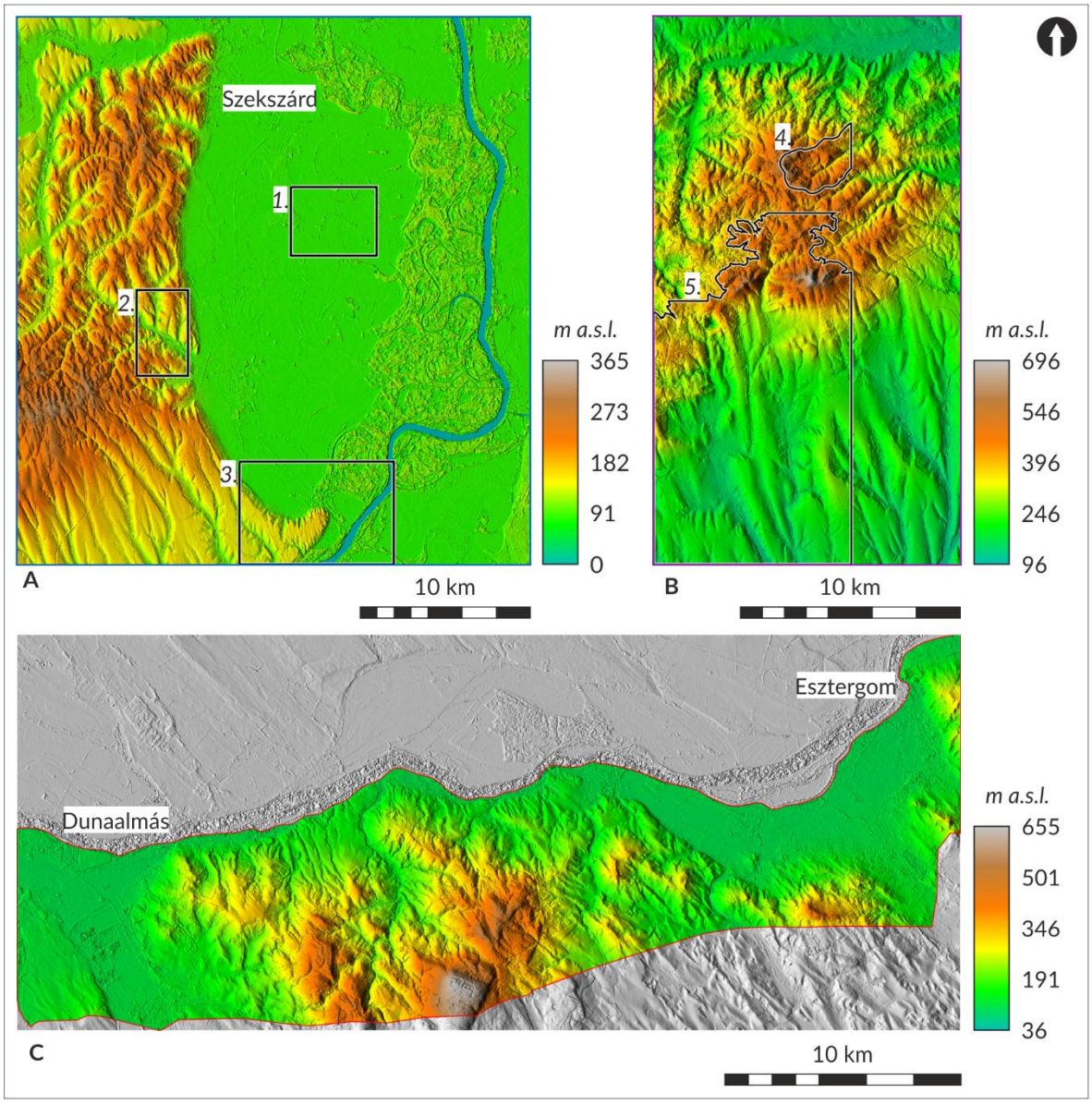

Figure 4. Topography of the 3rd level study areas shown on exaggerated, elevation coloured shaded relief maps derived from the TanDEM-X 12 m model. (A – Tolnai-Sárköz and hilly region, B – Eastern Mecsek Mountains and foreland, C – Gerecse Mountains and Danube Valley, 1 – Decs DTM, 2 – Bátaszék DTM, 3 – Báta DTM, 4 – Váralja DTM, 5 – Vasas-Belvárd DTM)

3.2.1. The Danube floodplain and the accompanying hills

The largest of the 3rd level study areas covers the southern section of the Tolnai-Sárköz floodplain region and the accompanying hilly landscape, which belongs to the Tolna-

Baranya Hills (612 000, 84 000 [SW]; 642 000, 116 000 [NE]). The main axis of the floodplain is the Danube Valley, extending primarily to the right bank areas, but also including a narrow strip of the left shore. For comparisons of the GDEMs' performance over the flat floodplain and the diverse hills, the area could be separated along the 99 m contour-line. This elevation has been selected, because possible terrace remnants of the Tolnai-Sárköz occur below this level (Pécsi, 1959).

Below Paks, the bed of the river moves away from the hills, forming the most uniform landscape in the region, the so called Tolnai-Sárköz. The floodplain narrows at Báta, but widens again near Mohács (Láng, 1957; Leél-Őssy, 1953). The height of the natural and man-made micromorphological features vary between 0.5–6 m (Lóczy & Gyenizse, 2011), though the GDEMs' horizontal and vertical resolution is not suitable to capture all these fine details. In general, the plain can be classified into a low and high floodplain level with the occurrence of flood-free terrace islands around Decs and Őcsény, the Holocene I. terrace along the edge of the hills and the Late Würm II/a terrace near Bátaszék (Leél-Őssy, 1953; Pécsi, 1959, 1967). Typical natural elements of the protected floodplain are the scroll bar and swale series ('gyűrök' and 'göröndök' in local terminology), natural levees, crevasse splays, enclosed backswamps and oxbow lakes and filled cut-off meanders of the Danube and Sárvíz (Láng, 1957; Leél-Őssy, 1953; Pécsi, 1959). Since the Holocene the area of the Tolnai-Sárköz is continuously sinking towards SE, which is evened by a stronger accumulation in the vicinity of Báta (Pataki, 1954).

The Szekszárd Hills and South-Baranya Hills show common features due to the thick loess and loess-like sediment layers covering their slopes. The chronologically dubious red clay layer at the lower section of the loess series (J. Kovács, 2003; J. Kovács et al., 2011) had a major role in the development of mass movements that characterise the heterogenous topography of the hills (Fábián et al., 2006). The Szekszárd Hills are generally higher, segmented by a complex, deeply incised valley network and the landscape is scarred by fossil and recent landslides (Ádám, 1964; Ádám, Marosi, & Szilárd, 1981; Láng, 1955). In contrast, the South-Baranya Hills region is rather characterised as a loess plateau with well-developed dolines, loess gorges incising from the steeper edges and wide, smooth interfluves between the long valleys (Leél-Őssy, 1953). The Geresdi Hills, wedged between these two regions, show significantly different geological structure and geomorphological features. The Palaeozoic granite core of the area was also covered by Pleistocene loess, however, due to the vivid relief, short and steep-sloped valleys and the erosional forms of the granite outcrops, the landscape can rather be considered as low mountainous (Fábián, Kovács,

Schweitzer, & Varga, 2005). The average elevation of the Szekszárd Hills is about 195–230 m, the South-Baranya Hills 180–210 m, while the Geresdi Hills is around 240–280 m (Ádám, 1962; Ádám et al., 1981; Ádám, Marosi, & Szilárd, 1990; Leél-Őssy, 1953).

The waters of the right bank floodplain are collected by the Sió, Szekszárd-Báta Channel and Lajvér Stream. The Danube's ice and spring floods largely impact the area, during flooding the width of the river can extend from the normal 500–600 m to 4.5 km under the confluence of the Sió at the Gemenc Forest. The nearly 9 m difference between the annual lowest and highest water levels also confirms the significance of the floods (Pécsi, 1967). A long dyke system is responsible to protect the area from the effects of the flooding river. Due to the typical floodplain sediments and remnants of the Sárvíz and Danube meanders, inland water is commonly covering extensive regions of the Sárköz (Pataki, 1954). On the contrary, the groundwater level in the permeable loess sediments of the hills sinks to a depth of 50 m (Láng, 1957; Leél-Őssy, 1953). On the floodplain oxbow lakes are typical, while over the hilly region mainly artificial lakes are to be found (rainwater reservoirs, fishing lakes).

For centuries the inhabitants of this region were able to benefit from the floods and the riparian forests, living in harmony with the river. They used the natural system of levees with crevasses and backwater channels ('fok culture') to fish (Andrásfalvy, 1973). Due to the economic changes in the 19th century, intensive river regulation and land drainage works were executed to extend the agricultural fields and reduce the flooded area (Lóczy & Gyenizse, 2011). Gemenc, Central-Europe's largest floodplain forest, is located in the regularly flooded right bank wetlands. The riparian forest consists of willow-poplar and oak-elm-ash associations. The protected area is managed by the Duna-Dráva National Park. Due to forestry there is an altering mosaic of clear-cuts and new plantations over the region, which can be noticed on the GDEMs. The natural vegetation of the hilly region has been drastically changed, agricultural fields and vineyards are characteristic, while the oak forests only remained in smaller patches (Dövényi, 2010). The settlements are sparsely located over the studied region and are mainly villages. The towns of Szekszárd, Bátaszék and Baja can be mentioned as more densely built-in areas causing elevation offset on the models.

3.2.2. The Eastern Mecsek Mountains

The second study area covers the easternmost region of the Mecsek Mountains and its southern hilly slopes between 591 000, 80 000 (SW) and 605 000, 105 000 (NE) EOV coordinates. From geomorphological point of view, the area is divided into a low mountainous and a piedmont region, the elevation ranges from approximately 139 m up to

682 m at the Zengő as the highest peak. Mecsekalja piedmont region is one of the typical Hungarian piedmont surfaces connected to a mountainous background. Landforms of the investigated area are mostly related to the syncline geological structure and paleoclimatic conditions.

Considering the geology of the study area three main units can be distinguished. The central low mountainous part is built-up by Mesozoic marine, fluvial and lacustrine sediments and crossing rift-type volcanic rocks. The Late Triassic Karolinavölgy Sandstone is the oldest formation that can be found on the western boundary of this area. It is overlain by Liassic fluvial–lacustrine–palustrine sediments with interbedded paralic coal-swamp deposits (Mecsek Coal). The opencast coal mining affected the elevation values over the study area, thus these sites must be excluded from the calculation of error statistics. The rapid subsidence of Mecsek half graben in Early and Middle Jurassic indicates increasing carbonate content and marl with limestone intercalations becomes characteristic (e.g. Hosszúhetény Marl). Siliceous and carbonate deep-sea sedimentation developed in the second half of the Jurassic. The Early Cretaceous basaltic magmatism penetrated the Jurassic layers and a basalt–tephrite–phonolite series developed (Mecsekjános Basalt). It is covered by conglomerate and sandstone (Haas, 2012). Radial horst ranges originating from the Dobogó-Zengő group dominate in this part of the study area. The relief was further intensified by a complex, dense erosional valley network due to the erodibility and impermeability of Mesozoic rocks (Ádám et al., 1981).

The second major unit consists of Miocene alluvial, marine and lacustrine sediments that encompasses the centre section of the mountain. The northern part of this unit is characterised by chiefly older (Szászvár Formation), while the southern by younger (Leitha Limestone) Miocene layers. The Mecsek was an island in the Late Miocene, and the long-life Pannonian Lake developed its sediments, which can be observed on both sides of Mecsek Mountains (Nagymarosy & Hámor, 2012). These parts of the study area are dominated by a lower hilly surface.

The third unit consists of a young aeolian loess series interbedded with paleosoils on the top of the interfluves and proluvial deposits in the dry valleys and on the slopes (Lovász, 1977; Pécsi, Gerei, Schweitzer, Scheuer, & Márton, 1988). The Mecsekalja region is characterised by fragmented, lowering hills with gentle sloping to south, while steeper slopes and deeper valleys can be found on the Mecsekhát (northern section) (Mészáros & Schweitzer, 2002).

The landscape and landform evolution of the southern foreland was described as a classical pedimentation process that formed a typical piedmont surface. According to Pécsi, M. (1963) this piedmont is generally younger than the Pannonian layers that were cut with a gentle plain, but older than Quaternary erosional valleys with fluvial terraces. On the southern slopes of Mecsek Mountains different pre-pedimentation denudation levels were observed (Fábián, Kovács, & Varga, 2001; Pécsi, 1963) which were formerly described as Middle and Late Miocene abrasion terraces or etchplains (I. P. Kovács, Bugya, Fábián, & Schweitzer, 2013). Formation of the Mecsekalja piedmont surface started after the retreat of Lake Pannon approximately 7 Ma ago (Magyar, Geary, & Müller, 1999) and continued in Early Pliocene under arid steppe climate (Sebe, Csillag, & Konrád, 2008). On Mecsekalja a dislocation zone (neotectonic fault system) has developed that resulted in a subsidence from Okorág towards Pécs, Ellend and Bóly, where basins were evolving as tectonic subsidence moved eastward. On Western Mecsekalja, Pécs basin dissected the original piedmont surface thus it changed the valley and water network considerably. Obsequent valleys sloping to north have cut deep into Upper Miocene and Pliocene beds (Fábián, Schweitzer, & Varga, 2005; Sebe et al., 2008), while subsequent valleys captured consequent streams. These river captions characterise the eastern and south-eastern part of Pécs basin and Eastern Mecsekalja is also affected by the processes. The study area consists the last remain of the original piedmont surface on the western section of Eastern Mecsekalja, however the traces of neotectonic subsidence (e.g. stream captures, valley asymmetry) have already appeared (M. Kovács, 2013).

The Völgység Stream is of regional significance, located in the northern section of the mountainous region and draining the watersheds of Várvölgy, Váralja and Öreg brooks to the Sió–Danube system. The Szellő and Varasd streams belong to the Karasica catchment area also reaching the Danube as the erosion base (Lovász, 1977). The valley network on the piedmont surface shows asymmetry as per the above-mentioned surface formation. Leaving the mountainous background, the Vasas-Belvárd and Ellend streams change their course to N-NW–S-SE on their path to the Karasica, and the tributaries align with this general orientation as well (M. Kovács, 2013). There are relatively few water bodies in the Eastern Mecsek Mountains: the Pisztrángos Lakes near Óbánya, the Püspökszentlászló Lake, the Lakes of Váralja Forest Park, the Dombay Lake near Pécsvárad and fishing lakes. Rainwater is of primary importance regarding the water supply, and the karstic water reservoirs feed several springs across the region (Dövényi, 2010; Lovász, 1977).

To date the mountainous area has only a sparse settlement network because of the large nature reserves and Natura 2000 areas of the Mecsek Mountains region. As a result of the strict protection, a wide forested area of about 145 km^2 is present in the study site, influencing the elevation values on the GDEMs. The extensive agricultural fields represent the other relevant land cover category (Dövényi, 2010).

3.2.3. The northern foreland of the Gerecse Mountains

The study area spans from the subsiding alluvial fans of the Little Hungarian Plain to the northern slopes of the Gerecse Mountains, along the Hungarian-Slovakian border, ending at the Esztergom Castle Hill before reaching the vicinity of the Danube Bend. The selected region is bounded by 589 146, 257 803 (SW) and 628 956, 274 519 (NE) EOV coordinates. The minimum elevations are found on the lower floodplain level at around 101–104 m, while the highest peak is the Nagy-Gerecse with 634 m.

The mountain is mainly built up of well karstified Triassic and Jurassic limestones, while the majority of the surface is covered by Quaternary clastic sediments and alluvial materials (Schweitzer, 1980). The geological and hydrological settings of the area offered ideal circumstances for the fluvial sedimentation and terrace formation between the subsiding and uplifting regions of the Danube Valley sections. The varying relative height of surfaces, different thickness of fluvial sediment sequences, erosional and accumulation processes are making parallelisation of the terrace system dubious; the loess and travertine deposits provide some further guidance for this task (Budai et al., 2018; Gábris & Nádor, 2007; Scheuer & Schweitzer, 1988). The mountainous background can be separated along the tectonic intermountain basins and deeply incised valleys draining to the Danube (Schweitzer, 1980). The bauxite and Eocene coal mining were significant in the region, but ended in the last decades. The excavation of limestones and marls for construction and decoration purposes continues in open-pit mines, leaving well recognisable damages on the landscape – even shown on the lower resolution GDEMs.

The mid-mountainous area is well dissected, comprises a series of slightly folded-imbricated and block-faulted horsts, while landforms of fossil and recent mass movements are also characteristic on the steep slope margins of upper Miocene unconsolidated materials and along the deepening erosional valleys (Ádám & Schweitzer, 1985; Budai et al., 2018; Schweitzer, 1980). Under 150 m the undulating surface is the terraced valley slope of the Danube, while above this level the strath terraces were formed on the upper Miocene, Oligocene, Eocene, Cretaceous and Triassic formations of the Gerecse Mountains (Pécsi

1959, Budai 2018). Where the floodplain narrows to a few km in width the terrace staircases are rising from the Danube level (Gábris & Nádor, 2007). Terrace researches identified the presence of up to 7–8 terrace levels in this marginal zone of the Transdanubian Range (Bulla, 1941; Gábris & Nádor, 2007; Kéz, 1934; Pécsi, 1959). The uppermost flat surfaces are not related to fluvial geomorphological processes, but are indeed pediment remnants (Pécsi, 2001). On the easternmost part of the Győr-Tata Terrace Region and on the western slopes of the Gerecse the Által Brook has also formed terrace surfaces (Ádám & Schweitzer, 1985; Budai et al., 2018).

The area between Almásfüzitő and Esztergom is the first section in Hungary where the Danube has a defined, antecedent valley. The 0 level of the Danube slightly drops from 103.88 m (at Komárom) to 100.92 m (at Esztergom). The region consists of several small catchments directly draining to the Danube (Által, Bikol, Piszke, Fuchs, Bajót streams). The stream network has a general S–N flow direction, though some valley sections reflect the influence of neotectonics in the Transdanubian mountainous background (Schweitzer, 1980). The karstic springs discharging from the carbonate background of the Gerecse Mountains deposited nine levels of travertine accumulations (Scheuer & Schweitzer, 1988). After the mining activities of the last century ended, the karst reservoirs slowly regenerated and karstic springs have recently resurfaced in the Transdanubian Range (Babák, Kiss, Kopecskó, Kovács, & Schweitzer, 2013).

The floodplain is typically covered by willow and softwood gallery forests, while most settlements, industrial areas and agricultural fields are located on the lower terrace levels. The central and eastern sections of the mountainous region belong to the Gerecse Protected Landscape Area since 1977, which is currently managed by the Duna-Ipoly National Park Directorate. The Gerecse is still extensively covered by forests; oak-hornbeam associations are generally dominant, while on the higher regions beech also appears. According to the geological conditions, patches of karst forests and scrub woodlands can occur over the uncovered limestones (Dövényi, 2010).

4. Data and Methods

4.1. Overview of the quasi-global DEMs

The appearance of gridded elevation data arrays in the mid-1950s and the acceleration of software development revolutionised the quantitative geomorphic analysis of the Earth's surface (Pike et al., 2009). However, the scientific community had to wait until the 1990s for the first public domain global DEMs to be released (Hastings & Dunbar, 1999). The widespread availability of topographic data triggered the increase of the user base and applications, even though resolution and quality of these datasets were at first limited (Berry, Hoogerboord, & Pinnock, 2000; Grohmann, 2016a; Miliaresis & Iliopoulou, 2004). Quality assessments performed by numerous researchers facilitated the improvement of these DEMs (from Berry, 1999 to Grohmann, 2018). Over the last decades a series of projects were dedicated to create better representations of the surface topography (*Figure 5*). The following section provides brief descriptions about the available global datasets in a chronological order, discusses DEM improvement attempts and on-going developments.

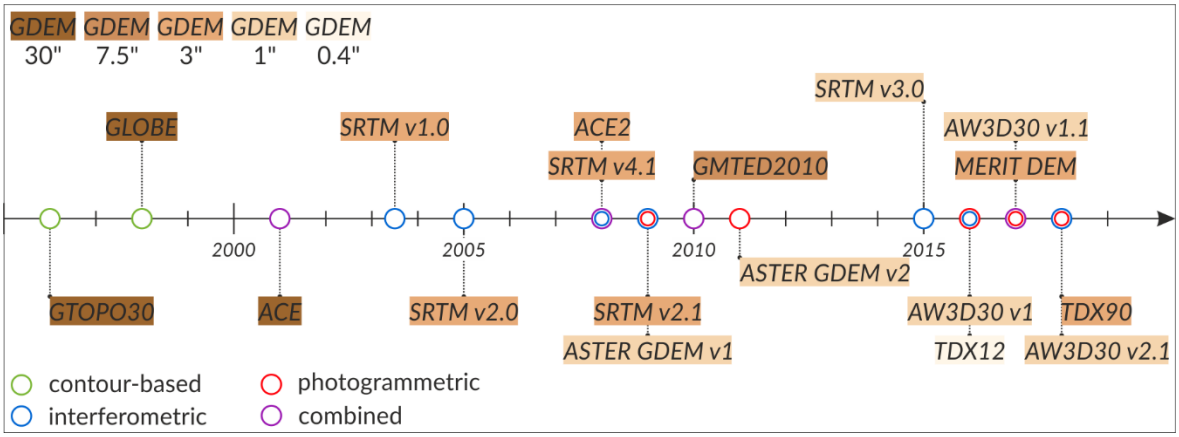

Figure 5. Timeline of the quasi-global DEM releases indicating the best available horizontal resolution of non-commercial, non-U.S. versions.

4.1.1. Before SRTM

Prior to SRTM the available elevation datasets with a quasi-global coverage had coarse horizontal spacing from 5' (~10 km) to 30" (~1 km) and were compiled from different data sources. As a result of this, accuracy varied by location, some regions were covered by lower resolution data that was up-sampled and elevation shifts occurred at the edge of tiles. A

uniform quality global DEM was, however, a prerequisite for the creation of the EGM96 geoid model. For this project NIMA and Hughes STX personnel developed the JGP95E (5') model on the bases of TUG87 (5' model of Technical University of Graz, Austria), ETOPO5 (5' model of NGDC), GGTOPO (1° model of Trent University, Canada) and TerrainBase (5' model of NGDC) (Lemoine et al., 1998).

In the literature GTOPO30 (30"), released in 1996 by USGS, is considered as the first publicly available GDEM. As there was no homogeneous data source to cover the complete land surface eight different raster and vector maps were merged. The base maps were mainly interpolated from digitized contour datasets, with two major contributors: resampled DTED Level 1 data (3" model of the U.S. DMA [later NIMA]) and Digital Chart of the World (1:1 000 000 scale cartographic data by NGA). According to the official documentation GTOPO30 had a 66 m RMSE globally (Danielson & Gesch, 2011).

Besides the model by USGS, an international research organisation was working on GLOBE GDEM, also having 30" horizontal resolution, released in 1998. In this dataset 11 different sources were merged, all of which underwent a thorough review, and also an auxiliary source map was created to identify the originating data. DMA provided DTED-1 data for this project as well, several regions were refined by using local DEMs (e.g. Italy). RMSE estimations suggested a vertical accuracy from 6 to 304 m (Danielson & Gesch, 2011). Moreover, applying the GLOBE data for watershed analysis revealed a good representation of derived river networks, which suggests that the model has been hydrologically treated (Jamieson, Sinclair, Kirstein, & Purves, 2004).

ACE GDEM was published in 2001 with 30" resolution by a UK based research group led by P.A.M. Berry (De Montfort University). The elevation model was improved by incorporating ERS-1 satellite altimeter data and avoiding the use of the DCW model (Berry, Hilton, Johnson, & Pinnock, 2000).

4.1.2. SRTM

The scientific community is referring to SRTM as a revolutionary dataset marking a milestone in remote sensing (Van Zyl, 2001) and having a significance comparable to Mercator (Massonnet & Elachi, 2006). The first spaceborne single-pass interferometric DEM covering Earth's land surface from 60° North to 56° South was realised in a collaborative effort by NASA, NGA, and German (DLR) and Italian (ASI) space agencies. Several versions of the SRTM C-band product are available worldwide, each incorporating improvements with regard to water bodies, voids, height offsets, etc. The recently released

SRTM v3.0 with 1” is available from LP DAAC repository (NASA JPL, 2014a), while the highly trusted SRTM v4.1 with 3” resolution is distributed by CGIAR-CSI (Jarvis, Reuter, Nelson, & Guevara, 2008). A DEM was also prepared from SRTM X-band data acquisitions by DLR and ASI, however, this dataset is limited to only 40% of the land surface and has not been publicly released (Rabus, Eineder, Roth, & Bamler, 2003).

The 10 days data acquisition mission was carried out by the Space Shuttle Endeavour on Flight STS-99, launched on 11 February 2000 (Farr & Kobrick, 2000; Van Zyl, 2001). The Endeavour was equipped with a C-band system (5.66 cm wavelength) provided by the U.S. party and an X-band system (3.10 cm wavelength) developed by the German party. As a result of the flight geometry (233 km nominal altitude, 57°orbital inclination) and the single-pass operation with the 60 m antenna baseline, 99.96% of the target land area was covered at least once (24% of the area at higher latitudes at least four times) with the C-band system; the SRTM raw data was 12.3 Terabytes in total (Van Zyl, 2001).

The interferograms from the data takes were composed of data from a minimum of two radar looks. A low-resolution GDEM, globally distributed ground control points from NGA and well-known ocean heights were used for mosaicking and geolocating the model (Farr et al., 2007). The SRTM interferometric product had an intrinsic resolution of about 30 m, however, in order to produce a seamless elevation model with reduced noise, the dataset was regridded using an adaptive smoothing approach. Over complex terrain less smoothing was applied, while in flat regions the resolution was degraded more by the used boxcar low-pass filter. Therefore, the effective spatial resolution of the SRTM model varies in different locations, typically between 45 to 60 m (Pierce, Kellndorf, Walker, & Barros, 2006; B. Smith & Sandwell, 2003). In the final product the elevations are reported in meters, the model is referenced to WGS84 and EGM96 (Farr et al., 2007).

The dataset created by NASA JPL is referred to as the *‘unfinished’ SRTM v1.0*, released region by region between 2003 and 2004, distributed by USGS at 1” resolution for the conterminous United States and 3” for non-U.S. territories. NGA contractors have processed the model further to improve inland water bodies, coastlines, remove outliers and fill small voids with interpolation (Slater et al., 2006). This model complied with the DTED-2 specifications and it was considered as *SRTM v2.0 ‘finished’* DEM released to the public in 2005 via USGS EROS and LP DAAC. Using the Delta Surface Fill Method (Grohman, Kroenung, & Strebeck, 2006) NGA produced a void filled model as well, but it was not publicly available. By 2009 NASA performed minor corrections on the 3” dataset and published the model as *SRTM v2.1*. Finally, in 2014 the White House announced that the

restrictions to distribute the SRTM model at 1" resolution have been lifted (NASA JPL, 2014b) and over the course of 2015 *SRTM v3.0* ('SRTM Plus', SRTMGL1) was released to the public. 'SRTM Plus' is an improved version of both the 1" and 3" DEMs, as NASA JPL have filled voids using non-commercial ASTER GDEM v2 and GMTED2010 data (Merryman Boncori, 2016; USGS, 2015). However, since 2004 CGIAR-CSI has independently published other void-filled versions of the 3" DEM. Different void-filling techniques were applied to the *SRTM v4.1* and since its release in 2008, it was widely used outside the conterminous United States (Reuter, Nelson, & Jarvis, 2007). In the frame of the *MEaSUREs* program a new version of SRTM, so-called NASADEM, is expected to be released by JPL in the near future (Buckley, 2018). For this project the original data takes will be reprocessed using state-of-the-art interferometric techniques, the absolute height bias will be reduced by using ICESat measurements and the remaining voids will be filled with refined ASTER GDEM v3 elevations (Crippen et al., 2016).

To validate the quality of the SRTM v1.0 product a global ground campaign was conducted to gather highly accurate kinematic GPS (KGPS) points. By the quality assessment the absolute vertical accuracy was found to be better than 6 m RMSE and 9 m LE90, absolute geolocation error was below 10 m. The error statistics indicated that the model exceeded the design specifications and matched the DTED-2 requirements. The largest errors were found over steep mountainous terrains and deserts. The remaining errors consisted of a systematic long wavelength component, spatially varying random noise at medium to short wavelengths and speckle noise. The 'Terrain Height Error Data' (THED) layer containing the error estimations was provided as an NGA product for internal use only (Rodríguez et al., 2006). A completely independent global validation of the 3" SRTM v2.0 was performed using 54 million ERS-1 and ENVISAT altimeter derived heights. The DEM showed good agreement with the altimeter dataset, the global statistics were estimated as 3 m mean difference with 16 m standard deviation (Berry, Garlick, & Smith, 2007).

Quality assessments focusing on the key error components or applicability in a wide variety of fields were continuously published over the last two decades (Carabajal & Harding, 2005, 2006; Hirt, 2018; Shortridge & Messina, 2011; G. Szabó, Singh, & Szabó, 2015; Wendleder, Felbier, Wessel, Huber, & Roth, 2016). The release of new GDEMs repeatedly boosted the realisation of comparative studies using SRTM as the standard (Grohmann, 2018; Józsa, Fábián, & Kovács, 2014; Purinton & Bookhagen, 2017; Satgé et al., 2016).

4.1.3. ASTER GDEM

ASTER GDEM is a 1" (30 m) horizontal resolution photogrammetric model, which was created by METI and NASA jointly and covers 99% of land surfaces (83° North to 83° South). The currently distributed model is ASTER GDEM v2 as per the project's website[4], downloadable via NASA Earthdata or LP DAAC Global Data Explorer.

GDEM is based on stereopair visible and near-infrared (VNIR) images with a 15 m pixel size, acquired in nadir and backward-looking modes by the ASTER instrument onboard the Terra satellite. The entire ASTER archive collected from 2000 to 2010 (for the current version) was used to produce over 1.52 million 30 m resolution scene models by stereo-correlation. After applying cloud and water masks, the individual DEMs were stacked and the remaining outliers were removed. The valid DEMs were averaged on a per cell basis to derive the elevation values (Fujisada, Urai, & Iwasaki, 2012). Elevations are referenced to WGS84 and EGM96 geoid. The distributed dataset also includes a quality assessment (QA) map, referred to as NUM file. Each QA cell provides information about the number of stacks (scene-based DEMs) contributing to the final elevation value or a negative number identifying the alternative dataset used to replace invalid cells (Tachikawa et al., 2011). Unlike SRTM, the ASTER GDEM is not a snapshot of the Earth's topography, therefore dynamically changing landscapes (e.g. dune fields or open-pit mines) could show a blurred average of the real topography (Guth, 2011).

ASTER GDEM v1 was released in June 2009, but contained several anomalies and artefacts and so it was considered as a 'research grade'/'experimental' dataset. From a technical point of view, the dataset met the accuracy goals of ±20 m vertical and 30 m horizontal accuracy (at 95% confidence level), yet in some regions, the representation of the topography wasn't reliable (Hengl & Reuter, 2011; Tachikawa et al., 2011).

Considering the feedback from the validation teams METI and NASA released an improved version of the model in October 2011. A stable correlation has been recognised between the RMSE and the number of stacks used to calculate the elevation value. Quality analyses performed over different regions and using different reference datasets indicated, that 10–15 stacks produced elevations with acceptable uncertainty (Carabajal 2011, Tachikawa 2011, Gesh 2012). The simplest and most effective way to reduce incorrect elevations in the ASTER GDEM v1 was to incorporate 260 000 new scenes and re-generate

[4] "ASTER Global Digital Elevation Map Announcement" 2011
https://asterweb.jpl.nasa.gov/gdem.asp

the model. In addition, georeferencing was improved and a smaller stereo-correlation kernel was used (5×5 instead of 9×9) to achieve an effective spatial resolution of 70 m, as opposed to the 120 m of the preceding model. The number of cells with two or less valid stacks were reduced to 7.5% (v1 rate was 12%) and the number of tiles with less than 1% of such bad elevations was increased to 54.3% (v1 rate was 43.5%). The RMSE of ASTER GDEM v2 was found to be 8.68 m (compared to 9.34 m for v1) in the global validation report, the differences to ICESat data showed a slight negative skewness (Carabajal, 2011; Tachikawa et al., 2011).

As the Terra satellite was continuously in operation, it was possible to acquire an additional 350 000 scenes over regions with high bad cell rate and less than 5 stacks used for elevation calculation (Urai et al., 2012). Furthermore, the water body dataset for masking inland water and coastlines was updated based on images from 13 years (Abrams, 2016). METI and NASA announced the release of ASTER GDEM v3 for 2016 and validation results were already published (Carabajal & Boy, 2016; Gesch, Oimoen, Danielson, & Meyer, 2016), however, to date the dataset is still not available for downloading at the above-mentioned official channels.

4.1.4. EU-DEM

The EU-DEM is a middle-precision, hybrid elevation model with a horizontal resolution of ~25 m (1”), first published in October 2013 covering the EEA38 countries. The dataset was created in the frame of the GMES RDA project and it is a realisation of the Copernicus program, managed by the European Commission and DG Enterprise and Industry. The model is available from the EU geospatial data repository on the website of the Copernicus project [5] as 5°×5° tiles in ETRS89-LAEA projection, the orthometric heights are given with respect to EGG08.

EU-DEM was created by an automated data fusion approach using weighted averaging to combine improved ASTER GDEM v2, 90 m SRTM and Russian topographic maps. Substantial steps of the data preparation consisted of removing ASTER GDEM elevation values where the number of scenes was less than 5, excluding cells where cloud cover caused errors or otherwise extreme outlier heights occurred, and finally filling these data voids with SRTM data. The concept of the model was to combine the advantages of both digital elevation models with additional improvements from a new hydrography dataset (EU-

[5] “EU-DEM v1.1” 2019
https://land.copernicus.eu/imagery-in-situ/eu-dem/eu-dem-v1.1?tab=download

Hydro) and NEXTMap data (Bashfield & Keim, 2011). Even though the horizontal resolution of the EU-DEM would indicate that the ASTER GDEM data is the dominant source, studies have revealed a generally stronger correlation of the model to the SRTM3 (Józsa, Fábián, & Kovács, 2014; Mouratidis & Ampatzidis, 2019). On the other hand, EU-DEM rather approximates ASTER GDEM for slopes exceeding 20°, which is related to the decreasing accuracy of SRTM over steep slopes (Mouratidis & Ampatzidis, 2019).

The first version was released in 2013 without a formal validation. This deficiency was addressed in 2014 when the official ICESat based statistical validation of the EU-DEM was published. The vertical accuracy has been found to be –0.56 m mean error and 2.9 m RMSE at 95% confidence level over the EEA38, with higher error in the Nordic countries where SRTM was not available (*EU-DEM Statistical Validation Report*, 2014). In order to gather direct feedback from the users ETC/ULS carried out a user consultation as an online survey in 2015, regarding the requirements and challenges with the DEM product (*User consultation – Requirements of European Community on DEM products*, 2015). Based on the DEM validations and the feedbacks from JRC, Eurostat and EEA experts, as well as the user community, the improved EU-DEM v.1.1 was published in April 2016. Improvement of the model was achieved by removing more than 75 000 artefacts, adjusting the absolute vertical bias using ICESat data, correcting geo-positioning issues (e.g. coastlines) and ensuring consistency of river network topology with the EU-Hydro dataset. The vertical accuracy of the upgraded model is estimated as 7 m RMSE, which complies with the contractual quality specifications (*EU-DEM Upgrade – Documentation EEA User Manual*, 2015).

4.1.5. TanDEM-X

TanDEM-X is treated as the new etalon of GDEMs with an unprecedented 12 m horizontal resolution, pole-to-pole spatial coverage, prominent horizontal and vertical accuracy and the ability to reliably depict even complex terrains (Grohmann, 2018). The mission was realised in a public-private partnership between the German Aerospace Center (DLR) and Astrium GmbH (member of the Airbus Group). The global DEM was finalised by September 2016. The dataset is available for scientific purposes with 0.4”, 1” and 3” resolutions after

submitting a research proposal to DLR[6], while the commercial WorldDEM[7] product is distributed by Airbus Defence and Space (Wessel et al., 2018). In October 2018, to comply with the EU data policies in the frame of the Copernicus Program, DLR publicly released the TanDEM-X 90 m version for scientific use ("The TanDEM-X 90 m Digital Elevation Model" 2018). The TanDEM-X product provided by DLR is not referenced to EGM96, the heights are given with respect to the WGS84-G1150 ellipsoid.

The TanDEM-X mission comprised of the twin satellites TerraSAR-X (TSX) and TanDEM-X (TDX) equipped with X-band SAR instruments, flying in a controlled helix formation at an altitude of around 500 km with typical baseline lengths of 250–500 m. Data acquisition was performed in bistatic InSAR stripmap mode. One of the satellites acted as the transmitter, while both TSX and TDX recorded the backscattered signal from the Earth's surface simultaneously. This mode enabled the dual use of the available transmitting power and essentially eliminated the temporal decorrelation and atmospheric disturbances. Data were collected over a four-year period from December 2010 to January 2015 covering all land surfaces at least twice, difficult terrains (e.g. deserts, mountain ranges) up to seven or eight times (Hueso González et al., 2012; Krieger et al., 2007; Rizzoli et al., 2017). In order to ensure the high quality of the TanDEM-X model, the acquisition strategy, processing of the first and second coverage, DEM calibration and mosaicking chain were closely monitored and consequently adapted throughout the mission (A. Gruber, Wessel, Huber, & Roth, 2012; Martone et al., 2012; Rizzoli et al., 2017; Rossi, Rodriguez Gonzalez, Fritz, Yague-Martinez, & Eineder, 2012; Wecklich et al., 2015).

The collected 350 Terabytes data volume was processed with the Integrated TanDEM-X Processor (ITP), the processing chain was specifically developed for the mission. ITP involved the steps of data takes' screening, focusing and interferometric processing, creating precalibrated and geocoded single-scene DEMs. The blocks of RawDEMs were the input for the Mosaicking and Calibration Processor (MCP), which performed a quality check of the phase unwrapping, then adjusted the DEM scenes to each other, and in the last step fused the blocks by applying an optimised logic to eliminate any residual phase unwrapping errors. To minimise height offsets and tilts ICESat GLA14 data were used as ground control points (GCPs) to reference the elevations to WGS84 (A. Gruber

[6] "TanDEM-X science service system" 2019
https://tandemx-science.dlr.de
[7] "WorldDEM(TM): The New Standard of Global Elevation Models" 2019
ttps://www.intelligence-
airbusds.com/files/pmedia/public/r49306_9_flyer_worlddem_en_january2019.pdf

et al., 2012; Rizzoli et al., 2017; Rossi et al., 2012; Zink & Moreira, 2015). Each distributed product contains information layers regarding the remaining height errors and applied water and shadow masks (Wessel, 2018).

TanDEM-X relative height errors correspond to a random noise, which resulted from lower interferometric coherence. Despite the efforts of multiple acquisitions and reprocessing by ITP, higher noise remains over slopes steeper than 20% or regions with dense vegetation (Rizzoli 2012, Rizzoli 2017). Official absolute vertical accuracy assessments were based on ICESat data excluded from the calibration, three million globally distributed kinematic GPS measurements and high-resolution DEMs from South Africa, Germany and Japan. The absolute global height accuracy was found to be 3.49 m LE90 compared to ICESat points and 1.4 m RMSE was reported for KGPS comparisons. The spatial coverage is also outstanding, from the total 19 389 1°×1° geocells only 0.107% contains voids (Wecklich 2018, Wessel 2018, Rizzoli 2017).

4.1.6. AW3D30

In May 2016 a new stereoscopic GDEM was published by JAXA with an unprecedented spatial resolution of 5 m (0.15”), covering the land surfaces approximately between 83° North to 82° South (Takaku et al., 2014). The high-resolution model is available for commercial users, however, JAXA has prepared a 30 m (1”) resolution mesh as well for scientific purposes, distributed free of charge via the project website[8].

Data was acquired by the PRISM optical instrument onboard ALOS satellite, which operated between January 2006 to May 2011 and produced a repository of 3 million scenes. The panchromatic radiometers obtained triplet stereoscopic images with 2.5 m ground resolution in nadir- (NDR), forward- (FWD), and backward- (BWD) views. The worldwide topographic data was prepared by automated stack processing of the multi-temporal scenes: tie-points are generated, the images are orthorectified, image matching is performed for height-calculation, then based on statistical classification outlier areas covered by cloud, snow or water are masked. The vertical shift of the individual DEMs is corrected based on existing global reference data (SRTM or ICESat), the scenes are then mosaicked to 1°×1° tiles, inland water surface heights are interpolated and the final product is quality checked based on auxiliary elevation data (SRTM or ASTER GDEM) to ensure no large matching errors, missing masks, systematic errors are present (Takaku et al., 2014). The height

[8] “ALOS Global Digital Surface Model "ALOS World 3D - 30m (AW3D30)” 2018 https://www.eorc.jaxa.jp/ALOS/en/aw3d30/

readings are referenced to WGS84 and EGM96. The corresponding information on masks, number of DEM-scene files, quality assurance and metadata on image geometry are also contained in the distributed data (Takaku, Tadono, Tsutsui, & Ichikawa, 2016).

The lower resolution dataset for public use was generated by applying two different resampling methods, an averaging and a median filter with a 7×7 cells kernel on the original AW3D dataset. Averaging on the 49 pixels reduces the effective spatial resolution, while keeping the 25th height value better reserves the texture of the terrain. A more complex resampling method (e.g. nearest neighbour algorithm) could not be used as it posed a conflict with the commercial purposes (Tadono et al., 2016).

Evaluation of the DEM tiles by JAXA revealed voids due to lack of suitable scenes related to unpreferable weather conditions (clouds) or insufficient ground textures (snow, water cover). Statistical analysis of the vertical accuracy was performed on the basis of ICESat data and independent GCPs and LiDAR datasets. Mean error compared to ICESat is around –0.08 m, the RMSE is 3.26 m. The GCPs and LiDAR datasets are localised and cover small regions, still, the findings align with the above mentioned error statistics (–0.30 m mean error, 3.28 m RMSE for GPS tracks, 1.81 m mean error, 2.70 m RMSE for LiDAR DEM) (Takaku et al., 2016).

Since the first release four new versions of AW3D30 were published. Voids between 60° North to 60° South have been filled with existing DEMs using the 'Delta Surface Fill' method (Grohman et al., 2006), water mask was enhanced, striping errors were corrected, absolute vertical offset was further reduced. JAXA also decided to only publish the 2.1 version as the average resampling product (Takaku & Tadono, 2017). The latest version 2.2 was just released in April 2019, therefore it has not been analysed in the current study.

4.1.7. MERIT DEM

MERIT DEM is a recent enhancement of quasi-global elevation datasets released to the public in 2017 by an international research team led by D. Yamazaki (Yamazaki et al., 2017). The elevation data is available with 3" horizontal resolution, referenced to WGS84 and EGM96, covers the land surface between 90° North to 60° South and distributed from the project website[9].

The elevation dataset is mainly based on SRTM3 v2.1 and AW3D30 v1, while auxiliary data sources from the Viewfinder Panoramas repository (VFP-DEM) were used to fill

[9] "MERIT DEM: Multi-Error-Removed Improved-Terrain DEM" 2018 http://hydro.iis.u-tokyo.ac.jp/~yamadai/MERIT_DEM/

remaining voids. The major error components removed from the dataset were stripe noise, absolute bias in reference to ICESat data, tree height bias and speckle noise. It quickly gained interest among terrain analysts, as the model is claimed to reflect the bare surface of the Earth and has a more reliable representation of major floodplains (Amatulli et al., 2018; Hirt, 2018; Iwahashi, Nakano, & Yamazaki, 2018; Moudrý et al., 2018). Built-in areas and so canopy in urban regions were not treated, thus in some regions, the model should be considered as a mixture of surface and terrain model (Hirt, 2018).

Visual inspection of the dataset and comparison to other DEMs revealed that MERIT DEM shows better agreement to the real topography, especially the hill-valley structures and lowland river networks are more recognisable. The research team has performed quality assessment of the corrected model based on ICESat data and UK airborne LiDAR DEM as well, which statistically confirmed the improvement of the elevation model. After the correction the number of cells with 2 m or better vertical accuracy increased by 19% (from 39% to 58%), the LE90 was reduced from 14 m to 12 m (Yamazaki et al., 2017).

4.1.8. Other quasi-global DEM projects

As all available datasets have limitations (spatial coverage, horizontal resolution, etc.) and deficiencies (e.g. voids, outliers, noise, offsets of vegetation and built objects) there have been several attempts to enhance the base models to create DEMs best fitting the application at hand. The offset due to tree coverage is considered among the major factors hindering the applicability of GDEMs for tasks such as flood inundation modelling or soil mapping. Different approaches were developed in order to remove the canopy heights from the models with the help of auxiliary datasets (Gallant & Read, 2016; Kulp & Strauss, 2018; O'Loughlin, Paiva, Durand, Alsdorf, & Bates, 2016; Seres & Dobos, 2010; Ungvári, 2015b; Zhao et al., 2018). Further efforts were made to eliminate the characteristic speckle noise from the radar-based DEMs implementing adaptive smoothing techniques capable of preserving the edges in the real topography (Gallant, 2011; Stevenson, Sun, & Mitchell, 2010). In addition, over the last decades, several research groups focused on deriving improved elevation datasets by fusing SRTM and ASTER GDEM versions (Kääb, 2005; Karkee, Steward, & Aziz, 2008; Pham, Marshall, Johnson, & Sharma, 2018; Robinson et al., 2014; Wang, Holland, & Gudmundsson, 2018; Yue et al., 2017).

It is also worth mentioning the Viewfinder Panoramas project (de Ferranti, 2014) operated by J. de Ferranti, which originally predated SRTM and aimed at collecting reliable elevation data from variable sources with better resolution than GTOPO30. The current

repository is mainly based on SRTM, but the gathered auxiliary datasets were used to improve that model as well.

Coarser resolution DEMs also stayed in the focus of scientific interest, as global scale simulations (e.g. numeric modelling in climatology) or continental, sub-continental level geological and geomorphological mapping projects still require reliable topographic datasets (Grohmann, 2016a). In 2008 the research group at De Montfort University released ACE2, an SRTM based model corrected with radar altimetry data, available at 5', 30", 9" and 3" resolutions (Berry, Smith, & Benveniste, 2010). USGS and NGA published GMTED2010 as the successor of GLOBE and GTOPO30 models with 30", 15" and 7.5" resolutions (Danielson & Gesch, 2011).

Lastly, Global Relief Models combine topographic and bathymetric data and constitute a further group of elevation datasets. The currently available ETOPO1 (2008) is the product of NGDC with 1' resolution (Amante & Eakins, 2009), SRTM30_PLUS with 30" resolution was prepared by the Scripps Institution of Oceanography (Becker et al., 2009), while Earth2014 with 1' resolution was developed by an international research team (Hirt & Rexer, 2015). Planetary DEMs are not in the focus of the current study, and thus not presented here.

4.1.9. DEMs subject to analysis

The quality assessment is intended to focus on a variety of GDEMs with different cell size, acquisition time and technique, DEM processing method and degree of post-processing. Several models were excluded from the quality assessment based on previous experiences of the author and the thorough review of the relevant literature. Furthermore, it has been decided prior to the general review of the newest GDEMs to use the SRTM1 model – as the most trusted data source according to the numerous plausibility studies – for the specific geomorphometric analyses over the Hungarian study sites. The 30 m horizontal resolution, is considered reasonable to delineate the landform elements and physiographic units over the whole country, and it also fits the operational scale requirements of the terrace-remnant extraction. The following models are chosen for further analysis:

- *TanDEM-X 0.4"* (referred to as TDX12): quality assessment;
- *SRTM v3.0* (referred to as SRTM1): quality assessment, relative accuracy enhancement, specific geomorphometric mapping;
- *AW3D30 v2.1* (referred to as AW3D30): quality assessment;
- *MERIT DEM*: quality assessment.

The elevation models with a horizontal resolution over 3" were excluded from the analysis, as such low-resolution data would not be suitable for mapping the landforms that this study focuses on. SRTM3 has been analysed previously by the author (Józsa, 2015a; Józsa, Fábián, & Kovács, 2014), the model is sufficient for geomorphometric purposes, however, since 2015 the same dataset is available with better cell size (NASA JPL, 2014b). TDX90 was not included in the followings, because it is not a new product, it has been created by averaging TDX12 elevation values. It is rather advised to evaluate the original data because averaging is also smoothing the model, which hinders the understanding of error characteristics. The ASTER GDEM versions have been analysed in several studies in the past, concluding that due to the bumpy texture of the surface and the nearly ~70 m effective resolution the model is not an appealing candidate for digital terrain analysis (Józsa, 2015a; Pipaud, Loibl, & Lehmkuhl, 2015; G. Szabó, Mecser, et al., 2015; G. Szabó, Singh, et al., 2015; Tachikawa et al., 2011). The applicability of ASTER GDEM v2 in geomorphological mapping over Southern Transdanubia was thoroughly evaluated by the author, however, the results were not satisfactory even after applying a correction process (Józsa, 2014). EU-DEM v1 has also been tested by the author for landform delineation in the Eastern Mecsek Mountains with moderate success. Even though the official quality assessment report of v1.1 suggests a significant improvement in error statistics, as the model is a combination of ASTER GDEM v2 and SRTM3 and is only available over the EEA38 countries it has rather been excluded from further analysis (*EU-DEM Upgrade – Documentation EEA User Manual*, 2015).

TDX12 is currently described as the best horizontal and vertical resolution model available with exceptional quality (Rizzoli et al., 2017; Wecklich, Gonzalez, & Rizzoli, 2018; Wessel et al., 2018). However, there has been only a limited number of applications published so far, most of the available studies were conducted by DLR and subcontractors. The TanDEM-X 12 m resolution model has been provided by DLR in the frame of a research proposal (DEM_OTHER0625). As a result of the unfortunate tiling of the dataset it was not possible to acquire TDX12 for the whole country, also due to data sensitivity issues over Bosnia and Herzegovina, the tile covering the southernmost parts of Transdanubia is missing. Considering the high spatial resolution and the preliminary quality assessments the AW3D30 also marks a milestone in global DEM production, and thus receives increasing scientific interest (Boulton & Stokes, 2018; Grohmann, 2018). The model is included in the quality assessment because to date there are no published validations over Hungary despite the promising feedbacks from other regions. The SRTM1 was considered as the best

candidate for the relative accuracy enhancement: this is the only model that is representing a snapshot of the Earth's topography – even if 20 years ago – instead of elevation values merged over longer periods; its cell size is matching the available water mask and tree cover datasets; the corrected data could be further distributed for scientific purposes. Besides the quality assessment and error correction, SRTM1 was selected for the application in the geomorphometric mapping projects because of its well-established quality amongst mid-resolution, quasi-global elevation models and the prior positive experiences of the author using this DEM (Józsa, 2015a, 2016, 2017d). Despite its 3" horizontal resolution it has been also decided to review the MERIT DEM, primarily to explore the effects of the error correction process on the model's quality and applicability in geomorphological mapping. The recent feedbacks on the model are ambiguous (Amatulli et al., 2018; Hirt, 2018), therefore further analyses over different terrain types are also beneficial for the scientific community.

4.2. Auxiliary datasets

4.2.1. Reference DTMs

The characteristics and the spatial arrangement of DEM errors have also been explored by raster-to-raster comparisons involving independent reference DTMs. The reference models were generated by interpolation of contour lines digitised from 1:10 000 EOV topographic maps, thus these models represent the elevations of the bare surface and their input data or creation process is not related to the quasi-global DEMs.

The contour lines for the Decs, Bátaszék and Báta DTMs were digitised by the author herself, the boundaries of these regions are following the borders of the topographic map sheets. The Váralja and Vasas-Belvárd models were generated for separate research projects of the department, these partially follow the natural borders of the studied watersheds. The contour spacing was changing according to the topography; over plains it was 1 m, while on the hilly and low mountainous regions 2.5 m or 5 m. The elevation of mapped peaks has also been digitised where available. The digitisation was executed in one of the older QGIS versions (1.8.0, 2.2.0) as per user preferences. Before the interpolation all vector datasets were thoroughly inspected to find topological inconsistencies or incorrect height attributes (e.g. displaying the contour lines with a DEM colour scheme, creating shaded relief maps of preliminary interpolations). During the verification of the digitised lines special attention was payed to inspect how precisely the lines fit to the contours of the topographic map. 0.5 mm inaccuracy would mean 5 m misalignment on the 1:10 000 scale (Goodchild, 2001).

It was also necessary to better distribute the vertices along the contour lines and modify the contours at steep areas (e.g. high bluff of Danube at Báta) so the interpolation method could use the representative elevation values for the selected cell size (Józsa, Fábián, Varga, & Varga, 2014).

The actual interpolation of the reference DTMs was preceded by thorough literature review and numerous attempts to compare the methods against each other (Mitas & Mitasova, 2005; Neteler & Mitasova, 2007; S. Szabó, Szabó, Szabó, & Németh, 2005; Telbisz, Székely, et al., 2013). Based on the available descriptions and feedbacks the chosen approach was the *Triangulation* method implemented in SAGA GIS 2.1.0, which eventually provides a raster output (Cimmery, 2010; Conrad et al., 2015). As IDW, nearest neighbour or natural neighbour interpolations this method is also an exact interpolation, the derived surface passes through the data points. The method is fast and easy to perform, but due to its design it could create flat surfaces within closed contour lines (Telbisz, Székely, et al., 2013). The reference DTMs were originally created with 10 m horizontal resolution and resampled to larger cell sizes to match the DEMs analysed.

It is reasonable to presume, that the reference data is a satisfactory representation of the land surface, however, one cannot have a fully accurate description of the topography, the derived surface models are always subject to unknown errors (Detrekői & Szabó, 2007). To assess the quality of independent models the reference dataset should be at least three times more accurate than the evaluated DEM (Blak, 2007). As mentioned above, from the analysed quasi-global DEMs the TanDEM-X and AW3D30 models have an exceptionally high vertical and horizontal accuracy, but official evaluations were based mostly on bare surfaces. Based on independent validations of the EOV topographic maps, the mean of height differences vary between ±0.47 and ±1.00 m depending on the contour spacing (Winkler, 2003). Further quality assessment of the reference models was performed by exaggerated 2.5D displays, shaded relief maps and statistical analysis of the elevation histograms (Hutchinson & Gallant, 2000; Wise, 1998). Though the general appearance of the DTMs is slightly rough as per the interpolation method, even the steeper slopes are represented reasonably well (e.g. Báta DTM). The elevation histograms only show significant peaks in case of the Decs DTM. This model represents a very smooth surface on the floodplain, there were several closed contours, thus the flat triangles are appearing on the histogram as spikes at the contour-lines' values. Taking into account the characteristics of the analysed DEMS, the contour-based reference DTMs are considered appropriate for the validation.

4.2.2. Land cover map, water body mask and tree canopy cover data

The Corine Land Cover 2006 dataset was selected to investigate the land cover properties over the study areas for the quality assessment. As previously clarified only the SRTM1 model is representing a snapshot of the Earth's surface, the other models are based on years of data acquisition. The 2006 dataset is a compromise from a temporal aspect, however, as the large forested regions are under national protection drastic changes were not anticipated. The dataset is publicly distributed by the EEA[10] and has a unified thematic content and nomenclature for the territory of the European Union. CLC2006 was created by refreshing the CLC2000 dataset with the changes detected via the interpretation of SPOT 4, SPOT 5 and IRS P6 satellite imagery. The dataset has 1:100 000 scale, which means that the smallest mapped entities cover 25 ha and minimum 100 m in width (water bodies, roads). According to the technical specification and the published quality assessment the geometric precision of the data is better than 100 m, while the thematic content is in 85% accurate. Another important feature of the database is that the mapped forest patches represent vegetation taller than 5 m with at least 30% closed canopy (Büttner, Kosztra, Maucha, & Pataki, 2012).

The CLC2006 watercourse (511) and water body (512) categories did not provide a complete coverage of the inland water surfaces. Despite the much finer spatial resolution, the TanDEM-X Water Indication Mask was also not suitable for this purpose. The information layer is not an actual Boolean map of inland water bodies per se because the cell values reflect the number of acquisitions detecting water based on the SAR amplitude and coherence information (Wessel, 2018). In most GDEM creation or quality assessment projects the commonly selected water mask is the SRTM Water Body Data with a 30 m horizontal resolution. This dataset was created in cooperation by NASA and NGA and it is provided as a vector layer ("SRTM Water Body Database v2.1" 2003). During the post-processing of SRTM only lakes greater than 600 m in length and rivers wider than 183 m were treated. Cells of rivers were replaced by a 'water surface' gradually decreasing towards the estuary (Slater et al., 2006). In the present study this water surface mask was extended by smaller lakes and reservoirs derived from the OpenStreetMap database ("OpenStreetMap contributors" 2015) and merged with the water surfaces from the CLC2006 map.

Considering that the GDEMs are all rather surface models, the density of forests over a cell is expected to be positively associated with the magnitude of DEM errors. To perform

[10] "Corine Land Cover 2006 seamless vector data" 2012
https://www.eea.europa.eu/data-and-maps/data/clc-2006-vector-data-version-2

the regression analysis the global forest cover data by the University of Maryland has been applied ("Global Forest Change 2000-2014 v1.2" 2015). The forest cover percentage for vegetation taller than 5 m was estimated by time-series analysis of Landsat multispectral imagery. The tree cover map is distributed with a 0.9" horizontal resolution, which yields a better fit to the GDEMs, than the CLC2006 dataset (Hansen et al., 2013). The subset of the data representing the tree cover over Hungary in 2000 is shown in *Figure 6*.

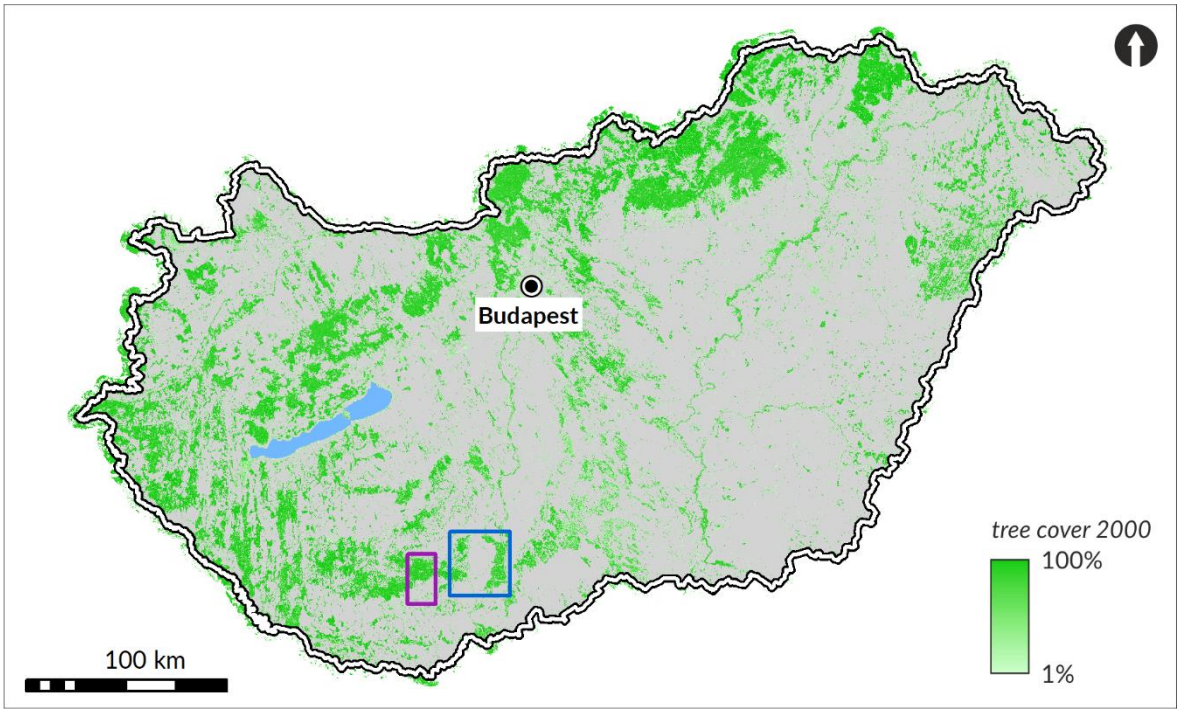

Figure 6. Tree canopy cover over Hungary in the year 2000.

4.3. Applied software

Managing the numerous input maps and digital elevation datasets, executing the quality assessment process, performing the geomorphometric analyses and preparing visually pleasing and meaningful output maps required the use of a universal, modern, platform independent GIS software. As the aims of the presented research was to provide new tools for the scientific community choosing *Free and Open Source Software* (*FOSS*) was evident.

The backbone of the current study is *GRASS GIS 7.4.0* ("GRASS Development Team" 2017; Hofierka, Mitasova, & Neteler, 2009) that was used to handle the large elevation models, while *R 3.5* ("R Core Team" 2019) was used as an intermediate analytical environment to perform the statistical analysis and create explanatory graphs. To prepare and test the R codes *RStudio 1.1.453* ("RStudio Team" 2016) was preferred as the integrated

development environment. For the quality assessment process RStudio was started from the GRASS GIS session for an easy access to the raster and vector datasets.

The self-developed r.tg.geom and r.terrace.geom tools are implemented as *Python 2.7.10* ("Python Software Foundation" 2013) script tools, which can be installed as extensions into GRASS GIS from GitHub (Józsa, 2017a, 2017b). Both tools are building on the capabilities of R, but the user is only interacting with the GRASS GIS GUI. In this scenario the R script is executed within GRASS GIS in batch mode. However, once the connection to R is initialised the system is able to execute the R commands and still has access to the GRASS GIS tools via the rgrass7 package (Bivand, 2018). With this interdependency it was possible to exploit the efficiency of both software.

Dependencies of the tools are the following:

- *GRASS GIS*: r.geomorphon extension (Jasiewicz & Stepinski, 2016),
- *Python*: os, platform, sys, subprocess, csv, grass.script modules,
- *R*: rgrass7, ggplot2 (Wickham, 2016), plyr (Wickham, 2011), data.table (Dowle, 2019) packages.

4.4. Quality assessment process

4.4.1. Key components of DEM errors

Before presenting the methods used to validate the accuracy and performance of the GDEMs it is first necessary to clarify the types of errors that can affect these products. Furthermore, it is worth highlighting that any attempt for the 2.5D representation of the real terrain introduces ambiguities, and leads to uncertainties when trying to use the model outside the operational scale for which it is suitable (Hengl, 2006).

The followings will focus on the spaceborne elevation models, but the user must keep in mind that different error types are typical according to the data source and DEM generation processes (Reuter et al., 2009). The key error components can be roughly grouped into three categories: (1) artefacts, blunders or gross errors; (2) systematic errors; (3) random errors or noise (Wise, 2000).

The most prominent errors are not compatible with the local topography (spurious sinks, spikes, voids, ghost lines, etc.), and are easily detected by checking on the basic elevation statistics (minimum and maximum) or by visual interpretation of shaded relief maps, first or second order DEM derivatives (Hutchinson & Gallant, 2000). These errors might occur due

to equipment failures, cloud anomalies, misregistration between measurements (Hebeler & Purves, 2009).

Systematic errors show either a common trend or clear dependency, they reflect a general bias, repetitive forms (e.g. striping) or non-terrain features (Shortridge, 2006). These errors are not clearly erroneous, therefore sophisticated statistical techniques are required to explore them, however, once the underlying causes are revealed it is also possible to reduce these errors (Hebeler & Purves, 2009; Reuter et al., 2009). Foreshortening and shadowing due to high-relief terrain; insufficient backscattering from snow, ice, water or sand surfaces; phase unwrapping errors in case of the radar technology; striping related to orbital adjustments; elevation steps at scene or track boundaries can be mentioned in this group (Farr et al., 2007; Rizzoli et al., 2017; Tachikawa et al., 2011). Even the vegetation offset and elevation of the man-made objects represented on these surface models belong to the systematic errors (Hengl, Gruber, & Shrestha, 2004; Reuter et al., 2009).

Noise is typical for the remote sensing-based DEMs, it shows no trend, but it is hiding the true terrain roughness. Random errors can originate from a variety of sources like the data acquiring process, DEM generation itself or the properties of the surface being measured (Fisher & Tate, 2006). This characteristic can be noticed by visual inspection or DEM derivatives as well (Reuter et al., 2009).

As an additional aspect of the quality assessment the accuracy goals, determined in the DEM specifications, should be also clarified. The SRTM1 model and accordingly other mid-resolution models meet the requirements of the DTED-2 specifications, while the TanDEM-X model follows the HRTI-3 standards (*Table 3*).

Table 3. Comparison of DTED-2 and HRTI-3 DEM specifications.
(Adopted from Krieger et al. (2007))

Requirement	**Specification**	**DTED-2**	**HRTI-3**
Relative Vertical Accuracy	90% linear point-to-point error over a 1×1° cell	12 m (slope < 20%) 15 m (slope > 20%)	2 m (slope < 20%) 4 m (slope > 20%)
Absolute Vertical Accuracy	90% linear error	18 m	10 m
Relative Horizontal Accuracy	90% circular error	15 m	3 m
Horizontal Accuracy	90% circular error	23 m	10 m
Spatial Resolution	independent cells	30 m (1” at the Equator)	12 m (0.4” at the Equator)

4.4.2. Preparing the datasets

The selected GDEMs were downloaded from the distributors mentioned in the detailed description in *GTiff* format. First these maps were imported to separate GRASS GIS *mapsets* and *locations*, which were created from the information incorporated in the georeferenced data files. This intermediate step provided the opportunity to review the original files before any projection and resolution transformation. For the quality assessment all GDEMs were projected to EOV and up-sampled or down-sampled to 30 m as the common resolution. As noted previously the models and reference DTMs were created using different projections and geoids, which can lead to deviation in the elevation values. However, based on the literature HD72 datum is fitting to the EGM96 well enough considering the reported vertical accuracy of the GDEMs (Winkler, Iván, Kay, Spruyt, & Zielinski, 2006). In case of the TDX12 model the elevations correspond to ellipsoidal heights, thus first it had to be referenced to the EGM96 geoid. The F477 program provided by NGA ("NGA/NASA EGM96" 2013) was used to interpolate the geoid heights necessary to convert the TDX12 model to orthometric heights. Reprojection and resampling was executed in one step with the r.proj tool (Schroeder, Hulden, & Kelly, 2016) by bicubic method. Bicubic interpolation is a commonly accepted option to resample continuous surfaces such as DEMs (Grohmann, 2018), however, it must be noted that this processing step lead to new floating point elevation values. The reference DTMs interpolated in SAGA GIS were imported similarly to GRASS GIS. The changes in the univariate statistics of the models are presented in *Appendix 2*.

The water body mask and tree cover map matched the resolution for the quality assessment, so those were only re-projected accordingly. The CLC2006 map was downloaded as a seamless vector dataset, and for further analysis it had to be re-projected with the v.proj tool (Kosinovsky, Holko, & Glenn, 2016) and converted to a 30 m resolution raster map with v.to.rast tool (Shapiro, Blazek, Hofierka, Mitasova, & Douglas, 2017). There are 19 different land cover types occurring over the 3rd level study areas, but for the feasibility of the analysis these were aggregated to six main groups (built-in, bare surface, low vegetation, forest, water surface, mining site). The forests are expected to cause bias between the GDEMs and reference DTMs, while the bare surfaces can be considered as ground truth values on the quasi-global models as well. *Appendix 3* describes the original land cover classes, while *Table 4* presents the distribution of the aggregated categories.

Table 4. Distribution of the aggregated CLC2006 categories over the 3rd level study areas used for quality assessment.

	Category (%)					
	built-in	bare surface	low vegetation	forest	water surface	mining site
EM study area	4.52	44.23	8.98	41.39	0.30	0.58
TS study area	3.49	55.60	10.58	27.10	3.19	0.04

Lastly, an important pre-processing step was to exclude the cells over water bodies and open-pit mining sites, as in these locations the elevation values are uncertain in case of the photogrammetric and radar-based models as well. This could be easily performed using raster algebra and the previously described auxiliary datasets.

4.4.3. Exploring the horizontal and vertical accuracy of GDEMs

Approximating the effective resolution

The official GDEM validations (Farr et al., 2007; Tachikawa et al., 2011) and independent quality assessment studies (Guth, 2006, 2010; Józsa, Fábián, & Kovács, 2014; Pierce et al., 2006; B. Smith & Sandwell, 2003) have revealed, that the nominal horizontal spacing of these elevation datasets is better, than their effective resolution. In geomorphometric analyses it is important to know the level of topography detail that is captured by the model, which is rather related to the effective resolution instead of the cell size selected to distribute the given elevation dataset (Boulton & Stokes, 2018; Grohmann, 2018; Pipaud et al., 2015). A fairly simple approach to estimate the effective resolution of the GDEMs is to find the cell size with comparable average slope values calculated from down-sampled reference DTMs (Guth, 2010). The reference DTMs were resampled with bicubic method from 10 to 110 m cell sizes at 10 m increments, and the slope map was calculated from all the models separately. The presence of noise and the edges around natural and man-made objects lead to an overestimation of the average slope over smooth topography (Guth, 2006), thus the calculations were based on the hilly and low mountainous study sites only.

Coregistration of the elevation models

Cell-by-cell comparison of the different elevation models is an important part of the GDEMs' quality assessment. The effect of horizontal shift between the models cannot be neglected especially in heterogenous terrain because the displacement can cause large, slope

and aspect dependent errors as shown in *Figure 7* (Nuth & Kääb, 2011; Van Niel, McVicar, Li, Gallant, & Yang, 2008).

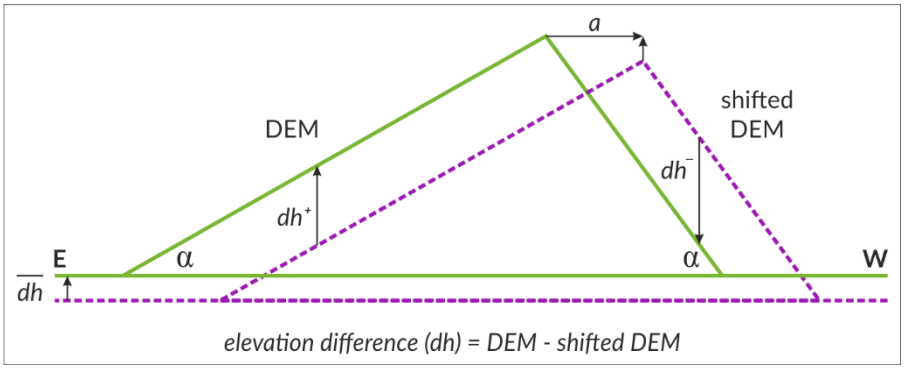

Figure 7. 2D scheme of elevation differences resulting from misregistration. (Based on Nuth & Kääb, 2011)

The misregistration of the models can be easily revealed by comparing the location of the prominent peaks in a region. The horizontal bias could also be explored by iteratively shifting one DEM to another and determining a displacement vector from the arrangement with the strongest correlation (Reuter, Strobl, & Mehl, 2011). According to the model specifications no significant shifts were expected, so the simpler method of visually investigating the displacement of peaks was sufficient. In GRASS GIS the raster data structure allows to relocate the maps by manipulating the bounding box coordinates. As the horizontal bias is most apparent in case of well-dissected terrain, the analysis was performed on the Váralja DTM, the Bátaszék DTM and the mountainous region of the Vasas-Belvárd DTM. The improvements were monitored by subtracting the reference DTMs from the shifted models and looking for the characteristic patterns on the valley slopes.

Visual quality assessment

Visual inspection with different approaches is an easy and fast way to obtain preliminary information about the quality of DEMs and the scale of captured topographic details. A common option is to prepare shaded relief maps with different illumination or 2.5D displays with exaggerating on the z-scale to highlight different types of terrain features (Neteler & Mitasova, 2007). The characteristic of the shaded relief map is defined by the altitude and azimuth of the light source, and while unreal settings can reveal specific details (e.g. fault lines), from a geomorphological point it is advised to avoid the inversion of the topography on the displayed image (Oguchi, 2003). The study area was investigated with classic greyscale shaded relief maps created with r.relief tool setting the azimuth as western direction (270°), the altitude as 25° and exaggerating the elevation values by a factor of four

(Westervelt & Metz, 2018). With the r.shade tool it was also possible to overlay the elevation-coloured DEM on the shaded relief map (Bowman & Petras, 2015).

To reveal the spatial distribution and degree of positive and negative elevation differences between two datasets it is necessary to subtract them from each other, eventually deriving a so-called DEM of Differences (DoD). This can also be the base for the calculation of the descriptive error statistics. Creating a DoD is a simple raster operation in the r.mapcalc tool (Shapiro & Clements, 2018). In the present study the reference DTMs are always the one being subtracted from the GDEMs, and thus the positive errors indicate cells where the heights on the GDEMs are higher (e.g. forest patches), while negative values reflect elevations below the reference surface. To have a good visual overview of the different error types a blue-white-red colour scale has been applied to the DoDs, where the more vibrant colours indicate significant differences. Furthermore, DoDs are created from the GDEMs as well to explore systematic errors between the models, general under- or overestimation of the represented surfaces and possible changes in the land cover, which is especially interesting in case of the forests.

Cross-sections are not only beneficial for geomorphological purposes (e.g. terraces, channel knickpoints), but when sampling different DEMs at the same locations they are useful in identifying horizontal displacement or systematic errors of the input models (Grohmann, 2018; Van Niel et al., 2008). In GRASS GIS the interactive *wxGUI profile tool* has been used to create cross-sections on multiple DEMs along various polylines drawn on the screen (Landa et al., 2017).

Descriptive statistics, error metrics, correlation and regression analysis

The comparative assessment of the selected GDEM versions (TDX12, SRTM1, AW3D30, MERIT DEM) with five reference DTMs over three different relief types (floodplain, hilly, low mountainous) and land cover categories (bare surfaces and forest patches as most important) produces an enormous amount of statistical information to be interpreted. The following section outlines the workflow for this process.

To explore the general topography captured by the GDEMs, elevation histograms and the descriptive statistics (minimum, maximum, mean, median and standard deviation) were determined for the 3rd level study areas used in the comparison. These can reveal outliers based on the preliminary knowledge of the terrain. In the preparation steps the water surfaces and open-pit mines were already excluded, as the elevation value of those cells is unreliable.

Additionally, correlations using the Spearman method were calculated to further explore how similar the three main relief types are represented by the GDEMs.

The detailed vertical accuracy assessment was performed using the DoDs created by subtracting the reference DTMs from the GDEMs ($h_{GDEM} - h_{ref}$). The distribution, skewness and kurtosis of the DEM errors were interpreted and visualised on histograms in order to see if the data is significantly different from the normal distribution. Besides deriving the overall error metrics, the calculations were also performed separately for the bare surfaces and the forested regions. The following error statistics were derived: Mean Error (*Equation 1*), Root Mean Square Error (*Equation 2*), Error Standard Deviation (*Equation 3*), Linear Error at 90% confidence level (*Equation 4*).

$$ME = \frac{1}{n}\sum_1^n \left[h_{GDEM} - h_{ref}\right] \quad (1)$$

$$RMSE = \sqrt{\frac{1}{n}\sum_1^n \left[h_{GDEM} - h_{ref}\right]^2} \quad (2)$$

$$ESD = \sqrt{\frac{1}{n-1}\sum_1^n \left[h_{GDEM} - h_{ref} - ME\right]^2} \quad (3)$$

$$LE90 = \hat{Q}_{|h_{GDEM} - h_{ref}|}(0.9) \quad (4)$$

Equations and assumptions are based on the recent TanDEM-X quality assessment studies and the related chapter of the *'Geomorphometry'* handbook (Fisher & Tate, 2006; Grohmann, 2018; Höhle & Höhle, 2009; Maune, Binder Maitra, & McKay, 2007; Reuter et al., 2009; Wessel et al., 2018). As per the previous findings, the DEM errors rarely show normal distribution, thus the LE90 means the absolute deviation between the models at the 90% quantile (Höhle & Höhle, 2009; Wessel et al., 2018). Outliers were excluded by applying the 3σ-rule (Höhle & Höhle, 2009; Vaze, Teng, & Spencer, 2010), in which approach the DEM errors outside ±3 times standard deviation, but no more than 5% of the sample, are omitted. As the cells typically affected with large errors (e.g. inland water, mining pits) were already omitted, these remaining outliers could provide further insights on DEM quality and necessary pre-processing steps before geomorphometric applications. To further investigate the possible underlying causes of DEM errors the relevant statistics were also calculated on the bases of elevation classes, the agricultural slope gradient categories (Pécsi, 1985) and the eight cardinal directions of the slope aspect. Finally, a simple linear regression analysis was performed to explore the influence of per cell tree cover rate on the DEM errors in case of different terrain types and data sources (Gallant & Read, 2016; Sadeghi, St-Onge, Leblon, Prieur, & Simard, 2018).

Effects of DEM uncertainty in general geomorphometry

Absolute vertical accuracy is not the primary factor of the GDEMs' performance for geomorphometric purposes, in the assessments the reliability of the derived land-surface parameters and objects is providing more insights. The geomorphological accuracy can be explored by inspecting how well the DEM resembles the topographic and hydrologic characteristics of the surface (e.g. slope, aspect, actual landform shapes, watercourses) (Hengl & Reuter, 2011; Mukherjee et al., 2013; Reuter et al., 2009). A geostatistical error propagation modelling is not part of the present study. The effect of elevation uncertainties on common land-surface parameters and objects is reviewed by comparing the output maps from the GDEMs and the reference DTMs. The following derivatives were selected for the analysis:

- *Slope* and *aspect*: First-order, local land-surface parameters commonly used in GIS-aided geomorphological analyses. These derivatives are relevant for the accuracy assessment because of their sensitivity to the changes of the cell size and DEM quality (Bishop et al., 2012; Grohmann, 2013; Wilson & Gallant, 2000a). The above-mentioned r.slope.aspect tool (Shapiro & Waupotitsch, 2015) is used to derive the parameters and the output maps are again reclassified according to the Hungarian agricultural slope categories (Pécsi, 1985) and the eight cardinal directions.
- *Drainage network*: Hydro-geomorphological features of the study area are prepared from the sink-filled models by the r.stream.* toolset in GRASS GIS (Jasiewicz & Metz, 2011). Streamlines are extracted by multiple flow direction algorithm with a catchment area threshold being approximately 1 km^2 (1110 cells at 30 m resolution) according to the local topography and climate (Hegedűs, 2005; Marosi & Somogyi, 1990). The locational accuracy of the drainage network is based on how well the mapped features are matching within a 120 m buffer zone. With the available toolset the streamlines are ordered per Strahler's hierarchy and general statistics are also extracted (e.g. total length of the network, average catchment area).
- *Topographic Wetness Index*: As the function of upslope contributing area and slope the TWI is a complex parameter describing the tendency of a cell to accumulate water (Wilson & Gallant, 2000a). Its importance in hydrologic, geomorphic, soil and ecological studies is well established (S. Gruber & Peckham, 2009). The TWI was calculated with the r.topidx tool (Cho, 2017).

4.5. Enhancing the relative accuracy of SRTM1

In order to reduce the effect of the common DEM errors on the specific geomorphometric analyses a multi-error removal algorithm has been compiled in GRASS GIS based on easily feasible tools and freely available auxiliary datasets. The performed steps were aiming to remove the gross errors and artefacts, therefore improve the approximation of the land surface; a direct hydrological correction (e.g. stream 'burning') was not employed. The challenge of the SRTM1 post-processing was to 'do no harm' to the original data and to build a correction process that could be transferable to other regions if needed. The performance of DEMs in geomorphometric applications is not linked so much to the mean error, rather than to the spatial arrangement of erroneous cells and to the good relative elevation between locations (Hengl et al., 2004; Reuter et al., 2009).

To improve the quality of the SRTM1 model five major correction tasks were necessary, each of which consists of several steps. In order of execution these processing tasks are the following:

- flattening inland water surfaces,
- removing tree offsets,
- adjusting the height values over built-in areas,
- smoothening speckle noise,
- removing outliers.

The order in which these five error removal steps were performed was decided to (1) keep the edges of forests crisp for tree height estimation, (2) clear small remaining tree height bias in patchy forests during noise and outlier filtering, (3) replace the values of outliers from cells not affected by speckle noise.

The heights of the major Hungarian rivers have already been adjusted as per the SRTM post-processing with the SWBD mask, and conspicuous errors were not identified in the smaller valleys, thus the rather complicated procedure to patch gradually decreasing surfaces to represent watercourses was not applied. Correction of the lakes was necessary because even the small inland water surfaces contained outliers clearly noticeable with visual interpretation of the shaded relief map (*Figure 8*). Using the extended water mask and the method described by Slater et al. (2006) the elevation of lakes was adjusted to a unified value aligning with the shore. The average value of the lake was compared against the lowest 5^{th} percentile of sampled shoreline elevations and the lower one was selected as the new lake-height value.

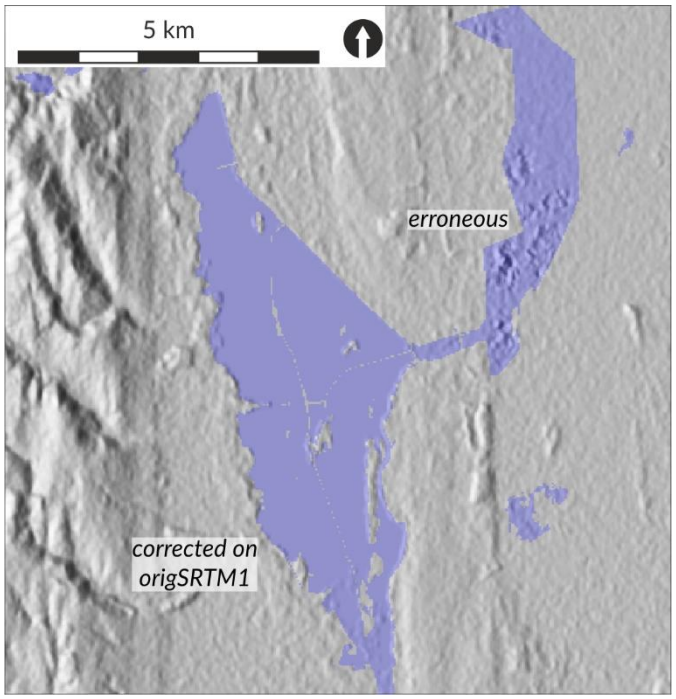

Figure 8. Correct cells of the Kis-Balaton and remaining errors in the north-eastern part. (Blue overlay shows the extended water mask)

Several attempts of vegetation offset removal from SRTM models have been published in the international (Gallant & Read, 2016; Gallant, Read, & Dowling, 2012; Köthe & Bock, 2009; O'Loughlin et al., 2016; Su & Guo, 2014; Yamazaki et al., 2017) and national (Seres & Dobos, 2010; Ungvári, 2015b) literature as well. Prerequisite for this step is a canopy cover map, preferably from the time of the DEM data acquisition, so the effect of clear-cuts or new plantings can be minimised. The tree canopy cover map from 2000 (Hansen et al., 2013) has been selected to delineate the forest patches as its horizontal resolution (0.9") and temporal coverage is appropriate for the SRTM1. The globally available forest canopy height map by Simard et al. (2011) was not included in this analysis because the tree heights are estimated using ICESat data from 2005 and the map only has 30" resolution. Based on visual inspection, the fit of the forest cover map to the forest edges, recognisable on the shaded relief map, was found suitable. Another advantage of the chosen forest cover layer is that it does not only provide information on whether or not tree groups are occurring in a particular cell, but also gives the percentage of the area covered by vegetation taller than 5 m.

As the available methods cannot provide accurate estimations of the tree heights on steeper slopes, based on the elevation differences along the border cells of forest and non-forest regions, the characteristics of topography had to be taken into consideration. Depending on the slope gradient and exposure the radar measurements penetrated the canopy to varying degree, and also the final smoothing of the original SRTM blended the values

more when applied over steeper terrain (Su & Guo, 2014). However, as high slope values occur also along the edges of forest patches, the moderate and low relief surfaces could not be separated by this land-surface parameter directly. To overcome this issue the elevation model was averaged by a 11×11 circular neighbourhood matrix, a new slope map was generated and the threshold of 7.5% was applied to classify the area as moderate or steep. Another challenging task was to find a method that is capable of handling small tree groups and such extensive, coherent forests as the Gemenc floodplain forest. Previous studies have either used an average patch value estimated from buffer zones at the forest edges (Seres-Dobos 2009, Ungvári 2015) or interpolated a tree height map using the difference values calculated at the border of forests (Gallant 2012), and finally subtracted the approximated bias from the original model. The presented algorithm attempted to account for the effect of the topography as well, by considering the tree height changes within forested regions as accurately as possible, therefore a multi-step approach was compiled (*Figure 9*). In the first step the border cells of forest patches were assigned the difference value between an inner and outer buffer zone. Based on the tree cover rate and the topography the unreliable values were filtered out. Afterwards a tree height map was interpolated for the given forest patch by IDW method, which has been then modified by the TPI values, so that the area of unidentified clearings on the forest cover map would not be affected. In the last step the tree height map has been smoothed with a 5×5 matrix to have a transition zone around the patches (Gallant et al., 2012) and finally subtracted from the SRTM1 model.

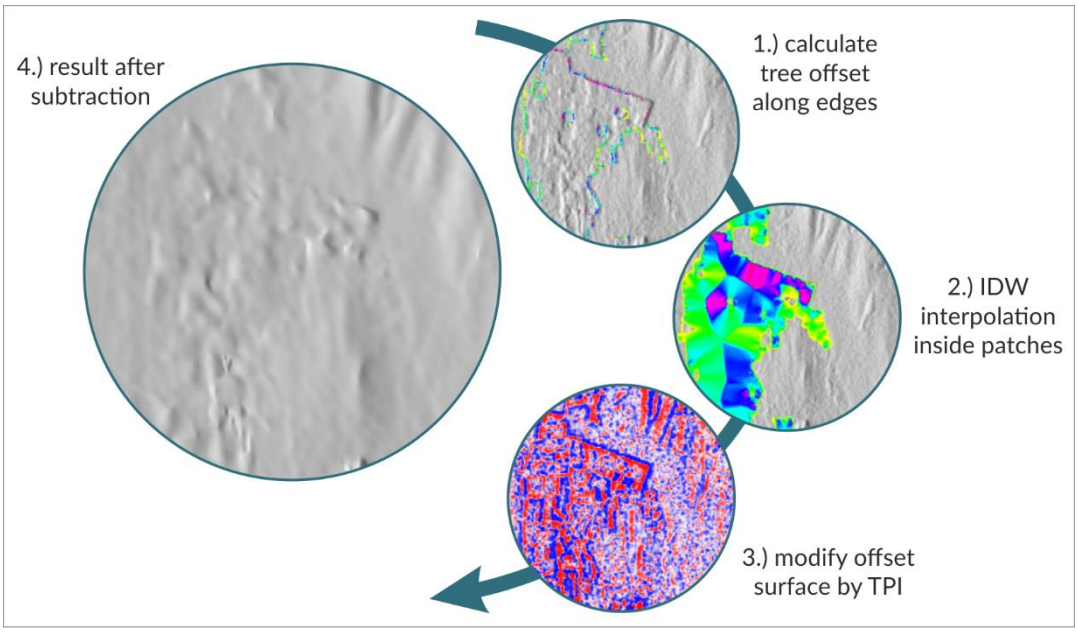

Figure 9. The compiled multi-step approach of tree offset removal explained on a forest patch north of Segesd.

As it has been previously mentioned, due to the horizontal resolution of the quasi-global DEMs, the buildings and other man-made objects are generally not distinguishable, but their height is rather increasing the elevation of the whole cell with an average value. The SRTM1 model also overestimates the bare earth heights depending on the type, size and density of the buildings in a region. The map of settlements and where available individual buildings from OSM has been used to screen the cells and identify locations that are significantly elevated from their surroundings ("OpenStreetMap contributors" 2015). Considering the local topography these cells have been replaced with average values generated by neighbourhood analysis.

A characteristic of the radar based DEMs is the noise-like error, which has been found to have no directional component, show no spatial autocorrelation or clustering and do not reach more than 2–3 m (Gallant et al., 2011). On the other hand, it is indeed more noticeable over flat areas. For smoothing the speckle noise and residual errors a readily available adaptive smoothing algorithm has been applied to the model (Stevenson et al., 2010; Sun, Rosin, Martin, & Langbein, 2007). The denoising tool is available as the r.denoise GRASS GIS Add-on (Grohmann, 2016b) or it could be executed from the command line on Windows (Mitchell, 2010). Setting the threshold parameter to preserve sharper features and the number of iterations to limit the smoothing gives a good control over the method, which is not obliterating important fine details of the topography, but effectively reduces the noise. Considering the tests of Stevenson et al. (2010) and also trying different combinations for denoising the SRTM1 over Hungary, the final edge-preserving threshold has been set as 0.99 and the number of normal-updating iterations as 7.

Outliers are typically independent cells or cell groups that are not compatible with the local topography, e.g. spurious pits or channels, point-like spikes or extremely high peaks. In order to identify and correct these cells a modified version of the method presented by Neteler (2005) has been followed. The algorithm is based on focal statistics; the difference of the original cell value and the averaged value is compared against the standard deviation of the surrounding cells, in order to determine whether a cell deviates 'enough' to be considered as outlier. Over flat regions a moving window of 7×7 size, while over steeper slopes a neighbourhood matrix of 5×5 cells were used to create the auxiliary maps, and the double of standard deviation has been selected as a threshold for the cell screening. The variability of aspect values has also been included as an additional parameter to locate incorrect groups of cells. The identified outliers were then masked out and the cells were updated with average values calculated from the surrounding area.

4.6. Semi-automated extraction of landforms from DEMs

4.6.1. Optimised search parameter to derive landform elements: r.tg.geom

The geomorphons approach (Jasiewicz & Stepinski, 2013) was selected for the purpose of multi-scale landform mapping. However, in order to exploit the full efficiency of this technique and to ensure that an objectively determined, representative search parameter is used a further GRASS GIS script tool – r.tg.geom – was developed (Józsa, 2017b).

The geomorphons method is a robust, cell-based landform mapping technique for the scale flexible identification of geomorphologic phonotypes (geomorphons). In a single scan of the input DEM the tool assigns a 'local ternary pattern' (LTP) to every cell based on the line-of-sight calculations performed in the eight cardinal directions (*Figure 2B*). The total combinations of higher, lower or same height relative positions around the central cell constitute of 498 geomorphologic phonotypes, and provides an exhaustive set of morphological elements. In the final processing step the geomorphons are reclassified into a general purpose geomorphometric map depicting the ten most common landform elements (*Figure 10*) (Jasiewicz & Stepinski, 2013).

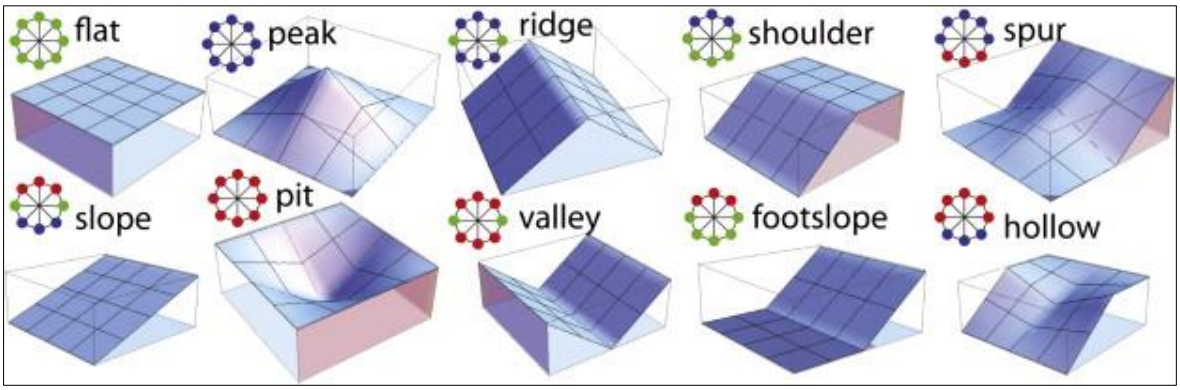

Figure 10. Schematic model of the 10 most common landform elements with the corresponding geomorphons. (Adopted from Jasiewicz & Stepinski, 2013, p. 150)

The appearance of the geomorphometric map is strongly dependent on the value of the lookup distance (outer search radius, *L*), which defines the maximum scale of mapping. The line-of-sight calculation is performed only within this distance, thus the landforms larger than the maximum search radius are broken down to smaller elements (*Figure 11*). The authors only provide a general suggestion to select a relatively large lookup distance (Jasiewicz & Stepinski, 2016; Stepinski & Jasiewicz, 2011). Based on experimentations with the tool it has been established, that in fact the optimal search parameter should be large enough to keep the relevant landforms, but small enough to avoid generalisation of the finer

terrain elements and slowing down the computation (Józsa, 2016; Sărășan, Józsa, Ardelean, & Drăguţ, 2019). The skip radius and flatness threshold parameters can be used to eliminate the influence of small irregularities and to classify flat surfaces respectively (Jasiewicz & Stepinski, 2013, 2016; Stepinski & Jasiewicz, 2011).

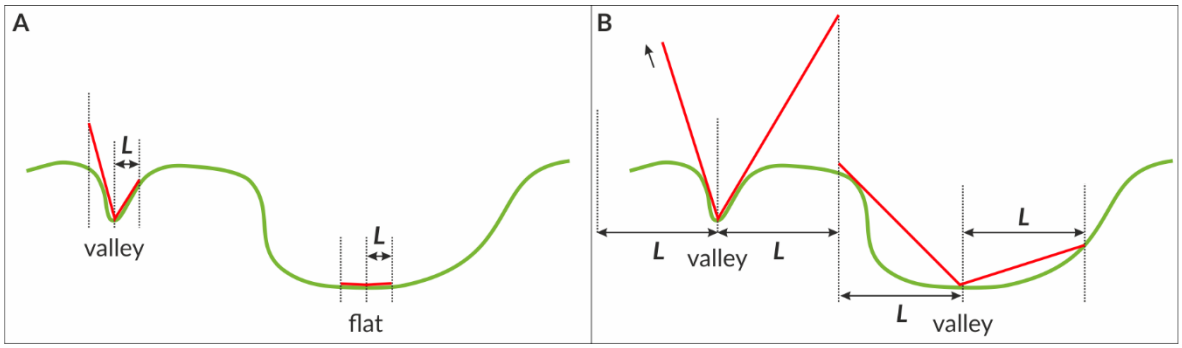

Figure 11. Detecting landforms by the line-of-sight principle. (A – local scale with a small search radius, B – multiple scales mapped simultaneously with a larger search radius). (Based on Stepinski & Jasiewicz, 2011)

The r.tg.geom tool provides an alternative way to derive the map of landform elements by first determining the representative scale over the AOI. The suitable value for the lookup distance is mostly based on the topographic grain principle (Pike et al., 1989; W. F. Wood & Snell, 1960), while the method's implementation also builds on the local variance concept used in GEOBIA applications to determine the scale parameter (Drăguţ & Eisank, 2012; Drăguţ et al., 2011). The topographic grain was considered as potentially optimal value of L as it is approximating the characteristic local ridgeline-to-channel wavelength (Guzzetti & Reichenbach, 1994), and also correlates well with the range and sill of the (semi)variogram within the local topography (Etzelmüller, Romstad, & Fjellanger, 2007).

The automated approach of Pike et al. (1989) was reinterpreted and implemented for GRASS GIS as a Python script tool accessing R functionality (*Figure 12*). The calculation is based on the relative relief values determined with nested neighbourhood matrices, and the topographic grain is defined as the break-point where the increase rate of local relief encountered by the sample is significantly reducing, while the least-squares values of the fitted regression models reach the smallest sum (*Figure 13*). Besides providing a generally representative topographic grain value of the study area the maps of cell-by-cell based characteristic scales and the corresponding maximum relative relief values can be generated as well (*Figure 12A*). These scale signature maps reveal substantial information for the interpretation of the landscape (Lindsay & Newman, 2018). As the main purpose of developing the r.tg.geom tool was to derive the geomorphons map of the study area with

objectively determined key parameters, it is possible to call the r.geomorphon module in a separate step with suggested default values (*Figure 12B*).

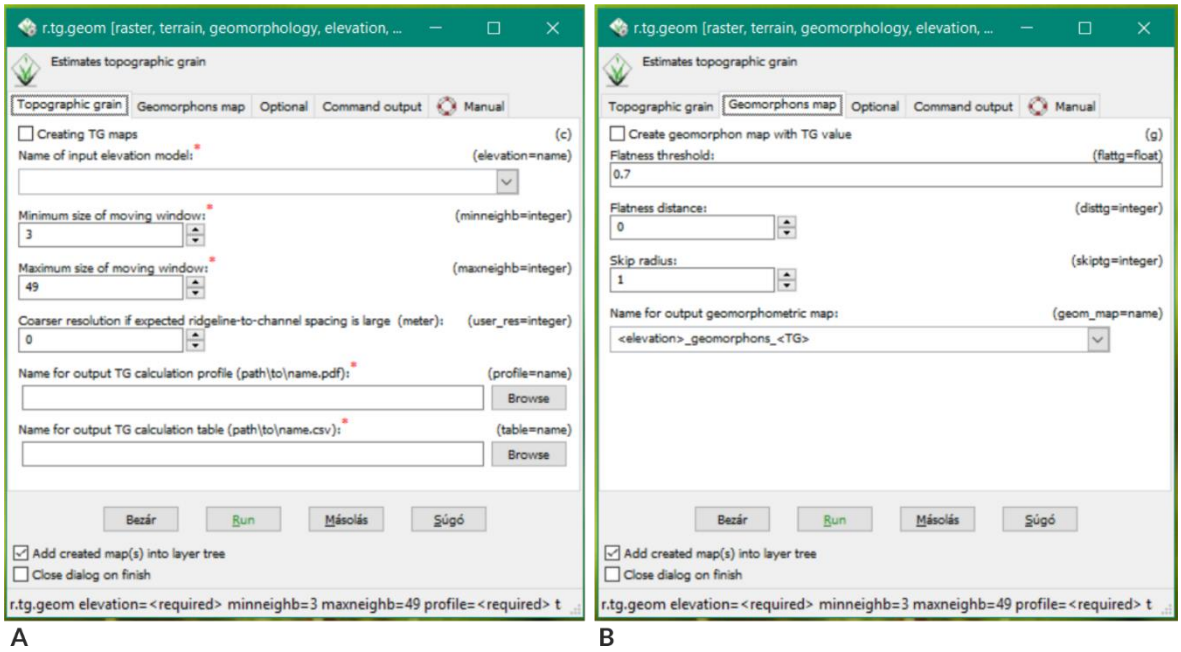

Figure 12. Screens of the r.tg.geom tool in GRASS GIS.
(A – tab to set the input elevation map, necessary parameters and requested outputs for topographic grain calculation, B – the suggested settings to create geomorphons map).

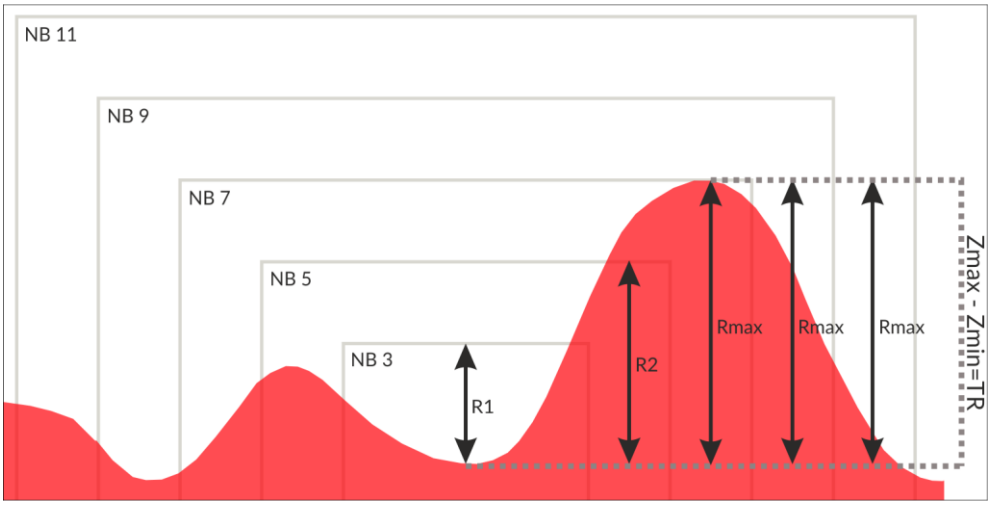

Figure 13. The topographic grain determined as the search window size (NB7) covering the total relief (Rmax, TR) of the local topography.

The r.geomorphon tool is amongst the newer developments of multi-scale terrain analysis techniques, and as such it is not yet part of the core GRASS GIS modules. Installation of the tool is possible with the extension manager from the GRASS GIS Add-ons repository (Jasiewicz & Stepinski, 2016). The r.tg.geom tool has a user friendly interface as per GRASS GIS requirements and it is distributed via GitHub with a manual and a detailed installation guide (Józsa, 2017b).

4.6.2. Pattern analysis to retrieve landscape types: GeoPAT toolbox

The geomorphometric map generated by the r.geomorphon tool – while providing valuable information on the complexity of the topography and the spatial arrangement of shorter and longer slopes, wide and narrow valleys, etc. – can still not be considered as a meaningful map with a traditional geomorphological purpose. The DEM-based geomorphological landscapes map of Hungary was prepared by a supervised classification algorithm – implemented as the Geospatial Pattern Analysis Toolbox (GeoPAT) (Dmowska, 2015; Netzel, Nowosad, Jasiewicz, Niesterowicz, & Stepinski, 2018). In the taxonomy the geomorphological landscapes are also referred to as physiographic units or relief types (Horváth, 1991; Pécsi, 1958; Seres & Dobos, 2010), which are characterised by patterns of landforms and on a sub-level composed of landform elements (Minár & Evans, 2008).

The outline of the methodology is shown in *Figure 14*. The landscape retrieval is based on the geomorphons map, however, in order to avoid misclassification it is advised to incorporate other independent parameters (e.g. elevation categories or relative topographic position), so that the base map distinctively represents the landscape types (Stepinski et al., 2015). Prior knowledge of the study area and the categories to be distinguished is required, as the classification is a similarity based supervised mapping approach. The horizontal resolution of the output map is degraded, as the similarity analysis is comparing the landform patterns of the study scenes to arbitrary square-shaped subsets of the base map (lattice of local landscapes). The size of the local landscape mosaics should be large enough to contain representative landform elements, but small enough to keep the diversity of landscape types and avoid overgeneralisation of the output map (Jasiewicz et al., 2014). The pattern of landform elements in the given scene is transformed into a histogram of the primitive features using the co-occurrence method as per suggestion for topographic data (Stepinski et al., 2015). The primitive features are defined as pairs of eight connected neighbouring cells around the central location (e.g. three slope–slope, four slope–footslope, one slope–valley combination). For DEM-derived base maps the dissimilarity (as reverse of similarity) can be derived by the normalized ‘Wave Hedges’ distance metric (Jasiewicz et al., 2014; Stepinski et al., 2015). In the so-called landscape search step, the overall affinity of the sub-sets to study scenes is built from the similarities of the corresponding bins of two histograms (Jasiewicz, Stepinski, & Netzel, 2013). The scenes are considered as landscape templates and the individual similarity maps representing a given geomorphological landscape type are aggregated by averaging. Finally, the physiographic units are delineated by taking the category with maximum likelihood value (Jasiewicz et al., 2014).

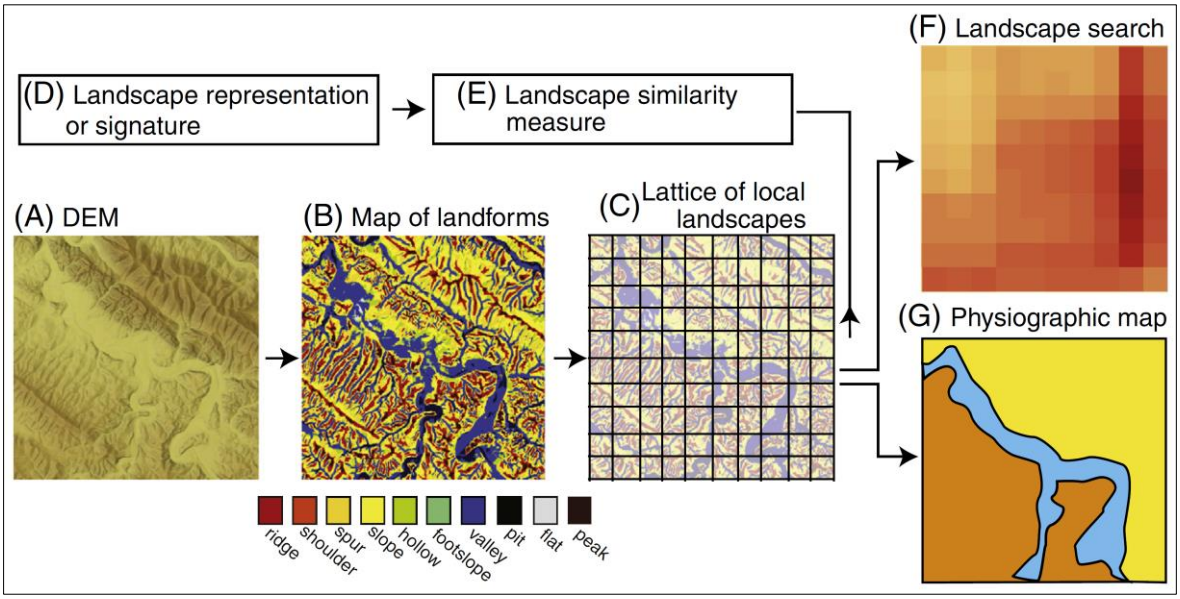

Figure 14. Analytical framework of geomorphological landscape delineation with the GeoPAT toolbox. (Adopted from Jasiewicz et al., 2014)

The GeoPAT toolbox is not designed exclusively for terrain analysis purposes, but to be used for pattern-based information retrieval from images and other raster datasets (Jasiewicz et al., 2015). The detailed description of processing steps with the theoretical background and the full scale of applications is presented in the user's manual (Netzel et al., 2018). The collection of GRASS GIS modules integrated within the GeoPAT1 toolbox are available on GitList ("GeoPAT" 2015), while the standalone GeoPAT2 is available from the website of Space Informatics Lab at the University of Cincinnati ("GeoPAT2" 2018).

4.6.3. Extracting fluvial terraces from DEMs: r.terrace.geom

The complementary functionality of GRASS GIS and R provided the possibility to develop a flexible terrain analysing tool for the delineation and quantitative analysis of terrace remnants (*Figure 15*). The r.terrace.geom tool builds on the method presented by Demoulin et al. (2007) and the R-based implementation published by Miller (2012). The core of the idea came from the terrace definition of Leopold et al. (1964), according to which terraces are composed of two units: a flat top-surface and a dividing slope. The original method tested in the Vesdre valley (Ardennes, Eastern Belgium) was found to be suitable for DEM-based delineation of even small fluvial terrace remnants (Demoulin et al., 2007), but to exploit its full potential it was advisable to compile a 'push-the-button' solution and also extend the analysing capabilities. Using R as an intermediate analytical environment (data.table package) and visualisation tool (ggplot2 package) gives great added value to the algorithm, while GRASS GIS is capable of handling the large digital elevation datasets and perform the

demanding computations to prepare necessary raster inputs (Bivand, Pebesma, & Gómez-Rubio, 2008). The r.terrace.geom tool is available on GitHub with a manual and a detailed installation guide (Józsa, 2017a).

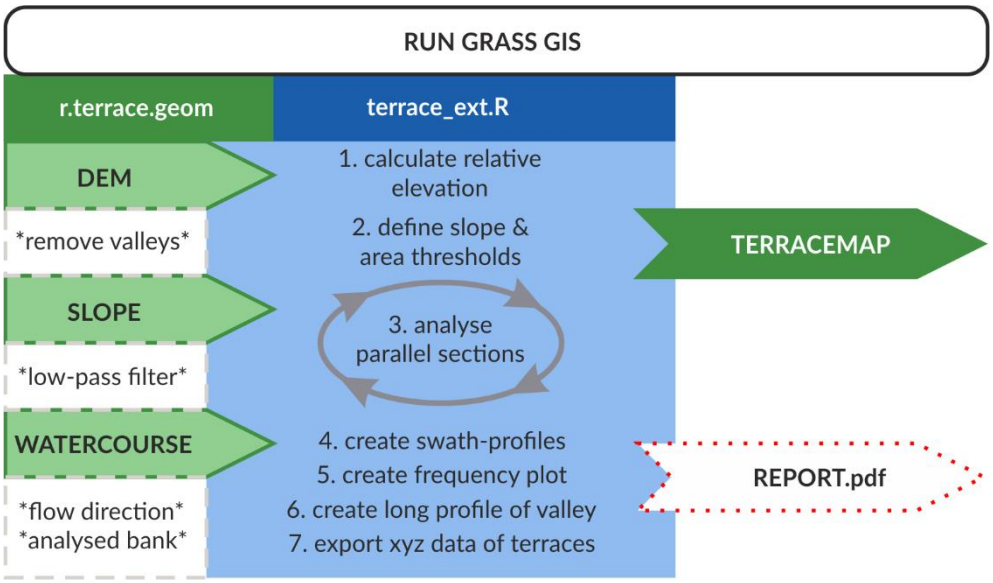

Figure 15. Flowchart of the terrace extraction procedure. (Sections in green are performed in GRASS GIS, blue in R, red represents the output report containing the generated plots)

In particular, the method was planned to be applied on the northern foreland of the Gerecse Mountains, an antecedent valley section of the Danube, with terrace remnants expected in 6 to 8 altitude ranges. Methodological issues arising during the algorithm optimisation were explored based on the available literature (Bugya, 2009; Bulla, 1941; Gábris & Nádor, 2007; Kéz, 1934; Pécsi, 1959), field work and an artificial hillslope model (*Figure 16*). Artificial or synthetic DEMs are useful tools to help the conceptualisation phase of quantitative landform analysis. The synthetic DEMs depict less complexity, than the real topography, and the noise from different DEM types can also be omitted. The synthetic landscape must be representative of the morphological observations about the study site, in order to allow the quantitative approach to be tested for mapping accuracy and completeness (Hani, Sathyamoorthy, & Asirvadam, 2014; Hillier & Smith, 2012; Hillier, Sofia, & Conway, 2015). The artificial hillslope model – created in Autodesk 3Ds Max 2015 – covers an area of 10×5 km, the elevation ranges from 104 to 350 m, the model is slightly tilted to represent lowering elevations along the theoretical river. There are 7 terrace levels, floodplain with narrower and wider sections and a flat top surface included. In order to mimic the effect of erosion and accumulation processes, different level of noise was added, increasing up to a few meters at the higher and therefore ‘older’ surfaces. Even though the

methodology was primarily tested on the synthetic and real DEMs of the Gerecse foreland, the algorithm has not been tailored for this area.

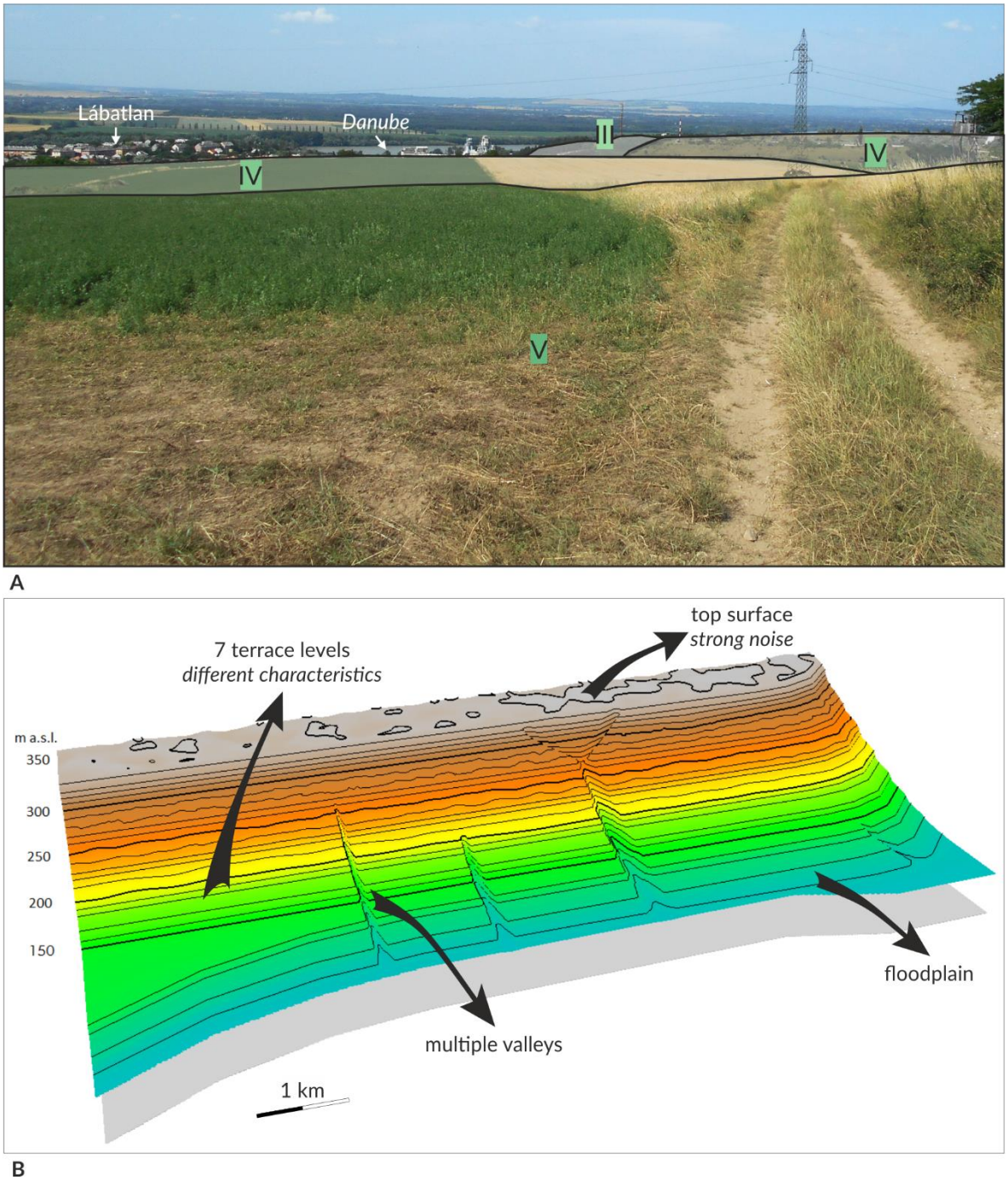

Figure 16. Terrace levels (III., IV., V.) identified on the field at Lábatlan (A) and the synthetic DEM used in conceptualisation phase and tests of the terrace extraction tool (B).

The screens of the tool are shown in *Appendix 4*. The analysis is based on an input DEM and heights representing the river for which the terraces are to be identified. The user has the option to decide in which elevation range the terrace extraction should be performed, there is no need to clip the study area before execution. The tool is automatically creating the

necessary slope map, which can be smoothed with a low pass filter as well. As per Demoulin et al. (2007) the maximum slope threshold to select candidate cells is 13%. Generally, the older, higher located surfaces are expected to be more eroded, therefore the area of terrace remnants is supposed to be smaller and the mean slope value of the forms higher. One of the innovations of r.terrace.geom tool is to define flexible maximum slope and minimum extent thresholds for every elevation range adapted to the topography of the AOI. In an iteration the algorithm cuts up the analysed region into parallel, overlapping sections of 330 m in the flow direction and determines cells potentially belonging to terrace surfaces based on the local slope characteristics and the minimum extent threshold (*Figure 17*). When selected, the tool is able to exclude cells that belong to valleys of tributaries based on the geomorphometric map by r.geomorphon.

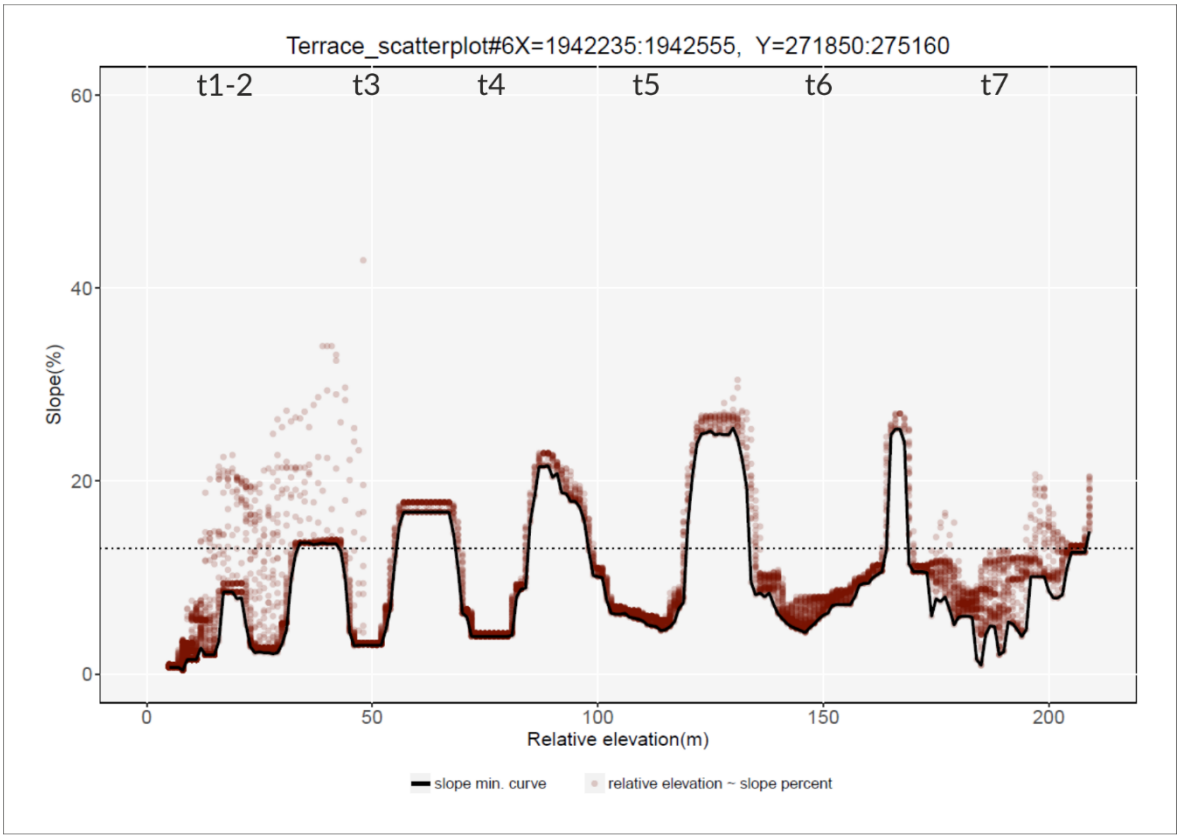

Figure 17. Bivariate scatterplot from R showing the relation of slope to relative elevation in case of section 33 of the artificial test surface. (The tone indicates the number of comprised cells, while the dotted line shows the 13% general slope threshold)

As a result, an output report is created in *pdf* format that contains a histogram of altitudes, swath-profiles of the landscape, scatter plots to represent the relation of the relative elevations and slope values in the analysed sections and final plots showing the frequency of potential cells by altitude and a longitudinal profile of the river with the determined height

ranges of possible terrace levels. Including swath analysis for the studied region is an innovation in the terrace extraction method (*Figure 18*). Classical elevation profiles can reveal slope breaks indicating levels of erosion or accumulation surfaces, but as per the design of the tool it was reasonable to create a swath profile, which represents statistical parameters of the analysed section (minimum, mean, maximum). The coding was implemented after Telbisz et al. (2012) and Telbisz et al. (2013b). The plot showing the frequency of terrace candidate cells can be combined with terrace level ranges based on other sources, therefore a visual comparison is easily feasible. The algorithm also produces a raster map containing the cells of extracted terrace candidates for further analysis.

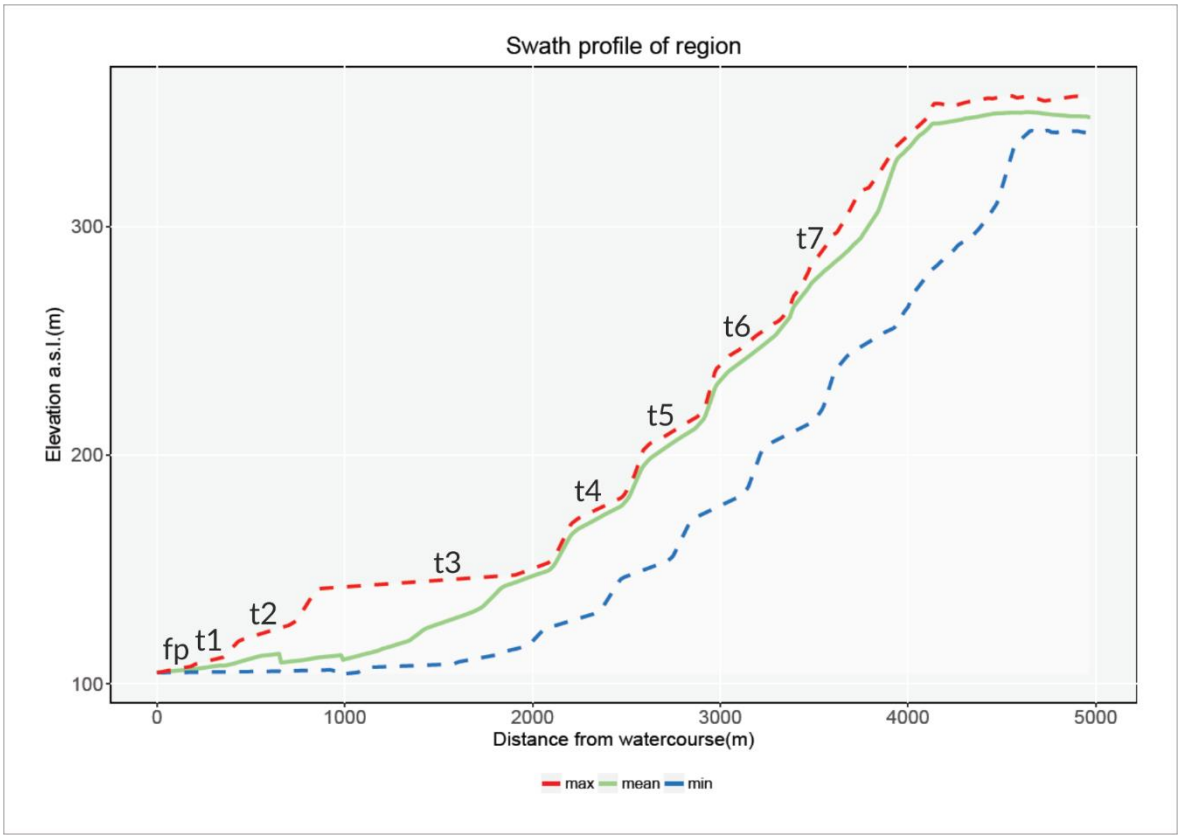

Figure 18. Swath profile of the artificial DEM.
(Blue – minimum curve, Green – mean curve, Red – maximum curve)

5. Results

5.1. Quality assessment of the quasi-global DEMs

5.1.1. Comparative analysis of horizontal and vertical accuracy

Following the presented guideline of the quality assessment the first step was to import all GDEMs, reference DTMs and auxiliary datasets to an EOV location in GRASS GIS. The software allows the organisation of the datasets into a hierarchical structure with a main mapset ('PERMANENT') and several user-defined mapsets to isolate the base maps and the task-specific outputs (Neteler & Mitasova, 2007). In the current analysis the determination of the effective resolution, the DoDs and the general geomorphometric applications were handled separately. However, before the base maps could be moved to the main mapset, the height values of the TanDEM-X model were registered to the EGM96 geoid to ensure the comparability of the elevations. Furthermore, the entire analysed tile of the SRTM1 model (N46E018) was 'lifted' by 1.5 m to account for the absolute negative bias detected by previous quality assessment projects (Józsa, 2015a; G. Szabó et al., 2013; Winkler et al., 2006).

Once the base maps were reprojected to EOV a systematic misregistration analysis was performed by the thorough review of exaggerated shaded relief maps, cross-directional elevation profiles and preliminary DEM difference surfaces. The location of the reference DTMs was assumed correct and signs of cell shifts were searched on the GDEMs. Elevation profiles crossing the valleys of the Lajvér Stream's tributaries or the edge of the South-Baranya Hills near Báta were especially helpful in this task. Furthermore, the highest cells representing the peaks of Zengő, Hármashegy and Szószék were also cross-referenced. Finally, the preliminary DoDs were draped over the shaded relief maps to see if a pattern occurs in the DEM errors, which would indicate that the valleys and ridges are not aligning correctly. A sub-pixel shift was noticed in case of the SRTM1 model, however, by the repeated analysis of DEM difference maps the relocation of the model was rejected. Besides the elevation models, the geolocation of the CLC2006 land cover and the forest patches map was also explored. The horizontal accuracy of these datasets was found satisfactory, the detectable patch edges on the shaded relief maps were fitting to the category boundaries.

The effective resolution of the models was determined as an estimation of the level of terrain shape complexity represented by the GDEMs. The connection between the resolution and mean slope was explored by resampled versions of the reference DTMs. Afterwards, the mean slope was also calculated for each GDEM on their nominal horizontal spacing and the effective resolution was derived by finding the cell size for these slope values. It has to be noted, that the resolution of the TDX12 model is nearly equal to the cell size of the contour-based reference DTMs, thus the simple mean slope analysis method is not optimal for precisely calculating the effective resolution. Based on extrapolation, the estimated effective cell size in this analysis is 4.37 m, but the TDX12's mean slope value is distorted by the steep edges of forest patches and other man-made objects. The AW3D30 model was found to have an effective resolution of 28.79 m, the SRTM1 43.46 m and the MERIT DEM 101.66 m respectively. These values are comparable to the previously published estimations (Florinsky, Skrypitsyna, & Luschikova, 2018; Grohmann, 2018; Józsa, 2015a; B. Smith & Sandwell, 2003) and reasonable when considering the GDEMs' characteristics and creation processes (e.g. final smoothing of SRTM1, AW3D30 being a resampled version of the 5 m original model). Furthermore, striking differences in the level of detail are visible on the exaggerated shaded relief maps also (*Figure 19*). On the TanDEM-X 12 m model even the scroll bar and swale series of the Danube floodplain are visible for the trained-eye, while the low resolution of the MERIT DEM results in a blurry appearance of the shaded relief map and generalisation of the landscape. Merging different DEM data sources and applying the multi-error correction process came at the price of losing terrain detail.

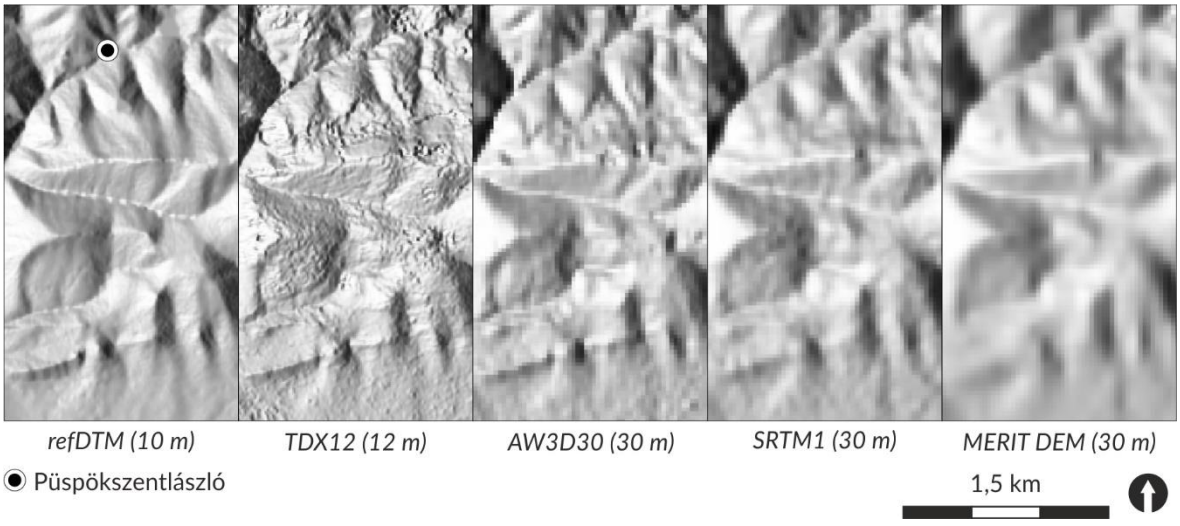

Figure 19. Exaggerated shaded relief maps of the analysed models showing the western section of the ridge leading up to Zengő.

As a next step of exploring the general similarities and differences between the GDEMs, the elevation histograms were generated for the total area, the floodplain (*Appendix 5*), the hilly region and the Eastern Mecsek Mountains 3rd level study areas as well. The elevation range below 99 m is significantly over-represented due to the extensive floodplain; however, the 10+ m vegetation bias is distorting the distribution on all GDEMs except the MERIT DEM. On the elevation histogram of the MERIT DEM the vast majority of the cells are grouped around 88–93 m. From this one could assume that the lower and higher floodplain level is represented well on the model, but in fact the correction of the Gemenc Forest left behind a slightly elevated surface. The elevation histogram of the TanDEM-X model also peaks around 88 m, and a less significant second peak appears near 103 m, which might indicate a typical 15 m tree height captured by the radar technique. The elevation of the AW3D30 and SRTM1 models don't show bimodality and the peak is appearing around 86–88 m, which indicates the underestimation of the surface. In case of the hilly or low mountainous regions such differences cannot be identified: the general appearance of the elevation histograms is similar; the variability of the terrain obscures the influence of the different DEM error components. These findings are supported by the Spearman correlation coefficients presented in *Table 5*. The corrected MERIT DEM and the SRTM1 model show a stronger relation, while the weakest correlation appears to be between the AW3D30 model and MERIT DEM. This could be associated with the general characteristic of the models: SRTM1 still underestimates the surface, thus the vegetation bias is 'smaller' across the large area of the Gemenc Forest, while the AW3D30 model is a photogrammetric product, which tends to capture the canopy top surface.

Table 5. Spearman correlation of the analysed GDEMs.

		TDX12	**AW3D30**	**SRTM1**	**MERIT DEM**
Total TS and EM study area	**TDX12**	1	0.9745	0.9756	0.9761
	AW3D30		1	0.9724	0.9664
	SRTM1			1	0.9880
	MERIT DEM				1
Danube floodplain in the TS study area	*TDX12*	*1*	*0.7216*	*0.7411*	*0.7597*
	AW3D30		*1*	*0.6895*	*0.6283*
	SRTM1			*1*	*0.8647*
	MERIT DEM				*1*

Further insights on the DEM errors were gained by calculating the descriptive error statistics based on the DoDs created from every GDEM and all of the contour-based reference DTMs. The error metrics were calculated over the total area of the reference DTMs and subsets of bare surface and forest categories of the CLC2006 land cover map, assuming that the vegetation offset is explaining a larger portion of the DEM error (*Table 6*). The DoDs' histograms are all unimodal, but the peak is below zero for the TDX12 (–1.04 m) and SRTM1 (–0.88 m) models, while it is positive 1.60 m for MERIT DEM and 0.84 m for AW3D30. The mean error, the skewness and kurtosis of the error distributions indicate that larger scale positive differences occur. A characteristic that is not revealed by the typically used error statistics is the proportion of cells with less, than 1 m error. In case of the GDEMs it is 44.42% for TDX12, 25.06% for AW3D30, 26.56% for SRTM1 and 23.64% for MERIT DEM respectively. The presented DEM error statistics are different for the MERIT DEM: due to the smoothing of small scale features, elevated valley bottoms and the slightly lifted residual 'plateau' of the Gemenc Forest this model generally overestimates the surface. The efficiency of the multi-error correction process is revealed by the similarity of error metrics over the bare surface and forest categories. Considering only bare surfaces the error metrics are satisfactory for the other GDEMs as well, however, it is clear that the vegetation offset must be considered and possibly eliminated in specific applications to reduce the consequences of error propagation.

Table 6. Error metrics of GDEMs compared to contour-based reference DTMs.

		ME (m)	**RMSE (m)**	**ESD (m)**	**LE90 (m)**	**skewness**	**kurtosis**
TDX12	Total area	3.11	6.94	6.21	13.18	1.78	2.80
	Bare surfaces	0.22	1.61	1.60	2.50	1.37	4.37
	Forests	11.60	15.16	9.76	25.55	0.24	–0.33
AW3D30	Total area	3.41	7.43	6.61	14.46	1.33	1.68
	Bare surfaces	0.42	2.73	2.70	4.16	0.62	2.36
	Forests	12.09	15.03	8.93	24.32	–0.06	–0.48
SRTM1	Total area	0.64	4.57	4.52	7.60	1.43	2.53
	Bare surfaces	–1.10	2.31	2.03	3.73	0.54	1.67
	Forests	6.05	9.24	6.99	16.16	0.46	–0.05
MERIT DEM	Total area	1.51	3.33	2.96	5.37	–0.12	2.25
	Bare surfaces	1.17	2.09	1.74	3.27	–0.55	1.93
	Forests	2.91	6.10	5.37	10.33	0.15	0.42

The main factors commonly assumed to have a significant influence on the DEM errors are the terrain morphology (relief type, slope, aspect) and land cover (Mukherjee et al., 2013; Purinton & Bookhagen, 2017; G. Szabó, Singh, et al., 2015). To reveal the effect of these factors on the vertical bias further analysis was executed by grouping the errors per elevation ranges, agricultural slope classes and cardinal directions. Furthermore, linear regression analysis was performed in order to explore to which extent the forest density could explain the DEM errors. Boxplot diagrams displayed next to each other are useful to interpret the error characteristics per elevation, slope and aspect groups for all GDEMs. The diagrams of elevation categories (*Appendix 6A*) are in good agreement with the boxplots of the agricultural slope categories (*Figure 20*). With the rise of elevation and slope value the DEM errors show more variability, and as typically the higher, steeper regions are covered by forest patches the median of the errors is also increasing. The characteristics of the TDX12 and AW3D30 model are similar, which can be related to the more detailed representation of the non-topographic objects, while the elevations on both the SRTM1 and MERIT DEM models are smoothed. Due to the orientation of the sensors it is a common assumption, that the slope aspect (*Appendix 6B*) has a strong influence on the DEM errors (Shortridge & Messina, 2011). The interquartile ranges in the N and NW directions are wider, however, a typical fluctuation which could be an indication of horizontal shifts is not detectable.

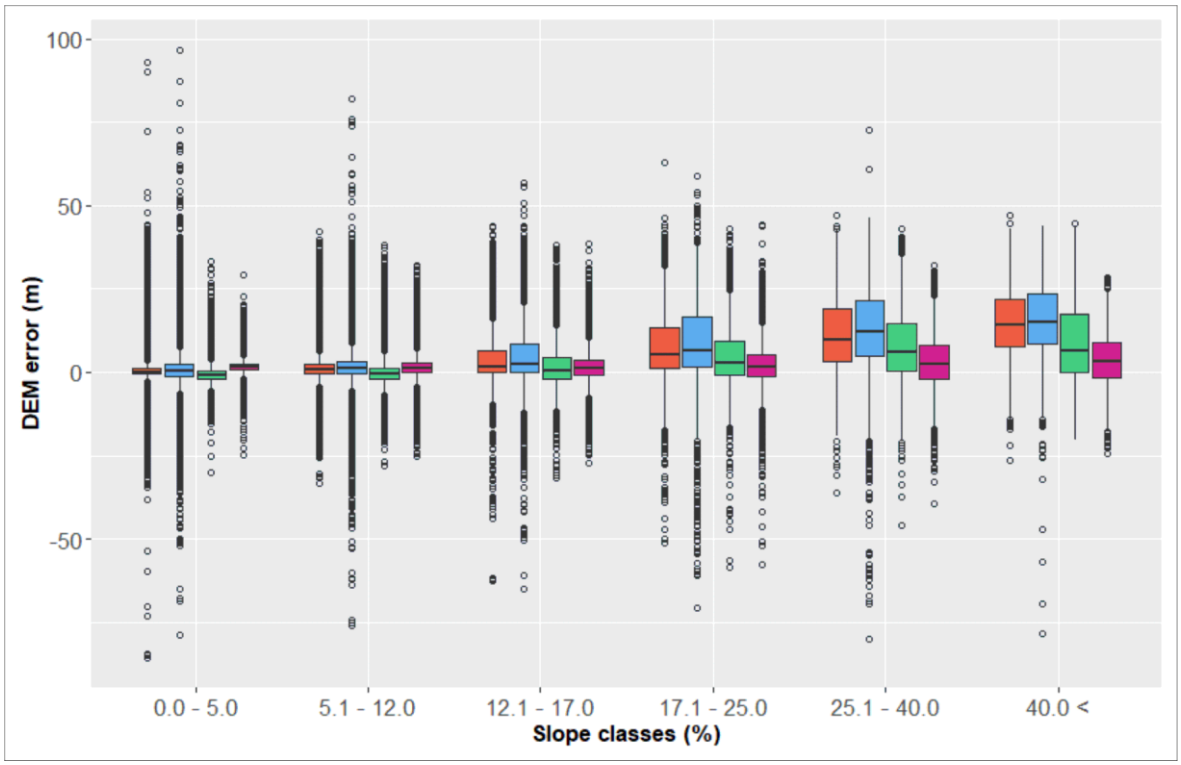

Figure 20. Boxplot diagrams showing the DEM errors grouped by agricultural slope categories. (Red – TDX12, Blue – AW3D30, Green – SRTM, Magenta – MERIT DEM)

By displaying the DEM errors exceeding the 3-σ rule it can be noted that most of these are located on N–NW facing, steeper slopes with at least 70% forest cover on the cells. These outliers occur on all four of the GDEMs, supporting what has been noticed on the aspect related boxplots regarding the wider DEM error ranges. As the TDX12 model is representing the ground truth so well in bare surface regions, the very dense forest patches often belong to the outlier's category. Other spots indicate spurious sinks and some cells along the Danube, which were not excluded by the water body mask. During the visual assessment of the AW3D30 model several unreal peaks and pits were noticed across the study areas, irrespective of the relief type. These are also marked as outliers based on the 3-σ rule and definitely degrade the performance of the model in hydrological or geomorphological analysis. The SRTM1 model shows less outliers over the flat surfaces, while some further cells are located around the open-pit mines near Pécs-Vasas, which indicates inaccuracy of the mining site's boundary from the CLC2006 map. A different characteristic of the outliers on the MERIT DEM is that these occur along the steep slopes of narrow valleys or the loess plateau's edge at the South-Baranya Hills, as a result of the smaller effective resolution and blended elevation values.

A stronger association was assumed between the tree cover of the cells and the scale of DEM errors over the flat regions, where the morphology has a smaller impact on the difference values. The linear regression analysis of the tree cover as the predictor and the DEM errors as response variable revealed a statistically significant relationship (p-value is less than 0.001 in all cases). As it could be expected, on the MERIT DEM after the vegetation offset removal the tree cover does not explain the remaining errors well, R^2 is under 0.05 for the hilly and low mountainous surfaces and only increases to 0.36 in case of the floodplain. Over the area of the Tolnai-Sárköz the TDX12 has 0.56, the AW3D30 has 0.52 and the SRTM1 has 0.45 R^2 values respectively. The tree cover did not predict the DEM errors well over the hilly region, however, it also has to be noted, that only small vegetation patches occur in this area. It has been concluded by DEM correction studies that the difference between the models increases with the vegetation bias, but the standard deviation of the error is also influenced by the slope value (Su & Guo, 2014). Over the Eastern Mecsek Mountains study area this characteristic of the DEM errors can be also noticed from the boxplot diagrams of the topographic conditions and the R^2 values, which are explaining around half of the variation in the elevation differences over the extensive forest region.

5.1.2. Applicability of quasi-global DEMs in general geomorphometry

The quality of the GDEMs determines the quality of the geomorphometric analysis, because even the most robust and scale-flexible methods cannot distinguish between natural and man-made features, eliminate severe artefacts and errors. Different error statistics reveal the general accuracy and possible weaknesses of the models, but in certain cases the errors might cancel out and remain hidden. In case of geomorphometric applications the preliminary assessment of how reasonable the surface is represented is essential. For this part of the analysis the r.fill.dir sink filling algorithm (Srinivasan & Miller, 2017) was applied on both the GDEMs and the reference DTMs, but no further error removal steps were executed.

First of all, the categorised slope (*Figure 21A*) and aspect maps were compared over the different relief types to determine how the different effective resolution and DEM errors affect these first order derivatives. The spatial arrangements of slope categories indicating the heterogenous or smooth terrain characteristics are represented reasonably well. An expected characteristic was the varying slope classes along forest clear-cuts and roads over the floodplain. For the TDX12 model such slope category variations draw the outline of road cuts and embankments, tree alleys and stream channels when the general topography is smooth. An unusual characteristic of the slope map of AW3D30 model is a nearly 6 km wide swath across the Tolnai-Sárköz region, which coincides with a small number of scene stacks used for the DEM creation. Due to the error removal process and lower effective resolution of the MERIT DEM the complete floodplain belongs to the 0–5% slope category, however, as a result of the denoising the steep slopes in the hilly and low mountainous regions were also smoothed over multiple cells.

As the surface in the floodplain is rather bumpy due to the vegetation offset and man-made objects, the aspect maps are showing variations which are not related to the actual topography. When analysing only the study sites in hilly or low mountainous environments it can be noted that aspect classes changed in the narrower valleys and ridges, as these forms are generalised on the GDEMs resolution and local sub-pixel misregistration can also occur. The categorised aspect map of AW3D30 shows spurious patterns as well, which are likely related to the peculiar bumpy texture and group of outlier cells found on the model.

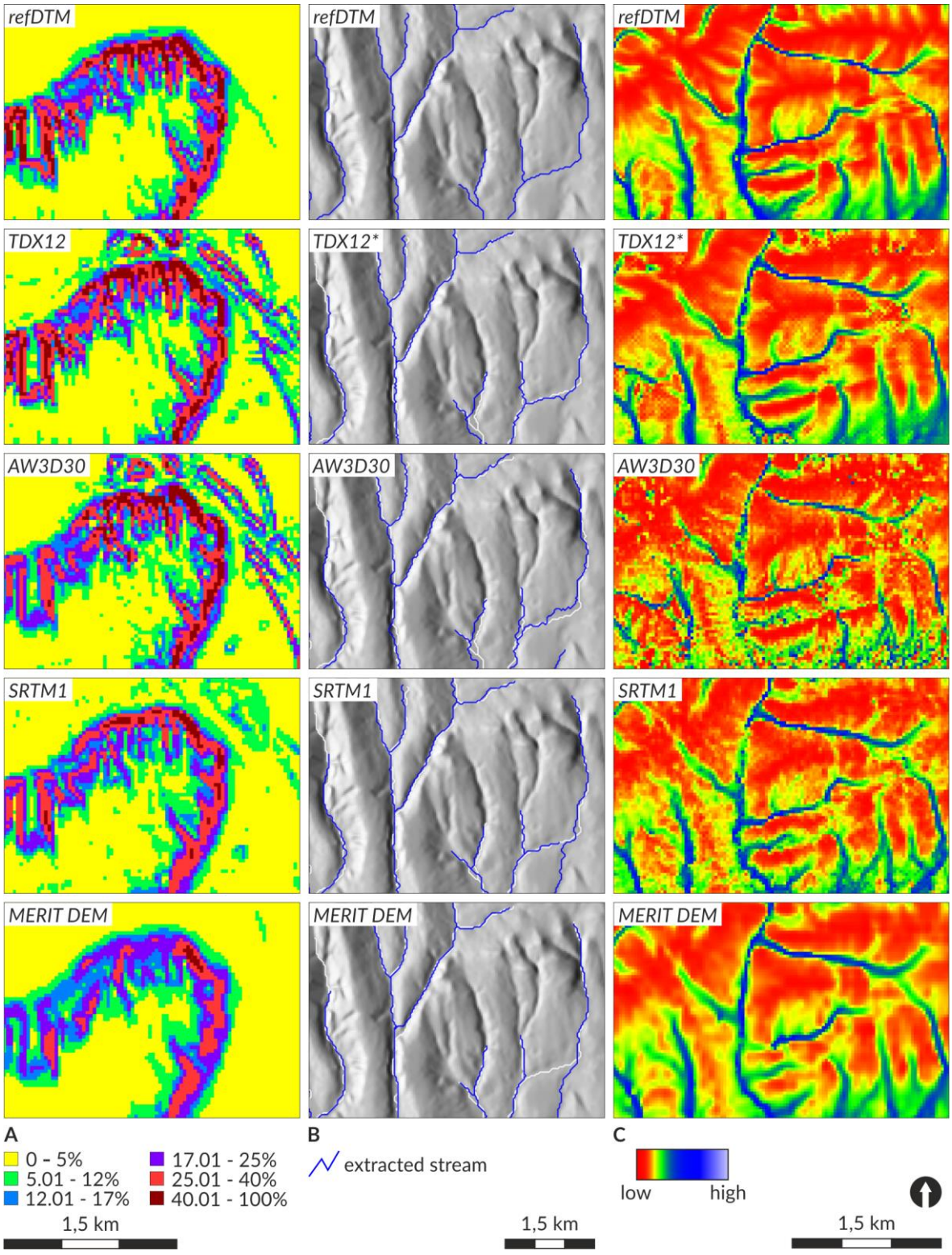

Figure 21. The categorised slope maps at Báta (A), extracted stream lines at Hird (B) and topographic wetness index maps at Hosszúhetény (C) from the reference DTMs and the analysed GDEMs. Exaggerated shaded relief map in the background is from the reference DTM. TDX12 indicate filtered TanDEM-X map.*

Stream networks (*Figure 21B*) were only extracted over the hilly and low mountainous landscape based on the above-mentioned considerations. Beforehand, the flow direction and flow accumulation maps were visually inspected, and in case of the TDX12 model remaining sinks were noticed. These were treated by applying a circular 3×3 average filter on the model. The characteristics of the drainage network demonstrate that the increasing DEM resolution does not necessarily result in more accurate streamline features. Even though, in case of the MERIT DEM the source of the small tributaries in the Eastern Mecsek Mountains region is often located more downstream, the channels align generally well with the results from the reference DTM. Besides the visual similarity this translates to 80.14% of the derived watercourses being located within the 120 m buffer zone around the reference features. The streamlines from the TDX12 and AW3D30 models often meander around the surface objects. Due to this characteristic in case of the TDX12 model the 75.92% of the stream cells are within the buffer zone, while for the AW3D30 model only 74.44%. On the SRTM1 77.05% of the streamlines are within the buffer zone around the reference dataset. *Figure 21B* shows that the stream captures of the piedmont surface are well mapped in case of TDX12 and AW3D30, while the drainage network from SRTM1 shows ambiguities in the vicinity of the subsequent and resequent valley section. On the MERIT DEM the slight elevation changes of these more recent channels are not significant enough for the flow tracing algorithm to distinguish.

Finally, the topographic wetness index (*Figure 21C*) maps were compared, in order to explore how this secondary geomorphometric parameter represents the surface runoff properties when derived from different GDEMs. As this variable is also based on flow direction and accumulation values, the unresolved sinks would cause trouble in case of the TDX12 model, thus the filtered DEM was used for TWI calculation instead. The embankments of roads still distorted the flow directions enough to cause peculiar patches on the TWI map. As a result of the smoothing and lower horizontal spacing the output from MERIT DEM showed more similarities to the map derived from the reference DTM. The high local variations caused by noise or group of outlier cells often translated to unrealistic patterns of TWI values on the AW3D30 and SRTM1 models. This hinders the separation of the bottom, middle and top of hillslopes and clearly indicates that more sophisticated pre-processing algorithms should be applied on these GDEMs before specific applications (e.g. landform delineation, soil mapping, hydrological analysis).

5.2. Assessment of improvements on SRTM1

The changes on SRTM1 model during the correction process were closely monitored by analysing the descriptive statistics, distribution of remaining errors, visual inspection of exaggerated shaded relief maps and DoDs. The correction of inland water surfaces (0.6% of cells), built-in areas (0.8% of cells) and outliers (0.04% of cells) only affected a fraction of the model, but these are still important from analytical point of view and also improve the visual appearance of the SRTM1. The removal of tree offsets resulted in a change of elevation in case of 21.7% of the total area, while the denoising step virtually involved all cells. *Figure 22* represents the achieved effect of corrections on cross-sections over regions of 'best-case-scenarios'.

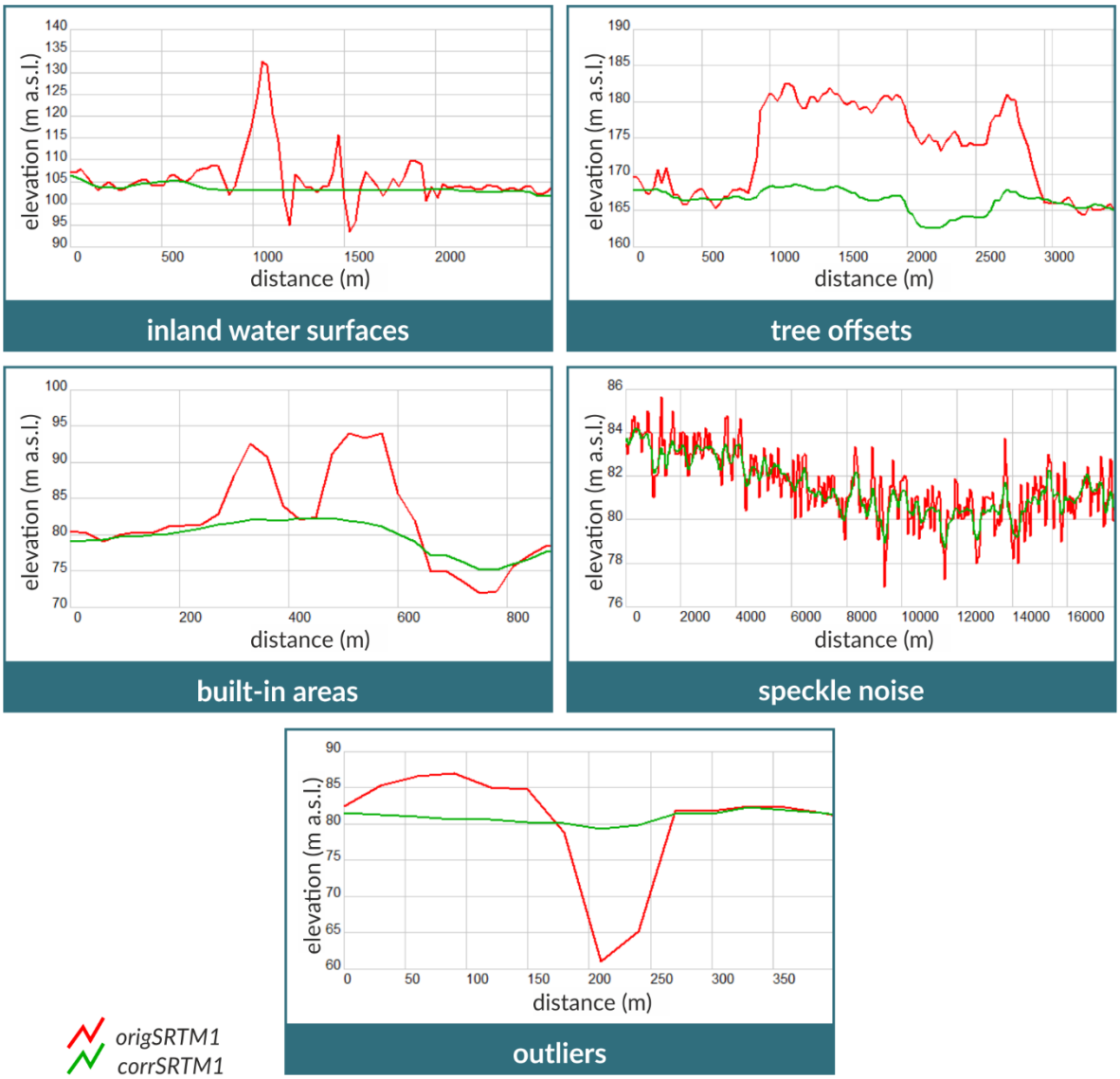

Figure 22. Cross-sections illustrating the effects of the applied corrections.

The correction of water surfaces by the extended water mask was an easily feasible process and successfully removed the spurious pits and peaks occurring over the lakes and reservoirs. Adjusting the elevation values over settlements provided more reliable results in case of less densely built-in regions, as the surrounding cells represented the real topography better when the original measurements of SRTM could reach the ground between the buildings. It is, however, important to note that for geomorphological analysis it may still be expedient to rather mask out the areas densely covered by tall building blocks, or at least pay close attention to the interpretation of the derived maps. Regarding the outliers it has been noticed, that replacing the unreliable height values with the average elevation of surroundings could not fully correct these errors. A partial correction is illustrated in case of the Kunkápolnás marsh system on the Hortobágy (*Figure 23*). From a general point of view the error statistics did improve, but as the neighbouring cells of an outlier were oftentimes also distorted by the faulty elevation, the average height of the patch not always represented the ground truth. Group of outliers have been typically observed over wetlands, like marshes, bogs or swamps. From a geomorphometric aspect these definitely hinder the delineation of landforms, yet interestingly they could provide beneficial information when looking for former meanders or paleochannels in geomorphological studies.

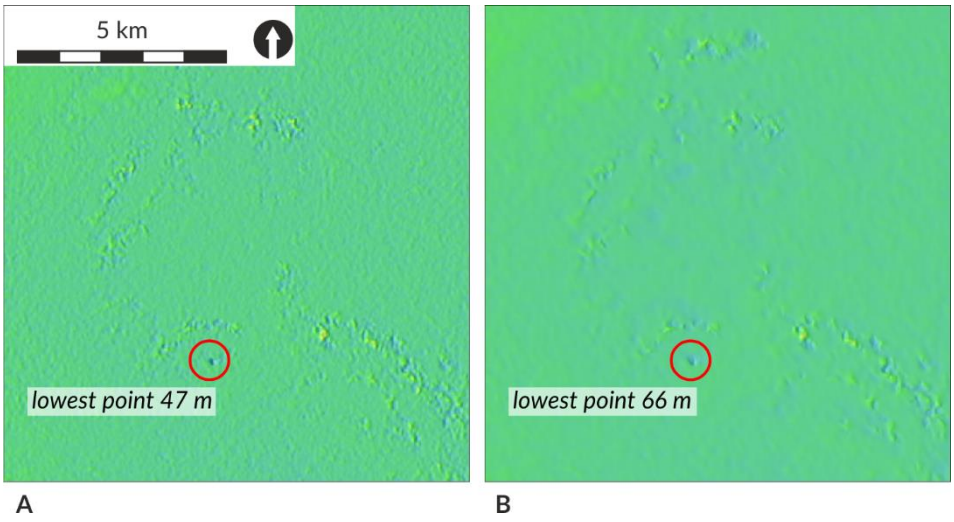

Figure 23. Groups of faulty cells in the Kunkápolnás marsh system before (A) and after (B) the outlier correction.

The effectiveness of the denoising algorithm in both flat or mid-mountainous regions is revealed by the exaggerated shaded relief maps (*Figure 24*). At the border of the Kalocsa-Sárköz and Illancs region near Hajós it can be observed, that the surface got smoothed, yet the edge created by the Danube was well preserved. Before corrections several tree patches and a general noisy appearance of the surface was clearly visible. With the applied

corrections the vegetation offset was successfully removed and the smoothing improved the representation of the landscape. The mid-mountainous site selected from the Northern Bükk area is a good example of the importance of edge preservation and adaptive smoothing. Even after applying the denoising algorithm, smaller valleys and ridges can be visually delineated, while on the flat surface of the central basin area, where generally stronger smoothing was required, the method also proved effective.

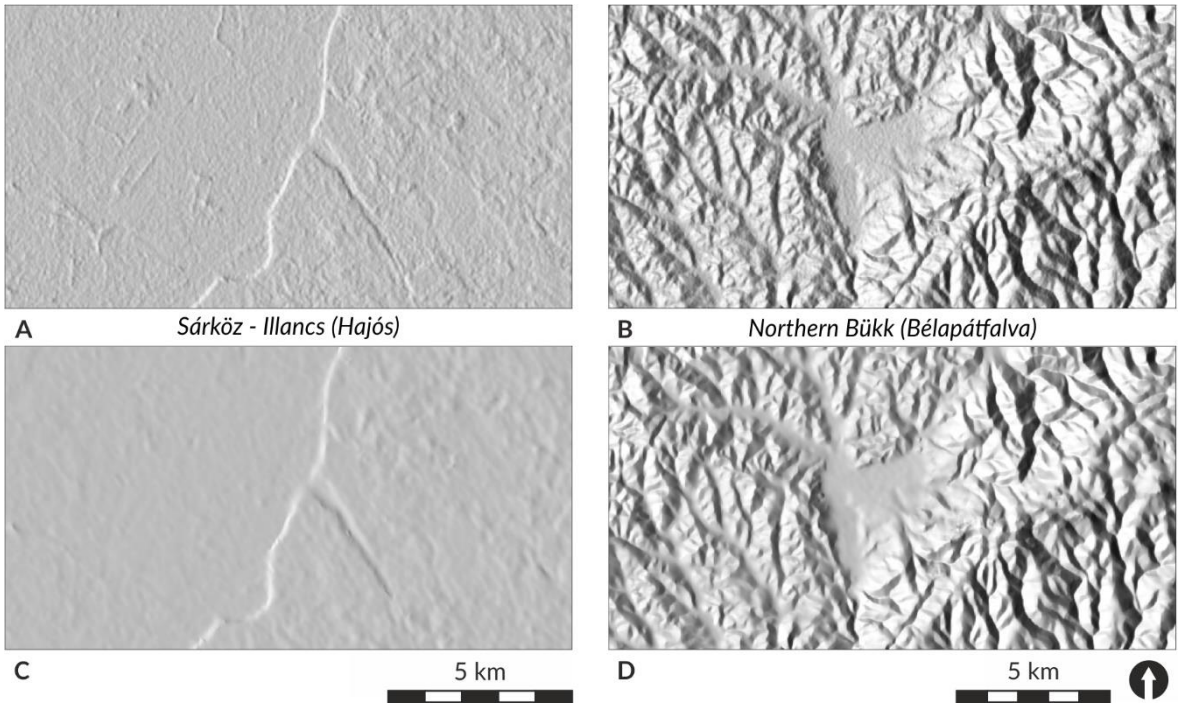

Figure 24. Effect of noise reduction in areas with different relief.
(A and B – before correction, C and D – shaded relief maps after denoising)

To explore the intensity and spatial arrangement of the changes, the surface of elevation differences has been calculated by subtracting the corrected SRTM1 from the original model. The chosen colour scheme is intended to give a better overview on where the correction lowered or filled the surface with the category breaks reflecting the European and global SRTM error statistics (*Figure 25*). Based on the map it can be noted that the vegetation bias on the original model was at least 6 m, while in some regions differences up to 16 m occurred. The blue colours represent the cells that have been filled by the correction process, however, the domination of lighter colours indicate that the heights were generally not increased with more than 6 m. Narrow valleys in the hilly and mountainous regions are typical examples for this type of elevation change, as the denoising and outlier removal process involved averaging of adjacent cells. In addition, the alternating occurrence of light red and blue shades over the plains is attributed to the correction of the speckle noise as well.

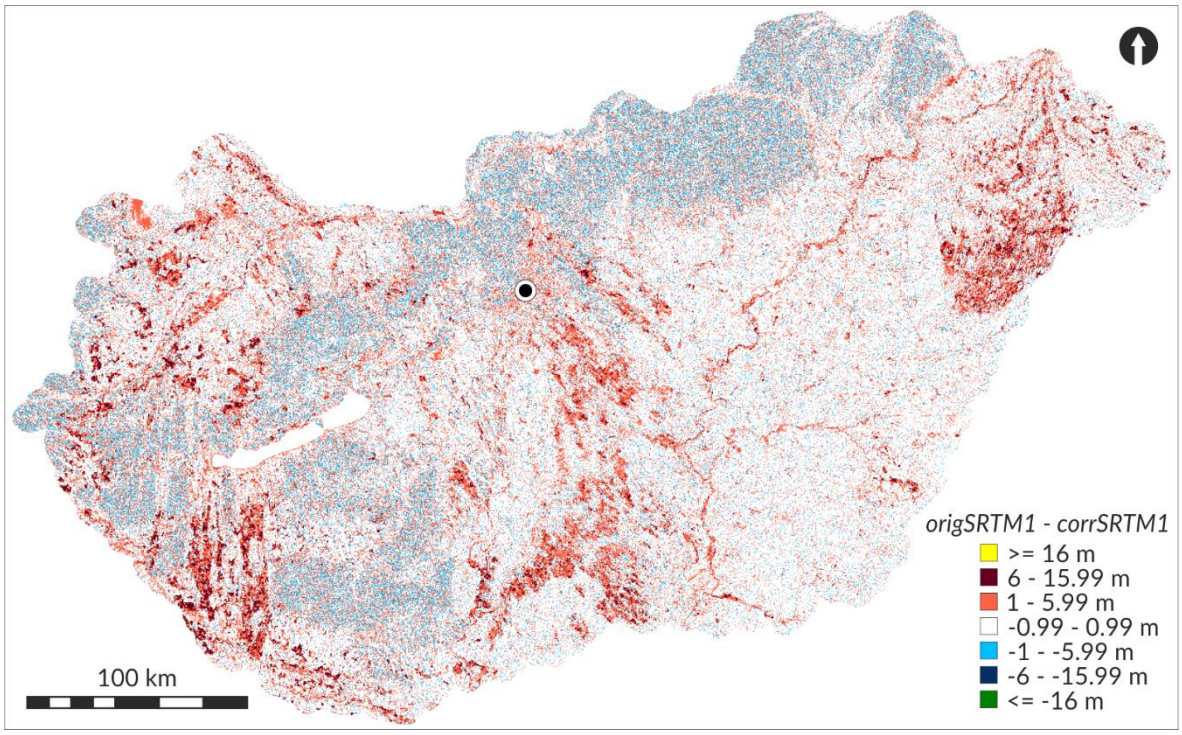

Figure 25. 'DEM of Differences' showing the change in elevation values after the corrections.

The cell most increased on the corrSRTM1 was changed by 72 m, while the largest value shaved off of the surface was 42 m. Apart from a few exceptionally high differences, the overall average of the absolute DEM difference values is only 1.11 m and the standard deviation is 1.84 m. *Table 7* is providing information on the distribution of the categorised elevation changes.

Table 7. Distribution of DEM difference values between origSRTM1 and corrSRTM1.

DEM differences	**Proportion of affected cells**
>= 16 m	0,01%
6 - 15,99 m	2,54%
1 - 5,99 m	20,87%
–0,99 - 0,99 m	67,26%
–1 - –5,99 m	9,32%
–6 - –15,99 m	-
<= –16 m	-

As previously, the quality of the corrected DEM has also been assessed by doing cell-by-cell comparisons and calculating error statistics using the contour-based reference DTMs. Regarding the origSRTM1 it has been found that it generally underestimates the surface and the vegetation bias compensates this characteristic when considering the mean error value.

The 0.28 m ME on the corrSRTM1 is slightly lower than before, which can be associated with the reduction of the falsely positive differences of the forest patches and reducing the noise on the model. The rate of DEM differences within ±1 m got slightly reduced (26.16%) as the bumpy texture on the flat areas was smoothed. On the other hand, from the histogram of the DEM errors it is noticeable that the number of cells at the mode significantly increased (*Figure 26*). The ESD (4.47 m), RMSE (4.48 m) and LE90 (7.34 m) error metrics all show lower values, but did not change drastically. However, the improvement in the relative accuracy of the model is detectable in case of the derived land-surface parameters and objects. For example, the ambiguity with the delineation of the streamline at the decapitated valley section on the Eastern Mecsek piedmont is resolved (*Figure 27*), which is promising when considering the geomorphic applicability of the corrSRTM1.

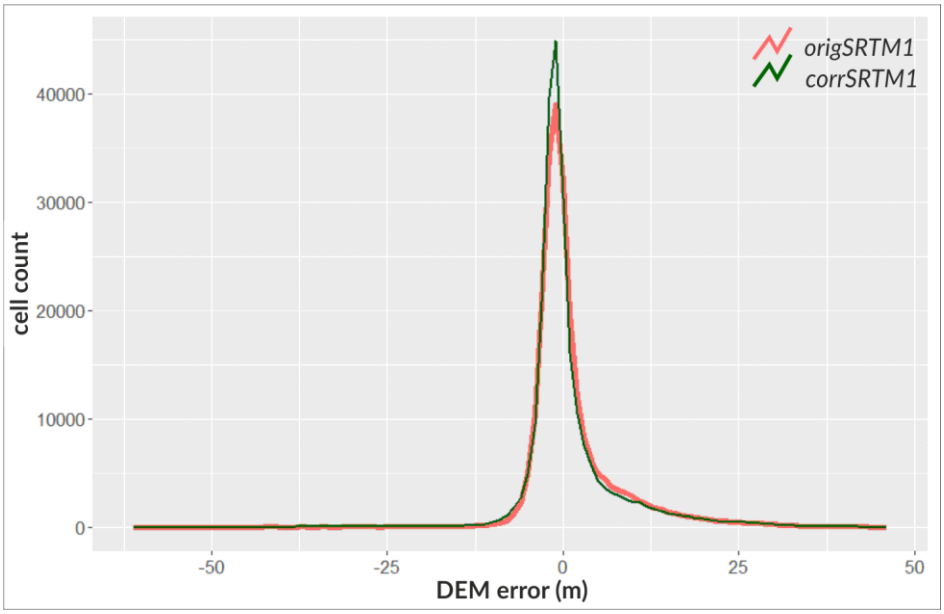

Figure 26. Frequency of elevation errors before and after the SRTM1 correction.

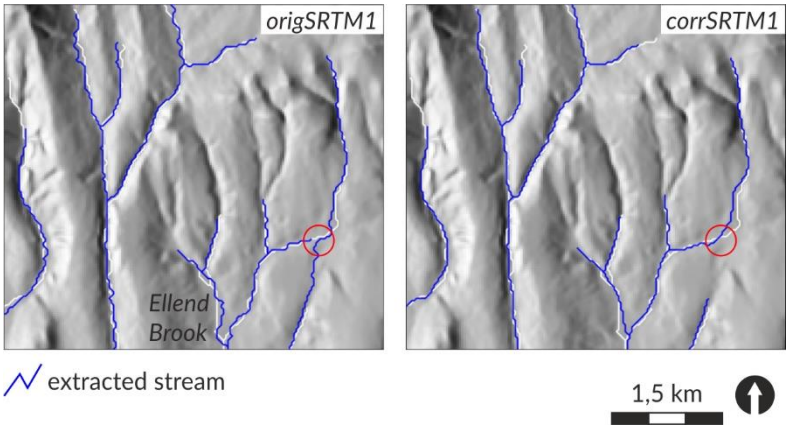

Figure 27. Stream capture at one of the unnamed tributaries of the Ellend Brook. (Exaggerated shaded relief map in the background is from the reference DTM)

5.3. Geomorphometric applications

The actual mapping techniques and the quality of the input DEMs and output maps cannot be interpreted independently, thus the presented results serve dual purpose. The primary objective is to provide an overview on the applicability of the selected and self-developed methods for digital geomorphological mapping. The secondary aspect is to reveal the advantages and drawbacks of using the *corrSRTM1* model in mapping of landforms and landscapes. The presented applications are organised according to increasing complexity of implementation and also considering the interdependence of the tasks.

5.3.1. Mapping landform elements: geomorphons at the topographic grain

Potentials and limitations of the geomorphons approach with the topographic grain-based search parameter has been tested on different terrain types over Southern Transdanubia. Previous experiences with r.geomorphon tool revealed that the character of the output geomorphometric map is highly dependent on the selected lookup distance. The search parameter should be optimised to represent the heterogenous topography well, without the disintegration of wider ridges, interfluves or valleys, yet also preserving the fine details. The clips in *Figure 28* show the Szekszárd Hills and north-eastern end of the Völgység microregion. The loess covered hills are well-dissected by the erosion-derasion valley network, loess denudation forms (dolines, steep-walled loess gorges, etc.) and 'coffins' of past slumps amongst the recent forms of the landslide prone region (Ádám, 1964). The area is lowering to the west; the smoother Börzsöny-Kakasd loess plateau is separated by the valley of the Rák Brook. The recognisable landform elements are limited by the horizontal and vertical resolution of the SRTM1 model, still when focusing on the character of the resulting geomorphometric map it is clear, that with a smaller search parameter (7 cells) even the narrower ridges and valleys are fragmented, while with a rather large value (17 cells) the valley floor seems to get overestimated and shoulders are extending to the slopes. This can be confirmed by comparing the distribution of the different landform categories over the whole study area as well (*Table 8*).

Over the heterogenous terrain of Southern Transdanubia the topographic grain method determined the characteristic local ridgeline-to-channel spacing as 330 m (*Figure 29*). The absolute relief of the area is 608.16 m, the neighbourhood matrix of 11×11 cells captures 189.68 m of this relief. This means, that with larger window sizes the relative relief is still steadily increasing and there could be other characteristic wavelengths. However, the general design of the tool is to find the local topographic grain value, which can be used to derive a

geomorphometric map representative of the typical slope lengths. Tailoring the r.tg.geom tool to find a local value was necessary, in order to keep the computational costs and processing time reasonable. The runtime of focal statistics grows exponentially with the increasing moving window sizes (Grohmann & Riccomini, 2009), which would eliminate the benefits of calculating the TG value instead of going with a trial-and-error approach to generate the acceptable geomorphometric map. When running the r.tg.geom tool for the total area of Hungary the characteristic ridgeline-to-channel value was determined as 450 m, but as represented by *Figure 28C* the geomorphometric map correlates well with the map generated using 330 m as lookup distance.

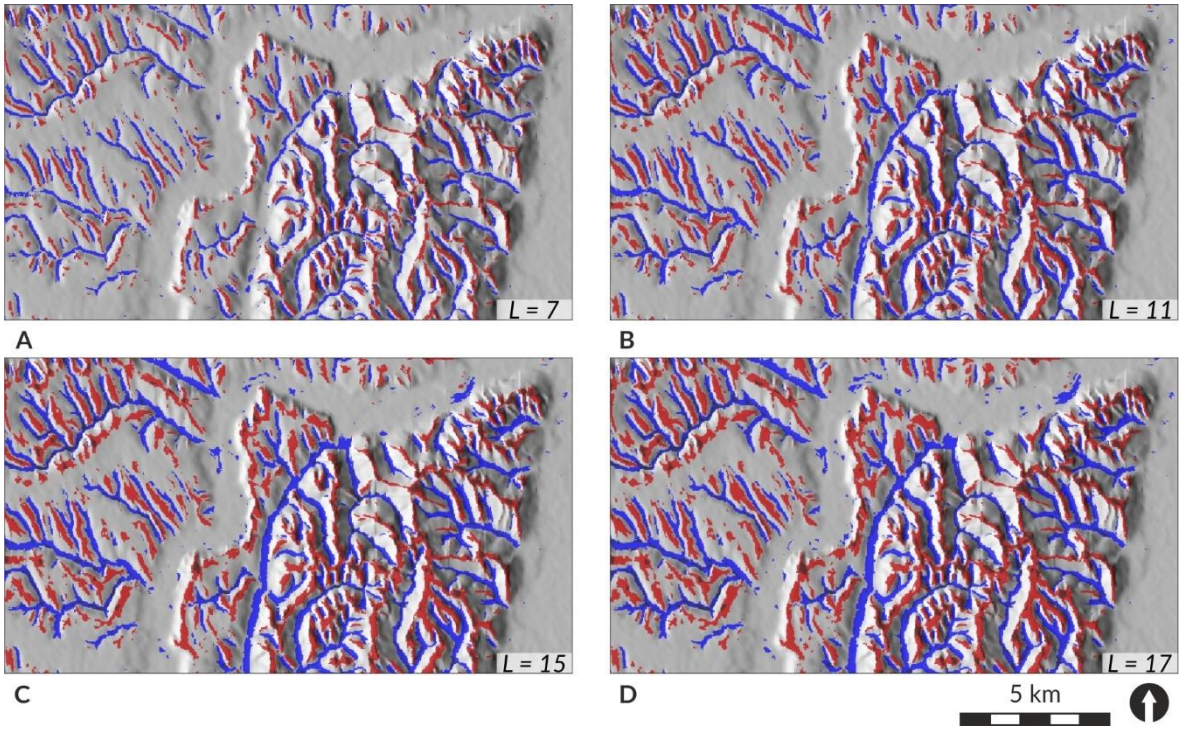

Figure 28. Subsets of the geomorphometric maps created by four different lookup distance (L) values showing the changes in the delineated pit, valley, ridge and shoulder landform elements. (Colours correspond to the header of Table 8)

Table 8. Distribution of the 10 main landform types by the different search parameters. (1 – flat, 2 – summit, 3 – ridge, 4 – shoulder, 5 – spur, 6 – slope, 7 – hollow, 8 – footslope, 9 – valley, 10 – depression)

L	1	2	3	4	5	6	7	8	9	10
7	34,28%	0,33%	4,96%	5,07%	7,30%	31,49%	5,60%	5,15%	5,59%	0,23%
11	31,59%	0,64%	7,04%	5,02%	8,36%	28,10%	6,23%	5,25%	7,32%	0,45%
15	30,03%	0,90%	8,37%	4,94%	8,81%	26,38%	6,39%	5,40%	8,12%	0,67%
17	29,32%	1,05%	8,99%	4,88%	8,99%	25,63%	6,43%	5,48%	8,42%	0,81%

The user has the option to generate a map providing the topographic grain value on a cell-by-cell basis as well (*Figure 30A*). For a better overview, the output map has been classified to only three main local TG categories. Due to the characteristics of the input corrSRTM1 model the values show a 'salt-and-pepper' appearance over the plains. The 270–330 m category dominates on most of the slopes over the well-dissected hilly and low mountainous terrains, while the wider valleys with larger TG values are also distinguishable.

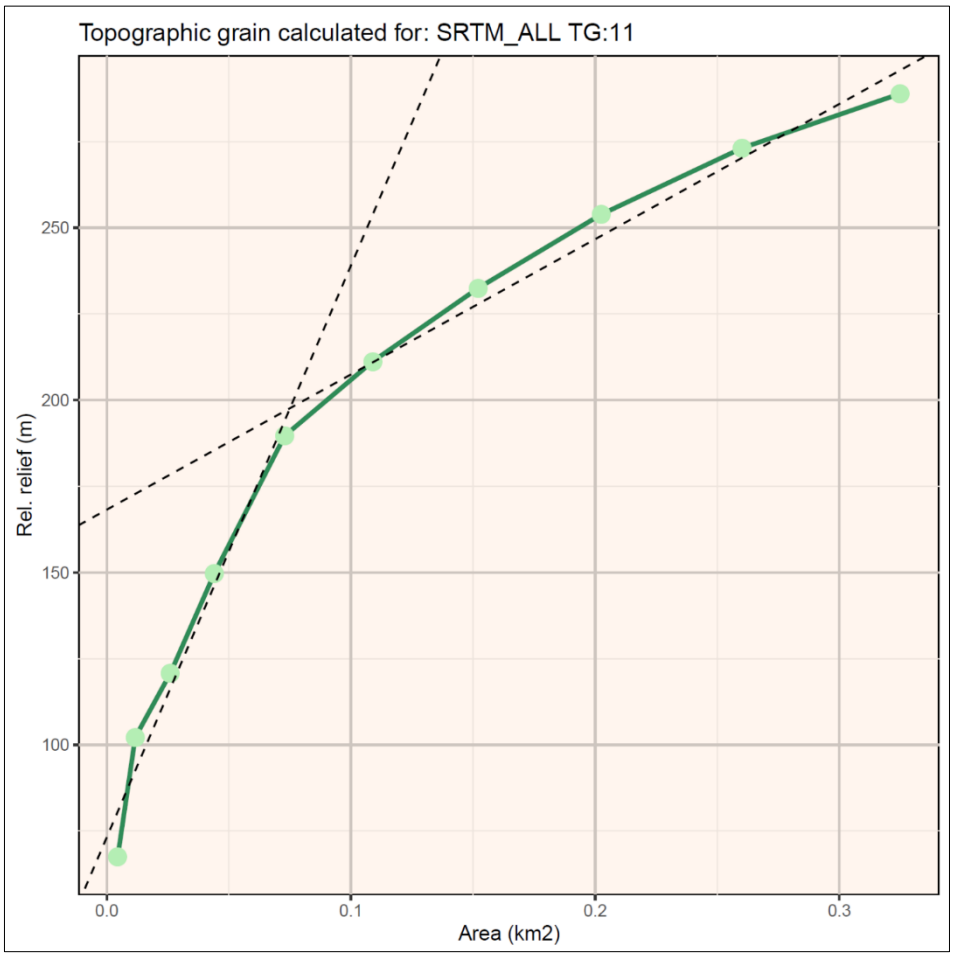

Figure 29. The resulting plot of the topographic grain calculation process in case of the Southern Transdanubia study area. (The maximum relative relief per neighbourhood matrix (green marks) is plotted against the approximated area that the moving window covers)

When considering the geomorphology of the region and the traditional approaches to map landforms, then the selected search parameter can appear as too small for geomorphological mapping purposes, however, one must note that r.tg.geom was primarily designed to work with the r.geomorphon tool. The geomorphons method adopts the Nyquist-Shannon theory in its design, as the lookup distance is eventually used as search radius. The TG value, which locally represents the characteristic length of slopes, will be actually doubled, thus making it possible to effectively delineate the representative landform elements.

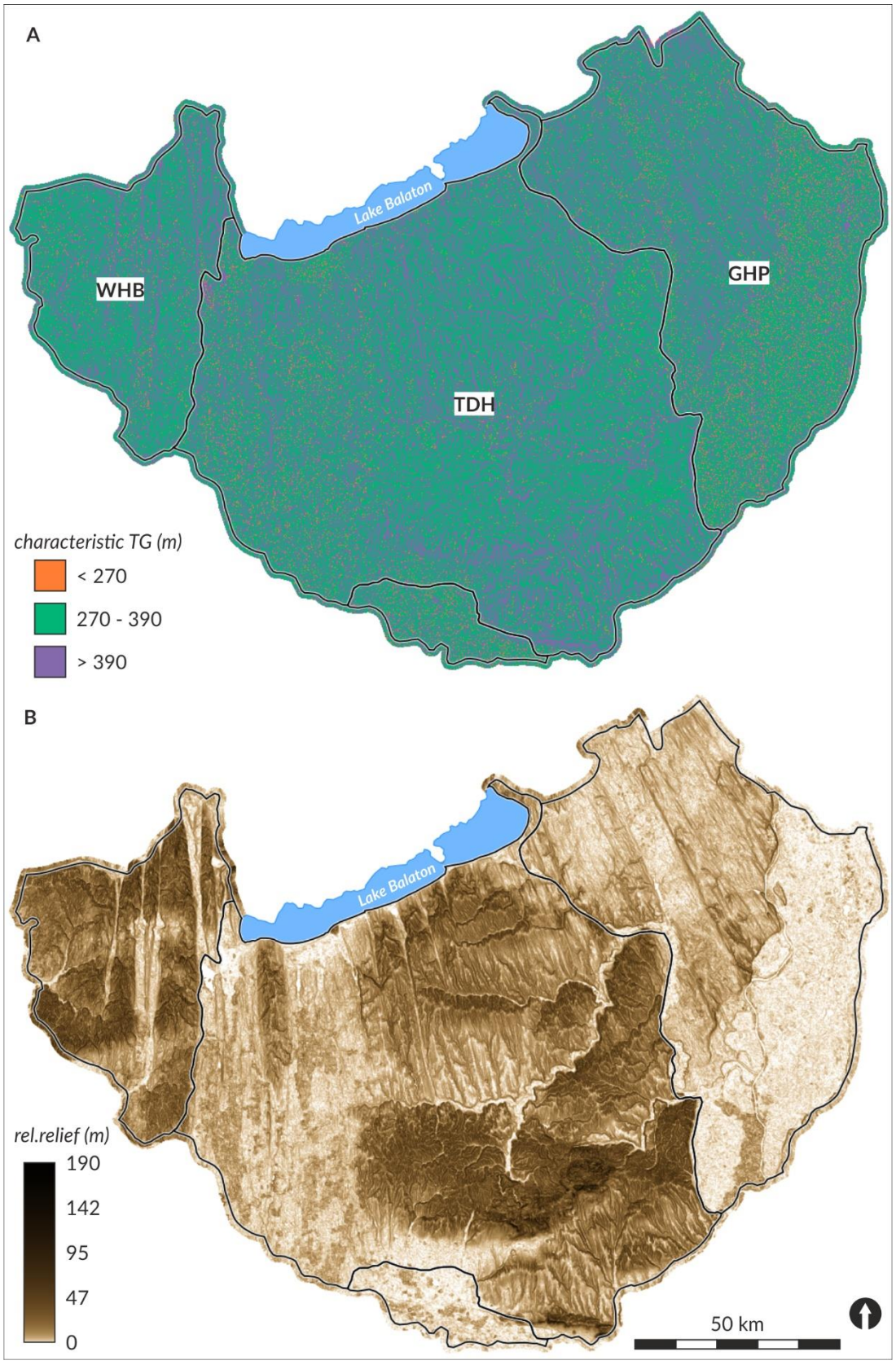

Figure 30. The characteristic TG values (A) and the associated relative relief map (B).

As a by-product of the r.tg.geom algorithm the relative relief map associated with the calculated topographic grain value can also be generated (*Figure 30B*). The map represents the relative relief values calculated with a circular neighbourhood matrix of 11 cells. Even though in the literature it is common to use 1 km^2 to define the relative relief, this map provides a better option for visual inspection. The values over flat regions are distorted by the remaining errors of the corrSRTM1 model, however, the map still provides a good overview of the spatial arrangement of relative relief in the different geomorphological landscapes.

5.3.2. Mapping the pattern of landforms: geomorphological landscapes of Hungary

Landscapes are fundamental spatial categories of geography (Mezősi & Bata, 2011), the delineation and characterisation of the different terrain types is of key importance in geomorphological mapping as well. The geomorphons-based landform map and the derived geomorphological landscape map reveal objective information about the spatial arrangement and characteristics of the topography with the potential to revise the traditional geomorphological maps.

As previously mentioned, the GeoPAT-based supervised regionalisation requires prior knowledge of the study area and the input data that is to be classified. The largest units of the hierarchic landscape system of Hungary are the macroregions i.e. Great Hungarian Plain (GHP), Little Hungarian Plain (LHP), West Hungarian Borderland (WHB), Transdanubian Hills (TDH), Transdanubian Range (TDR) and North Hungarian Range (NHR). These are territories with natural conditions significantly differing from their neighbouring regions and within their boundaries reflecting similar geomorphic characteristics (Mészáros & Schweitzer, 2002). Based on the spatial arrangement and connection of the natural factors (e.g. geology, relief, water network, soils, etc.) there are 33 mesoregions and 230 microregions with a more homogenous landscape potential on the lower levels of the system (Dövényi, 2010; Marosi & Somogyi, 1990). In addition to this hierarchical structure, the different authors discriminate different subtypes of landscapes. While these broadly coincide, their spatial delineation or exact categorisation typically varies, the boundaries don’t necessarily overlap. Exclusively on the basis of orographic and morphologic conditions the authors describe mountainous regions as medium and low mountains with narrower and wider ridges; discriminate between hills in mountain forelands and isolated hilly districts characterised by erosion-derasion valleys; and separate lowlands into the categories of flat floodplains and gently undulating alluvial plains, which are in some cases

heightened by loess or sand cover (Bulla, 1962; Lóczy, 2015; Pécsi, 1977, 1984, 1996; Pécsi & Somogyi, 1967; Prinz, 1936; Schweitzer, 2009).

In order to evaluate the DEM-based output map, a seamless reference dataset of geomorphological landscapes was necessary. The geomorphic and relief type maps available in the literature (Mészáros & Schweitzer, 2002; Pécsi, 1977; Pécsi & Somogyi, 1967) were in some cases incomplete or incompatible, therefore the microregions were classified into a primary and secondary category based on their geomorphic characteristics (*Figure 31*). For the purpose of this research each major relief type was divided into two subtypes of geomorphological landscapes resulting in six main types (floodplains, alluvial plains, low hills, dissected hills, low mountains and mountain ridges). Taking over the boundaries of the microregions to the categorised geomorphological landscapes map was reasonable because the original framework for the delineation of these spatial entities included the morpho-lithological elements, geostructural features and orographical conditions, which are key factors in geomorphological mapping (Pécsi, 1984).

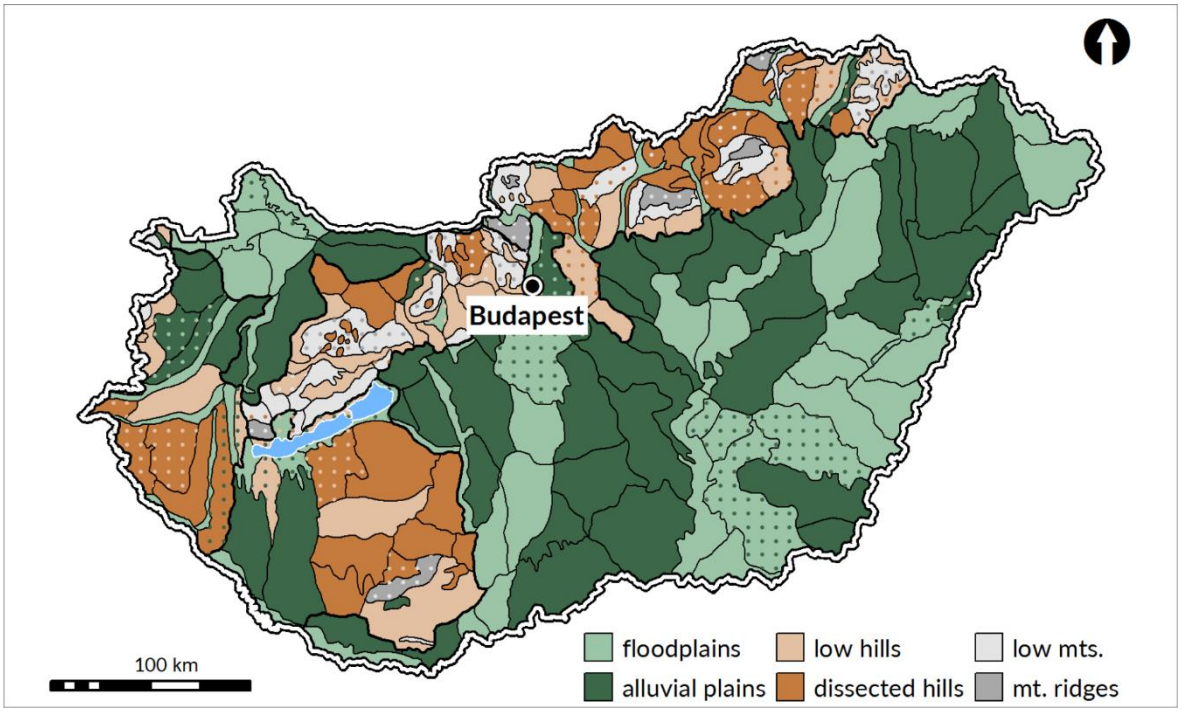

Figure 31. The microregions of Hungary classified into a characteristic geomorphological landscape category and a potential secondary type.
(Based on Dövényi, 2010; Marosi & Somogyi, 1990; Pécsi, 1977; Schweitzer, 2009)

The steps of the geomorphometric analysis from pre-processing the input SRTM1 dataset to the validation of the resulting geomorphological landscape map are outlined in *Figure 32*. As mentioned previously, the GeoPAT method was applied to the landform elements map. The r.tg.geom tool approximated 450 m as the topographic grain value, which

fits the basic rules of geomorphological mapping adopted in Hungary. Automatically the r.geomorphon module was also triggered using the TG as search parameter, 1 cell as skip radius to eliminate remaining DEM data noise and 0.7° as flatness threshold to only exclude perfect flats. The base geomorphometric map allows the statistical (*Table 9*) and spatial (*Figure 33*) analysis of the ten dominant landform elements in the country. Even though the flatness threshold was selected to represent only perfect plains as flat forms the vast majority of the cells belong to this category. On the other hand, the value is slightly lower than expected considering the literature (Schweitzer, 2009), which can be explained by the effect of erroneous cells on the corrSRTM1, where the method misinterpreted the more rugged surface of forested or built-in regions to different landform elements.

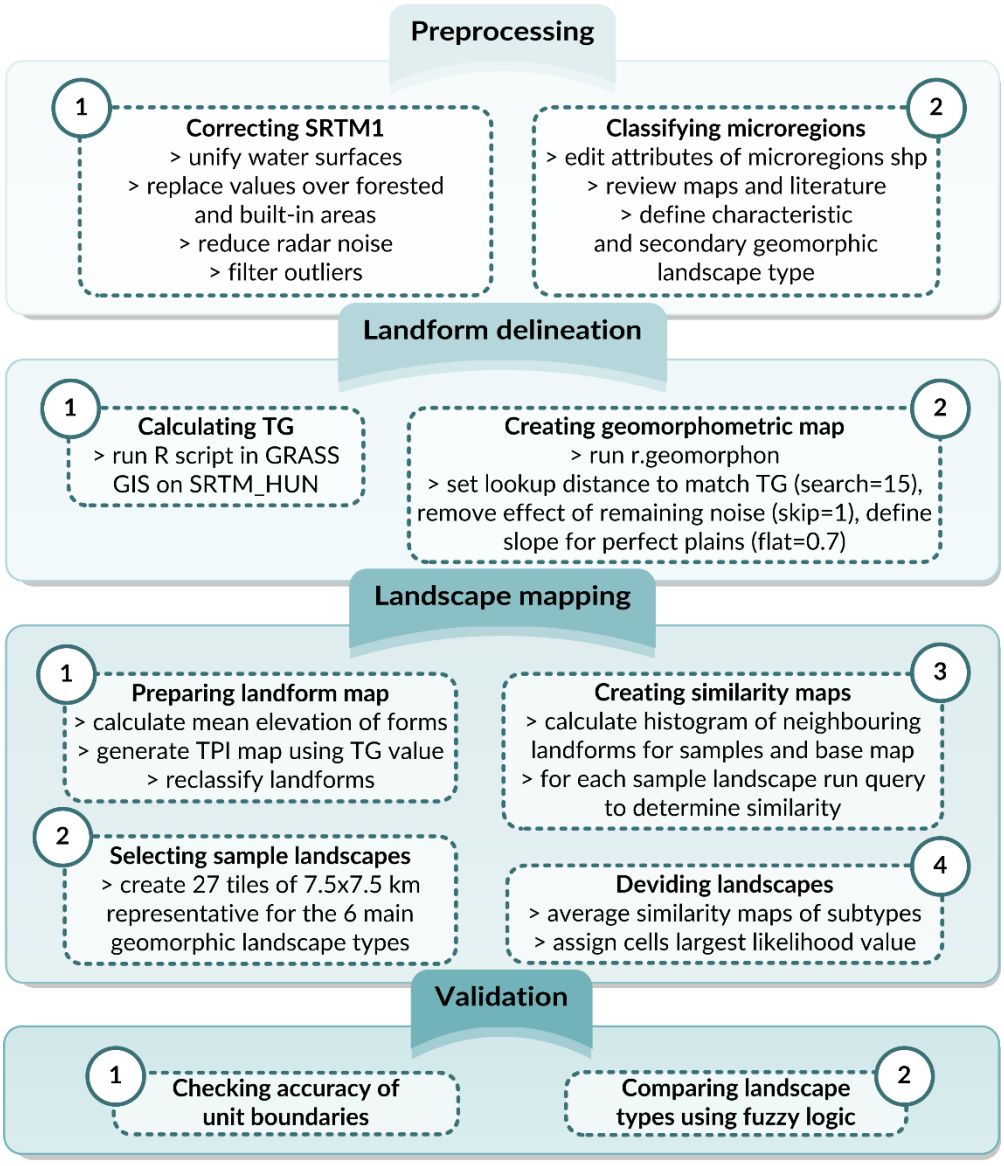

Figure 32. Flowchart of the landform and geomorphological landscape mapping procedure.

Table 9. Distribution and elevation characteristics of the 10 main landform elements. (1 – flat, 2 – summit, 3 – ridge, 4 – shoulder, 5 – spur, 6 – slope, 7 – hollow, 8 – footslope, 9 – valley, 10 – depression)

	1	**2**	**3**	**4**	**5**	**6**	**7**	**8**	**9**	**10**
proportion	52.3%	0.6%	5.0%	3.9%	6.1%	17.6%	4.5%	4.7%	4.9%	0.4%
min elev. (m)	69.6	73.6	72.3	71.0	32.3	29.9	28.9	69.7	23.5	22.6
max elev. (m)	462.4	1044.0	1031.8	831.0	1021.8	1007.8	997.6	819.4	919.0	885.5
standard deviation	25.3	127.2	110.6	37.4	111.4	93.1	103.5	35.1	88.9	86.6

The landform elements of plains show a well distinguishable pattern, even though the remaining errors of the corrSRTM1 are visible. Due to the small range of altitude in Hungary, the long-lasting denudation and the relatively minor effects of neotectonics on the landscape, the landform pattern of the hilly and mountainous environments show a high degree of similarity. The hills are typically made up of Tertiary molasse sediments and the lower regions of the mountains are also covered by loess or sand layers, thus the valleys and ridges are frequently smooth with gentle slopes (Csillag & Sebe, 2015). Characteristic N–S, NW–SE oriented valleys appear in the Transdanubian Hills, the western parts of the Great Hungarian Plain and the eastern region of the West Hungarian Borderland. Even though the general wind directions in Transdanubia coincide with these wide, meridional valleys dissecting the alluvial plains, it was proven that they have complex erosion-deflation origin (Pécsi, 1996; Sebe et al., 2011).

The raster map of the landform elements provides the opportunity to visually analyse the characteristics of the topography, but more importantly, the dataset allows for the automatic separation of landscapes by following a predefined set of rules. For the landscape search step of the GeoPAT process 27 representative study scenes were selected with 7.5×7.5 km spatial extent based on expert-knowledge of the typical geomorphological landscapes (*Figure 34*). For a good representation of the varying topographic characteristics 4–5 sample sites per geomorphic type were scattered across the country (*Figure 33 & Figure 34*). To successfully discriminate geomorphic landscapes of hills and mountains it was unavoidable to calculate auxiliary morphometric parameters and reclassify the original map of landform elements. The Topographic Position Index (Weiss, 2001) was used to separate flat top surfaces or valley bottoms. By calculating the mean elevation of summits, it was possible to distinguish between peaks of mountain ridges (above 400 m), outlier values on plains (below 100 m) and top surfaces in hilly regions (between 100–400 m).

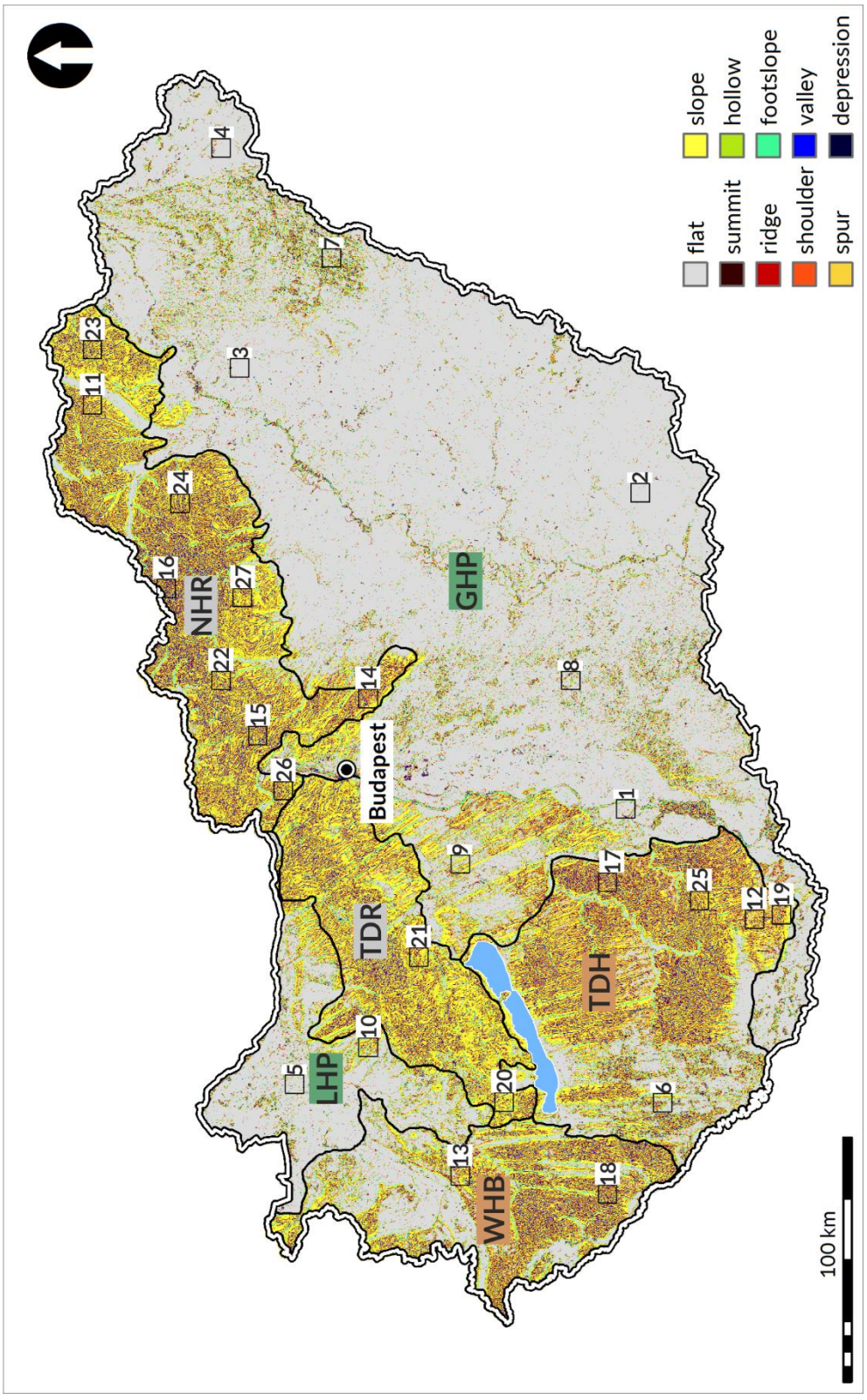

Figure 33. Geomorphometric map of Hungary with the locations of study scenes and boundaries of macroregions.

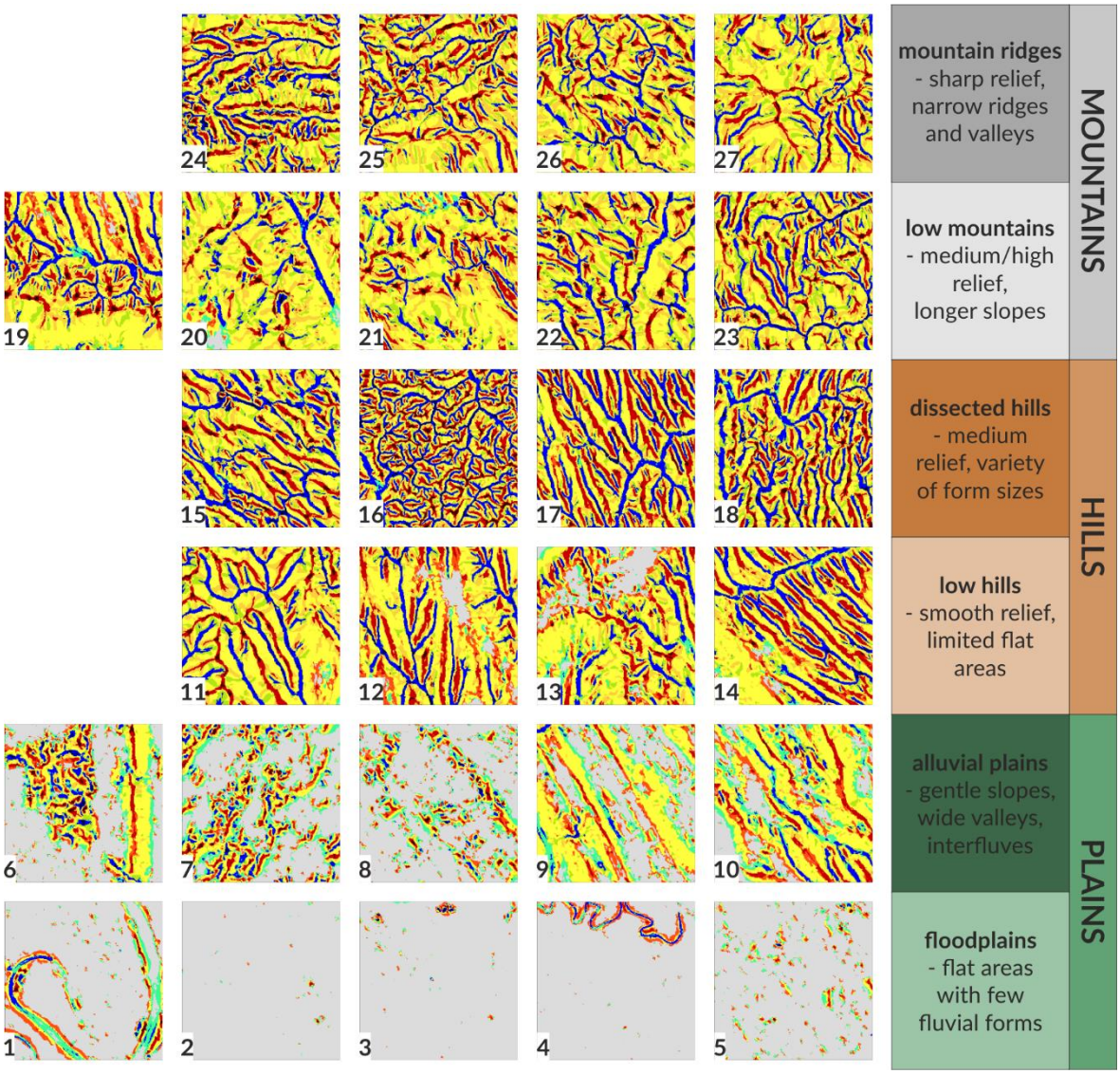

Figure 34. Landform elements of sample sites and description of analysed geomorphological landscape types. (Colours correspond to the legend of Figure 33)

In the next step the similarity maps of the given categories were averaged and lastly the six major landscape types were separated based on the maximum likelihood value of the cells. However, as an intermediate step, the similarity maps of the 3 main landscape types were also derived to visualise the spatial distribution of likelihood values (*Figure 35*). The hilly and mountainous regions are clearly distinguishable from the plains. On the other hand, as the characteristics of different landscape types (e.g. well-dissected hills and low mountains) are not so significantly distinct and the types are transitioning into one another, the similarity maps represent fuzzy boundaries instead of crisply defined regions. In the TDR and the NHR it can be observed, that the group of cells possibly belonging to mountains are surrounded by regions more similar to the hilly category. On the southern part of Transdanubia, in case of the Mecsek Mountains and Tolna-Baranya Hills it is more difficult

to separate these types. Flat landscapes show relatively smaller values of similarity, this being particularly evident over the nearly perfect plain between the Tisza, Körös and Maros rivers. This characteristic is related to the design of the tool; the number of landform elements falling into a tile is smaller over plains, thus a smaller number of meaningful and diverse input features can be used in the landscape search process (Jasiewicz et al., 2014).

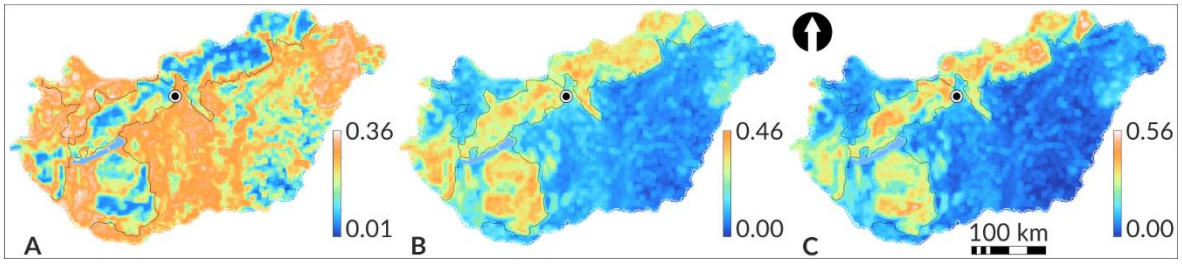

Figure 35. Spatial distribution of the likelihood values by the main geomorphic landscape types. (A – similarity map of plains; B – similarity map of hills; C – similarity maps of mountains)

The final map of geomorphological landscape types (*Figure 36*) was created by assigning every cell the category of the highest likelihood value from the six similarity maps. Due to the principles of the mapping technique the resulting map could only be prepared with ~1 km cell size despite the ~30 m resolution of the geomorphometric base map. Within the limits of DEM resolution and applied mapping scale, the output map is a realistic semi-automatic interpretation of the main landscape types on a lower level of generalisation than other published maps from global geomorphometric projects (Csillik & Drăguţ, 2018; Drăguţ & Eisank, 2012; Iwahashi, Kamiya, et al., 2018; Iwahashi & Pike, 2007). The map is a further element of a Digital Geomorphological Information System, and deeper analysis can be executed upon this dataset. The raster map could be converted to a set of vector polygons, and using overlay operations and incorporating auxiliary general geomorphometric parameters (e.g. slope, relative relief, shaded relief) it would be possible to update the boundaries of the geomorphological landscape types.

After the visual comparison, a strong similarity was expected between the expert- and algorithm-based maps, which was indeed confirmed by the statistical analyses. The most evident way to compare the reference map (*Figure 31*) and the result of the geomorphological landscape mapping algorithm (*Figure 36*) was to calculate the proportion of the main landscape categories. On the reference map 69.7% of the microregions belong to plains, 24.0% to hills and 6.3% to low mountains. In case of the raster dataset 70.9% of the cells were categorised as plains, 22.2% as hills and 6.9% as low mountains.

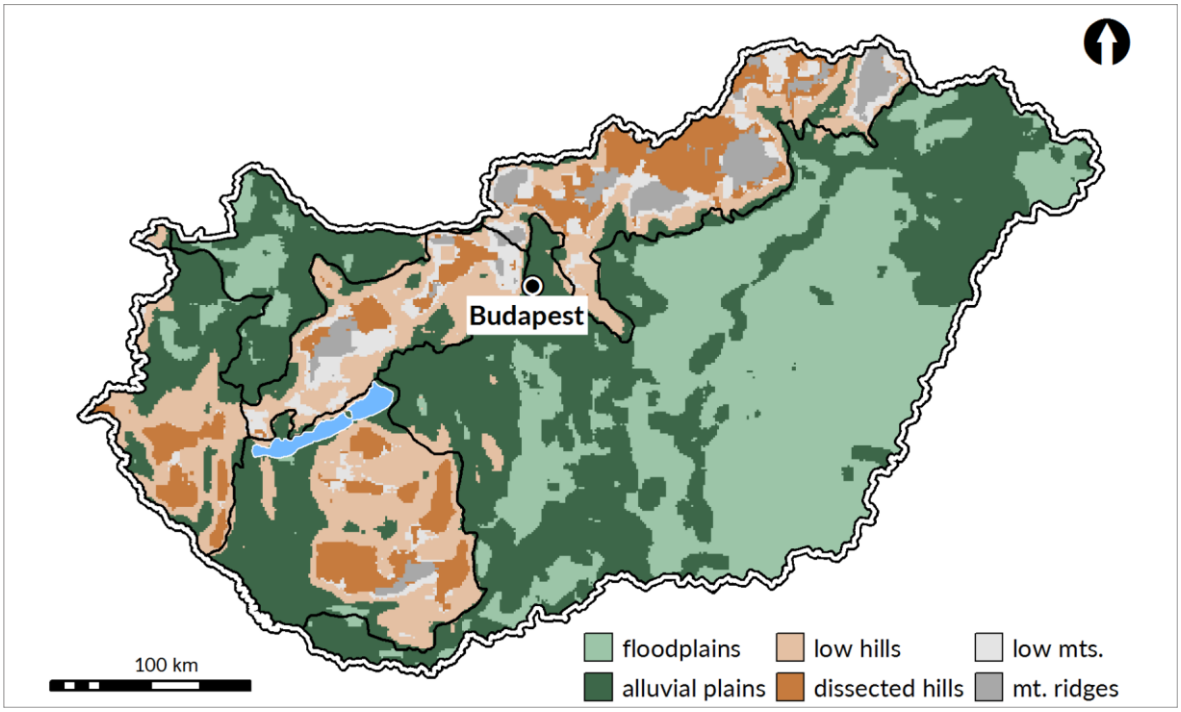

Figure 36. Algorithm-delineated geomorphological landscapes.

Table 10. Distribution of macroregions and results of validation.
(Colours represent the main geomorphic landscape types from Figure 31)

	proportion	*matching micro-regions/all*	*characteristics of landscape types*
GHP	55.1%	55.5/70	somewhat unclear expert categories missing units of alluvial plains
LHP	5.8%	9/12	floodplains underestimated alluvial plains correctly located
WHB	7.9%	17/25	mapped units better represent complexity floodplains misinterpreted
TDH	12.3%	16.5/25	expert map generalized reinterpretation is suggested
TDR	7.0%	22/47	mostly correct boundaries identification of categories varies
NHR	11.9%	37.5/68	automatically mapped categories represent relief types well

A more complex part of the quality assessment was the fuzzy category comparison on the basis of the microregions (*Table 10*). In every macroregion it was checked how many of the microregions were categorized correctly to the most dominant geomorphological landscape type, which meant the category represented by the majority of cells in the given area. The comparison was carried out in a sense of fuzzy logic, because half scores were given in cases when at least the main landscape type was correctly identified. The best match

was detected on the Hungarian plains, while relatively low number of microregions were appropriately categorised in the mountain ranges. However, one must bear in mind, that in several regions the expert-maps and literature were also not in agreement, as depicted by the secondary categories in *Figure 31*.

Most of the differences between the traditionally and semi-automatically derived datasets were expected. Distinguishing floodplains and alluvial plains based on a landform map that shows unreal features over wooded floodplains (e.g. Gemenc floodplain forest on the right bank of the Danube's southern course) was challenging, even with the supervised classification technique. The topographic similarity of hilly and mountainous environments mentioned above was also proven by the observations made during the quality assessment. However, on the reference map due to generalisation, the extent and spatial arrangement of the landscape types are not necessarily representing the real topography in every region, while the DEM-based approach was able to reveal the heterogeneity. On the other hand, as the resulting boundaries were obtained using an elevation dataset still loaded with erroneous height values, it is not possible to directly apply this map to update the questionable areas on the traditional relief type or geomorphological region maps.

5.3.3. Mapping a specific landform: Extracting terrace remnants along the Danube

In order to perform the terrace analysis, it was necessary to divide the region from Almásfüzitő to Esztergom by clearly recognisable structural-morphological boundaries. The microregions were found to be too generalised for the operational scale of the terrace extraction. The base-level, drainage density and stream-gradient index maps were prepared to reveal existing hydrological-geological-geomorphological borders (Jacques, Salvador, Machado, Grohmann, & Nummer, 2014; Józsa & Fábián, 2017; Józsa & Szeberényi, 2016; Luo & Stepinski, 2008); these were then visually interpreted and the whole area was divided into seven characteristic sections as shown on the map in *Appendix 7C*. The identified sections are the following: (1) Almásfüzitő Embayment, (2) Western slopes of Gerecse, (3) Western Gerecse, (4) Central Gerecse, (5) Eastern Gerecse, (6) Tát-Esztergom Embayment, (7) Esztergom Castle Hill.

With the intention to compile a unified knowledge base about the terrace levels in the Gerecse foreland several former studies have been consulted (Bugya, 2008; Bulla, 1941; Kéz, 1934; Pécsi, 1959, 1971, 1991; Ruszkiczay-Rüdiger et al., 2005). Over the more than 100 years of the Hungarian terrace morphological research there has not been a satisfactory synthesis of the spatial arrangement and chronology of the terrace levels. The above-

mentioned publications all include a number of uncertainties. All in all, one can conclude, that the most widely accepted terrace system for the Hungarian stretch of the Danube valley is still the summary published by Pécsi (1959). The terrace levels relevant in the AOI are listed in *Table 11*, these are displayed on the resulting plots to compare the GIS-based results directly to the reference data. Another challenging, yet essential, task for the validation of the automated terrace extraction results was to reinterpret and digitise the expert-based geomorphological map of the region (Schweitzer, 1980), to have a georectified vector layer of the landforms without overlapping or not touching polygons. The scanned geomorphological map is presented in *Appendix 9*.

Table 11. Terrace levels in the Gerecse Mountains according to Pécsi (1959).

Right bank settlement	Distance from mouth (km)	0 level of Danube (m a.b.s.l.)	m above Danube level								
			FLP (low)	I	II/a	II/b	III	IV	V	VI	VII
Szőny	*1753*	*103.18*		5	10	23		78			
Dunaalmás	*1751*	*103.13*	3	5	10	27	47	78	120	170	210
Neszmély	*1749*	*103.05*	3	5	9	22	37	72	120	150	210
Süttő	*1743*	*102.58*			8		43			170	170
Lábatlan	*1737*	*102.11*	3	5	7			72		160	200
Nyergesújfalu	*1733*	*101.95*		5	9	20	46	68		140	170
Tát	*1727*	*101.61*						80			
Esztergom	*1718*	*100.92*	2.5	6	10	18	48	78			

For the seven separated sections of the study area the r.terrace.geom tool has produced over 600 explanatory plots of the parallel analysis stripes, which can be reviewed to understand why given cells were marked as terrace candidates. The information vital to draw conclusions about the general terrain characteristics and the possible terrace levels in a section are the following:

- the plot showing the determination of maximum slope and minimum extent thresholds per altitude,
- the swath-profiles representing the minimum, mean and maximum elevation statistics of the section,
- the frequency diagram depicting the number of terrace candidate cells and literature-based terrace levels,

- the long profile of the Danube section with marks at possible terrace remnant elevations.

The mentioned results of Central Gerecse (section 4) were selected for detailed presentation here (*Figure 37*), while the other outputs are shown in *Appendix 8* (numbering according to the sections listed above). The section has clearly defined boundaries in the valley of Bikol Brook from West and Bajót Brook from East. The terrace level details relevant for this section are from Süttő, Lábatlan and Nyergesújfalu (*Table 11*). Based on the moderate, but well dissected topography of the region the trendline of maximum slope threshold changes from 5% to 8.5%, while the minimum extent rate of surfaces under 13% drops to 65% in the higher elevations, confirming the necessity of flexibly changing thresholds (*Figure 37A*). The swath-profile is meant to provide an overview of the whole section and the axes are adopting to the vertical range and width of the analysed area (*Figure 37B*). According to the traditional geomorphological map, terrace levels could be expected in a 5–6 km wide stripe along the Danube. As the Central Gerecse holds the highest peak (Nagy-Gerecse, 634 m) of the AOI, the represented elevation range is larger and the small height differences between the low terrace levels are generalised. In this region the floodplain and lower terraces are narrowing, which can be seen from the different appearance of the maximum and minimum profiles. By taking a closer look at the minimum curve two levels can be separated within a 10 m relative elevation range: a narrow level occurs around 20 m where terrace II/b could be expected, then terrace III. around 40 meter is not clearly recognisable on the minimum curve, but a clear step is visible on the maximum curve. Terrace IV., which should be found around 70 meter is not clearly recognisable on any of the elevation profiles, the step like form at this height on the minimum curve is too far inside from the bank, likely related to a valley floor. According to the literature, terrace V. is not occurring in the region; a break on the maximum curve around 150 m indicates terrace VI.; a bend at 170 m is also noticeable as per terrace VII. The frequency diagram in *Figure 37C* is in general agreement with the above findings: there is a high peak at 8 m, the level around 20 m is not clearly recognisable, the next peak appears around 40 m, a less dominant increase is seen in the height of terrace IV., then there is a peak around 100 m, but this is not mentioned by the literature, lastly the terrace levels in the higher regions are not decisive on the curve. The location of the cells seemingly belonging to terrace V. requires further investigation. *Figure 37D* provides an overview of the spatial arrangement (along the river profile), elevation ranges (colour) and spatial significance (tone intensity) of the terrace remnant candidates. The missing floodplain and lower terrace levels can be noticed in the

mid-section. In higher altitude ranges there are clearly less terrace remnants found, however, as the dividing slope between those is longer, they can be better grouped. This figure also suggests the possible occurrence of terrace V. between 200–220 m. Even though, these plots provide meaningful insights about the flat, terrace-like surfaces of the section, further analysis is required based on a map of the extracted terrace candidate cells (*Figure 38*).

The resulting map is presented as it was generated by the tool, overlaid by the terrace boundaries digitised from the traditional geomorphological map (*Figure 38A*). As per visual interpretation it can be concluded, that a low pass filter would improve the quality of the map by removing the small groups of cells along valleys and cleaning the rugged edges of the terrace remnants. However, the cells around peaks, top-surfaces should be kept as those are possibly what remained from the higher-level surfaces (Bugya, 2008). When compared with the geomorphometric map (*Figure 38B*) it can be seen, that oftentimes these slivers are along valleys, therefore likely resulting from the attempt to exclude valley floors from the terrace cells. On the other hand, it should be noted as well, that the number of these remaining cells is negligible, therefore these could not significantly distort the statistical analysis of terrace surfaces. Another obvious characteristic of the map is that several non-north facing cells were also selected as terrace candidates. This issue could possibly be avoided with an extra filter to omit cells with irrelevant slope exposure values, but this factor was not accounted for in the original method either (Demoulin et al., 2007).

Overall, the floodplain and lowest terraces have been found well, however, it is difficult to distinguish levels on the corrSRTM1 model considering its horizontal and vertical resolution. In the higher regions the method was moderately successful in mapping terrace-like surfaces. The interpretation of geomorphological levels in this region is complicated, as possible terraces of the tributaries (e.g. Által, Bikol, Bajót brooks), remnants of landslides and the eroded pediment surfaces could also show characteristics that the software considers as terrace-like. Auxiliary geological data and stricter maximum elevation thresholds could be useful to reclassify or remove these.

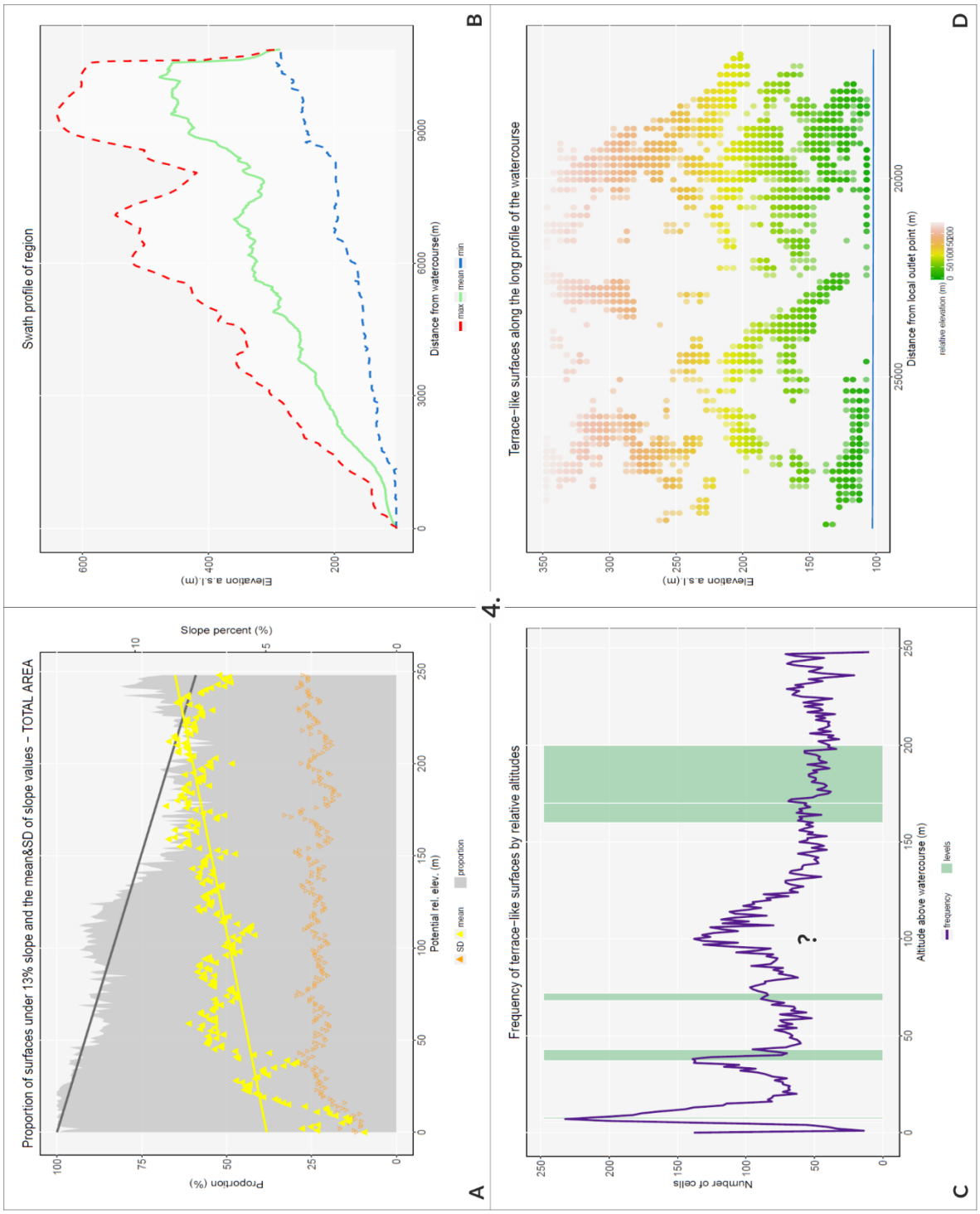

Figure 37. Plots from the output report in case of Central Gerecse.
(A – showing the determination of thresholds, B – swath-profile, C – comparison of automatically extracted cells to terrace levels from the literature, D – long profile with altitudes of terrace remnant candidates).

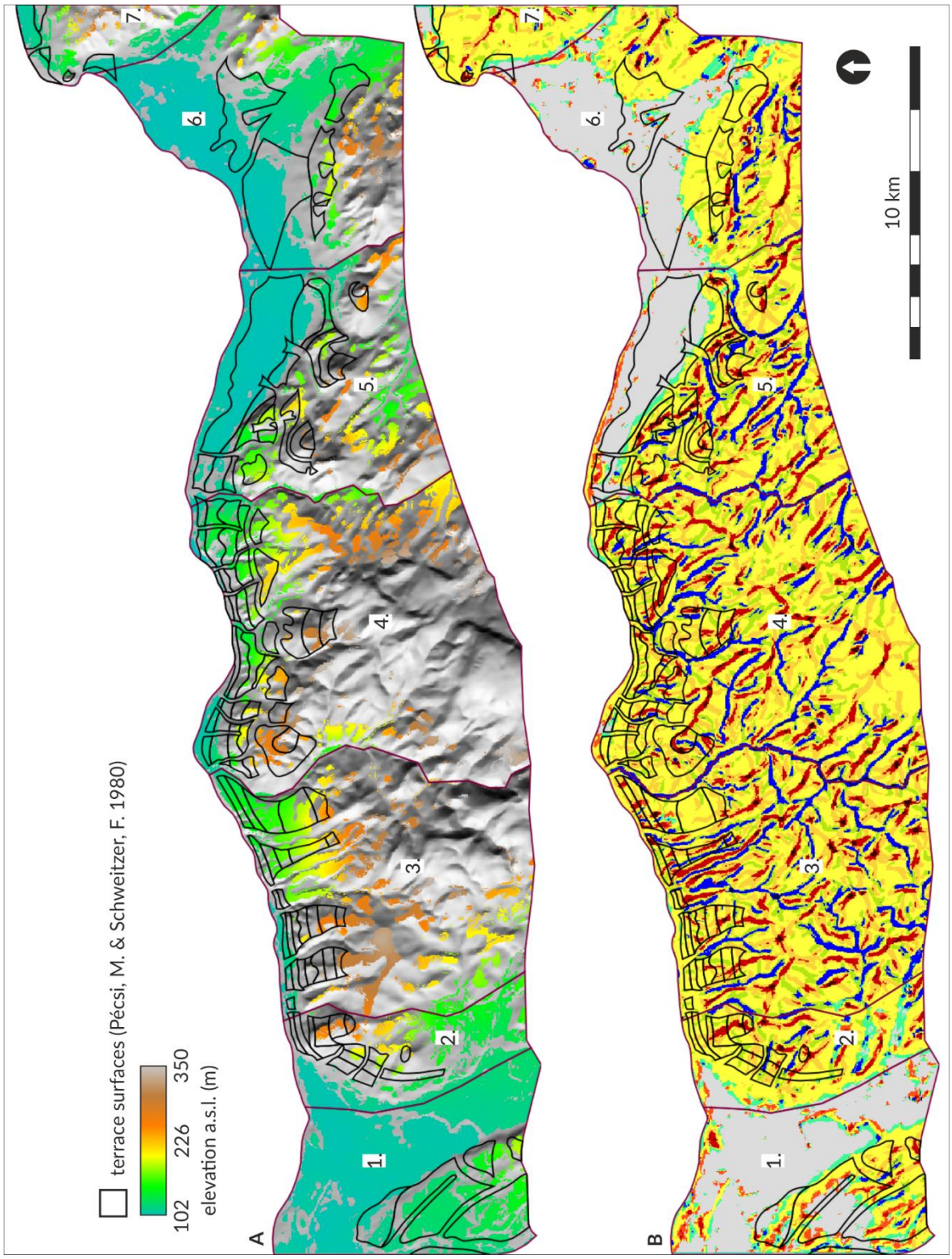

Figure 38. The output map depicting the possible terrace-top surfaces (A) and the geomorphometric map of the ten most common landform elements (B). (Landform categories in Figure 38B correspond to legend of Figure 33)

In *Figure 39* the terrace candidate cell numbers in all seven regions are combined and compared to the terrace levels from the literature. By excluding values below 8 m relative to the Danube level, the most significant peaks are found between 10–14 m and 20–22 m; cell count moderately increases between 26–30 m, 38–40 m, 54–58 m, 72–76 m, 98–102 m and 114–118 m; while in higher ranges only a slight fluctuation is noticeable on the curve (156–158 m, 190–196 m, 242–246 m). Bugya (2008) found that a significant number of peaks and thicker layer of Quaternary sediments coincide in the following elevation ranges: 10–19 m, 20–29 m, 40–49 m, 60–69 m, 80–89 m, 90–99 m, 110–119 m, 170–179 m, 200–209 m, 250–259 m. Both studies detected a level around 80-100 m, which has not been clearly described in other literature. Bugya (2008) concluded that this level possibly aligns with the Nyergesújfalu–Tokod high bluff section elevated by a thick loess cover (15–20 m), which has been mentioned, but not included in the summarising tables or general overviews by Pécsi (1959, p. 100).

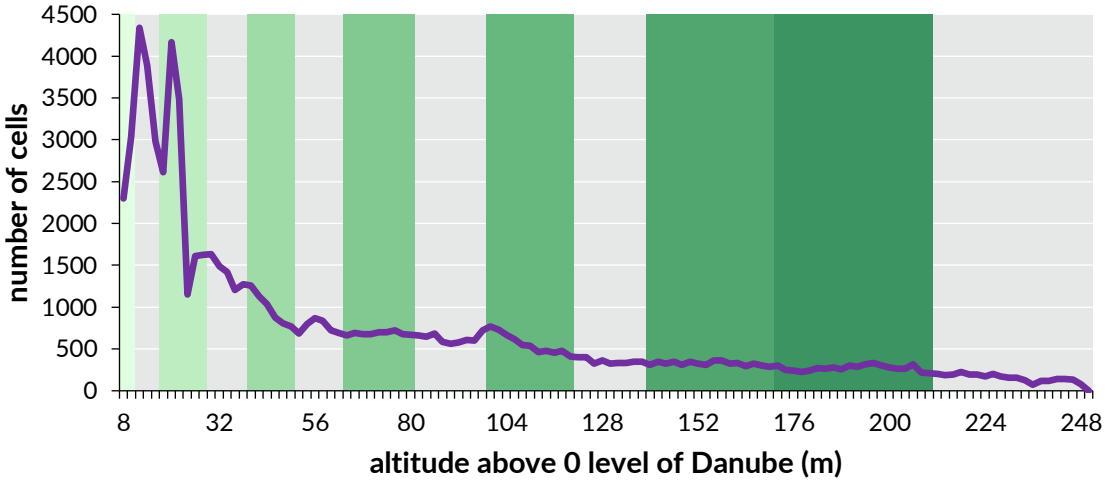

Figure 39. Frequency distribution of terrace candidate cells over the whole study area (purple curve) compared to the terrace levels documented in the literature (green bars).

6. Discussion

6.1. Comparative analysis of the GDEMs

The findings of the absolute accuracy assessment presented in *Chapter 5.1.1.* are in good agreement with the previously published validation reports: the error statistics over the bare surfaces match the DTED and HRTI requirements respectively; the typical differences of the DEM processing techniques are reflected by the different vegetation bias values and the varying correlation between the models; the relation of the DEM differences to the possible underlying causes (relief, slope, aspect, canopy density) also shows the expected characteristics. As the outliers are excluded by applying the 3-σ rule and the speckle noise only has a magnitude of 1–3 m, these error components are not reflected so strongly in the statistics. At this point of the analysis – making a compromise on the resolution and the unavoidable bias of vegetation and man-made objects – all the GDEMs could be considered as vital input for semi-automated geomorphological mapping. The exaggerated shaded relief view is a quick and easy way to get a preliminary impression about the landforms and artificial features represented by the models (*Figure 40*). The sensitivity of the land-surface parameters and objects to the DEM errors makes these derivatives a suitable tool to select the elevation model performing best from a geomorphic aspect.

The MERIT DEM is a promising step towards an error-free, globally uniform elevation dataset. The coarser resolution can be viewed as its drawback, causing a decrease in slope values and the different pattern of the drainage network as the flow barrier features are less distinctive. The applied smoothing algorithm could be further tuned as the flat top surfaces (e.g. loess covered plateaus) or wide valley bottoms still show speckle noise. The 30 m SRTM1 model is eventually a good compromise because once the relief exceeds the average height of the surface objects, the topographic features are well represented, the distortion of the landforms is not directly detectable. The mining sites and water contaminated cells are definitely leading to the occurrence of outliers, but by improved land cover masks and simple focal statistics these cells were treatable (*Chapter 5.2*). The AW3D30 model did not live up to the expectations; the frequent occurrence of outliers and the visible variation of the quality based on the number of stacks question the reliability of the model for geomorphological analyses. Although it is tempting to use the TDX12 model, considering its high resolution

and exceptional precision, it has been found that on the 12 m cell size the fluctuations of the canopy cover, tree avenues, road cuts, levees, etc. are misinterpreted by the terrain analysis tools as different landforms or inaccurate streamlines. It has also been noted that the typical errors of GDEMs are resulting in a 'salt-and-pepper' appearance of the geomorphons output map, and eventually lead to the underestimation of the TG values.

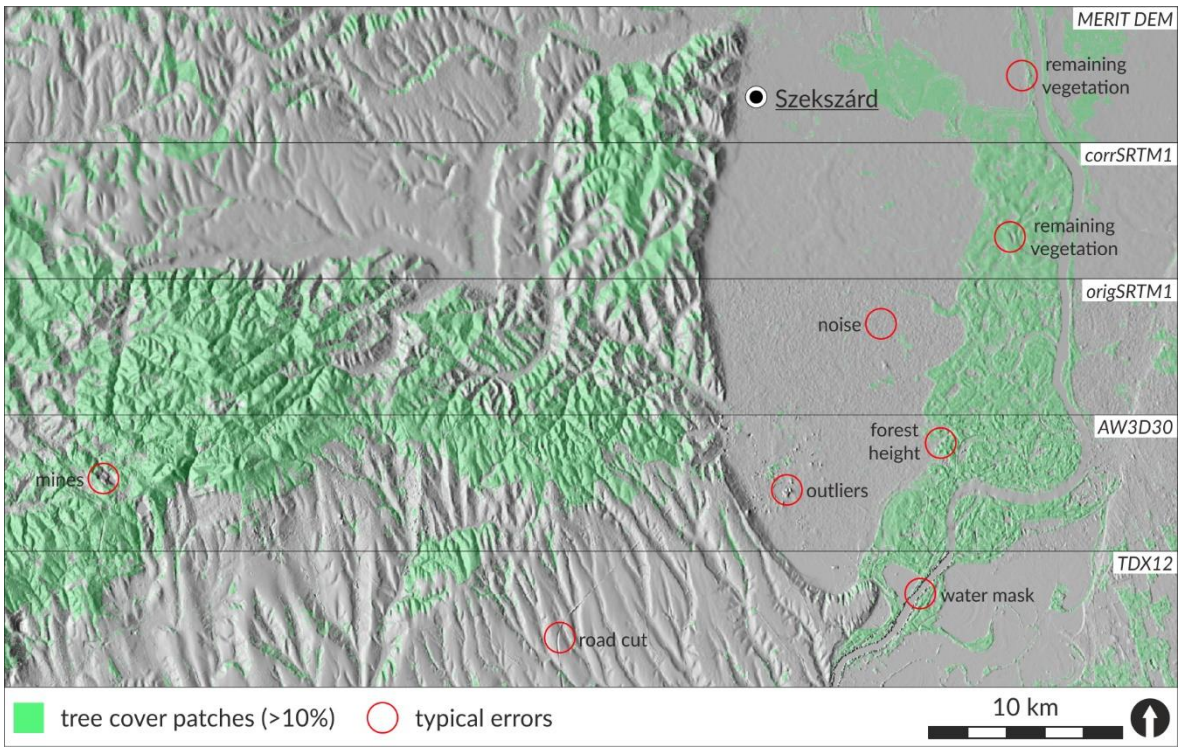

Figure 40. Exaggerated shaded relief maps showing the area within the bounding box of the EM and TS quality assessment regions representing the different typical DEM errors.

Finally, to further assess the results of the vegetation offset removal, the corrSRTM1 and MERIT DEM were compared by DoD creation, exaggerated shaded relief maps and cross-sections. In case of the MERIT DEM the level of detail had less emphasis, the primary goal of the author was to remove the pseudo-topography caused by the forests, especially over floodplains (Yamazaki et al., 2012, 2017). This resulted in a visually pleasing estimation of the terrain, however, the underlying microtopography was also erased (e.g. former channels, oxbow lakes). Applying a tree height map and ICESat observations, even if interpolation was used for up-sampling the data to the 90 m resolution, yielded better results over the area of Gemenc. The method compiled in the current study had difficulties in estimating tree heights over large forest patches. On the other hand, in case of the Eastern Mecsek study area it can be noticed even by visual inspection that the vegetation bias removal on the MERIT DEM undercut the original topography.

6.2. Possible utilisation of the Hungarian case studies

The specific geomorphometric analyses have been performed on rather larger scales, on the 1st, 2nd and 3rd level of the study areas' hierarchy. As mentioned earlier an important aspect of executing these mapping projects was to prove the applicability of the corrSRTM1 model coupled with state-of-the-art digital terrain analysis tools (two of which were implemented by the author) in semi-automated geomorphological mapping. The general overview of the results suggested that the selected GDEM and GRASS GIS methods are fitting for the task of delineating landform elements, classifying geomorphic regions and extracting terrace like surfaces. A closer look at some local examples can be helpful in revealing the potentials and limitations of the results for geomorphological researches in Hungary.

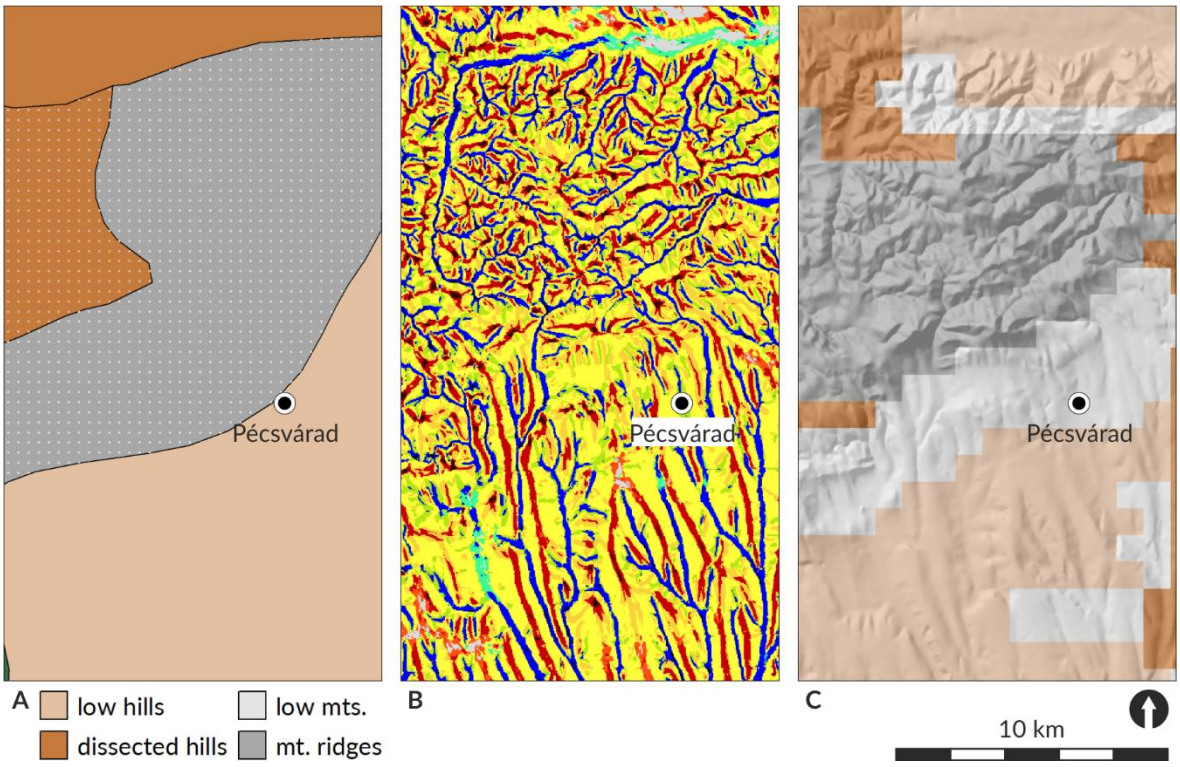

Figure 41. Subset of the expert-based geomorphological regions map (A), geomorphometric map (B) and GeoPAT algorithm-delineated geomorphic landscapes (C) over the EM study area.

The Eastern Mecsek Mountains study area has been selected to present the quality of the geomorphometric map, and showcase the similarities and differences between the expert-based and algorithm-delineated geomorphic units (*Figure 41*). Over the past years the author and co-authors have expressed the superiority of the geomorphons approach over other landform delineation tools in different publications (Józsa, 2014, 2016; Józsa & Kalmár, 2014; Sărășan et al., 2019), therefore the selection of the method has not been discussed in the dissertation. From the subsets on *Figure 28*, *Figure 34*, *Figure 41B* the reader can verify

that the landform elements are represented reasonably well on the resolution of the corrSRTM1 model. The boundaries of the expert-based geomorphological regions on basis of the microregions are rather generalised. Based on the 10 most common landforms the GeoPAT tool was able to classify the region into the categories of low hills, dissected hills, low mountains and mountain ridges. The central region with the radial horst ranges surrounding the highest mountain tops (Dobogó, Hármashegy and Zengő) has been correctly identified as the mountain ridges class. The northern foreland mainly belongs to the low hilly region of the Völgység, but the more dissected topography of the Mecsekhát is also recognised by the method. The Mecsekalja region is also separated into two geomorphic regions. It appears that the algorithm managed to distinguish the pre-pedimentation denudation level and oldest piedmont level from the gently sloping interfluves of the accumulation glacis (Pécsi, 1963). As presented by this local example, the algorithm-delineated geomorphic regions can provide a reasonable representation of the topographic variability (dissection, relief), however, some misinterpretations can still occur and the boundaries are not completely precise due to the 1 km cell size. A practical aspect of the GeoPAT-based landscape search – that has not been covered in the dissertation – is spatial decision support. Regions with similar geomorphic qualities could be easily retrieved, even on a global scale (Jasiewicz et al., 2015).

Compared to other GIS approaches that aim to map terrace surfaces at different stages of erosion (Bugya, 2008; Demoulin et al., 2007; Stout & Belmont, 2014), the novelties of the r.terrace.geom tool are the followings: the subjective interaction from the user is limited, the thresholds are adapted to the local topography and the results are not only statistics and plots to support the recognition of levels, but an actual output map containing the terrace-like cells. Even though *Chapter 5.3.3.* is discussing several shortcomings of the outputs (and also the options for improvement), the significance of these issues should be assessed in the light that the plots and the map of possible remnants are meant to be interpreted by geomorphologists with a priori knowledge about the studied area. In the example of the Central Gerecse section, the trained eye can easily exclude the stream terraces not sloping towards the Danube, flat pediments and horst top surfaces, and can rather focus on the typically found or missed terrace features. In fact, with a stricter delineation of the study area these could be directly omitted, however, the author admits that further tuning of the tool is necessary to assist less experienced users. Analysing the results directly in GRASS GIS, by overlapping the digitised geomorphological map (Schweitzer, 1980), the exaggerated shaded relief, the geomorphons, the output terrace cells map and even the location of peaks applied

by Bugya (2008), the operator has a wide range of information to draw conclusions from. For example, when reviewing these input maps, the GIS-based results seem to confirm that the travertine cover has protected the terrace surfaces from erosion, the tool rarely missed these cell groups. Another interesting finding is how well the mapped terrace remnants correlate with the built-in areas of Süttő, Lábatlan and Nyergesújfalu. One could debate, that the corrSRTM1 model is elevated here, however, the settlements are not so densely built in. The in-depth geomorphological analysis of the results could reveal further insights regarding the terrace system on the Gerecse foreland. All in all, the obtained plots and terrace remnants map are considered reliable, the results are corresponding well with the pre-existing maps, literature and other GIS-based approaches. The realisation of this terrace extraction approach in a 'push-the-button' tool could definitely facilitate the spread of this method, leading to consistent results along the Danube sections, its tributaries and other similar fluvial systems.

6.3. Transparency and transferability of the applied methods

As mentioned in the previous chapters transparency of the performed analysis is of vital importance to the author. Individual research teams are oftentimes compiling algorithms from a set of tools or they are writing codes intended to automate the analysis of the task at hand. The typical length of a scientific paper limits the presentation of the applied methods in such depth that would allow direct reproduction of the analysis. Furthermore, the authors rather stress the potentials and limitations of their methods, while sharing the code snippets as well could facilitate further development of these routines (Barnes, 2010). No technical support is demanded by publishing the computer codes on platforms like GitHub, however, social-networking aspect of these websites makes it possible to get feedback from experts or engage in collaborations. It would not have been possible to perform the presented research without the methods and codes shared on the designated 'GIS4Geomorphology' blog (Cooley, 2010), the source code of the GRASS GIS tools ("GRASS Development Team" 2017), online available R scripts for other geomorphometric analysis (Hengl, Grohmann, Bivand, Conrad, & Lobo, 2009) and the routine for the comparative analysis of DEMs on GitHub (Grohmann, 2018), which supported the development of the author's own tools.

Another aspect of transparency is related to the different DEM error metrics. In this regard it is important to clearly describe the used datasets, share the equations and point to the relevant literature. The results of regional or even global-scale studies with varying reference data sources publish error metrics that are not comparable in every case (Carabajal, 2011; Carabajal & Harding, 2005; Mukherjee et al., 2013; Rodríguez et al., 2006; G. Szabó,

Singh, et al., 2015; Tachikawa et al., 2011). Therefore, it is necessary to perform preliminary quality assessment of the GDEMs over the area of interest before specific applications. In large scale GDEM validations the ICESat GLA14 dataset could be employed as precise reference ground truth heights globally, but unfortunately the obtained granules of Laser 3 measurements were not overlapping with the designated 3rd level study areas. From another perspective, the auxiliary, tile-based quality check information and height error layers distributed with the AW3D30 and TanDEM-X models are useful for the inexperienced users as well (Takaku et al., 2016; Wessel, 2018). The 'NUM' files (e.g. with ASTER GDEM) that only indicate the number of stacks used for the estimation of elevation values provides less direct quality information (Tachikawa et al., 2011). Continuous, cell-based quality indicators would be beneficial in selecting the GDEMs for specific applications, however, it might pose a conflict with the commercial purposes of these elevation models (Tadono et al., 2016). Furthermore, standardised multi-error correction methods would also be welcome by the scientific community, as currently separated research groups are not cooperating well in this field, which results in duplicated efforts (Kulp & Strauss, 2018; Robinson et al., 2014; Yamazaki et al., 2017; Zhao et al., 2018). Enhancing the relative accuracy of SRTM1 was a prerequisite for its geomorphometric application, and hereby the author also admits that this work could have been channelled into other similar projects.

Transferability of the self-developed r.tg.geom and r.terrace.geom tools to other elevation models and study sites was tested in collaboration with fellow researchers. The suitability of the landform elements derived by the geomorphons approach with the search parameter being the TG value was assessed in an object-based image analysis routine to detect drumlins. In case of the Eberfinger drumlin field (Southern Germany) a 10 m resolution LiDAR-derived DEM was available, thus this analysis also tested the applicability of the r.tg.geom tool with non-GDEM data. The object-based classification achieved the highest drumlin detection rate (91.7%) with the 13 cells L value, which was determined as the characteristic ridgeline-to-channel distance in this study area (Sărășan et al., 2019). Applying the topographic grain concept to define the maximum scale of geomorphons proved superior to subjectively selecting the search parameter.

From the GDEMs the r.terrace.geom tool was applied on TDX12 dataset over the Central Gerecse region, with results comparable to the findings presented in *Chapter 5.3.3*. In case of the swath profile analysis and the terrace remnants map the interpretation was hindered by the bumpy texture, appearance of vegetation patches and man-made objects. On the other hand, even the higher terrace levels (IV., possible V., VI., VII.) were more

expressed on the frequency plot (Józsa, 2017c). A rather new direction in the analysis of the Hungarian terrace levels is to detect terrace remnants in the valleys of Danube tributaries (Szeberényi, Viczián, Fábián, & Józsa, 2013). For this purpose, the r.terrace.geom tool was used on the contour-based 10 m resolution DEM of the Török and Les streams' watershed in the South-Eastern Börzsöny. The extracted terrace remnant candidates are in good agreement with other GIS-based results and provide a suitable set of data for further statistical analysis, in order to reveal the possible connection of the stream terraces to the Visegrád Gorge terrace system (Józsa, 2015b; Szeberényi et al., 2013). On the other hand, despite the efforts to fine-tune the method, when applied on a pre-processed version of the ASTER GDEM v2 model, the terrace extraction algorithm could not derive meaningful results regarding the I., II/a, II/b and terrace-island surfaces potentially occurring in the southern section of the Tolnai-Sárköz (Józsa, 2013). The tool itself is not directly capable of distinguishing the geomorphic levels with small dividing elevation steps, however, the inadequacy of the results was here mainly caused by the low quality of the input ASTER GDEM v2 data.

As a final remark on the transferability of the tools it should be mentioned that any user with a basic familiarity of GRASS GIS could install and execute the r.tg.geom and r.terrace.geom tools. The GitHub documentation includes a step-by-step guide for installation on Linux and Windows devices as well (Józsa, 2017a, 2017b). The help section of the tools describes the necessary inputs and parameters in the typical manual page format of GRASS GIS. Lastly, with basic Python and R scripting knowledge the tools could be easily extended or tailored. As a future research opportunity the terrace analysis method of Bugya (2008) could be incorporated into the r.terrace.geom tool.

7. Conclusions

The presented work is a contribution to the discipline of geomorphometry from a geoinformatics and a geomorphologic perspective as well. The research explored the potentials and limitations of applying quasi-global digital elevation models coupled with robust, yet scale-flexible geomorphometric tools, in order to map landform elements, geomorphologic regions and terrace remnants in Hungary. In order to ensure the transparency and reproducibility of the performed analysis, the process from the quality assessment of GDEMs to the visualisation of the derived information was streamlined into the freely available R and GRASS GIS software, and the source codes of the developed tools were also published online on GitHub. To reflect on the outlined objectives, the conclusions are also following the guideline of the typical geomorphometric analysis; the theses of the dissertation are highlighted in bold.

1. *Acquiring the digital land surface model matching the research objectives*

   Since the realisation of the Shuttle Radar Topography Mission in 2000, newer GDEMs were released every few years, providing ever-increasing resolution and spatial accuracy for a wide variety of applications. **The comprehensive overview of the currently available quasi-global DEMs was timely, and it is expected to benefit the DEM user's community in finding the appropriate model for the task at hand.** Regarding the current study, the thorough literature review related to the accessible GDEMs was essential in order to narrow down the candidates for the comparative accuracy and geomorphometric plausibility assessment. **The TDX12, AW3D30, SRTM1 and MERIT DEM models were chosen** based on the recent GIS-aided geomorphological publications and the worth-wile research topics presented at the '*Geomorphometry 2018*' conference. The preliminary visual assessments and estimation of the effective resolution revealed that the TDX12 model could even be applied in micromorphology analysis, while the AW3D30 and SRTM1 models fit the general requirements to perform the mesoscale landform mapping, which the current study was aiming for. The MERIT DEM has its own potentials due to the multi-error correction process, however, the level of topographic detail was not satisfactory in the current case.

2. Quality assessment of the GDEMs

The evaluation focused on exploring the key error components present in the elevation models via visual inspection, calculation of the descriptive error statistics and derivation of land-surface parameters. The comparative analysis revealed that the main components of DEM errors are the extensive forests, remaining outliers of open-pit mines and water bodies, other spurious sinks and peaks (e.g. from low coherence or cloud shadow) and an uncorrelated noise (for some extent even on the smoothed MERIT DEM). **The descriptive statistics of the horizontal and vertical accuracy of the models, based on contour-derived reference DTMs, are in good agreement with previously published validation results for bare surfaces**, the scale of vegetation offset also corresponds with the varying acquisition techniques. **The relative accuracy assessment based on land-surface parameters and objects confirmed that the geomorphometric plausibility of the GDEMs needs to be estimated on a per study basis by the user.** As it was expected in this validation step, the effect of the natural and man-made surface objects distorted the values on the slope maps, the bumpy and noisy texture of the TDX12, AW3D30 and SRTM1 models led to the appearance of 'salt-and-pepper' effect on the TWI map, while the adaptive smoothing applied to the MERIT DEM caused ambiguities in the stream network extraction. **Based on the GDEMs' evaluation in the current study, the reviewed literature and the previous experiences of the author, the SRTM1 model has proven superior as the base elevation model of the specific geomorphometric analysis.**

3. Correcting errors and removing artefacts

A pre-processing algorithm was compiled to improve the relative accuracy of the SRTM1 model and to reduce the possibility of error propagation to the derived geomorphometric maps. The elevations of larger water bodies were replaced by single values approximated from heights of their shorelines. Forested and built-in areas were mapped using public domain auxiliary data (tree cover map from 2000 and OpenStreetMap data). The effect of vegetation was reduced by generating a bias surface based on the elevation difference of cells located on the inner and outer border of forest patches. Lastly, an adaptive smoothing algorithm was applied to treat the random noise component and the outliers were removed based on focal statistics. **Even though the error metrics do not show a drastic improvement of the corrSRTM1, the enhancement of the relative accuracy is detectable in the geomorphometric derivatives (slope, aspect, watercourses, TWI, geomorphons) and the repeated**

visual inspection. The weakness of this DEM pre-processing method is clearly the correction of the extensive forest patches. **From the presented five-step correction approach flattening of water bodies, removal of outliers, filtering of noise and elimination of small vegetation patches over flat regions are considered the least challenging and still generally beneficial steps in case of any GDEM.**

4. *Delineating landform elements, geomorphological landscapes and terrace remnants*

The users need to treat the obtained GIS-based results with caution – especially in case of the GDEMs –, but at the same time these geomorphometric derivatives should facilitate a critical review of the traditional geomorphological maps. Conceptualisation of the specific landforms from a DEM-based aspect and objective parametrisation of the tools need to dominate in the research projects, while the experimental fine-tuning of thresholds to digitally recreate existing expert-based maps should be avoided.

a. Delineation of the landform elements and physiographic units of Hungary was executed with the complementary geomorphons approach and GeoPAT toolset, which are developed by the same research team (Jasiewicz et al., 2014). **The geomorphons approach represents a new standard for the generation of objective and comparable landform element maps**, while still allowing the user to tune the results for specific applications. **Revisiting and implementing the topographic grain principle in the form of a GRASS GIS extension (r.tg.geom) is the author's contribution to improve this robust and scale-flexible mapping tool.** Applying the geomorphons tool in Hungary, by setting the 450 m topographic grain value as search parameter, enabled the derivation of a landform map fitting the various topographies occurring in the country, while keeping the computational cost low and avoiding the trial-and-error method.

b. **Based on the geomorphometric map and other land-surface variables (e.g. TPI) it was possible to map the physiographic units of floodplains, alluvial plains, low hills, dissected hills, low mountains and mountain ridges in Hungary.** As the GeoPAT toolset is a supervised classification method it requires interaction from the user to define the classes to be mapped and designate the learning areas, but otherwise the implementation of the steps is straightforward and objective. The comprehensive landform elements (geomorphons) and geomorphic regions map of the country provide the opportunity to carry out statistical analysis on the characteristics of the topography and reveal new insights on the spatial arrangement of the landforms.

c. **The applied terrace mapping algorithm is based on the work of Demoulin et al. (2007), but it was further improved in the form of a GRASS GIS script tool accessing R functionality (r.terrace.geom).** Using R as an intermediate analytical environment and visualisation tool gave great added value to the algorithm, while GRASS GIS was capable of handling the digital elevation datasets and perform the demanding computations to prepare necessary raster derivatives. The algorithm cuts up the analysed region into parallel sections in the flow direction and determines cells potentially belonging to terrace surfaces based on local slope characteristics and a minimum area size parameter. **The thresholds for the terrace extraction are not experimental, they are adaptively determined for every elevation range according to the local topography of the AOI.** The tool generates an output report with explanatory plots, which can be directly compared to the terrace levels from the literature, swath-profiles of the landscape and a final plot showing the longitudinal profile of the studied river with the determined height ranges of terrace levels, and also a raster map of the possible terrace remnants. The synthetic hillslope model with 7 terrace levels, widening floodplain and an 'eroded' pediment surface has helped in the conceptualisation phase of the terrace mapping algorithm. There are remaining methodological issues, not handled by the original approach either (e.g. terraces of the tributaries, landslide toes, pediments), which require the incorporation of filtering techniques based on auxiliary land-surface parameters (e.g. aspect).

5. Assessing and synthesising the geomorphologically relevant output

The possible error propagation from the GDEMs and the constraints of the horizontal and vertical accuracy must be taken into consideration when interpreting the output geomorphometric maps. **For geomorphological analysis the 30 m SRTM1 model is a good compromise because once the relief exceeds the average height of the surface objects, the topographic details are well represented, the landforms are not deformed.** Despite the erroneous cells remaining on the corrSRTM1 the present study concludes that the generated landform elements, geomorphological regions and terrace remnants maps are useful to review expert-based geomorphological maps and provide further insights for the compilation of a unified knowledge base. **The use of GDEMs, such as the corrSRTM1 dataset, is also beneficial considering the expandability of the presented geomorphological analyses** to the Carpathian Basin, as the physical geographical units continue over the national borders.

Even though, the geomorphons and GeoPAT approaches are not producing geomorphological maps in the traditional sense (where a multi-colour map contains information about the topography, genesis and geology of the region), these methods are an important step towards comparable and scale-flexible digital geomorphic maps. In the Hungarian case study, the expert-based reference maps and the algorithm-based geomorphic regions differ mainly in case of the floodplains and alluvial plains, where the remaining errors of the corrSRTM1 led to misleading landforms and the number of meaningful features for landscape search is limited. **Local examples from the hilly and mountainous landscapes (e.g. Eastern Mecsek Mountains, Cserhát, Zala Hills) confirm that the algorithm-delineated geomorphic units can represent the topographic variability reasonably well, however, some misinterpretations can still occur and the boundaries are not completely precise due to the 1 km cell size.**

This study focused on the terrace surfaces on the northern foreland of the Gerecse Mountains, where the algorithm performed fairly well to delineate the floodplain and lower terrace levels (II/a, II/b, III., IV.). The GIS-based results seem to confirm that the travertine deposits have protected the terrace surfaces from erosion, the tool rarely missed these cell groups. Furthermore, the location of the possible terrace surfaces correlates well with the built-in regions of the settlements of the Almás-Tát Danube Valley. Possible terrace candidates were mapped in higher elevations as well, however, due to level of erosion, occurrence of stream terraces, pediment surfaces and features of fossil and recent landslides the parallelisation of the terrace levels require further interpretation. **The obtained plots and terrace remnants map are considered reliable, the results are corresponding well with the pre-existing maps, literature and other GIS-based approaches.** From a technical point of view, the realisation of this terrace extraction approach in a 'push-the-button' tool is considered as an important contribution to the digital terrain analysis toolset available in GRASS GIS.

In the past ten years since the '*Geomorphometry*' handbook was published significant developments have been accomplished in the discipline. The author hopes that the presented work serves the geomorphometric community well, in order to overcome the challenges of finding the appropriate GDEM, the operational scale, the optimal mapping method and the user-friendly GIS or statistical tool to reveal the wealth of geomorphological information stored in digital land surface models. The final conclusion of the dissertation agrees with the following quote from Ian Evans: *'The "Holy Grail" of full automation remains elusive, but progress has been made'* (Evans, 2012, p. 105).

8. Acknowledgement

First of all, I would like to express my gratitude to my supervisor *Dr. Szabolcs Ákos Fábián* for his continuous support of my research projects ever since my bachelor studies. I am grateful for his scientific guidance and motivation to prepare my PhD thesis. I am also thankful to *Dr. Titusz Bugya*, who first drew my attention to the possibilities of free and open source software in GIS. Furthermore, my sincere appreciation goes to *Dr. Lucian Drăguț* and *Dr. Adriana Sărășan* from the West University of Timișoara for the discussions on my research topic and the cooperation in my methodological developments. Special thanks go to *Attila Polák*, *Dr. István Péter Kovács*, *Zsanett Kopecskó* and *Gábor Nagy* for clarifying scientific or additional questions and helping me with their constructive feedback to avoid overcomplication of my research.

I am also grateful for the professional framework and possibilities provided by the *Doctoral School of Earth Sciences* and *Institute of Geography and Earth Sciences* at Pécs to extend my knowledge, attend international conferences and prepare my research.

I would like to express my appreciation to *Viktória Nemes* for her help with the review of the English version of my dissertation. I am also grateful to *Anita Domján*, *Balázs Simon* and *Dr. Andrea Pálfi* for their moral and emotional support during my university years and while I was writing this thesis.

My sincere thanks go to fellow researchers of the GIS and geomorphometry community who are contributing to the development of open science with their data and code.

Finally, I would like to thank my manager *Tamás Schwarcz* for appreciating my scientific interest and supporting me to maintain my 'work – research' balance, even though my studies are not in the least related to enterprise resource planning.

During my PhD studies my research was supported by a scholarship from the National Talent Programme ('Nemzet Fiatal Tehetségeiért Ösztöndíj' – NTP-NFTÖ-16-0673). The 12 m resolution TanDEM-X data was provided by the DLR under the science proposal DEM_OTHER0625.

Bibliography

1. Abrams, M. (2016). ASTER global DEM version 3, and new ASTER Water Body Dataset. *ISPRS Annals of Photogrammetry, Remote Sensing and Spatial Information Sciences*, 107–110. Prague: Copernicus Publications.
2. Abshire, J. B., Sun, X., Riris, H., Sirota, J. M., McGarry, J. F., Palm, S., … Liiva, P. (2005). Geoscience Laser Altimeter System (GLAS) on the ICESat Mission: On-orbit measurement performance. *Geophysical Research Letters*, *32*(L21S02), 1–5.
3. Ádám, L. (1962). A Tolnai-dombság. *Földrajzi Értesítő*, *11*(1), 74–84.
4. Ádám, L. (1964). *A Szekszárdi-dombvidék kialakulása és morfológiája – Földrajzi Tanulmányok 2.* Budapest: Akadémiai Kiadó.
5. Ádám, L., Marosi, S., & Szilárd, J. (1981). *A Dunántúli-dombság – Magyarország tájföldrajza*. Budapest: Akadémiai Kiadó.
6. Ádám, L., Marosi, S., & Szilárd, J. (1990). A Dunántúli-dombság. In S. Marosi & S. Somogyi (Eds.), *Magyarország kistájainak katasztere* (pp. 564–567, 571–574, 578–583). Budapest: Magyar Tudományos Akadémia, Földrajztudományi Kutatóintézet.
7. Ádám, L., & Pécsi, M. (Eds.). (1985). *Mérnökgeomorfológiai térképezés*. Budapest: Magyar Tudományos Akadémia, Földrajztudományi Kutatóintézet.
8. Ádám, L., & Schweitzer, F. (1985). A Neszmély-Dunaalmás-Dunaszentmiklós közötti felszínmozgásos terület 1:10 000-es méretarányú geomorfológiai térképének magyarázója. In L. Ádám & M. Pécsi (Eds.), *Mérnökgeomorfológiai térképezés* (pp. 108–167). Budapest: Magyar Tudományos Akadémia, Földrajztudományi Kutatóintézet.
9. ALOS Global Digital Surface Model "ALOS World 3D – 30m (AW3D30)." (2018). Retrieved March 11, 2019, from https://www.eorc.jaxa.jp/ALOS/en/aw3d30/
10. Amante, C., & Eakins, B. W. (2009). *NOAA Technical Memorandum NESDIS NGDC-24 – ETOPO1 1 arc-minute Global Relief Model: procedures, data sources and analysis*. Boulder.
11. Amatulli, G., Domish, S., Kiesel, J., Sethi, T., Yamazaki, D., & Raymond, P. (2018). High-resolution stream network delineation using digital elevation models: assessing the spatial accuracy. In P. L. Guth (Ed.), *Geomorphometry 2018: 5th International Conference of the ISG* (pp. 1–3). Boulder: International Society for Geomorphometry.
12. Anders, N. S., Seijmonsbergen, A. C., & Bouten, W. (2011). Segmentation optimization and stratified object-based analysis for semi-automated geomorphological mapping. *Remote Sensing of Environment*, *115*(12), 2976–2985.
13. Andrásfalvy, B. (1973). *A Sárköz és a környező Duna-menti területek ősi ártéri gazdálkodása és vízhasználatai a szabályozás előtt – Vízügyi Történeti Füzetek 6.* Budapest: Vízügyi Dokumentációs és Tájékoztató Iroda.
14. Ardelean, F., Drăguţ, L. D., Urdea, P., & Török-Oance, M. (2013). Variations in landform definition: A quantitative assessment of differences between five maps of glacial cirques in the Ţarcu Mountains (Southern Carpathians, Romania). *Area*, *45*(3), 348–357.
15. Arundel, S. T., Li, W., & Zhou, X. (2018). The Effect of Resolution on Terrain Feature Extraction. In P. L. Guth (Ed.), *Geomorphometry 2018: 5th International Conference of the ISG* (pp. 1–4). Boulder: International Society for Geomorphometry.
16. ASTER Global Digital Elevation Map Announcement. (2011). Retrieved March 11, 2019, from https://asterweb.jpl.nasa.gov/gdem.asp
17. Babák, K., Kiss, I., Kopecskó, Z., Kovács, I. P., & Schweitzer, F. (2013). Regeneration process of the karst water springs in Transdanubian Mountains, Hungary. *Hungarian Geographical Bulletin*, *62*(3), 247–265.
18. Barnes, N. (2010). Publish your computer code: it is good enough. *Nature*, *467*(7317), 753.

19. Bashfield, A., & Keim, A. (2011). Continent-wide DEM Creation for the European Union. *34th International Symposium on Remote Sensing of Environment*, 1–4. Sydney.
20. Becker, J. J., Sandwell, D. T., Smith, W. H. F., Braud, J., Binder, B., Depner, J., … Weatherall, P. (2009). Global Bathymetry and Elevation Data at 30 Arc Seconds Resolution: SRTM30_PLUS. *Marine Geodesy*, *32*(4), 355–371.
21. Bédard, Y. (2005). Principles of spatial database analysis and design. In P. A. Longley, M. F. Goodchild, D. J. Maguire, & D. W. Rhind (Eds.), *Geographical Information Systems: Principles, Techniques, Management and Applications* (2nd ed., pp. 413–424). New York: John Wiley & Sons, Inc.
22. Berry, P. A. M. (1999). Global digital elevation models - fact or fiction? *Astronomy & Geophysics*, *40*(3), 310–313.
23. Berry, P. A. M., Garlick, J. D., & Smith, R. G. (2007). Near-global validation of the SRTM DEM using satellite radar altimetry. *Remote Sensing of Environment*, *106*(1), 17–27.
24. Berry, P. A. M., Hilton, R., Johnson, C. P. D., & Pinnock, R. A. (2000). ACE: A new Global Digital Elevation Model incorporating satellite altimeter derived heights. *ERS-Envisat Symposium, Vol. SP-461*, 1–9. Gothenburg: ESA.
25. Berry, P. A. M., Hoogerboord, J. E., & Pinnock, R. A. (2000). Identification of common error signatures in Global Digital Elevation Models based on satellite altimeter reference data. *Physics and Chemistry of the Earth, Part A: Solid Earth and Geodesy*, *25*(1), 95–99.
26. Berry, P. A. M., Smith, R. G., & Benveniste, J. (2010). Gravity, Geoid and Earth Observation. In S. P. Mertikas (Ed.), *Gravity, Geoid and Earth Observation: International Association of Geodesy Symposia* (Vol. 135, pp. 231–238). Chania, Crete: Springer.
27. Bishop, M. P., James, L. A., Shroder, J. F., & Walsh, S. J. (2012). Geospatial technologies and digital geomorphological mapping: Concepts, issues and research. *Geomorphology*, *137*(1), 5–26.
28. Bivand, R. S. (2018). Package "rgrass7." Retrieved April 11, 2019, from https://cran.r-project.org/web/packages/rgrass7/rgrass7.pdf
29. Bivand, R. S., Pebesma, E., & Gómez-Rubio, V. (2008). Handling Spatial Data in R. In *Applied Spatial Data Analysis with R* (pp. 21–154). New York: Springer.
30. Blak, T. A. (2007). DEM Quality Assessment. In D. F. Maune (Ed.), *Digital Elevation Model Technologies and Applications: The DEM Users Manual* (2nd ed., pp. 425–448). Bethesda.
31. Boulton, S. J., & Stokes, M. (2018). Which DEM is best for analyzing fluvial landscape development in mountainous terrains? *Geomorphology*, *310*, 168–187.
32. Bowman, M. H., & Petras, V. (2015). r.shade – GRASS GIS manual. Retrieved April 12, 2019, from https://grass.osgeo.org/grass74/manuals/r.shade.html
33. Bubenzer, O., & Bolten, A. (2008). The use of new elevation data (SRTM/ASTER) for the detection and morphometric quantification of Pleistocene megadunes (draa) in the eastern Sahara and the southern Namib. *Geomorphology*, *102*(2), 221–231.
34. Buckley, S. (2018). NASADEM: Creating a new NASA Digital Elevation Model and associated products. Retrieved March 8, 2019, from https://earthdata.nasa.gov/community/community-data-system-programs/measures-projects/nasadem
35. Budai, T., Fodor, L., Sztanó, O., Kercsmár, Z., Császár, G., Csillag, G., … Lantos, Z. (2018). Explanatory Book to the Geological Map of the Gerecse Mountains (1:50 000). In T. Budai (Ed.), *Geology of the Gerecse Mountains – Regional map series of Hungary* (pp. 255–408). Budapest: Magyar Bányászati és Földtani Szolgálat.
36. Bugnicourt, P., Guitet, S., Santos, V. F., Blanc, L., Sotta, E. D., Barbier, N., & Couteron, P. (2018). Using textural analysis for regional landform and landscape mapping, Eastern Guiana Shield. *Geomorphology*, *317*, 23–44.
37. Bugya, T. (2008). *Negyedidőszaki folyóteraszok azonosítása földtani fúrások adatai és térinformatikai eljárások alapján*. University of Pécs.
38. Bugya, T. (2009). Identification of Quaternary fluvial terraces using borehole data and digital elevation models. *Zeitschrift Für Geomorphologie, Supplementary Issues*, *53*(2), 113–121.
39. Bugya, T., & Halmai, Á. (2013). The Multiresolution Image Format. *Journal of Geographic Information System*, *5*(1), 87–95.

40. Bulla, B. (1941). A Magyar medence pliocén és pleisztocén terraszai. *Földrajzi Közlemények*, *69*(4), 199–230.
41. Bulla, B. (1962). Magyarország természeti tájai. *Földrajzi Közlemények*, *10*(1), 1–16.
42. Burrough, P. A., van Gaans, P. F. M., & MacMillan, R. A. (2000). High resolution landform classification using fuzzy k-means. *Fuzzy Sets and Systems*, *113*(1), 37–52.
43. Büttner, G., Kosztra, B., Maucha, G., & Pataki, R. (2012). *Implementation and achievements of CLC2006*. Budapest.
44. Carabajal, C. C. (2011). *ASTER Global DEM version 2.0 evaluation using ICESat geodetic ground control*.
45. Carabajal, C. C., & Boy, J.-P. (2016). Evaluation of ASTER GDEM V3 using ICESat laser altimetry. *ISPRS Annals of Photogrammetry, Remote Sensing and Spatial Information Sciences*, 117–124. Prague: Copernicus Publications.
46. Carabajal, C. C., & Harding, D. J. (2005). ICESat validation of SRTM C-band digital elevation models. *Geophysical Research Letters*, *32*(22), 1–5.
47. Carabajal, C. C., & Harding, D. J. (2006). SRTM C-Band and ICESat Laser Altimetry Elevation Comparisons as a Function of Tree Cover and Relief. *Photogrammetric Engineering & Remote Sensing*, *72*(3), 287–298.
48. Cho, H. (2017). r.topidx – GRASS GIS manual. Retrieved April 13, 2019, from https://grass.osgeo.org/grass74/manuals/r.topidx.html
49. Cimmery, V. (2010). *User Guide for SAGA (version 2.0.5)* (p. 393). p. 393.
50. Conrad, O., Bechtel, B., Bock, M., Dietrich, H., Fischer, E., Gerlitz, L., … Böhner, J. (2015). System for Automated Geoscientific Analyses (SAGA) v. 2.1.4. *Geoscientific Model Development*, *8*(7), 1991–2007.
51. Cooley, S. (2010). GIS4Geomorphology blog (2010-2019). Retrieved March 21, 2019, from http://gis4geomorphology.com
52. Corine Land Cover 2006 seamless vector data. (2012). Retrieved April 20, 2014, from https://www.eea.europa.eu/data-and-maps/data/clc-2006-vector-data-version-2
53. Crippen, R. E., Buckley, S., Agram, P., Belz, E. J., Gurrola, E. M., Hensley, S., … Tung, W. (2016). NASADEM global elevation model: Methods and Progress. *ISPRS Annals of Photogrammetry, Remote Sensing and Spatial Information Sciences*, 125–128. Prague: Copernicus Publications.
54. Csillag, G., & Sebe, K. (2015). Long-Term Geomorphological Evolution. In D. Lóczy (Ed.), *Landscapes and Landforms of Hungary* (pp. 29–38). Leverkusen: Springer International Publishing.
55. Csillik, O., & Drăguţ, L. D. (2018). Towards a global geomorphometric atlas using Google Earth Engine. In P. L. Guth (Ed.), *Geomorphometry 2018: 5th International Conference of the ISG* (pp. 1–4). Boulder: International Society for Geomorphometry.
56. Cunha, N. S., Magalhães, M. R., Domingos, T., Abreu, M. M., & Withing, K. (2018). The land morphology concept and mapping method and its application to mainland Portugal. *Geoderma*, *325*, 72–89.
57. Danielson, J. J., & Gesch, D. B. (2011). Global Multi-resolution Terrain Elevation Data 2010 (GMTED2010). In *U.S. Geological Survey*. Virginia.
58. de Ferranti, J. (2014). Viewfinder Panoramas Digital Elevation Data. Retrieved March 12, 2019, from http://viewfinderpanoramas.org/dem3.html
59. De Reu, J., Bourgeois, J., Bats, M., Zwertvaegher, A., Gelorini, V., De Smedt, P., … Crombé, P. (2013). Application of the topographic position index to heterogeneous landscapes. *Geomorphology*, *186*, 39–49.
60. Dekavalla, M., & Argialas, D. (2017). Object-based classification of global undersea topography and geomorphological features from the SRTM30_PLUS data. *Geomorphology*, *288*, 66–82.
61. DEM, DSM & DTM Differences – A Look at Elevation Models in GIS. (2018). Retrieved March 9, 2019, from https://gisgeography.com/dem-dsm-dtm-differences/
62. Demek, J., Embleton, C., Gellert, J. F., & Verstappen, H. T. (Eds.). (1972). *Manual of Detailed Geomorphological Mapping*. Prague: International Geographical Union Commission on Geomorphological Survey and Mapping.

63. Demek, J., Kirchner, K., Mackovčin, P., & Slavík, P. (2012). Geomorphodiversity derived by a GIS-based geomorphological map: case study the Czech Republic. *Zeitschrift Für Geomorphologie*, *55*(4), 415–435.
64. Demeter, G., Szabó, S., Szalai, K., & Püspöki, Z. (2007). Statisztikai lejtőprofil és a digitális magasságmodell-felbontás kapcsolatának vizsgálata. In E. Dobos & A. Hegedűs (Eds.), *Lehetőségek a domborzatmodellezésben - a HUNDEM 2006 konferencia közleményei* (pp. 1–14). Miskolc: Miskolci Egyetem Földrajzi Intézet.
65. Demoulin, A. (2011). Basin and river profile morphometry: A new index with a high potential for relative dating of tectonic uplift. *Geomorphology*, *126*(1–2), 97–107.
66. Demoulin, A., Bovy, B., Rixhon, G., & Cornet, Y. (2007). An automated method to extract fluvial terraces from digital elevation models: The Vesdre valley, a case study in eastern Belgium. *Geomorphology*, *91*(1), 51–64.
67. Deng, Y., Wilson, J. P., & Bauer, B. O. (2007). DEM resolution dependencies of terrain attributes across a landscape. *International Journal of Geographical Information Science*, *21*(2), 187–213.
68. Detrekői, Á., & Szabó, G. (2007). *Térinformatika*. Budapest: Nemzeti Tankönyvkiadó Rt.
69. Digital elevation model – Wikipedia article. (2018). Retrieved March 9, 2019, from https://en.wikipedia.org/wiki/Digital_elevation_model
70. Dikau, R., Brabb, E. E., & Mark, R. M. (1991). *Landform classification of New Mexico by computer. Open-File Report 91-634*.
71. Dmowska, A. (2015). Manual Guide – How to use GeoPAT toolbox. *Computers and Geosciences*, pp. 62–73.
72. Dövényi, Z. (Ed.). (2010). *Magyarország kistájainak katasztere*. Budapest: Magyar Tudományos Akadémia, Csillagászati és Földtudományi Kutatóintézet.
73. Dowle, M. (2019). Package "data.table." Retrieved April 11, 2019, from https://cran.r-project.org/web/packages/data.table/data.table.pdf
74. Drăguţ, L. D., & Blaschke, T. (2006). Automated classification of landform elements using object-based image analysis. *Geomorphology*, *81*(3–4), 330–344.
75. Drăguţ, L. D., Csillik, O., Eisank, C., & Tiede, D. (2014). Automated parameterisation for multi-scale image segmentation on multiple layers. *ISPRS Journal of Photogrammetry and Remote Sensing*, *88*, 119–127.
76. Drăguţ, L. D., & Eisank, C. (2011). Object representations at multiple scales from digital elevation models. *Geomorphology*, *129*(3–4), 183–189.
77. Drăguţ, L. D., & Eisank, C. (2012). Automated object-based classification of topography from SRTM data. *Geomorphology*, *141–142*, 21–33.
78. Drăguţ, L. D., Eisank, C., & Strasser, T. (2011). Local variance for multi-scale analysis in geomorphometry. *Geomorphology*, *130*(3–4), 162–172.
79. Drăguţ, L. D., Eisank, C., Strasser, T., & Blaschke, T. (2009). A Comparison of Methods to Incorporate Scale in Geomorphometry. In R. Purves, G. Stephan, T. Hengl, & R. Straumann (Eds.), *Geomorphometry 2009 Conference Proceedings* (pp. 133–139). Zürich: University of Zürich, Department of Geography.
80. Elek, I. (2004a). Domborzati modellek és a mintavételi tétel (I . rész). *Geodézia És Kartográfia*, *56*(10), 21–24.
81. Elek, I. (2004b). Domborzati modellek és a mintavételi tétel (II. rész). *Geodézia És Kartográfia*, *56*(10), 21–24.
82. Etzelmüller, B., Romstad, B., & Fjellanger, J. (2007). Automatic regional classification of topography in Norway. *Norwegian Journal of Geology*, *87*(1–2), 167–180.
83. *EU-DEM Statistical Validation Report*. (2014).
84. *EU-DEM Upgrade – Documentation EEA User Manual*. (2015).
85. EU-DEM v1.1. (2019). Retrieved March 11, 2019, from https://land.copernicus.eu/imagery-in-situ/eu-dem/eu-dem-v1.1?tab=download
86. Evans, I. S. (1972). General geomorphometry, derivatives of altitude, and descriptive statistics. In R. J. Chorley (Ed.), *Spatial Analysis in Geomorphology* (pp. 17–90). London: Methuen & Co. Ltd.

87. Evans, I. S. (2012). Geomorphometry and landform mapping: What is a landform? *Geomorphology*, *137*(1), 94–106.
88. Evans, I. S., Hengl, T., & Gorsevski, P. V. (2009). Applications in Geomorphology. In T. Hengl & H. I. Reuter (Eds.), *Geomorphometry: Concepts, Software, Applications. Developments in Soil Science, vol. 33* (pp. 497–525). Amsterdam: Elsevier.
89. Evans, I. S., & Minár, J. (2011). A classification of geomorphometric variables. In T. Hengl, I. S. Evans, J. P. Wilson, & M. Gould (Eds.), *Proceedings of Geomorphometry 2011* (pp. 105–108). Redlands: International Society for Geomorphometry.
90. Fábián, S. Á., Kovács, J., Lóczy, D., Schweitzer, F., Varga, G., Babák, K., … Nagy, A. (2006). Geomorphological hazards in the Carpathian Foreland, Tolna County (Hungary). *Studia Geomorphologica Carpatho-Balcanica*, *40*, 107–118.
91. Fábián, S. Á., Kovács, J., Schweitzer, F., & Varga, G. (2005). Természeti erő- és veszélyforrások. In N. Pap (Ed.), *Terület- és településfejlesztés Tolna megyében* (pp. 9–45). Szekszárd: Babits Kiadó.
92. Fábián, S. Á., Kovács, J., & Varga, G. (2001). Újabb szempontok a pedimentáció problémájához a Keszthelyi-hegység alapján. In S. Á. Fábián & J. Tóth (Eds.), *Geokronológia és domborzatfejlődés* (pp. 43–56). Pécs: PTE TTK Földrajzi Intézet.
93. Fábián, S. Á., Schweitzer, F., & Varga, G. (2005). A Pécsi-víz völgyének kialakulása és kora. In Z. Dövényi & F. Schweitzer (Eds.), *A földrajz dimenziói: Tiszteletkötet a 65 éves Tóth Józsefnek* (pp. 461–472). Budapest: Magyar Tudományos Akadémia, Földrajztudományi Kutatóintézet.
94. Farr, T. G., & Kobrick, M. (2000). Shuttle Radar Topography Mission Produces a Wealth of Data. *Eos*, *81*(48), 583–585.
95. Farr, T. G., Rosen, P. A., Caro, E., Crippen, R. E., Duren, R., Hensley, S., … Alsdorf, D. E. (2007). The Shuttle Radar Topography Mission. *Reviews of Geophysics*, *45*(RG2004), 1–33.
96. Fisher, P., & Tate, N. J. (2006). Causes and consequences oferror in digital elevation models. *Progress in Physical Geography*, *30*, 467–489.
97. Fisher, P., Wood, J. D., & Cheng, T. (2004). Where is Helvellyn? Fuzziness of multi-scale landscape morphometry. *Transactions of the Institute of British Geographers*, *29*(1), 106–128.
98. Florinsky, I. V. (2017). An illustrated introduction to general geomorphometry. *Progress in Physical Geography*, *41*(6), 723–752.
99. Florinsky, I. V., Skrypitsyna, T. N., & Luschikova, O. S. (2018). Comparative accuracy of the AW3D30 DSM, ASTER GDEM, AND SRTM1 DEM: A case study on the Zaoksky testing ground, central European Russia. *Remote Sensing Letters*, *9*(7), 706–714.
100. Frankl, A., Lenaerts, T., Radusinović, S., Spalevic, V., & Nyssen, J. (2016). The regional geomorphology of Montenegro mapped using Land Surface Parameters. *Zeitschrift Für Geomorphologie*, *60*(1), 21–34.
101. Franklin, S. E. (1987). Geomorphometric processing of digital elevation models. *Computers and Geosciences*, *13*(6), 603–609.
102. Fujisada, H., Urai, M., & Iwasaki, A. (2012). Technical methodology for ASTER global DEM. *IEEE Transactions on Geoscience and Remote Sensing*, *50*(10), 3725–3736.
103. Gábris, G., & Nádor, A. (2007). Long-term fluvial archives in Hungary: response of the Danube and Tisza rivers to tectonic movements and climatic changes during the Quaternary: a review and new synthesis. *Quaternary Science Reviews*, *26*(22–24), 2758–2782.
104. Gallant, J. C. (2011). Adaptive smoothing for noisy DEMs. In T. Hengl, I. S. Evans, J. P. Wilson, & M. Gould (Eds.), *Proceedings of Geomorphometry 2011* (pp. 37–40). Redlands: International Society for Geomorphometry.
105. Gallant, J. C., Dowling, T. I., Read, A. M., Wilson, N., Tickle, P., & Inskeep, C. (2011). *1 second SRTM Derived Products User Guide (Version 1.0.4)*. Canberra.
106. Gallant, J. C., & Read, A. M. (2016). A near-global bare-Earth DEM from SRTM. *ISPRS Annals of Photogrammetry, Remote Sensing and Spatial Information Sciences*, 137–141. Prague: Copernicus Publications.
107. Gallant, J. C., Read, A. M., & Dowling, T. I. (2012). Removal of tree offsets from SRTM and other Digital Surface Models. *International Archives of the Photogrammetry, Remote Sensing and Spatial Information Sciences*, *XXXIX-B4*, 275–280. Melbourne.

108. Geach, M. R., Stokes, M., Telfer, M. W., Mather, A. E., Fyfe, R. M., & Lewin, S. (2014). The application of geospatial interpolation methods in the reconstruction of Quaternary landform records. *Geomorphology*, *216*, 234–246.
109. GeoPAT. (2015). Retrieved March 27, 2019, from http://sil.uc.edu/gitlist/geoPAT/
110. GeoPAT2. (2018). Retrieved March 26, 2019, from http://sil.uc.edu/cms/index.php?id=geopat2
111. Gesch, D. B., Oimoen, M. J., Danielson, J. J., & Meyer, D. (2016). Validation of the ASTER global digital elevation model version 3 over the Conterminous United States. *ISPRS Annals of Photogrammetry, Remote Sensing and Spatial Information Sciences*, 143–148. Prague: Copernicus Publications.
112. Global Forest Change 2000-2014 v1.2. (2015). Retrieved January 8, 2016, from https://earthenginepartners.appspot.com/science-2013-global-forest/download_v1.2.html
113. Goodchild, M. F. (2001). Metrics of scale in remote sensing and GIS. *ITC Journal*, *3*(2), 114–120.
114. Goodchild, M. F. (2011). Scale in GIS: An overview. *Geomorphology*, *130*(1–2), 5–9.
115. Gorini, M. A. V., & Mota, G. L. A. (2011). Which is the best scale? Finding fundamental features and scales in DEMs. In T. Hengl, I. S. Evans, J. P. Wilson, & M. Gould (Eds.), *Proceedings of Geomorphometry 2011* (pp. 67–70). Redlands: International Society for Geomorphometry.
116. GRASS Development Team. (2017). Retrieved April 11, 2019, from Geographic Resources Analysis Support System (GRASS GIS) Software, version 7.4.0 website: https://grass.osgeo.org/
117. Griffiths, J. S., Smith, M. J., & Paron, P. (2011). Introduction to Applied Geomorphological Mapping. In M. J. Smith, P. Paron, & J. S. Griffiths (Eds.), *Geomorphological Mapping – Methods and Applications* (1st ed., pp. 3–11). Amsterdam: Elsevier Science.
118. Grohman, G., Kroenung, G., & Strebeck, J. (2006). Filling SRTM voids: the Delta Surface Fill method. *Photogrammetric Engineering & Remote Sensing*, *72*(3), 213–216.
119. Grohmann, C. H. (2013). Effects of spatial resolution on slope and aspect derivation for regional-scale analysis. In T. Guoan, Z. Qiming, H. Mitasova, T. Hengl, L. Xuejun, & L. Fayuan (Eds.), *Proceedings of Geomorphometry 2013* (pp. O11–O14). Nanjing: Nanjing Normal University, International Society for Geomorphometry.
120. Grohmann, C. H. (2015). Effects of spatial resolution on slope and aspect derivation for regional-scale analysis. *Computers and Geosciences*, *77*, 111–117.
121. Grohmann, C. H. (2016a). Comparative analysis of global Digital Elevation Models and ultra-prominent mountain peaks. *ISPRS Annals of Photogrammetry, Remote Sensing and Spatial Information Sciences*, 17–23. Prague: Copernicus Publications.
122. Grohmann, C. H. (2016b). r.denoise – GRASS GIS manual. Retrieved April 4, 2019, from https://grass.osgeo.org/grass74/manuals/addons/r.denoise.html
123. Grohmann, C. H. (2018). Evaluation of TanDEM-X DEMs on selected Brazilian sites: Comparison with SRTM, ASTER GDEM and ALOS AW3D30. *Remote Sensing of Environment*, *212*, 121–133.
124. Grohmann, C. H., & Riccomini, C. (2009). Comparison of roving-window and search-window techniques for characterising landscape morphometry. *Computers and Geosciences*, *35*(10), 2164–2169.
125. Gruber, A., Wessel, B., Huber, M., & Roth, A. (2012). Operational TanDEM-X DEM calibration and first validation results. *ISPRS Journal of Photogrammetry and Remote Sensing*, *73*, 39–49.
126. Gruber, F. E., Baruck, J., & Geitner, C. (2017). Algorithms vs. surveyors: A comparison of automated landform delineations and surveyed topographic positions from soil mapping in an Alpine environment. *Geoderma*, *308*, 9–25.
127. Gruber, S., & Peckham, S. (2009). Land-Surface Parameters and Objects in Hydrology. In T. Hengl & H. I. Reuter (Eds.), *Geomorphometry: Concepts, Software, Applications. Developments in Soil Science, vol. 33* (pp. 171–194). Amsterdam: Elsevier.
128. Gustavsson, M., & Kolstrup, E. (2009). New geomorphological mapping system used at different scales in a Swedish glaciated area. *Geomorphology*, *110*(1–2), 37–44.

129. Gustavsson, M., Kolstrup, E., & Seijmonsbergen, A. C. (2006). A new symbol-and-GIS based detailed geomorphological mapping system: Renewal of a scientific discipline for understanding landscape development. *Geomorphology*, *77*(1–2), 90–111.
130. Guth, P. L. (2006). Geomorphometry from SRTM: Comparison to NED. *Photogrammetric Engineering & Remote Sensing*, *72*(3), 269–277.
131. Guth, P. L. (2010). Geomorphometric Comparison of ASTER GDEM and SRTM. *ISPRS Archives – Geospatial Data and Geovisualization: Environment, Security, and Society*, 1–10. Orlando.
132. Guth, P. L. (2011). Quantifying linear dune morphology: Examples with SRTM, GDEM, and multibeam bathymetry. In T. Hengl, I. S. Evans, J. P. Wilson, & M. Gould (Eds.), *Proceedings of Geomorphometry 2011* (pp. 139–142). Redlands: International Society for Geomorphometry.
133. Guth, P. L. (2018). What Should a Bare Earth Digital Terrain Model (DTM) Portray? In P. L. Guth (Ed.), *Geomorphometry 2018: 5th International Conference of the ISG* (pp. 1–4). Boulder: International Society for Geomorphometry.
134. Guzzetti, F., & Reichenbach, P. (1994). Towards a definition of topographic divisions for Italy. *Geomorphology*, *11*(1), 57–74.
135. Haas, J. (Ed.). (2012). *Geology of Hungary*. Heidelberg: Springer.
136. Hammond, E. H. (1964). Analysis of properties in land form geography: An application to broad-scale land form mapping. *Annals of the Association of American Geographers*, *44*, 11–19.
137. Hani, A. F. M., Sathyamoorthy, D., & Asirvadam, V. S. (2014). Computing uncertainty of physiographic features extracted from multiscale digital elevation models. *Computers and Geosciences*, *64*, 15–23.
138. Hansen, M. C., Potapov, P. V., Moore, R., Hancher, M., Turubanova, S. A., Tyukavina, A., … Townshend, J. R. G. (2013). High-Resolution Global Maps of 21st-Century Forest Cover Change. *Science*, *342*(6160), 850–853.
139. Hastings, D. A., & Dunbar, P. K. (1999). *Global Land One-kilometer Base Elevation (GLOBE) Digital Elevation Model, Documentation, Volume 1.0*. Boulder.
140. Hebeler, F., & Purves, R. S. (2009). The influence of elevation uncertainty on derivation of topographic indices. *Geomorphology*, *111*(1–2), 4–16.
141. Hegedűs, A. (2005). A domborzat fõ formáinak vizsgálata digitális domborzatmodell alapján. In D. Endre & H. András (Eds.), *HUNDEM 2004 konferencia közleményei* (pp. 1–11). Miskolc: Miskolci Egyetem Földrajzi Intézet.
142. Hegedűs, A. (2012). Felszínalaktani szintek keresése, kijelölése domborzatmodell segítségével. In A. Hegedűs (Ed.), *Lehetőségek a domborzatmodellezésben - a HUNDEM 2011 konferencia közleményei* (pp. 1–16). Miskolc: Miskolci Egyetem Földrajzi Intézet.
143. Hengl, T. (2006). Finding the right pixel size. *Computers and Geosciences*, *32*(9), 1283–1298.
144. Hengl, T., & Evans, I. S. (2009). Mathematical and Digital Models of the Land Surface. In T. Hengl & H. I. Reuter (Eds.), *Geomorphometry: Concepts, Software, Applications. Developments in Soil Science, vol. 33* (pp. 31–63). Amsterdam: Elsevier.
145. Hengl, T., Grohmann, C. H., Bivand, R. S., Conrad, O., & Lobo, A. (2009). SAGA vs GRASS: A Comparative Analysis of the Two Open Source Desktop GIS for the Automated Analysis of Elevation Data. In R. Purves, G. Stephan, T. Hengl, & R. Straumann (Eds.), *Geomorphometry 2009 Conference Proceedings* (pp. 22–27). Zürich: University of Zürich, Department of Geography.
146. Hengl, T., Gruber, S., & Shrestha, D. P. (2004). Reduction of errors in digital terrain parameters used in soil-landscape modelling. *International Journal of Applied Earth Observation and Geoinformation*, *5*(2), 97–112.
147. Hengl, T., & Reuter, H. I. (Eds.). (2009). *Geomorphometry: Concepts, Software, Applications. Developments in Soil Science, vol. 33*. Amsterdam: Elsevier.
148. Hengl, T., & Reuter, H. I. (2011). How accurate and usable is GDEM? A statistical assessment of GDEM using LiDAR data. In T. Hengl, I. S. Evans, J. P. Wilson, & M. Gould (Eds.), *Proceedings of Geomorphometry 2011* (pp. 45–48). Redlands: International Society for Geomorphometry.

149. Hillier, J. K., & Smith, M. J. (2012). Testing 3D landform quantification methods with synthetic drumlins in a real digital elevation model. *Geomorphology*, *153–154*, 61–73.
150. Hillier, J. K., Sofia, G., & Conway, S. J. (2015). Perspective - Synthetic DEMs: A vital underpinning for the quantitative future of landform analysis? *Earth Surface Dynamics*, *3*(4), 587–598.
151. Hirt, C. (2018). Artefact detection in global digital elevation models (DEMs): The Maximum Slope Approach and its application for complete screening of the SRTM v4.1 and MERIT DEMs. *Remote Sensing of Environment*, *207*, 27–41.
152. Hirt, C., & Rexer, M. (2015). Earth2014: 1 arc-min shape, topography, bedrock and ice-sheet models - Available as gridded data and degree-10,800 spherical harmonics. *International Journal of Applied Earth Observation and Geoinformation*, *39*, 103–112.
153. Hofierka, J., Mitasova, H., & Neteler, M. (2009). Geomorphometry in GRASS GIS. In T. Hengl & H. I. Reuter (Eds.), *Geomorphometry: Concepts, Software, Applications. Developments in Soil Science, vol. 33* (pp. 387–410). Amsterdam: Elsevier.
154. Höhle, J., & Höhle, M. (2009). Accuracy assessment of digital elevation models by means of robust statistical methods. *ISPRS Journal of Photogrammetry and Remote Sensing*, *64*(4), 398–406.
155. Horváth, G. (1991). A domborzat formáinak osztályozása és tipizálása. *Földrajzi Értesítő*, *40*(1–2), 39–54.
156. Hueso González, J. H., Antony, J. M. W., Bachmann, M., Krieger, G., Zink, M., Schrank, D., & Schwerdt, M. (2012). Bistatic system and baseline calibration in TanDEM-X to ensure the global digital elevation model quality. *ISPRS Journal of Photogrammetry and Remote Sensing*, *73*, 3–11.
157. Hutchinson, M. F. (1989). A new procedure for gridding elevation and stream line data with automatic removal of spurious pits. *Journal of Hydrology*, *106*, 211–232.
158. Hutchinson, M. F., & Gallant, J. C. (2000). Digital Elevation Models and Representation of Terrain Shape. In J. P. Wilson & J. C. Gallant (Eds.), *Terrain Analysis: Principles and Applications* (pp. 29–50). New York: John Wiley & Sons, Inc.
159. Hutchinson, M. F., Xu, T., & Stein, J. A. (2011). Recent Progress in the ANUDEM Elevation Gridding Procedure. In T. Hengl, I. S. Evans, J. P. Wilson, & M. Gould (Eds.), *Proceedings of Geomorphometry 2011* (pp. 19–22). Redlands: International Society for Geomorphometry.
160. Iwahashi, J., Kamiya, I., Matsuoka, M., & Yamazaki, D. (2018). Global terrain classification using 280 m DEMs: segmentation, clustering, and reclassification. *Progress in Earth and Planetary Science*, *5*(1), 1–31.
161. Iwahashi, J., Nakano, T., & Yamazaki, D. (2018). Classification of topography in artificially modified alluvial plains using DEMs. In P. L. Guth (Ed.), *Geomorphometry 2018: 5th International Conference of the ISG* (pp. 1–4). Boulder: International Society for Geomorphometry.
162. Iwahashi, J., & Pike, R. J. (2007). Automated classifications of topography from DEMs by an unsupervised nested-means algorithm and a three-part geometric signature. *Geomorphology*, *86*(3–4), 409–440.
163. Jacques, P. D., Salvador, E. D., Machado, Rô., Grohmann, C. H., & Nummer, A. R. (2014). Application of morphometry in neotectonic studies at the eastern edge of the Paraná Basin, Santa Catarina State, Brazil. *Geomorphology*, *213*, 13–23.
164. Jamieson, S. S. R., Sinclair, H. D., Kirstein, L. A., & Purves, R. S. (2004). Tectonic forcing of longitudinal valleys in the Himalaya: morphological analysis of the Ladakh Batholith, North India. *Geomorphology*, *58*(1–4), 49–65.
165. Jarvis, A., Reuter, H. I., Nelson, A. D., & Guevara, E. (2008). Hole-filled SRTM for the globe Version 4, available from the CGIAR-CSI SRTM 90m Database. Retrieved March 13, 2019, from http://srtm.csi.cgiar.org/
166. Jasiewicz, J., & Metz, M. (2011). A new GRASS GIS toolkit for Hortonian analysis of drainage networks. *Computers and Geosciences*, *37*(8), 1162–1173.
167. Jasiewicz, J., Netzel, P., & Stepinski, T. F. (2014). Landscape similarity, retrieval, and machine mapping of physiographic units. *Geomorphology*, *221*, 104–112.

168. Jasiewicz, J., Netzel, P., & Stepinski, T. F. (2015). GeoPAT: A toolbox for pattern-based information retrieval from large geospatial databases. *Computers and Geosciences*, *80*, 62–73.
169. Jasiewicz, J., & Stepinski, T. F. (2013). Geomorphons-a pattern recognition approach to classification and mapping of landforms. *Geomorphology*, *182*, 147–156.
170. Jasiewicz, J., & Stepinski, T. F. (2016). r.geomorphon – GRASS GIS manual. Retrieved March 21, 2019, from https://grass.osgeo.org/grass74/manuals/addons/r.geomorphon.html
171. Jasiewicz, J., Stepinski, T. F., & Netzel, P. (2013). Content-based landscape retrieval using geomorphons. In T. Guoan, Z. Qiming, H. Mitasova, T. Hengl, L. Xuejun, & L. Fayuan (Eds.), *Proceedings of Geomorphometry 2013* (pp. O51–O54). Nanjing: Nanjing Normal University, International Society for Geomorphometry.
172. Jenness, J. S. (2006). Topographic Position Index (TPI) v. 1.2. Retrieved April 9, 2019, from http://www.jennessent.com/downloads/TPI_Documentation_online.pdf
173. Józsa, E. (2013). *Az ASTER GDEM értékelése és geomorfológiai alkalmazhatóságának vizsgálata ártéri mintaterületen*. University of Pécs.
174. Józsa, E. (2014). *Az ASTER GDEM alkalmazása geomorfológiai kutatásokban a Dél-Dunántúlon*. University of Pécs.
175. Józsa, E. (2015a). An evaluation of EU-DEM and SRTM1 in comparison with ASTER GDEM , SRTM3 and reference DEMs – geomorphometric approaches. In J. Boda (Ed.), *Az elmélet és a gyakorlat találkozása a térinformatikában VI. = Theory meets practice in GIS* (pp. 117–125). Debrecen: Debrecen Egyetemi Kiadó.
176. Józsa, E. (2015b). Extracting possible terrace surfaces from digital elevation models – methodological issues and case study from Hungary. In J. Jasiewicz, Z. Zwoliński, H. Mitasova, & T. Hengl (Eds.), *Geomorphometry for Geosciences* (p. 235). Poznań: Adam Mickiewicz University in Poznań - Institute of Geoecology and Geoinformation, International Society for Geomorphometry.
177. Józsa, E. (2016). The topographic grain concept in DEM-based geomorphometric mapping. *EGU Geophysical Research Abstracts*, *18*, 1. Vienna: EGU General Assembly.
178. Józsa, E. (2017a). GitHub project: terrace_extraction_grassgis. Retrieved March 28, 2019, from https://github.com/edinaj0zs4/terrace_extraction_grassgis
179. Józsa, E. (2017b). GitHub project: topographic_grain_grassgis. Retrieved March 28, 2019, from https://github.com/edinaj0zs4/topographic_grain_grassgis
180. Józsa, E. (2017c). Mapping fluvial terraces from DEMs with semi-automated geostatistical approach. In V. Dumbrovská (Ed.), *Abstract Book – 9th International Student and Early Career Conference: NEW WAVE 2017* (p. 40). Prague: Charles University.
181. Józsa, E. (2017d). Spatial analysis of fluvial terraces in GRASS GIS accessing R functionality. *EGU Geophysical Research Abstracts*, *19*, 1. EGU General Assembly.
182. Józsa, E., & Fábián, S. Á. (2017). Folyóvízi teraszok térképezése és elemzése térinformatikai módszerekkel a Gerecse északi peremén. In I. L. Szigyártó & A. Szikszai (Eds.), *XIII. Kárpát-medencei Környezettudományi Konferencia* (pp. 90–95). Kolozsvár: Ábel Kiadó.
183. Józsa, E., Fábián, S. Á., & Kovács, M. (2014). An evaluation of EU-DEM in comparison with ASTER GDEM, SRTM and contour-based DEMs over the Eastern Mecsek Mountains. *Hungarian Geographical Bulletin*, *63*(4), 401–423.
184. Józsa, E., Fábián, S. Á., Varga, G., & Varga, T. (2014). Meredek lejtőkkel elválasztott sík felszínek domborzatmodellezésének sajátosságai dunai magaspartok példáján. *Modern Geográfia*, *9*(2), 1–20.
185. Józsa, E., & Kalmár, P. (2014). Assessing the applicability of EU-DEM dataset to landform classification using the geomorphons approach: the case study of the Eastern Mecsek Mountains region. *Kartografické Listy*, *22*(2), 90–101.
186. Józsa, E., & Szeberényi, J. (2016). Geomorfometriai vizsgálatok a tektonika domborzatra gyakorolt hatásainak feltárására börzsönyi mintaterületen. In B. Balázs (Ed.), *Az elmélet és a gyakorlat találkozása a térinformatikában VII. = Theory meets practice in GIS* (pp. 193–200). Debrecen: Debrecen Egyetemi Kiadó.
187. Kääb, A. (2005). Combination of SRTM3 and repeat ASTER data for deriving alpine glacier flow velocities in the Bhutan Himalaya. *Remote Sensing of Environment*, *94*(4), 463–474.

188. Karkee, M., Steward, B. L., & Aziz, S. A. (2008). Improving quality of public domain digital elevation models through data fusion. *Biosystems Engineering*, *101*(3), 293–305.
189. Kéz, A. (1934). A Duna győr–budapesti szakaszának kialakulásáról. *Földrajzi Közlemények*, *62*(10–12), 175–193.
190. Kienzle, S. (2004). The Effect of DEM Raster Resolution on First Order, Second Order and Compound Terrain Derivatives. *Transactions in GIS*, *8*(1), 83–111.
191. Király, G. (2005). Domborzatmodellek előállításához felhasználható forrásadatok összehasonlító vizsgálata. In E. Dobos & A. Hegedűs (Eds.), *HUNDEM 2004 konferencia közleményei* (pp. 1–13). Miskolc: Miskolci Egyetem Földrajzi Intézet.
192. Kosinovsky, I., Holko, M. L., & Glenn, R. L. (2016). v.proj – GRASS GIS manual. Retrieved April 15, 2019, from https://grass.osgeo.org/grass74/manuals/v.proj.html
193. Köthe, R., & Bock, M. (2009). Preprocessing of Digital Elevation Models - derived from Laser Scanning and Radar Interferometry - for terrain analysis in Geosciences. In R. Purves, G. Stephan, T. Hengl, & R. Straumann (Eds.), *Geomorphometry 2009 Conference Proceedings* (pp. 155–161). Zürich: University of Zürich, Department of Geography.
194. Kovács, I. P., Bugya, T., Fábián, S. Á., & Schweitzer, F. (2013). Review on denudation levels of the Western Mecsek Mountains (SW Transdanubia, Hungary). *Studia Geomorphologica Carpatho-Balcanica*, *47*(1), 49–67.
195. Kovács, J. (2003). Vörösagyagok geomorfológiai helyzete és kora a Kárpát-medencében. *Közlemények a PTE Földrajzi Intézetének Természetföldrajzi Tanszékéről*, *24*, 1–8.
196. Kovács, J., Fábián, S. Á., Varga, G., Újvári, G., Varga, G., & Dezső, J. (2011). Plio-Pleistocene red clay deposits in the Pannonian basin: A review. *Quaternary International*, *240*(1–2), 35–43.
197. Kovács, M. (2013). Egy Pécs közeli vízfolyás vizsgálata geomorfológiai módszerekkel. In R. Balogh & P. Schmidt (Eds.), *A földtudományi kutatások új aspektusai* (pp. 27–32). Pécs: Publikon Kiadó.
198. Kramm, T., Hoffmeister, D., Curdt, C., Maleki, S., Khormali, F., & Kehl, M. (2017). Accuracy assessment of landform classification approaches on different spatial scales for the Iranian Loess Plateau. *ISPRS International Journal of Geo-Information*, *6*(11), 366–387.
199. Krieger, G., Moreira, A., Fiedler, H., Hajnsek, I., Werner, M., Younis, M., & Zink, M. (2007). TanDEM-X: A Satellite Formation for High-Resolution SAR Interferometry. *IEEE Transactions on Geoscience and Remote Sensing*, *45*(11), 3317–3341.
200. Kulp, S. A., & Strauss, B. H. (2018). CoastalDEM: A global coastal digital elevation model improved from SRTM using a neural network. *Remote Sensing of Environment*, *206*, 231–239.
201. Landa, M., Barton, M., Calvelo-Aros, D., Ceipcky, J., Metz, M., Kratochvilova, A., … Krejci, M. (2017). wxGUI profile tool – GRASS GIS manual. Retrieved April 12, 2019, from https://grass.osgeo.org/grass74/manuals/wxGUI.html
202. Láng, S. (1955). Geomorfológiai megfigyelések a szekszárdi dombvidéken. *Különnyomat a Földrajzi Közleményekből*, 151–156.
203. Láng, S. (1957). Természeti földrajzi tanulmányok a Sárköz környékén. *Földrajzi Értesítő*, *6*(2), 137–154.
204. Leél-Őssy, S. (1953). Geomorfológiai megfigyelések Baja és Bátaszék vidékén. *Földrajzi Közlemények*, *77*(1–2), 101–114.
205. Lemoine, F. G., Kenyon, S. C., Factor, J. K., Trimmer, R. G., Pavlis, N. K., Chinn, D. S., … Olson, T. R. (1998). *The Development of the Joint NASA GSFC and NIMA Geopotential Model EGM96*. Greenbelt.
206. Leopold, L. B., Wolman, M. G., & Miller, J. P. (1964). *Fluvial Processes in Geomorphology*. San Francisco: W. H. Freeman and Co.
207. Li, Z. (2008). Multi-scale terrain modelling and analysis. In Q. Zhou, B. Lees, & G. Tang (Eds.), *Advances in Digital Terrain Analysis* (pp. 59–83). Berlin: Springer Berlin Heidelberg.
208. Li, Z., Zhu, Q., & Gold, C. (2005a). *Digital Terrain Modeling: Principles and Methodology* (1st ed.). Boca Raton: CRC Press.
209. Li, Z., Zhu, Q., & Gold, C. (2005b). Digital Terrain Surface Modeling. In Z. Li, Q. Zhu, & C. Gold (Eds.), *Digital Terrain Modeling: Principles and Methodology* (1st ed., pp. 65–86). Boca Raton: CRC Press.

210. Li, Z., Zhu, Q., & Gold, C. (2005c). Introduction. In Z. Li, Q. Zhu, & C. Gold (Eds.), *Digital Terrain Modeling: Principles and Methodology* (1st ed., pp. 1–12). Boca Raton: CRC Press.
211. Li, Z., Zhu, Q., & Gold, C. (2005d). Techniques for Acquisition of DTM Source Data. In Z. Li, Q. Zhu, & C. Gold (Eds.), *Digital Terrain Modeling: Principles and Methodology* (1st ed., pp. 31–64). Boca Raton: CRC Press.
212. Liao, W.-H. (2010). Region description using extended local ternary patterns. *Proceedings - 2010 20th International Conference on Pattern Recognition*, 1003–1006. Istanbul: IEEE Computer Society.
213. Lidar Surface Topography (LIST). (2007). Retrieved March 8, 2019, from https://cce.nasa.gov/pdfs/LIST.pdf
214. Lindsay, J. B. (2016). Whitebox GAT: A case study in geomorphometric analysis. *Computers and Geosciences*, *95*, 75–84.
215. Lindsay, J. B., Cockburn, J. M. H., & Russell, H. A. J. (2015). An integral image approach to performing multi-scale topographic position analysis. *Geomorphology*, *245*, 51–61.
216. Lindsay, J. B., & Newman, D. R. (2018). Hyper-scale analysis of surface roughness. In P. L. Guth (Ed.), *Geomorphometry 2018: 5th International Conference of the ISG* (pp. 1–4). Boulder: International Society for Geomorphometry.
217. Lisenby, P. E., & Fryirs, K. A. (2017). 'Out with the Old?' Why coarse spatial datasets are still useful for catchment-scale investigations of sediment (dis)connectivity. *Earth Surface Processes and Landforms*, *42*(10), 1588–1596.
218. Lóczy, D. (2015). Geomorphological Regions. In D. Lóczy (Ed.), *Landscapes and Landforms of Hungary* (pp. 39–46). Leverkusen: Springer International Publishing.
219. Lóczy, D., & Gyenizse, P. (2011). Fluvial micromorphology influenced by tillage on a Danubian floodplain in Hungary. *Zeitschrift Für Geomorphologie, Supplementary Issues*, *55*(1), 66–75.
220. Lovász, G. (Ed.). (1977). *Baranya megye természeti földrajza*. Pécs: Baranya Megyei Levéltár.
221. Luo, W., & Stepinski, T. (2008). Identification of geologic contrasts from landscape dissection pattern: An application to the Cascade Range, Oregon, USA. *Geomorphology*, *99*(1), 90–98.
222. MacMillan, R. A., Pettapiece, W. W., Nolan, S. C., & Goddard, T. W. (2000). A generic procedure for automatically segmenting landforms into landform elements using DEMs, heuristic rules and fuzzy logic. *Fuzzy Sets and Systems*, *113*(1), 81–109.
223. MacMillan, R. A., & Shary, P. A. (2009). Landforms and Landform Elements in Geomorphometry. In T. Hengl & H. I. Reuter (Eds.), *Geomorphometry: Concepts, Software, Applications. Developments in Soil Science, vol. 33* (pp. 227–254). Amsterdam: Elsevier.
224. Magyar, I., Geary, D. H., & Müller, P. (1999). Paleogeographic evolution of the Late Miocene Lake Pannon in Central Europe. *Palaeogeography Palaeoclimatology Palaeoecology*, *147*(3–4), 151–167.
225. Marosi, S., & Somogyi, S. (Eds.). (1990). *Magyarország kistájainak katasztere I–II*. Budapest: Magyar Tudományos Akadémia, Földrajztudományi Kutatóintézet.
226. Martone, M., Bräutigam, B., Rizzoli, P., Gonzalez, C., Bachmann, M., & Krieger, G. (2012). Coherence evaluation of TanDEM-X interferometric data. *ISPRS Journal of Photogrammetry and Remote Sensing*, *73*, 21–29.
227. Massonnet, D., & Elachi, C. (2006). High-resolution land topography. *Comptes Rendus - Geoscience*, *338*(14–15), 1029–1041.
228. Maune, D. F. (Ed.). (2007). *Digital Elevation Model Technologies and Applications: The DEM Users Manual* (2nd ed.). Bethesda: American Society for Photogrammetry and Remote Sensing.
229. Maune, D. F., Binder Maitra, J., & McKay, E. J. (2007). Accuracy Standards. In D. F. Maune (Ed.), *Digital Elevation Model Technologies and Applications: The DEM Users Manual* (2nd ed., pp. 65–97). Bethesda: American Society for Photogrammetry and Remote Sensing.
230. Maune, D. F., Heidemann, K., Kopp, S., & Crawford, C. (2007). Introduction to DEMs. In D. F. Maune (Ed.), *Digital Elevation Model Technologies and Applications: The DEM Users Manual* (2nd ed., pp. 1–36). Bethesda: American Society for Photogrammetry and Remote Sensing.
231. Mentlík, P., Jedlička, K., Minár, J., & Barka, I. (2006). Geomorphological information system: Physical model and options of geomorphological analysis. *Geografie-Sbornik CGS*, *111*(1), 15–32.

232. MERIT DEM: Multi-Error-Removed Improved-Terrain DEM. (2018). Retrieved March 11, 2019, from http://hydro.iis.u-tokyo.ac.jp/~yamadai/MERIT_DEM/
233. Merryman Boncori, J. P. (2016). Caveats Concerning the Use of SRTM DEM Version 4.1 (CGIAR-CSI). *Remote Sensing*, *8*(10), 793–806.
234. Mészáros, E., & Schweitzer, F. (2002). Geomorfológiai tájak, felszíni formakincsek. In E. Mészáros & F. Schweitzer (Eds.), *Magyar tudománytár – Föld, Víz, Levegő* (pp. 123–176). Budapest: Akadémiai Kiadó.
235. Mezősi, G., & Bata, T. (2011). A földrajzi tájak határai. *Földrajzi Közlemények*, *135*(1), 33–43.
236. Miliaresis, G. C., & Iliopoulou, P. (2004). Clustering of Zagros Ranges from the Globe DEM representation. *International Journal of Applied Earth Observation and Geoinformation*, *5*(1), 17–28.
237. Miller, R. (2012). GIS Terrace Extraction. Retrieved April 2, 2019, from http://blog.raptorrob.com/search/label/GIS
238. Minár, J., & Evans, I. S. (2008). Elementary forms for land surface segmentation: The theoretical basis of terrain analysis and geomorphological mapping. *Geomorphology*, *95*(3–4), 236–259.
239. Minár, J., Krcho, J., & Evans, I. S. (2016). Geomorphometry: Quantitative Land-Surface Analysis. *Reference Module in Earth Systems and Environmental Sciences*, 1–13.
240. Minár, J., Mentlík, P., Jedli, K., & Barka, I. (2005). Geomorphological information system: Idea and options for practical implementation. *Geografický Časopis*, *57*(3), 247–266.
241. Minár, J., Minár Jr, J., & Evans, I. S. (2015). Towards exactness in geomorphometry. In J. Jasiewicz, Z. Zwoliński, H. Mitasova, & T. Hengl (Eds.), *Geomorphometry for Geosciences* (pp. 27–30). Poznań: Adam Mickiewicz University in Poznań - Institute of Geoecology and Geoinformation, International Society for Geomorphometry.
242. Mitas, L., & Mitasova, H. (2005). Spatial interpolation. In P. A. Longley, M. F. Goodchild, D. J. Maguire, & D. W. Rhind (Eds.), *Geographical Information Systems: Principles, Techniques, Management and Applications* (2nd ed., pp. 481–492). New York: John Wiley & Sons, Inc.
243. Mitasova, H., Harmon, R. S., Weaver, K. J., Lyons, N. J., & Overton, M. F. (2012). Scientific visualization of landscapes and landforms. *Geomorphology*, *137*(1), 122–137.
244. Mitchell, N. C. (2010). Using Sun's denoising algorithm on topographic data. Retrieved April 4, 2019, from https://personalpages.manchester.ac.uk/staff/neil.mitchell/mdenoise/
245. Moudrý, V., Lecours, V., Gdulová, K., Gábor, L., Moudrá, L., Kropáček, J., & Wild, J. (2018). On the use of global DEMs in ecological modelling and the accuracy of new bare-earth DEMs. *Ecological Modelling*, *383*(January), 3–9.
246. Mouratidis, A., & Ampatzidis, D. (2019). European Digital Elevation Model validation against extensive Global Navigation Satellite Systems Data and comparison with SRTM DEM and ASTER GDEM in Central Macedonia (Greece). *ISPRS International Journal of Geo-Information*, *8*(3), 108–125.
247. Mukherjee, S., Joshi, P. K., Mukherjee, S., Ghosh, A., Garg, R. D., & Mukhopadhyay, A. (2013). Evaluation of vertical accuracy of open source Digital Elevation Model (DEM). *International Journal of Applied Earth Observation and Geoinformation*, *21*(1), 205–217.
248. Nagymarosy, A., & Hámor, G. (2012). Genesis and Evolution of the Pannonian Basin. In J. Haas (Ed.), *Geology of Hungary* (pp. 149–200). Heidelberg: Springer.
249. NASA JPL. (2014a). NASA Shuttle Radar Topography Mission Global 1 arc second. Retrieved March 13, 2019, from NASA EOSDIS Land Processes DAAC website: https://lpdaac.usgs.gov/dataset_discovery/measures/measures_products_table/srtmgl1_v003
250. NASA JPL. (2014b). U.S. Releases Enhanced Shuttle Land Elevation Data. Retrieved March 14, 2019, from https://www.jpl.nasa.gov/news/news.php?release=2014-321
251. Nelson, A. D., Reuter, H. I., & Gessler, P. (2009). DEM Production Methods and Sources. In T. Hengl & H. I. Reuter (Eds.), *Geomorphometry: Concepts, Software, Applications. Developments in Soil Science, vol. 33* (pp. 65–85). Amsterdam: Elsevier.
252. Neteler, M. (2005). SRTM and VMAP0 data in OGR and GRASS. *GRASS Newsletter*, *3*, 2–6.
253. Neteler, M., & Mitasova, H. (2007). *Open Source GIS: A GRASS GIS Approach* (3rd ed.). New York: Springer.

254. Netzel, P., Nowosad, J., Jasiewicz, J., Niesterowicz, J., & Stepinski, T. F. (2018). *GeoPAT2 user's manual* (pp. 1–68). pp. 1–68. Cincinnati.
255. Newman, D. R., Lindsay, J. B., & Cockburn, J. M. H. (2018). Evaluating metrics of local topographic position for multiscale geomorphometric analysis. *Geomorphology*, *312*, 40–50.
256. NGA/NASA EGM96. (2013). Retrieved April 15, 2019, from WGS 84 EGM96 15-Minute Geoid Height File and Coefficient File website: http://earth-info.nga.mil/GandG/wgs84/gravitymod/egm96/egm96.html
257. Nuth, C., & Kääb, A. (2011). Co-registration and bias corrections of sattelite elevation data sets for quantifying glacier thickness change. *The Cryosphere*, *5*, 271–290.
258. O'Loughlin, F. E., Paiva, R. C. D., Durand, M., Alsdorf, D. E., & Bates, P. D. (2016). A multi-sensor approach towards a global vegetation corrected SRTM DEM product. *Remote Sensing of Environment*, *182*, 49–59.
259. Oguchi, T. (2003). Identification of an active fault in the Japanese Alps from DEM-based hill shading. *Computers and Geosciences*, *29*, 885–891.
260. Olaya, V. (2009). Basic Land-Surface Parameters. In T. Hengl & H. I. Reuter (Eds.), *Geomorphometry: Concepts, Software, Applications. Developments in Soil Science, vol. 33* (pp. 141–169). Amsterdam: Elsevier.
261. OpenStreetMap contributors. (2015). Retrieved January 8, 2016, from Planet dump website: http://planet.openstreetmap.org
262. Pataki, J. (1954). *A Sárköz természeti földrajza*. Szekszárd: Tolna Megye Tanácsa V.B. XIII. Népművelési Osztálya.
263. Pécsi, M. (1958). A földfelszín formacsoportjainak ábrázolása. *Földrajzi Közlemények*, *6*(1), 27–35.
264. Pécsi, M. (1959). *A magyarországi Duna-völgy kialakulása és felszínalaktana*. Budapest: Akadémiai Kiadó.
265. Pécsi, M. (1963). Hegylábi (pediment) felszínek a magyarországi középhegységekben. *Földrajzi Közlemények*, *87*(3), 195–212.
266. Pécsi, M. (1967). Alföldi Duna-völgy. In S. Marosi & J. Szilárd (Eds.), *Magyarország tájföldrajza – A dunai Alföld* (pp. 171–175). Budapest: Akadémiai Kiadó.
267. Pécsi, M. (1971). The development of the Hungarian section of the Danube valley. *Geoforum*, *2*(2), 21–32.
268. Pécsi, M. (1977). Geomorphological map of the Carpathian and Balkan Regions (1:1,000,000). *Studia Geomorphologica Carpatho-Balcanica*, *11*, 3–31.
269. Pécsi, M. (1984). Magyarország domborzati formáinak minősítése. *Földrajzi Közlemények*, *32*(2), 81–94.
270. Pécsi, M. (1985). Domborzatminősítő térképek. In L. Ádám & M. Pécsi (Eds.), *Mérnökgeomorfológiai térképezés* (pp. 7–14). Budapest: Magyar Tudományos Akadémia, Földrajztudományi Kutatóintézet.
271. Pécsi, M. (1991). A magyarországi Duna-völgy teraszai és szintjei. In *Geomorfológia és Domborzatminősítés* (pp. 36–47). Budapest: Magyar Tudományos Akadémia, Földrajztudományi Kutatóintézet.
272. Pécsi, M. (1996). *Geomorphological regions of Hungary*. Budapest: Magyar Tudományos Akadémia, Földrajztudományi Kutatóintézet.
273. Pécsi, M. (2001). Geomorfológiai felszínek képződése a lepusztulás, a felhalmozódás és a lemeztektonika tér- és időbeni változásának hatására (A Dunántúli-középhegység felszínformálódásának modellje). *Földrajzi Értesítő*, *50*(1–4), 33–48.
274. Pécsi, M., Gerei, L., Schweitzer, F., Scheuer, G., & Márton, P. (1988). Ciklikus éghajlatváltozás és rosszabbodás visszatükröződése a magyarországi löszök és eltemetett talajok sorozatában. *Időjárás*, *92*(2–3), 75–86.
275. Pécsi, M., & Somogyi, S. (1967). Magyarország természeti földrajzi tájai és geomorfológiai körzetei. *Földrajzi Közlemények*, *15*(4), 285–304.
276. Pham, H. T., Marshall, L., Johnson, F., & Sharma, A. (2018). A method for combining SRTM DEM and ASTER GDEM2 to improve topography estimation in regions without reference data. *Remote Sensing of Environment*, *210*, 229–241.

277. Pierce, L. E., Kellndorf, J., Walker, W. S., & Barros, O. (2006). Evaluation of the Horizontal Resolution of SRTM Elevation Data. *Photogrammetric Engineering & Remote Sensing*, *72*(11), 1235–1244.
278. Pike, R. J. (1988). The geometric signature: quantifying landslide-terrain types from digital elevation models. *Mathematical Geology*, *20*(5), 491–511.
279. Pike, R. J. (2000). Geomorphometry – diversity in quantitative surface analysis. *Progress in Physical Geography*, *24*(1), 1–20.
280. Pike, R. J., Acevedo, W., & Card, D. H. (1989). Topographic grain automated from digital terrain elevation models. *Auto-Carto 9 – Proceedings of the International Symposium on Computer-Assisted Cartography*, 128–137. Baltimore: ASPRS/ACSM.
281. Pike, R. J., Evans, I. S., & Hengl, T. (2009). Geomorphometry: A Brief Guide. In T. Hengl & H. I. Reuter (Eds.), *Geomorphometry: Concepts, Software, Applications. Developments in Soil Science, vol. 33* (pp. 1–30). Amsterdam: Elsevier.
282. Pipaud, I., Loibl, D., & Lehmkuhl, F. (2015). Evaluation of TanDEM-X elevation data for geomorphological mapping and interpretation in high mountain environments - A case study from SE Tibet, China. *Geomorphology*, *246*, 232–254.
283. Prinz, G. (1936). Magyarország tájföldrajza. In L. Bartucz, J. Cholnoky, P. Teleki, & G. Prinz (Eds.), *Magyar föld, Magyar faj. Magyar földrajz I.* (pp. 295–298). Budapest: Királyi Magyar Egyetemi Nyomda.
284. Prinz, G. (1950). A geomorfológia mai alapkérdése. *Földrajzi Értesítő*, *1*(1–3), 153–158.
285. Purinton, B., & Bookhagen, B. (2017). Validation of digital elevation models (DEMs) and comparison of geomorphic metrics on the southern Central Andean Plateau. *Earth Surface Dynamics*, *5*(2), 211–237.
286. Python Software Foundation. (2013). Retrieved April 11, 2019, from Python Programming Language, version 2.7.10 website: http://www.python.org/
287. R Core Team. (2019). Retrieved April 11, 2019, from R: A language and environment for statistical computing website: https://www.r-project.org/
288. Rabus, B., Eineder, M., Roth, A., & Bamler, R. (2003). The shuttle radar topography missin - a new class of digital elevation models acquired by spaceborne radar. *ISPRS Journal of Photogrammetry and Remote Sensing*, *57*, 241–262.
289. Reuter, H. I. (2018). Geomorphometry – 10 years after the book – challenges ahead? In P. L. Guth (Ed.), *Geomorphometry 2018: 5th International Conference of the ISG* (pp. 1–3). Boulder: International Society for Geomorphometry.
290. Reuter, H. I., Hengl, T., Gessler, P., & Soille, P. (2009). Preparation of DEMs for Geomorphometric Analysis. In T. Hengl & H. I. Reuter (Eds.), *Geomorphometry: Concepts, Software, Applications. Developments in Soil Science, vol. 33* (pp. 87–120). Amsterdam.
291. Reuter, H. I., Nelson, A. D., & Jarvis, A. (2007). An evaluation of void-filling interpolation methods for SRTM data. *International Journal of Geographical Information Science*, *21*(9), 983–1008.
292. Reuter, H. I., Strobl, P., & Mehl, W. (2011). How to merge a DEM? In T. Hengl, I. S. Evans, J. P. Wilson, & M. Gould (Eds.), *Proceedings of Geomorphometry 2011* (pp. 87–90). Redlands: International Society for Geomorphometry.
293. Rizzoli, P., Martone, M., Gonzalez, C., Wecklich, C., Borla Tridon, D., Bräutigam, B., … Moreira, A. (2017). Generation and performance assessment of the global TanDEM-X digital elevation model. *ISPRS Journal of Photogrammetry and Remote Sensing*, *132*, 119–139.
294. Robinson, N., Regetz, J., & Guralnick, R. P. (2014). EarthEnv-DEM90: A nearly-global, void-free, multi-scale smoothed, 90m digital elevation model from fused ASTER and SRTM data. *ISPRS Journal of Photogrammetry and Remote Sensing*, *87*, 57–67.
295. Rodríguez, E., Morris, C. S., & Belz, E. J. (2006). A Global Assessment of the SRTM Performance. *Photogrammetric Engineering & Remote Sensing*, *72*(3), 249–260.
296. Rossi, C., Rodriguez Gonzalez, F., Fritz, T., Yague-Martinez, N., & Eineder, M. (2012). TanDEM-X calibrated Raw DEM generation. *ISPRS Journal of Photogrammetry and Remote Sensing*, *73*, 12–20.
297. RStudio Team. (2016). Retrieved April 11, 2019, from RStudio: Integrated Development Environment for R website: http://www.rstudio.com/

298. Ruszkiczay-Rüdiger, Z., Fodor, L., Bada, G., Leél-Össy, S., Horváth, E., & Dunai, T. J. (2005). Quantification of Quaternary vertical movements in the central Pannonian Basin: A review of chronologic data along the Danube River, Hungary. *Tectonophysics*, *410*(1–4), 157–172.
299. Sadeghi, Y., St-Onge, B., Leblon, B., Prieur, J.-F., & Simard, M. (2018). Mapping boreal forest biomass from a SRTM and TanDEM-X based on canopy height model and Landsat spectral indices. *International Journal of Applied Earth Observation and Geoinformation*, *68*, 202–213.
300. Sărășan, A., Józsa, E., Ardelean, A. C., & Drăguț, L. D. (2019). Sensitivity of geomorphons to mapping specific landforms from a digital elevation model: A case study of drumlins. *Area*, *51*(2), 257–267.
301. Satgé, F., Denezine, M., Pillco, R., Timouk, F., Pinel, S., Molina, J., … Bonnet, M. P. (2016). Absolute and relative height-pixel accuracy of SRTM-GL1 over the South American Andean Plateau. *ISPRS Journal of Photogrammetry and Remote Sensing*, *121*, 157–166.
302. Scheuer, G., & Schweitzer, F. (1988). *A Gerecse- és a Budai-hegység édesvízi mészkőösszletei*. Budapest: Akadémiai Kiadó.
303. Schmidt, J., & Andrew, R. (2005). Multi-scale landform characterization. *Area*, *37*(3), 341–350.
304. Schroeder, M., Hulden, M., & Kelly, P. (2016). r.proj – GRASS GIS manual. Retrieved April 15, 2019, from https://grass.osgeo.org/grass74/manuals/r.proj.html
305. Schutz, B., Zwally, H. J., Shuman, C. A., Hancock, D., & DiMarzio, J. P. (2005). Overview of the ICESat mission. *Geophysical Research Letters*, *32*(L21S01), 1–4.
306. Schweitzer, F. (1980). Gerecse-hegység. In L. Ádám, S. Marosi, & J. Szilárd (Eds.), *A Dunántúli-középhegység – Regionális tájföldrajz* (pp. 369–380). Budapest: Akadémiai Kiadó.
307. Schweitzer, F. (2009). Relief and Landscapes. In K. Kocsis & F. Schweitzer (Eds.), *Hungary in Maps* (pp. 38–44). Budapest: Magyar Tudományos Akadémia, Földrajztudományi Kutatóintézet.
308. Sebe, K., Csillag, G., & Konrád, G. (2008). The role of neotectonics in fluvial landscape development in the Western Mecsek Montains and related foreland basin (SE Transdanubia, Hungary). *Geomorphology*, *102*, 55–67.
309. Sebe, K., Csillag, G., Ruszkiczay-Rüdiger, Z., Fodor, L., Thamó-Bozsó, E., Müller, P., & Braucher, R. (2011). Wind erosion under cold climate: A Pleistocene periglacial mega-yardang system in Central Europe (Western Pannonian Basin, Hungary). *Geomorphology*, *134*(3–4), 470–482.
310. Seijmonsbergen, A. C., Hengl, T., & Anders, N. S. (2011). Semi-Automated Identification and Extraction of Geomorphological Features Using Digital Elevation Data. In M. J. Smith, P. Paron, & J. S. Griffiths (Eds.), *Geomorphological Mapping – Methods and Applications* (1st ed., pp. 297–336). Amsterdam: Elsevier Science.
311. Seres, A., & Dobos, E. (2010). Területhasználati térkép készítése műholdfelvételek alapján az SRTM magasságmodell pontosítására. In A. Hegedűs (Ed.), *Geoinformatika és domborzatmodellezés 2009 - A HunDEM 2009 és a GeoInfo 2009 konferencia és kerekasztal válogatott közleményei* (pp. 1–14). Miskolc: Miskolci Egyetem Földrajzi Intézet.
312. Shannon, C. E. (1949). Communication in the Presence of Noise. *Proceedings of the Institute of Radio Engineers*, *37*(1), 10–21.
313. Shapiro, M., Blazek, R., Hofierka, J., Mitasova, H., & Douglas, B. (2017). v.to.rast – GRASS GIS manual. Retrieved April 15, 2019, from https://grass.osgeo.org/grass74/manuals/v.to.rast.html
314. Shapiro, M., & Clements, G. (2018). r.mapcalc – GRASS GIS manual. Retrieved April 12, 2019, from https://grass.osgeo.org/grass74/manuals/r.mapcalc.html
315. Shapiro, M., & Waupotitsch, O. (2015). r.slope.aspect – GRASS GIS manual. Retrieved April 13, 2019, from https://grass.osgeo.org/grass74/manuals/r.slope.aspect.html
316. Shortridge, A. (2006). Shuttle radar topography mission elevation data error and its relationship to land cover. *Cartography and Geographic Information Science*, *33*, 65–75.
317. Shortridge, A., & Messina, J. (2011). Spatial structure and landscape associations of SRTM error. *Remote Sensing of Environment*, *115*(6), 1576–1587.
318. Simard, M., Pinto, N., Fisher, J. B., & Baccini, A. (2011). Mapping forest canopy height globally with spaceborne lidar. *Journal of Geophysical Research*, *116*(G04021), 1–12.

319. Slater, J. A., Garvey, G., Johnston, C., Haase, J., Heady, B., Kroenung, G., & Little, J. (2006). *The SRTM Data "Finishing" Process and Products*. *72*(3), 237–247.
320. Smith, B., & Sandwell, D. T. (2003). Accuracy and resolution of shuttle radar topography mission data. *Geophysical Research Letters*, *30*(9), 201–204.
321. Smith, M. J., & Clark, C. D. (2005). Methods for the visualization of digital elevation models for landform mapping. *Earth Surface Processes and Landforms*, *30*(7), 885–900.
322. Speight, J. G. (1990). Landform. In R. C. McDonald, R. F. Isbell, J. G. Speight, J. Walker, & M. S. Hop (Eds.), *Australian Soil and Land Survey Field Handbook* (pp. 9–57). Melbourne: Inkata Press.
323. Srinivasan, R., & Miller, R. S. (2017). r.fill.dir – GRASS GIS manual. Retrieved April 18, 2019, from https://grass.osgeo.org/grass74/manuals/r.fill.dir.html
324. SRTM Water Body Database v2.1. (2003). Retrieved April 14, 2019, from https://dds.cr.usgs.gov/srtm/version2_1/SWBD/
325. Stepinski, T. F., & Jasiewicz, J. (2011). Geomorphons - a new approach to classification of landforms. In T. Hengl, I. S. Evans, J. P. Wilson, & M. Gould (Eds.), *Proceedings of Geomorphometry 2011* (pp. 109–112). Redlands: International Society for Geomorphometry.
326. Stepinski, T. F., Jasiewicz, J., Netzel, P., & Niesterowicz, J. (2015). Doing Geomorphometry with Pattern Analysis. In J. Jasiewicz, Z. Zwoliński, H. Mitasova, & T. Hengl (Eds.), *Geomorphometry for Geosciences* (pp. 141–144). Poznań: Adam Mickiewicz University in Poznań - Institute of Geoecology and Geoinformation, International Society for Geomorphometry.
327. Stevenson, J. A., Sun, X., & Mitchell, N. C. (2010). Despeckling SRTM and other topographic data with a denoising algorithm. *Geomorphology*, *114*, 238–252.
328. Stout, J. C., & Belmont, P. (2014). TerEx Toolbox for semi-automated selection of fluvial terrace and floodplain features from lidar. *Earth Surface Processes and Landforms*, *39*(5), 569–580.
329. Su, Y., & Guo, Q. (2014). A practical method for SRTM DEM correction over vegetated mountain areas. *ISPRS Journal of Photogrammetry and Remote Sensing*, *87*, 216–228.
330. Sun, X., Rosin, P. L., Martin, R. R., & Langbein, F. C. (2007). Fast and effective feature-preserving mesh denoising. *IEEE Transactions on Visualisation and Computer Graphics*, *13*, 925–938.
331. Szabó, G. (2007). Eltérő alapú DEM-ekből származtatott kvantitatív geomorfológiai térképek pontosságának vizsgálata. In E. Dobos & A. Hegedűs (Eds.), *Lehetőségek a domborzatmodellezésben - a HUNDEM 2006 konferencia közleményei* (pp. 1–8). Miskolc: Miskolci Egyetem Földrajzi Intézet.
332. Szabó, G., Mecser, N., & Karika, A. (2013). Assessing data quality of remotely-sensed DEMs in a Hungarian sample area. *Acta Geographica Debrecina: Landscape and Environment*, *7*(2), 42–47.
333. Szabó, G., Mecser, N., & Karika, A. (2015). Szabad hozzáférésű felszínmodellek összehasonlító vizsgálata hazai mintaterületen. *Geodézia És Kartográfia*, *67*(5–6), 4–8.
334. Szabó, G., Singh, S. K., & Szabó, S. (2015). Slope angle and aspect as influencing factors on the accuracy of the SRTM and the ASTER GDEM databases. *Physics and Chemistry of the Earth*, *83–84*, 137–145.
335. Szabó, G., & Szabó, S. (2010). A Shuttle Radar Topography Mission (SRTM) során nyert adatbázis pontosságának vizsgálata hazai mintaterületeken. *Geodézia És Kartográfia*, *62*(3), 31–35.
336. Szabó, S., Szabó, G., Szabó, J., & Németh, G. (2005). Digitális magasságmodellek és űrfelvételek alkalmazása geomorfológiai értékeléshez a Bodrogzug példáján. In E. Dobos & A. Hegedűs (Eds.), *HUNDEM 2004 konferencia közleményei* (pp. 1–11). Miskolc: Miskolci Egyetem Földrajzi Intézet.
337. Szeberényi, J., Viczián, I., Fábián, S. Á., & Józsa, S. (2013). The relation of the South-Eastern Börzsöny Hills to the Visegrad Gorge, Hungary. *Studia Geomorphologica Carpatho-Balcanica*, *47*, 81–93.
338. Tachikawa, T., Kaku, M., Iwasaki, A., Gesch, D. B., Oimoen, M. J., Zhang, Z., … Carabajal, C. C. (2011). *ASTER Global Digital Elevation Model version 2 – Summary of validation results*.

339. Tadono, T., Nagai, H., Ishida, H., Oda, F., Naito, S., Minakawa, K., & Iwamoto, H. (2016). Generation of the 30 M-MESH global digital surface model by ALOS PRISM. *ISPRS Annals of Photogrammetry, Remote Sensing and Spatial Information Sciences*, 157–162. Prague: Copernicus Publications.
340. Takaku, J., & Tadono, T. (2017). Quality updates of "AW3D" global DSCM generated from ALOS PRISM. *IEEE International Geoscience and Remote Sensing Symposium (IGARSS)*, 5666–5669. Fort Worth.
341. Takaku, J., Tadono, T., & Tsutsui, K. (2014). Generation of high resolution global DSM from ALOS PRISM. *International Archives of the Photogrammetry, Remote Sensing and Spatial Information Sciences XL-4*, *40*(4), 243–248.
342. Takaku, J., Tadono, T., Tsutsui, K., & Ichikawa, M. (2016). Validation of "AW3D" global DSM generated from ALOS PRISM. *ISPRS Annals of Photogrammetry, Remote Sensing and Spatial Information Sciences*, 25–31. Prague: Copernicus Publications.
343. TanDEM-X science service system. (2019). Retrieved March 12, 2019, from https://tandemx-science.dlr.de
344. Telbisz, T., Kovács, G., Székely, B., & Karátson, D. (2012). A sávszelvényelemzés (swath analysis) módszere digitális terepmodell (DTM) alapján. *Földtani Közlöny*, *142*(2), 193–200.
345. Telbisz, T., Kovács, G., Székely, B., & Szabó, J. (2013). Topographic swath profile analysis: a generalization and sensitivity evaluation of a digital terrain analysis tool. *Zeitschrift Für Geomorphologie*, *57*(4), 485–513.
346. Telbisz, T., Székely, B., & Timár, G. (2013). *Digitális Terepmodellek – Adat, látvány, elemzés*. Budapest: Eötvös Loránd Tudományegyetem Természettudományi Kar Földrajz- és Földtudományi Intézet, Természetföldrajzi Tanszék.
347. The TanDEM-X 90 m Digital Elevation Model. (2018). Retrieved March 12, 2019, from https://geoservice.dlr.de/web/dataguide/tdm90/
348. Troiani, F., & Della Seta, M. (2011). Geomorphological response of fluvial and coastal terraces to Quaternary tectonics and climate as revealed by geostatistical topographic analysis. *Earth Surface Processes and Landforms*, *36*, 1193–1208.
349. Ungvári, Z. (2015a). Domborzatmodellek alkalmazása a térképkészítésben. *Geodézia És Kartográfia*, *67*(11–12), 23–28.
350. Ungvári, Z. (2015b). Valós tengerszint feletti magasságok meghatározása erdőfelületek alatt SRTM és CORINE adatok alapján. In J. Boda (Ed.), *Az elmélet és a gyakorlat találkozása a térinformatikában VI. = Theory meets practice in GIS* (pp. 429–436). Debrecen: Debrecen Egyetemi Kiadó.
351. Urai, M., Tachikawa, T., & Fujisada, H. (2012). Data acquisition strategies for ASTER Global DEM generation. *ISPRS Annals of the Photogrammetry, Remote Sensing and Spatial Information Sciences*, 199–202. Melbourne: Copernicus Publications.
352. *User consultation – Requirements of European Community on DEM products*. (2015).
353. USGS. (2015). *The Shuttle Radar Topography Mission (SRTM) Collection User Guide*. 1–17.
354. van Asselen, S., & Seijmonsbergen, A. C. (2006). Expert-driven semi-automated geomorphological mapping for a mountainous area using a laser DTM. *Geomorphology*, *78*(3–4), 309–320.
355. Van Niel, T. G., McVicar, T. R., Li, L., Gallant, J. C., & Yang, Q. (2008). The impact of misregistration on SRTM and DEM image differences. *Remote Sensing of Environment*, *112*(5), 2430–2442.
356. Van Zyl, J. J. (2001). The Shuttle Radar Topography Mission (SRTM): A breakthrough in remote sensing of topography. *Acta Astronautica*, *48*(5–12), 559–565.
357. Vaze, J., Teng, J., & Spencer, G. (2010). Impact of DEM accuracy and resolution on topographic indices. *Environmental Modelling and Software*, *25*(10), 1086–1098.
358. Verstappen, H. T. (2011). Old and New Trends in Geomorphological and Landform Mapping. In M. J. Smith, P. Paron, & J. S. Griffiths (Eds.), *Geomorphological Mapping – Methods and Applications* (1st ed., pp. 13–38). Amsterdam: Elsevier Science.
359. Walker, W. S., Kellndorfer, J. M., & Pierce, L. E. (2007). Quality assessment of SRTM C- and X-band interferometric data: Implications for the retrieval of vegetation canopy height. *Remote Sensing of Environment*, *106*(4), 428–448.

360. Walsh, S. J., Butler, D. R., & Malanson, G. P. (1998). An overview of scale, pattern, process relationships in geomorphology: a remote sensing and GIS perspective. *Geomorphology*, *21*(3–4), 183–205.
361. Wang, X., Holland, D. M., & Gudmundsson, G. H. (2018). Accurate coastal DEM generation by merging ASTER GDEM and ICESat/GLAS data over Mertz Glacier, Antarctica. *Remote Sensing of Environment*, *206*(December 2016), 218–230.
362. Wecklich, C., Gonzalez, C., & Bräutigam, B. (2015). Height Accuracy for the First Part of the Global TanDEM-X DEM Data. In J. Jasiewicz, Z. Zwoliński, H. Mitasova, & T. Hengl (Eds.), *Geomorphometry for Geosciences* (pp. 5–8). Poznań: Adam Mickiewicz University in Poznań - Institute of Geoecology and Geoinformation, International Society for Geomorphometry.
363. Wecklich, C., Gonzalez, C., & Rizzoli, P. (2018). Height Accuracy and Data Coverage for the Final Global TanDEM-X DEM Data. In P. L. Guth (Ed.), *Geomorphometry 2018: 5th International Conference of the ISG* (pp. 1–4). Boulder: International Society for Geomorphometry.
364. Weiss, A. D. (2001). Topographic Position and Landforms Analysis (poster presentation). *ESRI User Conference*, 1. San Diego.
365. Wendleder, A., Felbier, A., Wessel, B., Huber, M., & Roth, A. (2016). A method to estimate long-wave height errors of SRTM C-band DEM. *IEEE Geoscience and Remote Sensing Letters*, *13*(5), 696–700.
366. Wessel, B. (2018). *TanDEM-X ground segment DEM products specification document*. Oberpfaffenhofen.
367. Wessel, B., Huber, M., Wohlfart, C., Marschalk, U., Kosmann, D., & Roth, A. (2018). Accuracy assessment of the global TanDEM-X Digital Elevation Model with GPS data. *ISPRS Journal of Photogrammetry and Remote Sensing*, *139*, 171–182.
368. Westervelt, J., & Metz, M. (2018). r.relief – GRASS GIS manual. Retrieved April 12, 2019, from https://grass.osgeo.org/grass74/manuals/r.relief.html
369. Wickham, H. (2011). The Split-Apply-Combine Strategy for Data Analysis. *Journal of Statistical Software*, *40*(1), 1–29.
370. Wickham, H. (2016). *ggplot2: Elegant Graphics for Data Analysis*. New York: Springer.
371. Wieczorek, M., & Migoń, P. (2014). Automatic relief classification versus expert and field based landform classification for the medium-altitude mountain range, the Sudetes, SW Poland. *Geomorphology*, *206*, 133–146.
372. Wilson, J. P. (2012). Digital terrain modeling. *Geomorphology*, *137*(1), 107–121.
373. Wilson, J. P. (2018). Geomorphometry: Today and Tomorrow. In P. L. Guth (Ed.), *Geomorphometry 2018: 5th International Conference of the ISG* (pp. 1–4). Boulder: International Society for Geomorphometry.
374. Wilson, J. P., & Gallant, J. C. (2000a). Digital Terrain Analysis. In J. P. Wilson & J. C. Gallant (Eds.), *Terrain Analysis: Principles and Applications* (pp. 1–27). New York: John Wiley & Sons, Inc.
375. Wilson, J. P., & Gallant, J. C. (Eds.). (2000b). *Terrain Analysis: Principles and Applications*. New York: John Wiley & Sons, Inc.
376. Winkler, P. (2003). Magyarország digitális ortofotó programja (MADOP) és nagyfelbontású digitális domborzat modell (DDM) az ország teljes területére. *Geodézia És Kartográfia*, *55*(12), 3–10.
377. Winkler, P., Iván, G., Kay, S., Spruyt, P., & Zielinski, R. (2006). Űrfelvételekből származtatott digitális felületmodell minőségének ellenőrzése a magyarországi nagyfelbontású digitális domborzatmodell alapján. *Geodézia És Kartográfia*, *58*(2), 22–31.
378. Wise, S. (1998). The Effect of GIS Interpolation Errors on the Use of Digital Elevation Models in Geomorphology. In S. N. Lane, K. S. Richards, & J. H. Chandler (Eds.), *Landform Monitoring, Modelling and Analysis* (pp. 139–164). New York: John Wiley & Sons, Inc.
379. Wise, S. (2000). Assessing the quality for hydrological applications of digital elevation models derived from contours. *Hydrological Processes*, *14*, 1909–1929.
380. Wood, J. D. (1996). *The geomorphological characterisation of Digital Elevation Models*. University of Leicester.

381. Wood, J. D. (2009a). Geomorphometry in LandSerf. In T. Hengl & H. I. Reuter (Eds.), *Geomorphometry: Concepts, Software, Applications. Developments in Soil Science, vol. 33* (pp. 333–349). Amsterdam: Elsevier.
382. Wood, J. D. (2009b). Overview of Software Packages Used in Geomorphometry. In T. Hengl & H. I. Reuter (Eds.), *Geomorphometry: Concepts, Software, Applications. Developments in Soil Science, vol. 33* (pp. 257–267). Amsterdam.
383. Wood, W. F., & Snell, J. B. (1960). *A Quantitative System for Classifying Landforms*. Natick.
384. WorldDEM(TM): The New Standard of Global Elevation Models. (2019). Retrieved March 12, 2019, from ttps://www.intelligence-airbusds.com/files/pmedia/public/r49306_9_flyer_worlddem_en_january2019.pdf
385. Wu, L., Wang, N., Han, M., Ren, F., & Chen, Y. (1993). Methods and applications of a geomorphological GIS: a case study in the Ordos region of China. *ISPRS Journal of Photogrammetry and Remote Sensing*, *48*(6), 38–45.
386. Yamazaki, D., Baugh, C. A., Bates, P. D., Kanae, S., Alsdorf, D. E., & Oki, T. (2012). Adjustment of a spaceborne DEM for use in floodplain hydrodynamic modeling. *Journal of Hydrology*, *436–437*, 81–91.
387. Yamazaki, D., Ikeshima, D., Tawatari, R., Yamaguchi, T., O'Loughlin, F. E., Neal, J. C., … Bates, P. D. (2017). A high-accuracy map of global terrain elevations. *Geophysical Research Letters*, *44*(11), 5844–5853.
388. Yokoyama, R., Shirasawa, M., & Pike, R. J. (2002). Visualizing topography by openness: A new application of image processing to digital elevation models. *Photogrammetric Engineering & Remote Sensing*, *68*(3), 257–265.
389. Yue, L., Shen, H., Zhang, L., Zheng, X., Zhang, F., & Yuan, Q. (2017). High-quality seamless DEM generation blending SRTM-1, ASTER GDEM v2 and ICESat/GLAS observations. *ISPRS Journal of Photogrammetry and Remote Sensing*, *123*, 20–34.
390. Zhao, X., Su, Y., Hu, T., Chen, L., Gao, S., & Wang, R. (2018). A global corrected SRTM DEM product for vegetated areas. *Remote Sensing Letters*, *9*(4), 393–402.
391. Zink, M., & Moreira, A. (2015). TanDEM-X: A Challenging Radar Mission for Generating a New Earth's Topography. In J. Jasiewicz, Z. Zwoliński, H. Mitasova, & T. Hengl (Eds.), *Geomorphometry for Geosciences* (pp. 1–4). Poznań: Adam Mickiewicz University in Poznań - Institute of Geoecology and Geoinformation, International Society for Geomorphometry.
392. Zwoliński, Z., & Stefańska, E. (2015). Relevance of moving window size in landform classification by TPI. In J. Jasiewicz, Z. Zwoliński, H. Mitasova, & T. Hengl (Eds.), *Geomorphometry for Geosciences* (pp. 273–277). Poznań: Adam Mickiewicz University in Poznań - Institute of Geoecology and Geoinformation, International Society for Geomorphometry.

Appendices

Appendix 1. Microregions included in the specific geomorphometric analysis of the 2nd AOI level.

Macroregion	Map code of microregion	Name of microregion
Great Hungarian Plain	1.1.22	Solti-sík
	1.1.23	Kalocsai-Sárköz
	1.1.24	Tolnai-Sárköz
	1.4.21	Közép-Mezőföld
	1.4.24	Sárvíz-völgy
	1.4.25	Dél-Mezőföld
	1.4.31	Enyingi-hát
	1.4.32	Kálóz-Igari löszhátak
	1.4.33	Sió-völgy
	1.5.12	Fekete-víz síkja
West Hungarian Borderland	3.4.13	Közép-Zalai-dombság
	3.4.21	Egerszeg-Letenyei-dombság
	3.4.22	Principális-völgy
	3.4.23	Zalaapáti-hát
	3.4.24	Alsó-Zala-völgy
	3.4.25	Zalavári-hát
Transdanubian Hills	4.1.11	Kis-Balatoni-medence
	4.1.12	Nagyberek
	4.1.13	Somogyi parti sík
	4.2.11	Nyugat-Külső-Somogy
	4.2.12	Kelet-Külső-Somogy
	4.2.13	Dél-Külső-Somogy
	4.3.11	Marcali-hát
	4.3.12	Kelet-Belső-Somogy
	4.3.13	Nyugat-Belső-Somogy
	4.4.11	Mecsek-hegység
	4.4.12	Baranyai-Hegyhát
	4.4.21	Völgység
	4.4.22	Tolnai-Hegyhát
	4.4.23	Szekszárdi-dombság
	4.4.31	Pécsi-síkság
	4.4.32	Geresdi-dombság
	4.4.33	Villányi-hegység
	4.4.34	Dél-Baranyai-dombság
	4.4.41	Észak-Zselic
	4.4.42	Dél-Zselic

Appendix 2. The univariate statistics of the models before and after resampling.

	min (m)		max (m)		mean		standard deviation	
	orig.	**resamp.**	**orig.**	**resamp.**	**orig.**	**resamp.**	**orig.**	**resamp.**
TDX12	46.81	50.02	697.58	693.58	210.52	210.54	117.32	117.30
SRTM1	79.50	79.48	682.50	682.27	206.59	208.02	117.02	116.93
AW3D30	26.00	40.07	696.00	694.51	211.09	211.02	118.29	118.20
MERIT	84.01	84.00	674.78	674.73	208.31	208.56	114.48	114.48
ref. DTMs	84.43	84.15	681.16	680.44	206.66	206.70	113.58	113.61

Appendix 3. The CORINE CLC2006 categories and the aggregated landcover classes.

CORINE nomenclature	**CLC code**	**Aggregated group**	**Proportion (%)**	
			TS	**EM**
Discontinuous urban fabric	112	BUILT-IN AREA	*2.85*	*4.32*
Industrial or commercial units	121	BUILT-IN AREA	*0.64*	*0.21*
Mineral extraction sites	131	MINING SITE	*0.04*	*0.58*
Dump sites	132	LOW VEGETATION		*0.05*
Sport and leisure facilities	142	LOW VEGETATION	*0.16*	
Non-irrigated arable land	211	BARE SURFACE	*51.55*	*34.30*
Vineyards	221	LOW VEGETATION	*4.44*	*1.40*
Fruit trees and berry plantations	222	LOW VEGETATION	*0.39*	*1.19*
Pastures	231	BARE SURFACE	*1.62*	*3.46*
Complex cultivation patterns	242	BARE SURFACE	*1.56*	*6.19*
Land principally occupied by agriculture, with significant areas of natural vegetation	243	LOW VEGETATION	*2.00*	*2.55*
Broad-leaved forest	311	FOREST	*26.20*	*41.10*
Coniferous forest	312	FOREST	*0.13*	
Mixed forest	313	FOREST	*0.77*	*0.42*
Natural grasslands	321	BARE SURFACE	*0.18*	*0.26*
Transitional woodland-scrub	324	LOW VEGETATION	*3.58*	*3.82*
Inland marshes	411	BARE SURFACE	*0.69*	*0.14*
Watercourses	511	WATER SURFACE	*2.44*	
Water bodies	512	WATER SURFACE	*0.75*	*0.30*

Appendix 4. Necessary input elevation (A) and watercourse map (B) with the required and optional settings and the screen to select requested outputs (C) of the r.terrace.geom tool.

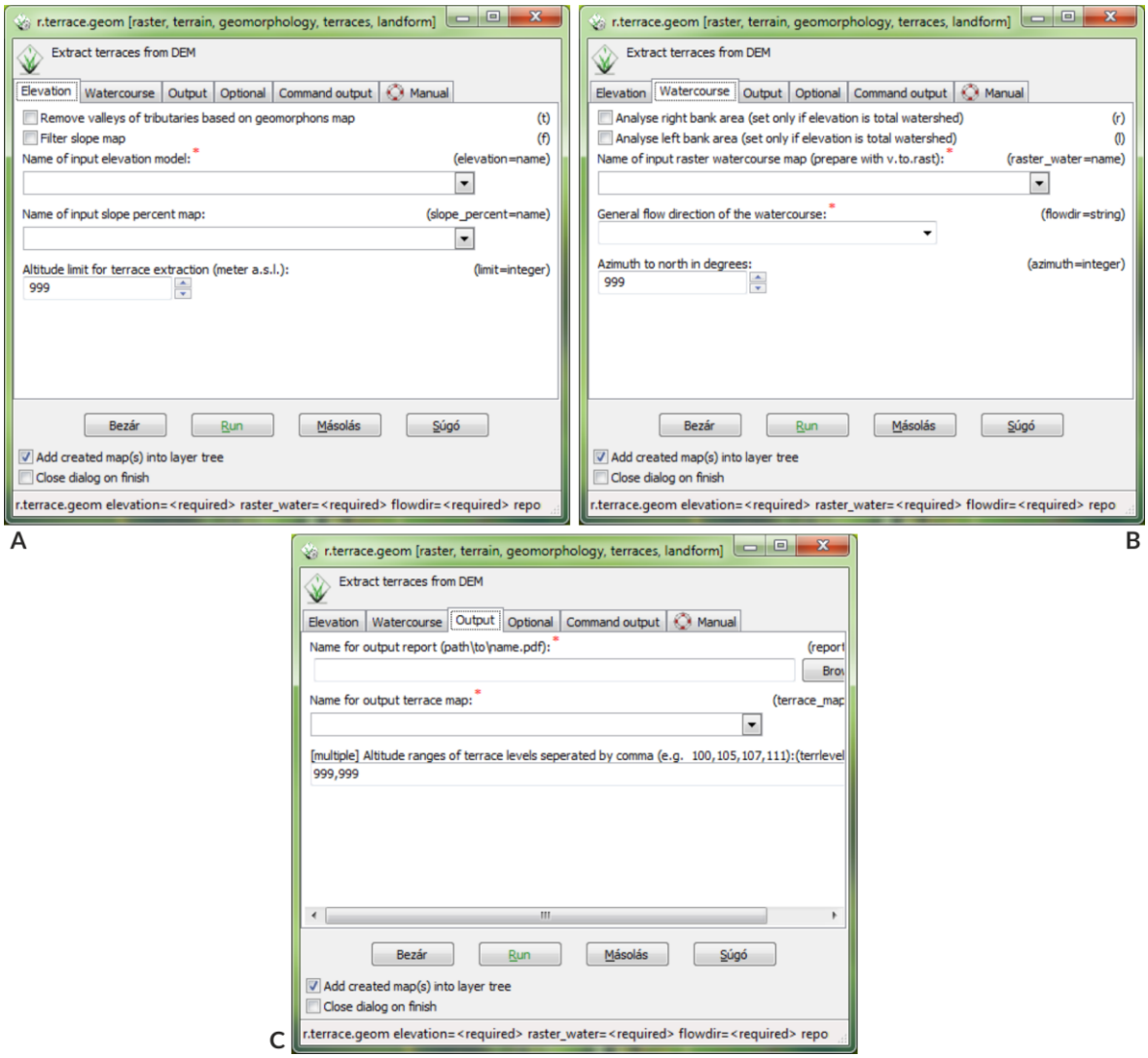

Appendix 5. Elevation histograms of the GDEMs over the Danube floodplain region in the Tolnai-Sárköz study area.

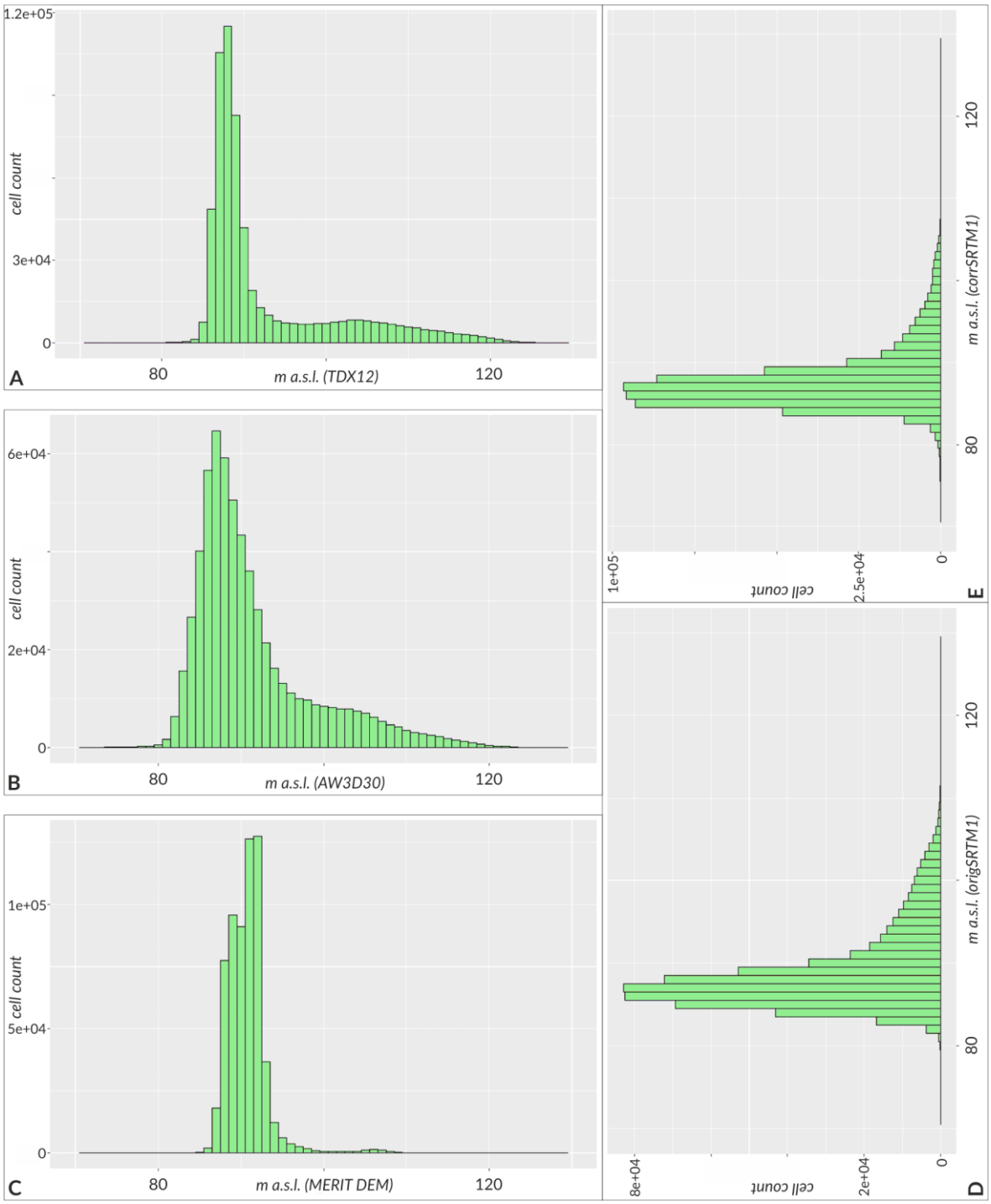

Appendix 6. Boxplot diagrams showing the DEM errors grouped by elevation categories (A) and cardinal directions (B). (Red – TDX12, Blue – AW3D30, Green – SRTM, Magenta – MERIT DEM)

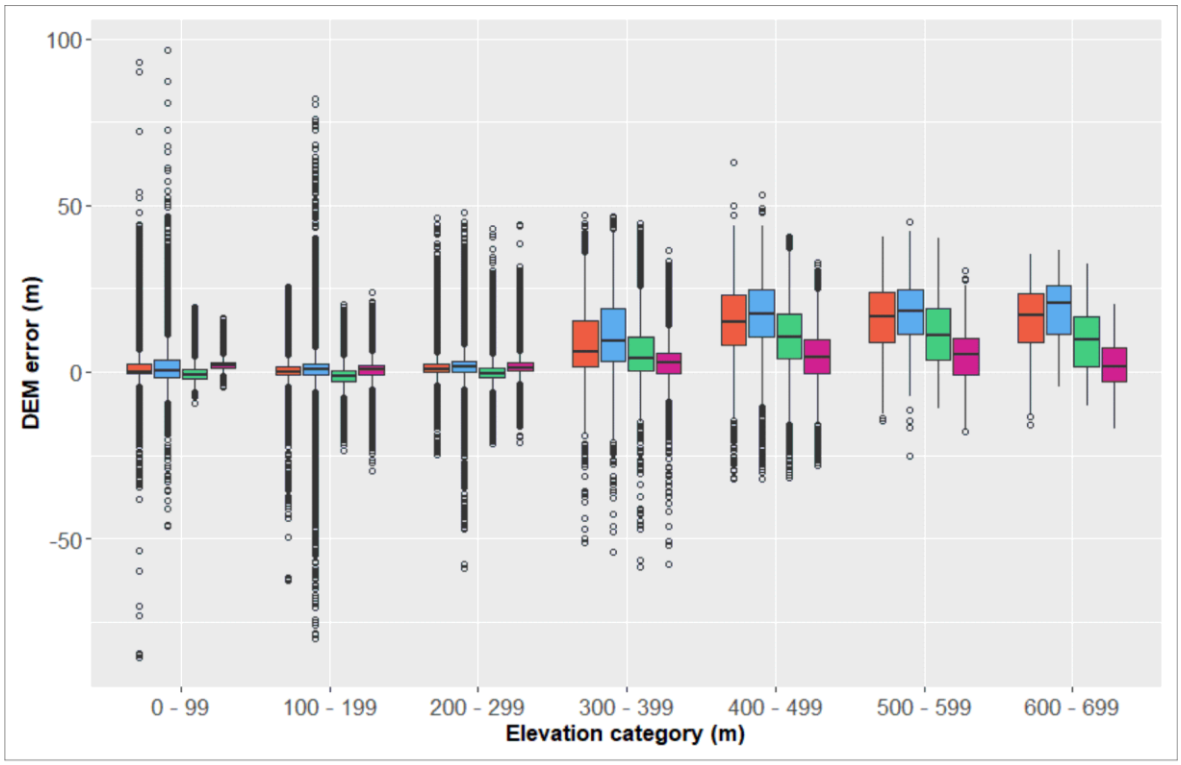

A

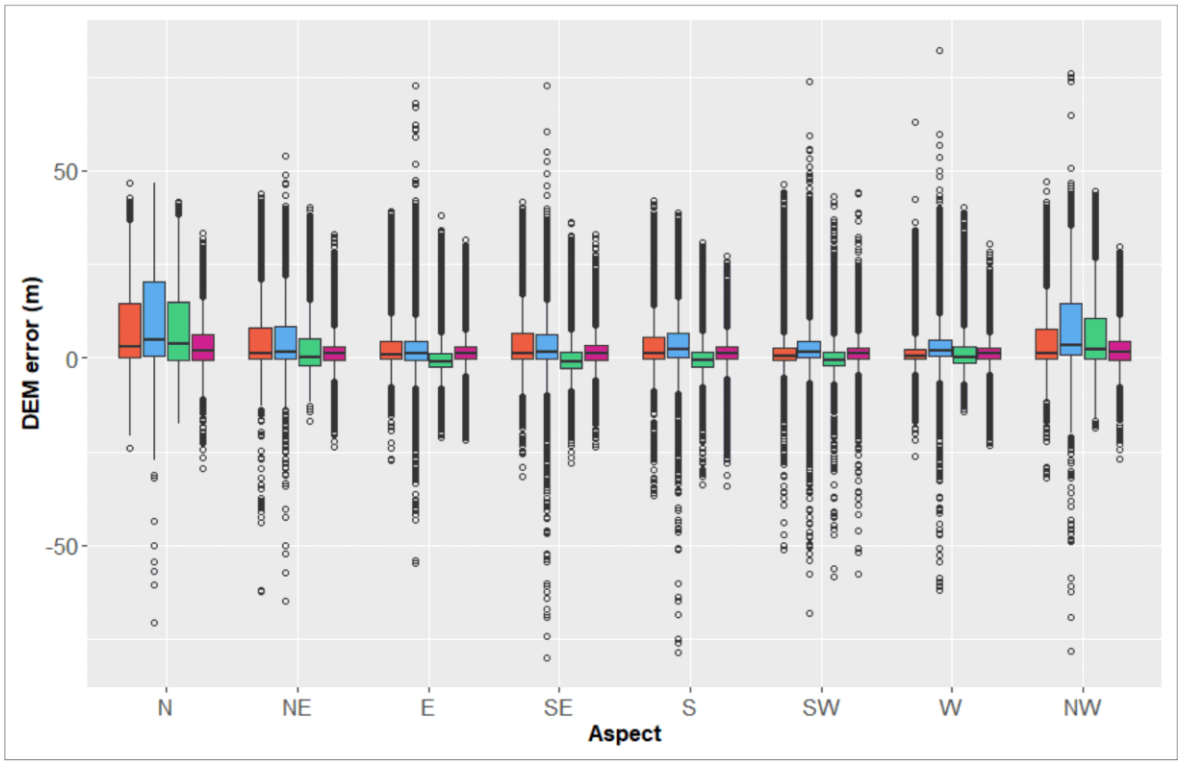

B

Appendix 7. Location (A), surface geology (B) and analysed hydro-geomorphological regions between Almásfüzitő and Esztergom (C). (Sources: satellite imagery from ESRI base layers; 1:100 000 surface geological map from MBFSZ map server)

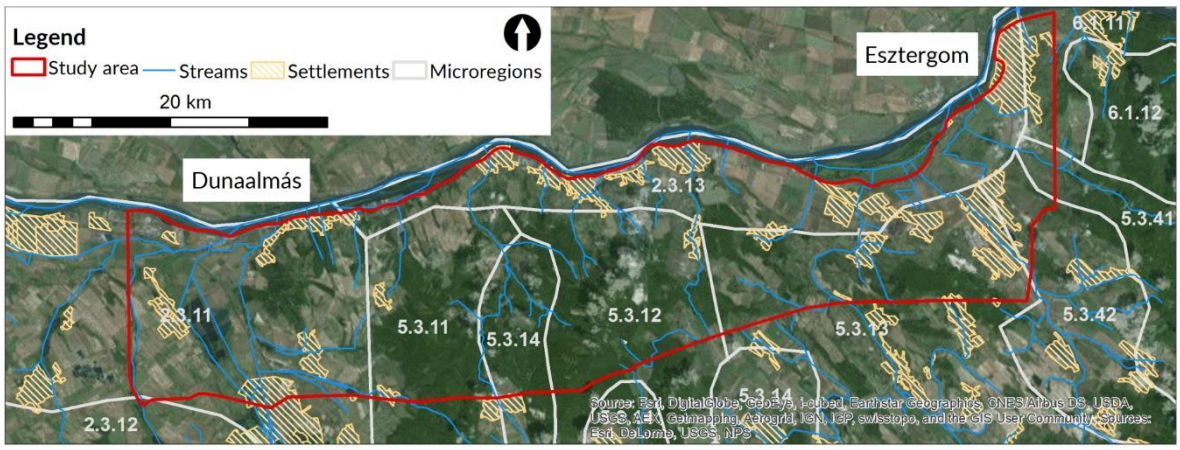

A

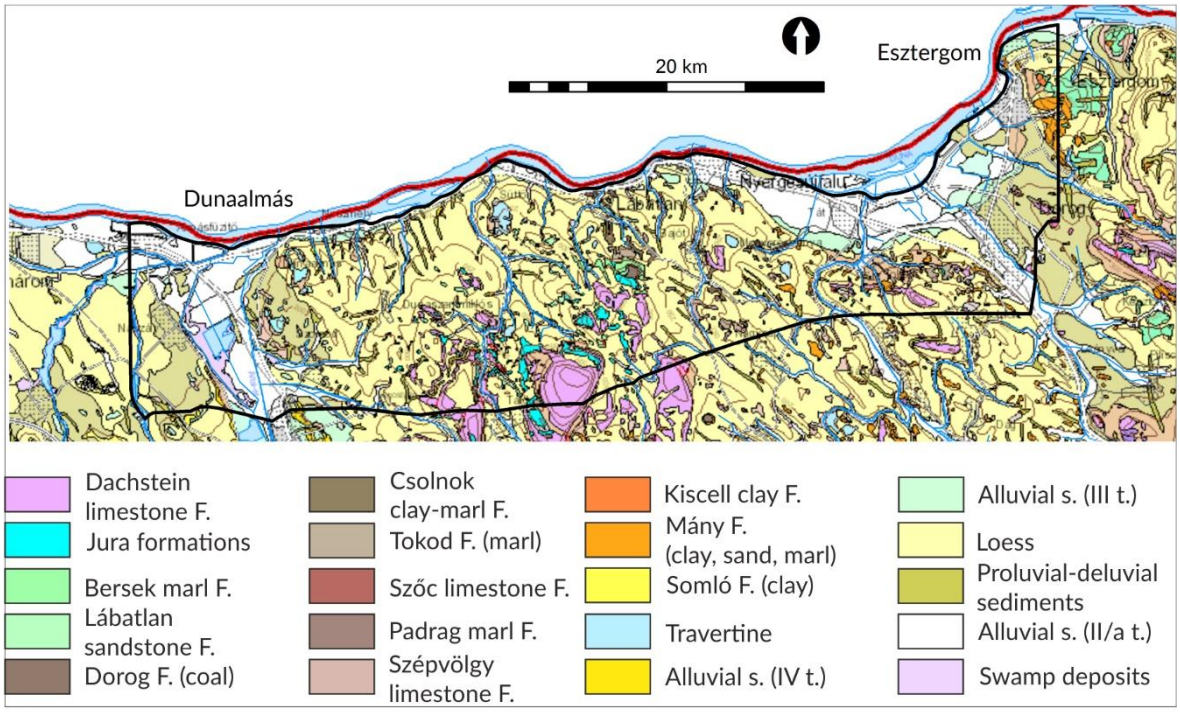

B

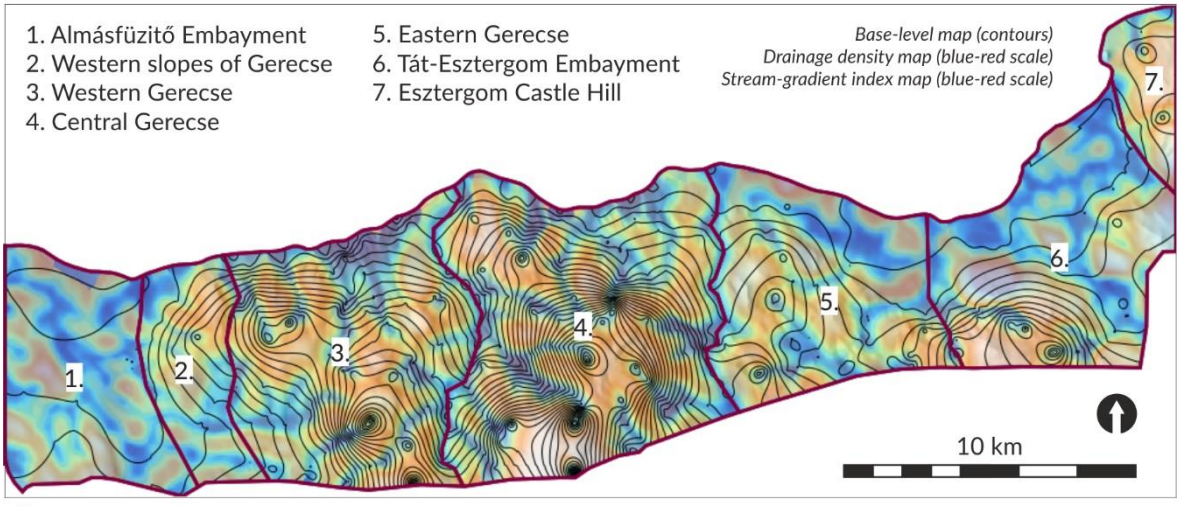

C

Appendix 8. Scatter plots, swath profiles, frequency distributions and possible terrace heights for the other analysed sections of the Gerecse foreland.

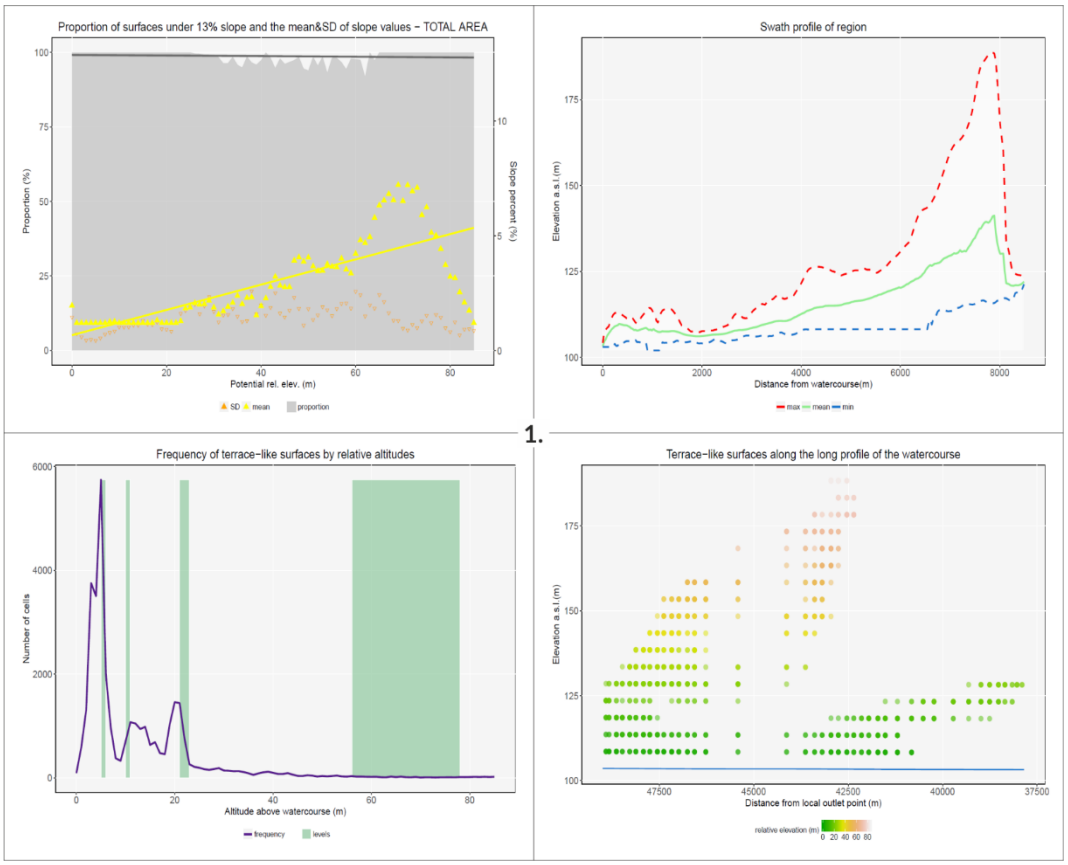

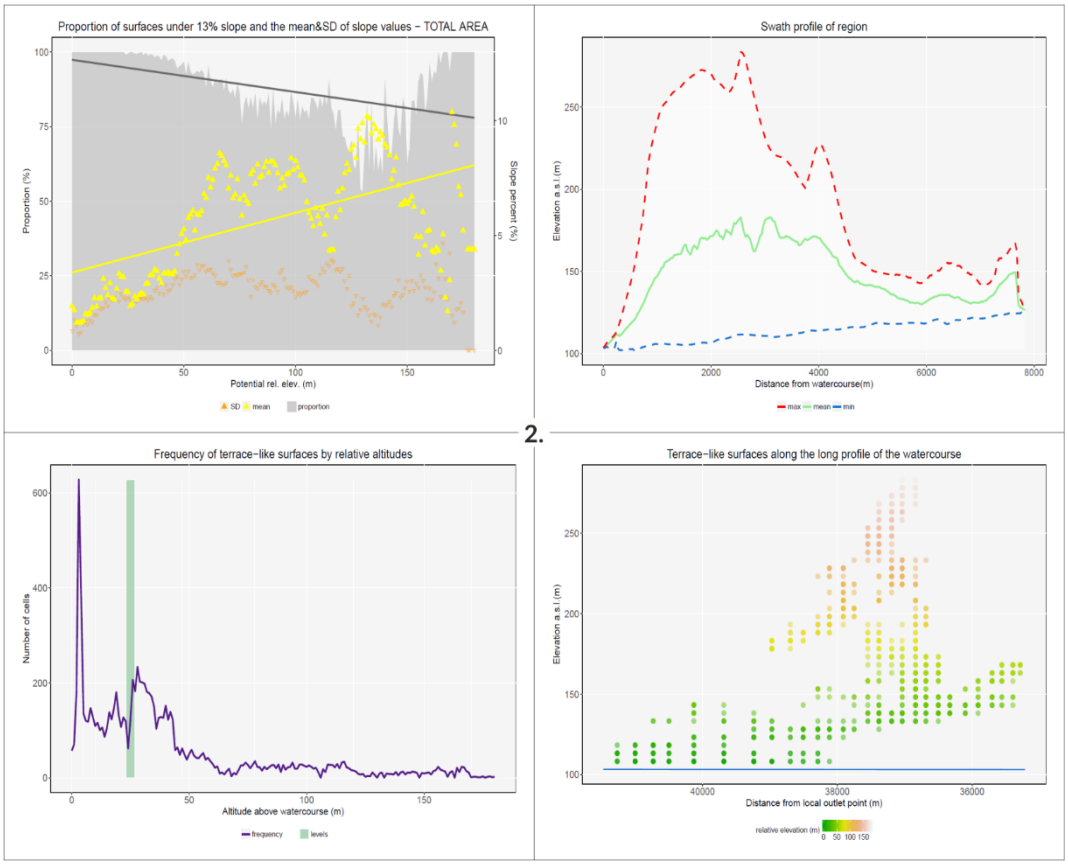

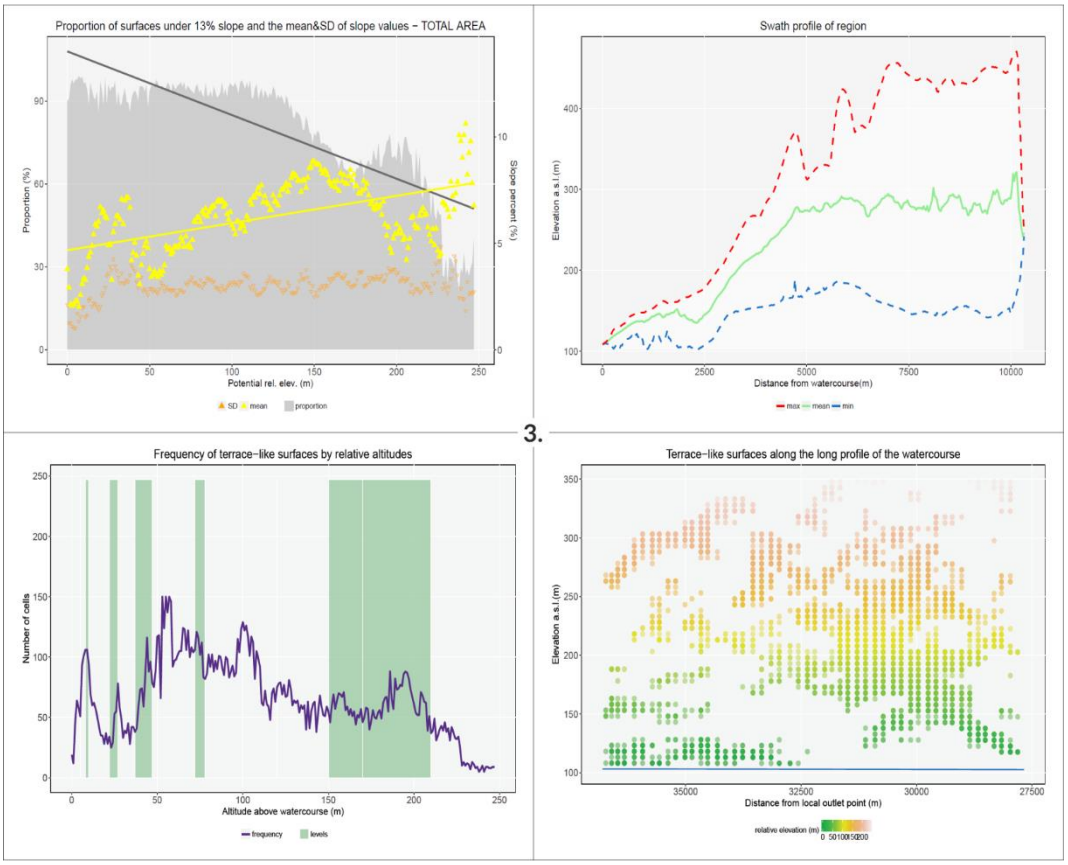
Proportion of surfaces under 13% slope and the mean&SD of slope values – TOTAL AREA
Proportion (%)
Slope percent (%)
Potential rel. elev. (m)
SD
mean
proportion
Swath profile of region
Elevation a.s.l.(m)
Distance from watercourse(m)
max
mean
min
3.
Frequency of terrace–like surfaces by relative altitudes
Number of cells
Altitude above watercourse (m)
frequency
levels
Terrace–like surfaces along the long profile of the watercourse
Elevation a.s.l.(m)
Distance from local outlet point (m)
relative elevation (m)

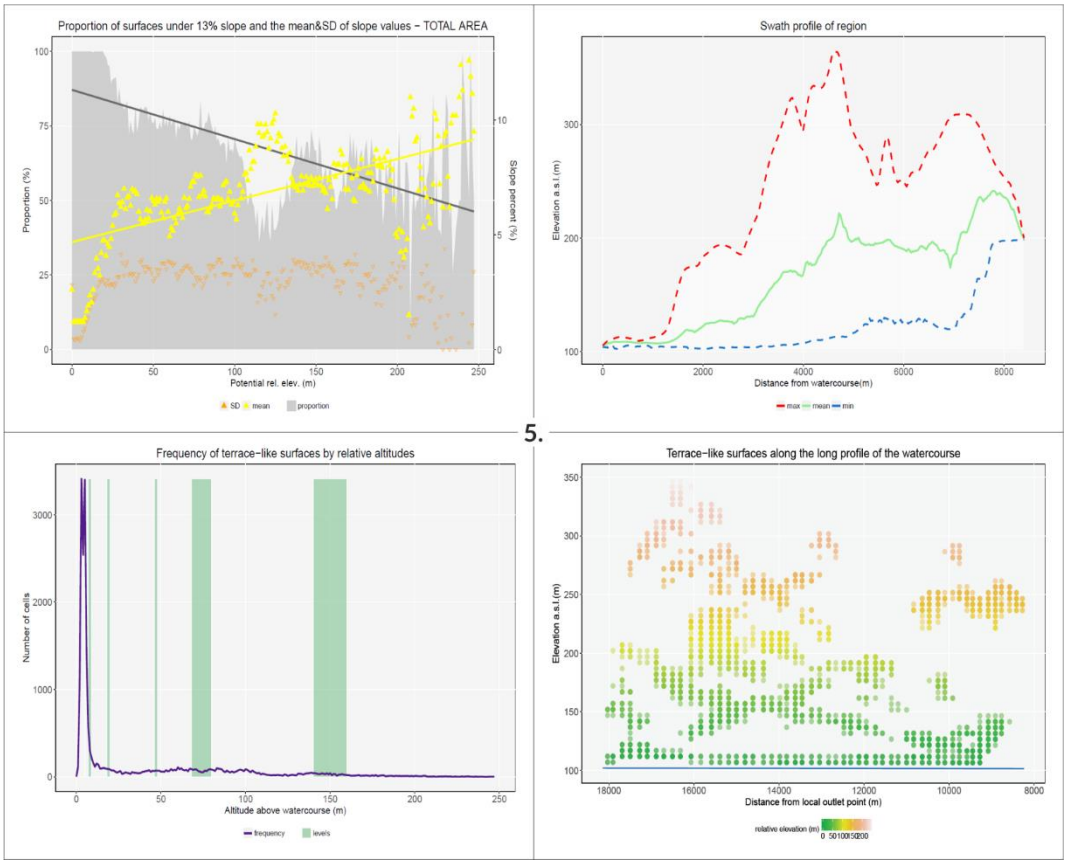
Proportion of surfaces under 13% slope and the mean&SD of slope values – TOTAL AREA
Proportion (%)
Slope percent (%)
Potential rel. elev. (m)
SD
mean
proportion
Swath profile of region
Elevation a.s.l.(m)
Distance from watercourse(m)
max
mean
min
5.
Frequency of terrace–like surfaces by relative altitudes
Number of cells
Altitude above watercourse (m)
frequency
levels
Terrace–like surfaces along the long profile of the watercourse
Elevation a.s.l.(m)
Distance from local outlet point (m)
relative elevation (m)

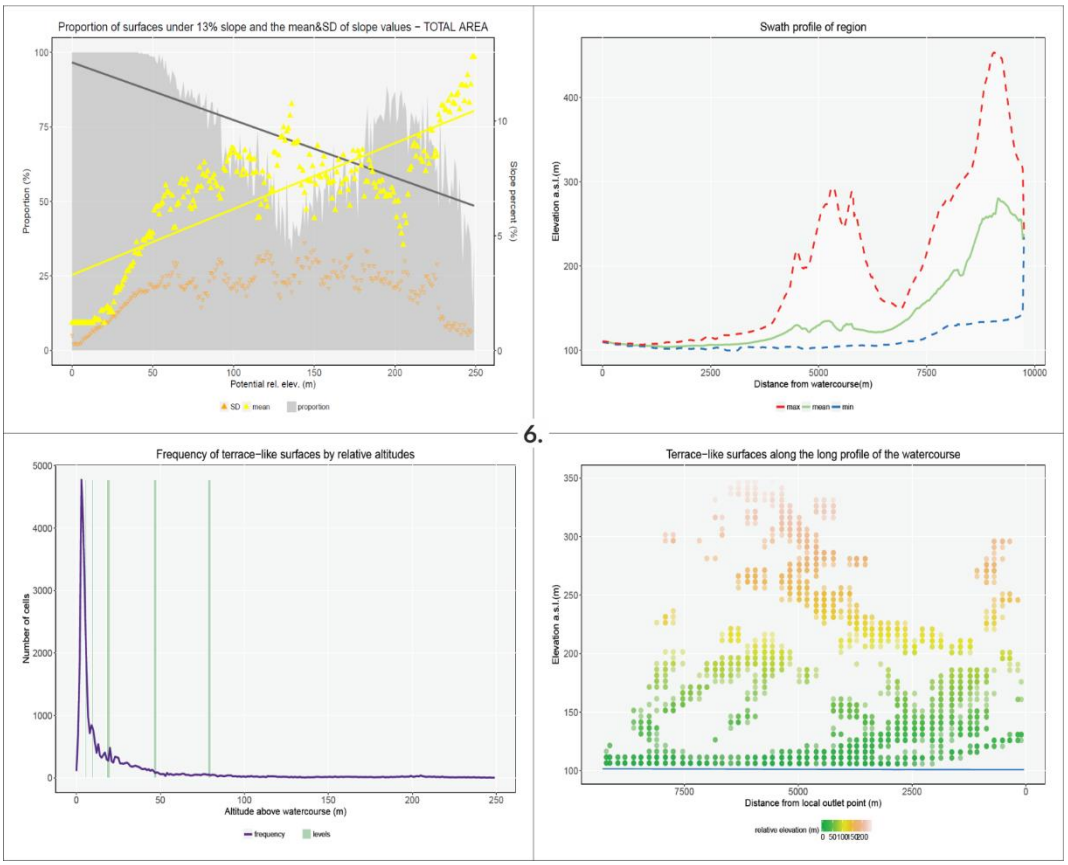
Proportion of surfaces under 13% slope and the mean&SD of slope values − TOTAL AREA
Proportion (%)
Slope percent (%)
Potential rel. elev. (m)
SD
mean
proportion
Swath profile of region
Elevation a.s.l.(m)
Distance from watercourse(m)
max
mean
min
Frequency of terrace−like surfaces by relative altitudes
Number of cells
Altitude above watercourse (m)
frequency
levels
Terrace−like surfaces along the long profile of the watercourse
Elevation a.s.l.(m)
Distance from local outlet point (m)
relative elevation (m)

6.


Proportion of surfaces under 13% slope and the mean&SD of slope values − TOTAL AREA
Proportion (%)
Slope percent (%)
Potential rel. elev. (m)
SD
mean
proportion
Frequency of terrace−like surfaces by relative altitudes
Number of cells
Altitude above watercourse (m)
frequency
levels
Swath profile of region
Elevation a.s.l.(m)
Distance from watercourse(m)
max
mean
min
Terrace−like surfaces along the long profile of the watercourse
Elevation a.s.l.(m)
Distance from local outlet point (m)
relative elevation (m)

7.

Appendix 9. Geomorphological map between Almásfüzitő and Esztergom.
(Adopted from Schweitzer, 1980)